

https://dspace.org/

Seismotectonic and seismic hazard studies for Madagascar

Rakotondraibe, Tsiriandrimanana

2022

https://hdl.handle.net/10539/37150

Downloaded from a DSpace repository. https://dspace.org/

UNIVERSITY OF THE WITWATERSRAND, JOHANNESBURG

Seismotectonic and seismic hazard studies for Madagascar

by

Tsiriandrimanana Rakotondraibe

A thesis submitted to the Faculty of Science, University of the Witwatersrand, Johannesburg, in fulfillment of the requirements for the degree of Doctor of Philosophy

Declaration

I declare that this thesis is my individual work. It is submitted in fulfillment of the requirements for the Degree of Doctor of Philosophy in the University of the Witwatersrand, Johannesburg. This thesis was not submitted before for any degree or examination in any other University.



Date: 24th October 2022

Abstract

Madagascar is an island that was once situated in the centre of the Gondwana supercontinent but is now located 1000 km from the East African Rift and about 2000 km from the mid-ocean ridge of the Indian Ocean. Its separation from the African continent (ca. 165-130 Ma) and the Indian sub-continent (ca. 90 Ma) and mantle upwelling that gave rise to the recent volcanism (ca. 28-0.5 Ma) has had significant impact on the geological structure and neotectonics of the island. This thesis focuses on the seismotectonic evolution of Madagascar and assesses the seismic hazard. Data for this project was derived from the 28-station MAdagascar – COmoros-MOzambique (MACOMO) array, as well as stations from the concurrent SEismological signatures in the Lithosphere/Asthenosphere system of SOuthern MAdagascar (SELASOMA) and Réunion Hotspot and Upper Mantle - Réunions Unterer Mantel (RHUM-RUM) projects, and permanent stations of the national seismological network. The combined 56 stations provided a better distribution and density than any previous study.

The thesis is presented in three main parts. The first part focuses on seismicity and focal mechanisms. The 695 events recorded and located during the 23-month period of MACOMO observations in 2011-2013 have magnitudes that vary from M1 to M5.3. Twenty-three focal mechanism solutions were determined using P-wave first motion polarities and some clear S-wave polarities. In agreement with previous studies, it was found that central Madagascar is the most seismically-active region. Most earthquakes are located near known faults. Normal faulting dominates the central area, while strike-slip and reverse fault mechanisms are predominantly observed near the Antsaba and Sandrakota shear zones in the north, and the Bekily and Ampanihy shear zones in the south. The focal mechanism studies revealed extensional faulting in central Madagascar, which can be explained by the reactivation of older faults by a thermal bulge underlying the region. The faulting style was not well defined in the northern and southern parts as few solutions were determined due to the lower density of stations.

In the second part of this thesis, 182 focal mechanism solutions were used to study the characteristics of the stress field. Calculations were performed using a linear inversion technique based on the Michael (1984) method and using a recently calculated velocity model of Madagascar. Results give shape ratios (i.e., relative magnitude of stress axes) that vary from 0.7 to 0.9; a maximum principal stress axis (σ_1) that is near-vertical and a minimum principal stress axis (σ_3) that is near-horizontal with a NW-SE orientation. This corresponds to a normal faulting regime. The regional variation of stress and the characteristics of the shape ratio and friction values were determined. The average direction of the stress field is approximately NW-SE in central Madagascar, and trends W-E in the southern and northern parts of the island. In central Madagascar the shape ratio and friction vary from 0.83 to 0.97 and 0.45 to 0.65, respectively; while in the northern and southern parts of Madagascar they vary from 0.3 to 0.5 and 0.5 to 0.7, respectively.

The third part of the thesis reports on the assessment of the seismic hazard in Madagascar using data from a catalogue that combines data from the NDC (National Data Center), bulletins produced by the current study for the period between 1975 and 2016, as well as historical earthquake data. The analysis reveals that Madagascar has moderate seismic activity with local magnitude $M_L \leq 6$. The relationship between the moment magnitude M_W and local magnitude M_L values was estimated in order to unify magnitude characteristics and create the homogeneous catalogue that is required for seismic hazard studies. A Probabilistic Seismic Hazard Assessment approach (PSHA) was performed using the Kijko and Sellevoll (KS) and Cornell-McGuire methods with two different ground motion models. In order to implement the alternative parameter values in seismic hazard calculation and to attribute uncertainties associated to the input parameter, a logic tree formalism was applied. The Peak Ground Acceleration (PGA) values near major towns in the central region for 10% and 2% probability of occurrence in 50 years are 0.04 g and 0.11 g, respectively. The spectral acceleration for 1.0 s and 3.0 s vary from 0.001 g to 0.01 g and 0.001 g to 0.005 g for 10% probability of

occurrence in 50 years, respectively; and from 0.02 g to 0.10 g and 0.002 g to 0.01 g for 2% probability of occurrence in 50 years.

This work demonstrates that the deployment of additional temporary seismic stations significantly improved our understanding of the seismotectonics of Madagascar, particularly in the northern and southern regions. In summary, we obtained a new magnitude relation, more accurate epicenter locations, better focal mechanism descriptions, and improved the assessment of seismic hazard.

Dedication

In memory of my mother

Rasoanirina Justine Claire

1952-2012

Acknowledgements

Primary, I would like to thank God for giving me strength during this research.

This PhD thesis has been done mostly at the School of Geosciences, University of the Witwatersrand Johannesburg, South Africa under guidance of Prof. Raymond Durrheim and Prof. Andrew Nyblade. It was a great work under their consideration; I really appreciate their concern, comment, and advice. I would like to give special thanks to Prof. Michael Wysession for his help, encouragement, and acceptance of me as member on his team during the deployment of the MACOMO stations. I would like to thank Prof. Gerard Rambolamanana for giving me the opportunity to participate to the deployment of the MACOMO stations and for his encouragements and advice. I would like to thank also Profs Frederic Tillman, Karin Sigloch and Guilhem Barruol for allowing me to use the data from the SELASOMA and RHUM-RUM projects.

I am so grateful to all of the field team members during the MAdagascar-COmoros-Mozambique (MACOMO) installation, Ghassan Aleqabi, Patrick Shore, Martin Pratt, Fenitra Andriampenomanana, Rina Randrianasolo and the drivers. I am so grateful to Mrs. Sharon Ellis, Mrs. Antonia Money and Mrs. Barbara Peragine, the administrative assistants, for their support and assistance during my study period.

I acknowledge all the members of the AfricaArray group at the Department of Geosciences, School of Earth and Mineral Sciences, Penn State University, USA. I am grateful to all members of the group meeting in the Seismic Lab at the School of Geosciences, University of the Witwatersrand, Johannesburg, South Africa, for their support and encouragement. I would like to thank the School of Geosciences as a whole; the staff including the head of the Department of Geosciences.

I would like to thank Michele Chernega for her support during my stay in State College while at PennState University, USA. I am heartily thankful for her encouragement, advice and for care and everything and my friends Carol Destro, Atefeh Mohammadpour, Laiz Fiorilli, Jocely Souza for making it memorable.

I would like to thank all the staff at the Institut et Observatoire de Géophysique d'Antananarivo (IOGA), all the members at the "Laboratoire de Sismologie et Infrason (LSI)" at the IOGA and the University of Antananarivo, Madagascar for their encouragement and help during the preparation of this study.

I would like to thank Dr Andriamiranto Raveloson, Dr Elisa Rindraharisaona, Dr Fenitra Andriampenomanana and Khile Homann for their help with scripts and advice.

I would like to thank all of my friends from Madagascar, South Africa and the USA that helped me to accomplish this study.

I would like to thank all of my family members, especially for their continuous support and encouragement over the years. Their support, love and encouragement have helped me during the challenging times, and also my mom who passed away before I started this study.

This study was funded by NSF awards EAR-0838426 and 0838387, and supported by the AfricaArray Program. Prof. Raymond Durrheim acknowledges the support of the National Research Foundation through the South African Research Chairs Initiative.

List of publications

Peer-reviewed publication

Andriampenomanana, F., Nyblade, A.A., Wysession, M.E., Durrheim, R.J., Tilmann, F., Barruol, G., Rambolamanana, G., and **Rakotondraibe, T**. (2020). Seismic velocity and anisotropy of the uppermost mantle beneath Madagascar from Pn tomography, Geophysical Journal International, https://doi.org/10.1093/gji/ggaa458

Rakotondraibe T., Nyblade,A.A., Wysession, M.E., Durrheim, R.J., Rambolamanana, G., Aleqabi, G., Shore, P.J., Pratt, M.J., Andriampenomanana, F., Rümpker, G., and Rindraharisaona, E. (2020). Seismicity and seismotectonics of Madagascar revealed by the 2011- 2013 deployment of the island-wide MACOMO broadband seismic array, Tectonophysics, 790, 228547, https://doi.org/10.1016/j.tecto.2020.228547

Ramirez, C., Nyblade, A.A., Wysession, M.E., Pratt, M.J., Andriampenomanana, F., and **Rakotondraibe, T**. (2018). Complex seismic anisotropy in Madagascar revealed by shear wave splitting measurements, Geophysical Journal International, 215(3), 1718-1727, https://doi.org/10.1093/gji/ggy367

Andriampenomanana, F., Nyblade, A.A., Wysession, M.E., Durrheim, R.J., Tilmann, F., Julià, J., Pratt, M.J., Rambolamanana, G., Aleqabi, G., Shore, P.J., and **Rakotondraibe T**. (2017). The structure of the crust and uppermost mantle beneath Madagascar, Geophysical Journal International, 210 (3), 1525 - 1544,http://doi:10.1093/gji/ggx243

Pratt, M.J., Wysession, M.E., Aleqabi, G.I., Wiens, D.A., Nyblade, A.A, Shore, P. J., Rambolamanana, G., Andriampenomanana, F., **Rakotondraibe, T**., Tucker, R.D., Barruol, G., and Rindraharisaona, E. (2017). Shear-velocity structure of the crust and uppermantle of Madagascar derived from surface wave tomography, Earth and Planetary Science Letters, 458, 405 - 417, http://doi:10.1016/j.epsl.2016.10.041

Peer-reviewed conference proceedings

06 - 09 October 2019: 16th Biennial Conference and Exhibition of the South African Geophysical Association (SAGA) (South Africa). Oral presentation: "*Seismic hazard studies in Madagascar*".

07 - 12 July 2019: 14th Annual AfricaArray Scientific Workshop at the School of Geosciences of the University of Witwatersrand (South Africa). Oral presentation: "*Seismic hazard studies for Madagascar*".

02 – 07 September 2018: 36th General Assembly of the European Seismological Commission in Valletta, Malta (ESC2018-S20-435). Oral and Poster presentation: "*Preliminary results of stress derivation from earthquake focal mechanisms in Madagascar*".

25 June – 26 June 2018: 13th Annual Africa Array Scientific Workshop at the School of Geosciences of the University of Witwatersrand (South Africa). Poster Presentation "*Preliminary results of stress derivation from earthquake focal mechanisms in Madagascar*".

11 - 15 December 2017: Fall Meeting of the American Geophysical Union, New Orleans, USA. Wysession, ME, Andriampenomanana, F, Nyblade, AA, Durrheim, R, Wiens, DA, Rambolamanana, G, Pratt, MJ, Aleqabi, G, Shore, PJ, **Rakotondraibe, T**, Tucker, RD and Tilmann, F, 2017, T41E-03: *Normal-Faulting in Madagascar: Another Round of Continental Rifting?*

13 - 14 November 2017: National Data Center (NDC) Capacity building Workshop and RSTT model (Namibia). Poster presentation: "*Seismotectonic studies in Madagascar*".

10 -13 September 2017: 15th Biennial Conference and Exhibition of the South African Geophysical Association (SAGA) (South Africa). Oral presentation: "*Focal mechanism and stress field inversion in the central part of Madagascar*".

29 June – 30 June 2017: 12th Annual AfricaArray Scientific Workshop at the School of Geosciences of the University of Witwatersrand (South Africa). Oral presentation: "*Probabilistic seismic hazard for Madagascar*".

27 August - 04 September 2016: 35th International Geological Congress (IGC) (South Africa). Poster presentation: "*Seimotectonic studies for Madagascar*".

02-05 April 2016: 1 st General Assembly of the African Seismological Commission (AfSC), (Egypt). Poster presentation: "*Seismotectonics studies for Madagascar*".

17 - 23 January 2016: 11th Annual AfricaArray Scientific Workshop at the School of Geosciences of the University of Witwatersrand (South Africa). Oral presentation: "*Determination of Fault structure for Madagascar*".

06 - 09 September 2015: 14th Biennial Conference and Exhibition of the South African Geophysical Association (SAGA) (South Africa). Oral presentation: "Seismicity and Local Magnitude scale for Madagascar". *Champagne Castle, SOUTH AFRICA, pp. 173-176.*

19 - 20 January 2015: 10th Annual AfricaArray Scientific Workshop at the School of Geosciences of the University of Witwatersrand (South Africa). Oral presentation: "*Seismicity map of Madagascar using data from MACOMO project*".

Contents

Declaration ... **iii**

Abstract ... **v**

Dedication ... **viii**

Acknowledgements ... **x**

List of publications ... **xii**

List of figures ... **xx**

List of tables ... **xxvi**

List of Acronyms ... **xxviii**

Chapter 1: General Introduction ... **1**

1.1 Introduction ... 1

1.2 Objectives ... 2

1.3 Outline ... 2

1.3.1 Seismicity studies ... 2

1.3.2 Fault mechanisms and stress field model ... 3

1.3.3 Magnitude scale and seismic hazard assessment ... 3

1.4 Problem statement ... 3

1.5 Literature review: geological setting ... 4

1.5.1 Precambrian basement ... 6

1.5.2 Sedimentary cover ... 9

1.5.3 Volcanic fields ... 9

1.6 Literature review: previous geophysical work ... 11

1.6.1 Seismicity studies of Madagascar ... 12

1.6.2 Magnitude scale ... 14

1.6.3 Velocity structure ... 15

1.6.4 Focal mechanisms ... 18

1.6.5 Hazard studies ... 19

Chapter 2: Theory ... **20**

2.1 Seismic waves 20
2.2 Source parameters and mechanisms 22
2.2.1 Location and origin time 22
2.2.2 Correction for instrument response 26
2.2.3 Fault geometry 27
2.2.4 Focal mechanism solutions 29
2.3 Stress field 37
2.3.1 Basic concepts 37
2.3.2 Mohr's circle of stress 38
2.3.3 P- and T-axis 41
2.3.4 Stress inversion 41
2.4 Earthquake magnitudes 47
2.4.1 Local magnitude 47
2.4.2 Duration magnitude 50
2.4.3 Moment magnitude 51
2.4.4 Relation between M_W, M_L, M_S, m_B and m_b 54
2.5 Seismic Hazard Assessment 55
2.5.1 Basic concepts 55
2.5.2 Cornell-McGuire approach 58
2.5.3 Kijko and Sellevoll approach (KS) 62
2.5.4 Logic tree 68
2.6 Computational packages 69
2.6.1 ANTELOPE software 69
2.6.2 HYPOELLIPSE 70
2.6.3 HYPODD 72
2.6.5 STRESSINVERSE program 74
2.6.6 HA3 program 75
2.6.7 CRISIS software 75
Chapter 3: Data and Methodology 77
3.1 Data 77
3.1.2 Permanent seismic network 77

3.1.3 Temporary seismic networks 79
3.2 Methodology 90
3.2.1 Completeness of the catalogue 90
3.2.2 Declustering method 90
3.2.3 Seismic source zone 92
3.2.4 Earthquake catalogue 92
3.2.5 Magnitude homogenization 93
Chapter 4: Seismotectonics of Madagascar 98
4.1 Introduction 98
4.2 Seismicity 99
4.2.1 Location of earthquakes 99
4.2.2 Northern region 102
4.2.3 Central region 103
4.2.4 Southern region 107
4.3 Focal mechanisms 109
4.3.1 Computation 109
4.3.2 Discussion 113
4.4 Magnitude calibration 117
4.5 Discussion 120
4.6 Conclusion 123
Chapter 5: Stress field inversion 125
5.1 Introduction 125
5.2 Focal mechanisms 125
5. 3 Stress Inversion 130
5.4 Results of inversion 131
5.4.1 Bemarivo 132
5.4.2 Bekily 133
5.4.3 Famoizankova 135
5.4.4 Alaotra 136
5.4.5 Ankaratra 141
5.4.6 Itremo 145

5.5 Discussion 148
5.5.1 Northern region 148
5.5.2 Central region 149
5.5.3 Bekily region 150
5.6 Conclusion 151
Chapter 6: Seismic hazard analysis 152
6.1 Introduction 152
6.2 Methodology 153
6.2.1 Declustering 158
6.2.2 Definition and characterization of source zones 165
6.2.3 Ground Motion Prediction Equations 174
6.3 Results 181
6.3.1 Hazard maps in term of PGA 181
6.3.2 Uniform hazard spectrum 184
6.4 Discussions and conclusion 185
6.4.1 Northern and southern part of Madagascar 187
6.4.2 Central part of Madagascar 188
Chapter 7: Discussion and Conclusion 189
7.1 Introduction 189
7.2 General discussion and conclusion 190
7.2.1 Seismicity and magnitude 190
7.2 2 Focal mechanisms 191
7.2.3 Stress field 193
7.2.4 Seismic hazard 195
7. 3 Recommendations for future studies 197
References 199
Appendix A: Seismotectonic studies of Madagascar (Published Paper) 220
Appendix B: Example of input files for HYPOELLIPSE and HYPODD 245
Appendix C: Earthquake location and relocation lists 247
Appendix D: Example of FOCMEC input files 273

Appendix E: Paper about Stress field in Madagascar paper (In Prep.) 277

Appendix F. Focal mechanism list for stress determination 294

Appendix G: Paper about Seismic hazard (In prep.) 300

Appendix H: Moment magnitude determination 315

List of figures

Figure 1. 1: Gondwana showing the position of Madagascar at the end of the Neoproterozoic Era (~550 Ma) (Kusky et al., 2003). 5

Figure 1. 2: Displacement of Madagascar along the Davie Fracture Zone (Mascle et al., 1987).....5

Figure 1. 4: Ankaratra and Lac Itasy volcanic fields in central Madagascar (after Bésairie, 1964). 11

Figure 1. 5: Seismicity and focal mechanisms determined by earlier studies.Red circles are events in the ISC Bulletin with magnitudes M>4.....13

Figure 1. 6: (a) S-wave velocity model from all stations (Andriampenomanana et al. 2017), (b) Calculated vertical P-wave velocity structure for Madagascar using results from the (c) Wadati plot. 16

Figure 2. 1: Main types of waves produced by an earthquake. (https://courses.lumenlearning.com/geo/chapter/reading-studying-the-earths-interior).....21

Figure 2. 2: Vertical component seismogram recorded at the SBV seismic station produced by a M3.5 earthquake on March 16th, 2012 at 11:56:55 UTC. 21

Figure 2. 3: Earthquake focus (hypocenter) and epicenter. 22

Figure 2. 4: Triangulation method to locate earthquakes. http://www.bbc.co.uk/education/guides/zq7ycdm/revision/2).....23

Figure 2. 5: Geometrical description of a fault plane $\boldsymbol{\gamma}$ is the rake direction and n is the normal to the fault plane.....28

Figure 2. 6: Illustration of the method for calculating strike, dip, and rake angles 29

Figure 2. 7: Measurement of the azimuth angle.....30

Figure 2. 8: Definition of the take-off angle 30

Figure 2. 9: Illustration of P-wave upward and downward first motions (Havskov and Ottemöller, 2010) 31

Figure 2. 10: Transformation of ZNE to ZRT and LQT 32

Figure 2. 11: Examples of polarity picking on a local M3.1 event recorded at station BKTA on 4 July 2013 at 13:40:59.08. 33

Figure 2. 12: Fault mechanisms and ‘beach ball’ diagrams. 34

Figure 2. 13: Focal mechanism for a normal faulting earthquake with the actual fault plane and auxiliary plane in a section BB'. 35

Figure 2. 14: Normal fault plane solution showing the P- and T-axes. 35

Figure 2. 15: Ternary diagram to display focal mechanisms (Frohlich, 1992) 36

Figure 2. 16: Difference between trend angle and plunge angle, N represents North. 37

Figure 2. 17: Stress and fault mechanisms 38

Figure 2. 18: Mohr diagram in 2-D with appropriate points in stress space 41

Figure 2. 19: An example of Mohr circle within its associated stress shape ratio values (R) in an overall strike-slip regime. 45

Figure 2. 20: Different forces that give definition of friction. 45

Figure 2. 21: Determination of the friction value from Mohr Coulomb failure criterion. 46

Figure 2. 22: Estimation of local magnitude using the Richter method. 48

Figure 2. 23: Illustration of the earthquake coda, which is normally used to estimate duration magnitude 50

Figure 2. 24: Frequency-domain transformation of the ground displacement wave. ...52

Figure 2. 25: Deterministic seismic hazard analysis (Kramer, 1996) 57

Figure 2. 26: Probabilistic seismic hazard analysis. 58

Figure 2. 27: Source zone geometries (a) point source *e.g.* from a short fault, (b) linear source defined as shallow fault modeled, c) a three-dimensional source zone (Kramer, 1996). 59

Figure 2. 28: Methods of source to site distance measurement. 59

Figure 2. 29: An example of curve showing the Gutenberg-Richter relation 60

Figure 2. 30: Kijko and Sellevoll (1992) method to obtain seismic hazard parameters.. 66

Figure 2. 31: An example of logic tree in which different parameters are inserted for computing seismic hazard. 69

Figure 2. 32: Hypoellipse error ellipsoid relationships with SEH= MAXH/1.87, and SEZ=MAXZ/1.87. MAXZ is the radius of the 68% confidence ellipsoid (after Lahr, 1999). 71

Figure 3. 1: Seismic stations in Madagascar 78

Figure 3. 2: Seismometers (1) CMG-3T, (2) STS-2, and (3) Trillium-120 81

Figure 3. 3: Schematic of a typical MACOMO seismic station. 82

Figure 3. 4: Installation of Vatomandry (VATO) station.. 83

Figure 3. 5: A set of equipment inside the blue barrel (DAS – Power box-Batteries- Cables-PVC tube) 83

Figure 3. 6: Field servicing by Tsiriandrimanana Rakotondraibe and Fenitra Andriampenomanana in the SOLA station in northern Madagascar. 87

Figure 3. 7: Histogram showing data collected from MACOMO, local permanent, SELASOMA, and RHUM-RUM seismic stations. 89

Figure 3. 8: Characteristics of the waveform from signal-to-noise ratio that allowed reliable measurements of the peak amplitude and the spectral plateau for estimates of M_L and M_W 96

Figure 3. 9: Topographic map of Madagascar with 18,970 earthquakes from the combined MACOMO and Madagascar NDC catalogue between the time periods 1975-2016. 97

Figure 3. 10: Earthquakes and seismic stations used to determine M_W. 97

Figure 4. 1: Seismicity map for Madagascar using data from the MACOMO project. 100

Figure 4. 2: Computed depth distributions from (a) HYPOELLIPSE program (for 695 events) and (b) HYPODD program (for 422 events) 101

Figure 4. 3: Earthquake distribution in Bemarivo area. 103

Figure 4. 4: Earthquake distribution in Alaotra area. 105

Figure 4. 5: Earthquake distribution in the Ankaratra area. 106

Figure 4. 6: Earthquake distribution in the Itremo area (ITR). 107

Figure 4. 7: Map showing the earthquake distribution in Bekily area (BEK) from HYPOELLIPSE (grey circles) and the effects of event relocation by the HYPODD double-difference relocation method (red circles). 108

Figure 4. 8: Depth constraints for the 23 focal mechanisms, plotting the RMS travel-time residuals vs depth at intervals of 5 km. 112

Figure 4. 9: Focal mechanisms of 23 earthquakes in Madagascar. 114

Figure 4. 10: Focal mechanism solutions, constructed using P-wave first polarities and S-wave polarities, for 23 Madagascar intraplate earthquakes with good station coverage. 115

Figure 4. 11: Frequency-magnitude analysis of the 695 intraplate Madagascar earthquakes. 119

Figure 5. 1: A total of 12,727 earthquakes with M_L>2.5 in Madagascar (2000-2016) from the MACOMO bulletin and Madagascar NDC including all 182 earthquake events used for stress field inversion. 127

Figure 5. 2: Focal mechanisms for 182 earthquake events 128

Figure 5. 3: Ternary diagram showing the classification of the focal mechanisms used for the stress inversion calculation 129

Figure 5. 4: Stress field inversion for 20 earthquakes in the Bemarivo zone (1). 132

Figure 5. 5: Stress direction results for the Bemarivo area. 133

Figure 5. 6: Same as Figure 5. 4 but for 23 events in Bekily zone. 134

Figure 5. 7: Stress direction results in the Bekily area. 134

Figure 5. 8: Same as Figure 5. 4 but for the Famoizankova zone. 135

Figure 5. 9: Stress direction results in the Famoizankova region 136

Figure 5. 10: Same as Figure 5. 4 but for the events in the sub-zone A of Alaotra 137

Figure 5. 11: Same as Figure 5. 4 but for the events in the sub-zone B of Alaotra…….....138

Figure 5. 12: Same as Figure 5. 4 but for the events in the sub-zone C of Alaotra…….....139

Figure 5. 13: Stress direction results in the Alaotra region.....140

Figure 5. 14: Same as Figure 5. 4 but for the events in the sub-zone D of Ankaratra…….....142

Figure 5. 15: Same as Figure 5. 4 but for the events in the sub-zone E of Ankaratra…….....143

Figure 5. 16: Stress direction results in the Ankaratra region.....144

Figure 5. 17: Stress direction results in the Itremo region 145

Figure 5. 18: Map showing the results of the minimum (blue) and maximum (red) stress direction after the inversion from each selected region. 147

Figure 6. 1: Plot of the estimated relation between M_w and M_L for 80 eartthquakes reported in the MACOMO catalogue (black) and events derived from ISC bulletin (blue). 158

Figure 6. 2: Declustering using the Reasenberg (1985) method after testing different values into the parameter files.....162

Figure 6. 3: Magnitude-time distribution and magnitude-distance distribution for declustered events in the whole area of Madagascar. 164

Figure 6. 4: Timeline showing the annual number of earthquakes as a function of magnitude in the period 1975-2016, $M_w \geq 2.9$.....170

Figure 6. 5: Histogram showing the moment magnitude of all earthquakes in Madagascar, 1975-2016 inclusive.....170

Figure 6. 6: Completeness estimation for all source zones for 42 years (1975-2016, inclusive). Red stars indicate the M_C values. 171

Figure 6. 7: Results from ZMAP using data from the combined two catalogues (NDC+MACOMO) but plotted using GMT (Wessel and Smith, 1998).....172

Figure 6. 8: Madagascar's location in the southeastern part of Africa https://platetectonicsafrica.weebly.com/cer.html.....175

Figure 6. 9: Predicted ground motion for an M=3.5 earthquake with a 15 km focal depth calculated.....176

Figure 6. 10: Map of Madagascar showing the 510 nodes (red squares) and seismic source zones (black boxes).....178

Figure 6. 11: Logic tree for median ground motions for determining the branches at the final branches. 180

Figure 6. 12: Seismic hazard maps showing the expected PGA, estimated spectral acceleration for a period 1.0 s and 3.0 s at 10% probability of being exceeding in 50 year period (474-year return period). 182

Figure 6. 13: Seismic hazard maps showing the expected PGA, estimated spectral acceleration for a period 1.0 s and 3.0 s at 2% probability of being exceeding in 50 year period (2,475-year return period). 183

Figure 6. 14: Example of uniform hazard spectrum calculated for a site in the Ankaratra region in central Madagascar for a return period of 474- and 2,475-years (10% and 2% probability of exceedance in 50 years). 184

Figure 6. 15: Earthquake hazard map for Africa in units of g with a 10% probability of being exceeded in 50 years (Poggi et al., 2017).....186

Figure 6. 16: Seismic hazard map showing PGA values in units of g with a 10% probability of being exceeded in 50 years (Razafindrakoto et al., 2009) 187

List of tables

Table 1. 1: Malagasy earthquakes with M≥5 14

Table 1. 2: Crustal velocity models for Madagascar..... 17

Table 1. 3: Focal mechanism solutions for Malagasy earthquakes. Source: (1) Shudofsky (1985), (2) Grimison and Chen (1988), (3) CMT-Harvard (http://www.globalcmt.org/CMTsearch.html) and (4) Craig et al. (2011) 18

Table 2. 1: Hypocentre quality factors based on the SEH and SEZ values (the vertical and horizontal errors) 71

Table 2. 2: Parameters for double difference relocation using hypoDD.inp 73

Table 3. 1: Seismic stations used in the study (Shown in Figure 3. 1). 84

Table 3. 2: Stations that failed or were vandalized, 2011-2013. 87

Table 4. 1: Focal mechanism solutions for 23 Madagascar intraplate earthquakes 116

Table 4. 2: The numbers of earthquakes in the different binned M_L magnitudes. 120

Table 5. 1: Stress inversion results for 182 events recorded from 1 January 2000 - 31 December 2016 in Madagascar. 146

AZ and PLG indicate Azimuth and Plunge. AZ is measured clockwise from the north and PLG downwards from the horizontal plane. 146

Table 6. 1: Earthquakes used to determine the M_L-M_w relation. (A) Earthquakes from the MACOMO bulletin, (B) Earthquakes from the ISC bulletin; "σ" is the average uncertainty value for M_w in m.u. (magnitude units). 155

Table 6. 2: Parameters set for the declustering method following Reasenberg (1985) method after inserting 18,970 seismic events..... 159

Table 6. 3: Parameter values inserted for declustering method using the Gardner and Knopoff (1974) approach. 165

Table 6. 4: Mc values from the two bulletins NDC and MACOMO. (a) 1897-1974, (b) 1975-2008; (c) 2009-2013; (d) 2013-2016..... 169

Table 6. 5: Largest earthquakes between November 1897 and December 1995 169

Table 6. 6: Characteristics of all seismic hazard parameters for all sources, where m_{max} is the maximum magnitude value, Beta (β) is equal to b*ln(10) a Gutenberg-Richter parameter. 174

Table 6. 7: Parameters used to create the grid for seismic hazard 178

List of Acronyms

BRSZ	Bongolava-Ranotsara Shear Zone
BRTT	Boulder Real Time Technology
CMAP	Central Madagascar Alkaline Province
CMT	Centroid Moment Tensor
DAS	Data Acquisition System
DSHA	Deterministic Seismic Hazard Assessment
FDSN	Federation of Digital Seismograph Networks
FPS	Fault Plane Solution
GFZ	GeoForschungsZentrum (Geo-research Centre)
GMT	Generic Mapping Tools
GPS	Global Position System
G-R	Gutenberg-Richter
HYPODD	Hypo Double Difference
IMAX	Intensity Maximum
IOGA `	Institut et Observatoire de Géophysique d'Antananarivo
IRIS	Incorporated Research Institutions for Seismology
ISC	International Seismological Center
MACOMO	Madagascar Comoros Mozambique
MAG	Magnitude
Ma	Million years from present
Mya	Million years ago
M_D	Magnitude Duration
M_L	Local Magnitude
M_W	Moment magnitude
NDC	National Data Central
NMAP	Northern Madagascar Alkaline Province
NRF	National Research Foundation (South Africa)
P	Primary wave
PASSCAL	Portable Array Seismic Studies of the Continental Lithosphere
PSHA	Probabilistic Seismic Hazard Assessment

RHUM-RUM Réunion Hotspot and Upper Mantle – Réunions Unterer Mantel

RMS Root Mean Square

SMAP Southern Madagascar Alkaline Province

SELASOMA Seismological Signatures in the Lithosphere/Asthenosphere system of Southern Madagascar

SEH Standard Horizontal Errors

SEZ Standard Vertical Errors

Chapter 1: General Introduction

1.1 Introduction

The island of Madagascar was at the centre of a major rifting event that led to the break-up of Gondwana during the Jurassic and Cretaceous periods, which is indicated by its position relative to its one-time neighbors, East Africa and the Indian subcontinent. The seismicity of the island has been studied since the early decades of the 20th century (Poisson, 1924, 1930), while more detailed seismotectonic studies were initiated following the deployment of local seismic stations in 1977 (Bertil and Regnoult, 1998; Rindraharisaona et al., 2013). Clusters of earthquakes in the central part of Madagascar are believed to be related to volcanic activity during the Quaternary in the Ankaratra volcanic field, while linear zones of seismicity are attributed to active extensional faulting (Bertil and Regnoult, 1998; Norton and Sclater, 1979; Mahoney et al., 1991). The central region of Madagascar is the most seismically active. To date, no earthquake is known to have exceeded magnitude M6, and thus the level may be described as 'moderate'.

Recent deployments of seismic stations have helped to advance our understanding of the causes of seismic activity and the assessment of seismic hazard in Madagascar. In this study I analysed waveforms recorded by an island-wide temporary network of broadband stations, supplemented by waveforms from several permanent broadband and short-period stations. I used standard modern methods to locate hypocenters and determine fault plane solutions. I used the results from the central part of the island to define the orientation of the main stress axis. Finally, I carried out a Probabilistic Seismic Hazard Assessment (PSHA) in order to determine the spatial variation of Peak Ground Acceleration (PGA) values and the statistical value of earthquake occurrence in Madagascar.

This preliminary chapter presents the problems to be solved and the principal objectives of this research following reviews of the geology of Madagascar and the results of previous geophysical studies.

1.2 Objectives

This study uses high-quality newly available seismic data to examine the spatial distribution of earthquakes, fault characteristics, orientation of the stress field, and seismic hazard for the whole of Madagascar. Immediately prior to the MAdagascar-COmoros-MOzambique (MACOMO) project, 11 permanent stations were operational, four broadband and seven short-period. MACOMO deployed 28 temporary broadband seismic stations spread over the whole of Madagascar from 2011 to 2013 (details are given in Chapter 2). Standard methods were used to process, analyze and interpret that data (see Chapter 2). The novelty of this work lies in a significantly better understanding of the distribution and causes of seismicity in Madagascar, enabling a more reliable assessment of seismic hazard. In summary, this study aimed to:

(a) Produce a new seismicity map for Madagascar using data from recently deployed temporary seismic stations, especially MACOMO;
(b) Identify earthquake clusters and determine the focal mechanisms of selected earthquakes in order to define and characterize seismic source zones.
(c) Determine the main direction of the stress field that is responsible for zones of active extensional faulting.
(d) Assess the seismic hazard for Madagascar.

1.3 Outline

This dissertation has three important topics, which are outlined in the following three sections.

1.3.1 Seismicity studies

The first topic focuses on the distribution of earthquake activity during the period 2011-2013. Earthquakes recorded by the MACOMO network were located using the HYPOELLIPSE software (Lahr, 1989, 1999). The accuracy of the relative locations of nearby events was improved by applying the Double Difference

method implemented in HYPODD software (Waldhauser and Ellsworth, 2000; Waldhauser, 2001) (See Chapter 2).

1.3.2 Fault mechanisms and stress field model

The second theme focuses on the seismotectonic structure of Madagascar. The geometry and form of the active faults in the central area of Madagascar was obtained after determining focal mechanisms using polarities of P- and S-wave first arrivals and the FOCMEC code (Snoke et al., 1984).

1.3.3 Magnitude scale and seismic hazard assessment

For the final theme, an earthquake catalogue for the period 1975 to 2016 was compiled by merging data from bulletins produced by the National Data Centre (NDC), the International Seismological Centre (ISC) and the MACOMO project. Magnitude values were then homogenized to a common magnitude, M_W, using a relation developed in this study. The seismic hazard parameters for identified source zones on the island were then determined and used in the seismic hazard calculation.

1.4 Problem statement

Prior to this study, the seismotectonics and hence the seismic hazard in Madagascar was poorly characterized owing to shortcomings in the national seismic network. Most of the permanent seismic stations are single-component short-period instruments located in the central part of the island. There were some first-order questions that needed to be answered. For example:

1. Why are there volcanoes in the middle of this plate?
2. Does a boundary between the Nubian and Somalian plates (or various other micro-plates) pass through Madagascar? If so, where?

Even though the island-wide broadband MACOMO network was deployed for only two years, it gathered data of sufficient quantity and quality to attempt to answer these questions and produce an improved assessment of the seismic hazard.

1.5 Literature review: geological setting

The current geological setting of Madagascar is due to two major rifting events: the separation of Madagascar from the Africa continent at ~160 Ma; and the separation of Seychelles and India from Madagascar at ~90 Ma (Kusky et al., 2007). The island once occupied a central position within the Gondwana supercontinent (Figure 1. 1, Stern, 1994), but rifted away from Africa (De Wit, 2003) and was displaced southwards parallel to the Davie Fracture Zone (Figure 1. 2 Coffin and Rabinowitz, 1992). However, its original position in Gondwana has been the subject of debate. Darracott (1974) and Förster (1975) place it in a position similar to that shown in Figure 1. 2 (*i.e.* it's present day location); Wegener (1924) and Tarling (1971) placed Madagascar closer to present-day Mozambique; while others suggested that Madagascar was once adjacent to the Kenya-Somalia-Tanzania coast (*e.g.* Du Toit, 1937).

Madagascar is divided into two major geological domains (Figure 1. 3). Precambrian rocks that pre-date Gondwana crop out in the eastern two-thirds of the island, while the western third is covered by younger sedimentary strata. Outcrops of younger volcanic rocks are found throughout Madagascar and range in age from the Cretaceous (beginning 145 Mya) to the Quaternary (see Figure 1. 3 and Figure 1. 4).

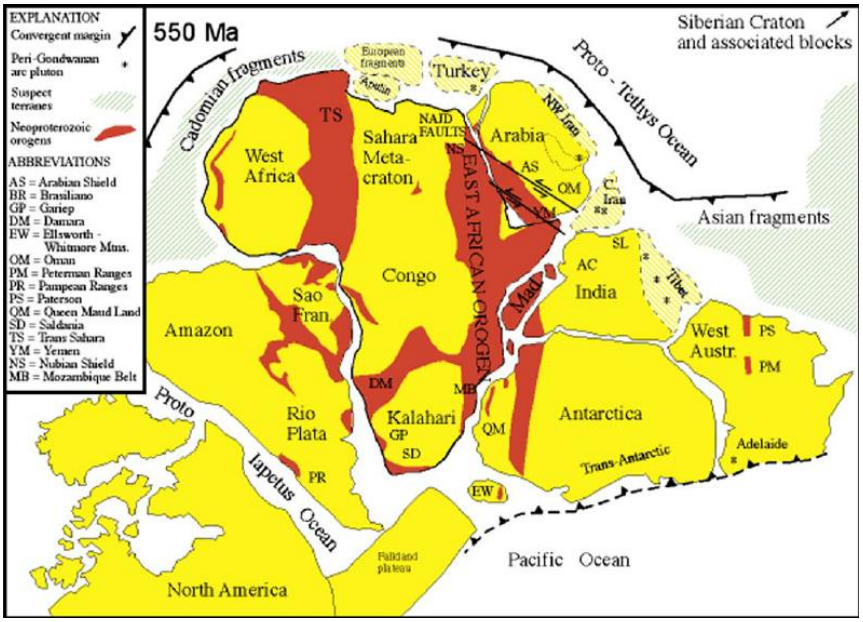

Figure 1. 1: Gondwana showing the position of Madagascar at the end of the Neoproterozoic Era (~550 Ma) (Kusky et al., 2003).

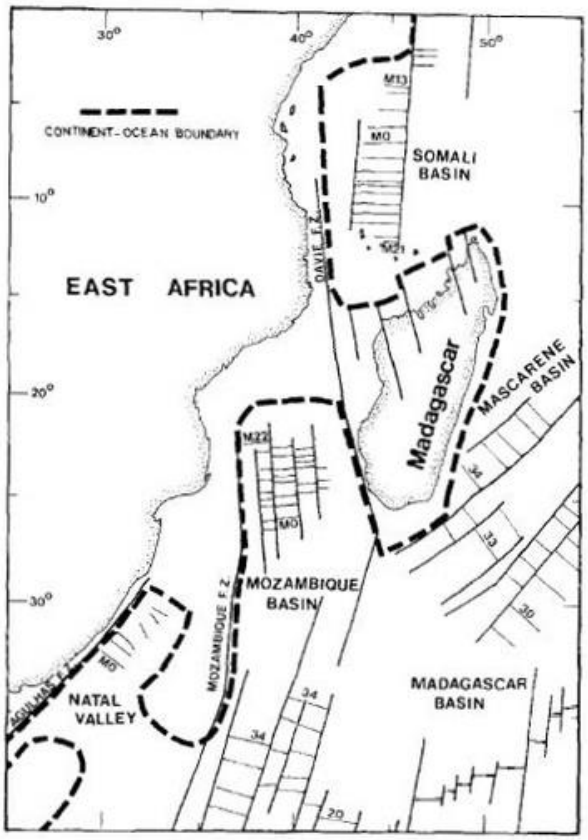

Figure 1. 2: Displacement of Madagascar along the Davie Fracture Zone (Mascle et al., 1987).

1.5.1 Precambrian basement

The Precambrian basement of Madagascar is bounded to the west by the Bongolava - Ranotsara shear zone (BRSZ) (Figure 1. 3). This Cambrian-age (542-488 Ma) structure was active during the last stages of the assembly of Gondwana, when the landmass consisting of present-day East Antarctica, East Africa and the Arabian-Nubian Shield coalesced, and is related to the Mozambican continental collision zone (Shackleton, 1996). The northern part of the Precambrian shield is composed of six geological units (Collins and Windley, 2002):

Antongil Group, found in the northeastern region, inshore of Antongil Bay, where it forms the Antongil Craton; on the small islands of Nosy Boraha (Île Sainte Marie) and Nosy Mangabe; and in the central east coast, where it forms the Masora Craton (

i. Figure 1. 3). The group consists of migmatites, gneiss, and early Archaean granites, dated at about 3000 Ma (Jourde, 1971). The Antongil and Masora Cratons are Neoarchaean and Mesoarchaean in age with Indian (Dharwar Craton) affinities (Tucker et al., 1999; Kröner et al., 1999; Collins and Windley, 2002; Collins et al., 2012).
ii. **Tsaratanana Group**, formed of gneiss, tonalites, ultramafic rocks, chromite-bearing paragneisses and greenstones, with zircon, dates between 2.75 and 2.49 Ga. (Tucker et al., 1999; Collins et al., 2000). The Tsaratanana and the Antananarivo blocks are divided by a mylonite zone (Tucker et al., 1999).
iii. **Bemarivo Group,** defined by the Neoproterozoic amphibolite- and granulite-facies calc-alkaline volcanic, sedimentary and clastic rocks (Jöns et al., 2006; Thomas et al., 2008). The northern area of Madagascar is formed by the belt in the Bemarivo region. Low angle thrust faulting is observed in the southern part of the Bemarivo Belt. The Antongil Craton was thrust northwards over the Bemarivo block.
iv. **Antananarivo Group** crops out in the central-northwest parts of the island. This Group consists of Neoarchaean gneisses, migmatites, granitoids and gabbros that were metamorphosed to granulite facies

between 700 and 550 Ma (Cox et al., 1998). Stratoid granites were emplaced at 630 Ma (Paquette and Nédélec, 1998). The east-west flexure that led to the formation of the north-south Angavo shear belt (Nédélec et al., 2003; Thomas et al., 2008) was accompanied by the intrusion of the porphyritic Carion granites at 532 Ma (Meert et al., 2001).

v. **Itremo Group** is a Paleoproterozoic succession of low-grade shallow water sedimentary rocks composed of quartzite, mica schist and marble, and was subjected to low grade metamorphism. The Itremo Group was thrust onto the Antananarivo Group (Nédélec et al., 2003).

vi. **Ikalamavony Group**, which is formed mostly of Proterozoic intermediate to mafic orthogneisses, formed between 1.03 Ga and 0.98 Ga, and has abundant volcano–clastic metasediments and quartzites (Tucker et al., 2011a, b).

The southern part of the Precambrian shield is composed of three geological units (Hirtz et al., 1954; Boulanger and Pavlovsky, 1954; Bésairie, 1956, 1968-1971, Nicollet 1990).

i. **Vohibory Group** consists of metasediments deposited during the Neoproterozoic Era from ~720 Ma to ~635 Ma (Collins et al., 2012) and amphibolite that are the products of granulite-facies metamorphism (Nicollet, 1990; Jöns and Schenk, 2008; Rakotovao, 2009). This Group also contains abundant mafic-ultramafic lenses of an unknown age. As the BRSZ has a left-lateral displacement, the Vohibory Group is tectonically associated with the eastern side of the Mozambique belt.

ii. **Ampanihy Group** (also known as the Graphite Group) lies between the Androyen and Vohibory groups. It comprises a variety of rock types that have been metamorphosed to granulite facies. The most common rocks are graphite schists.

iii. **Androyen Group** consists of Neoproterozoic metasediments and graphitic gneiss.

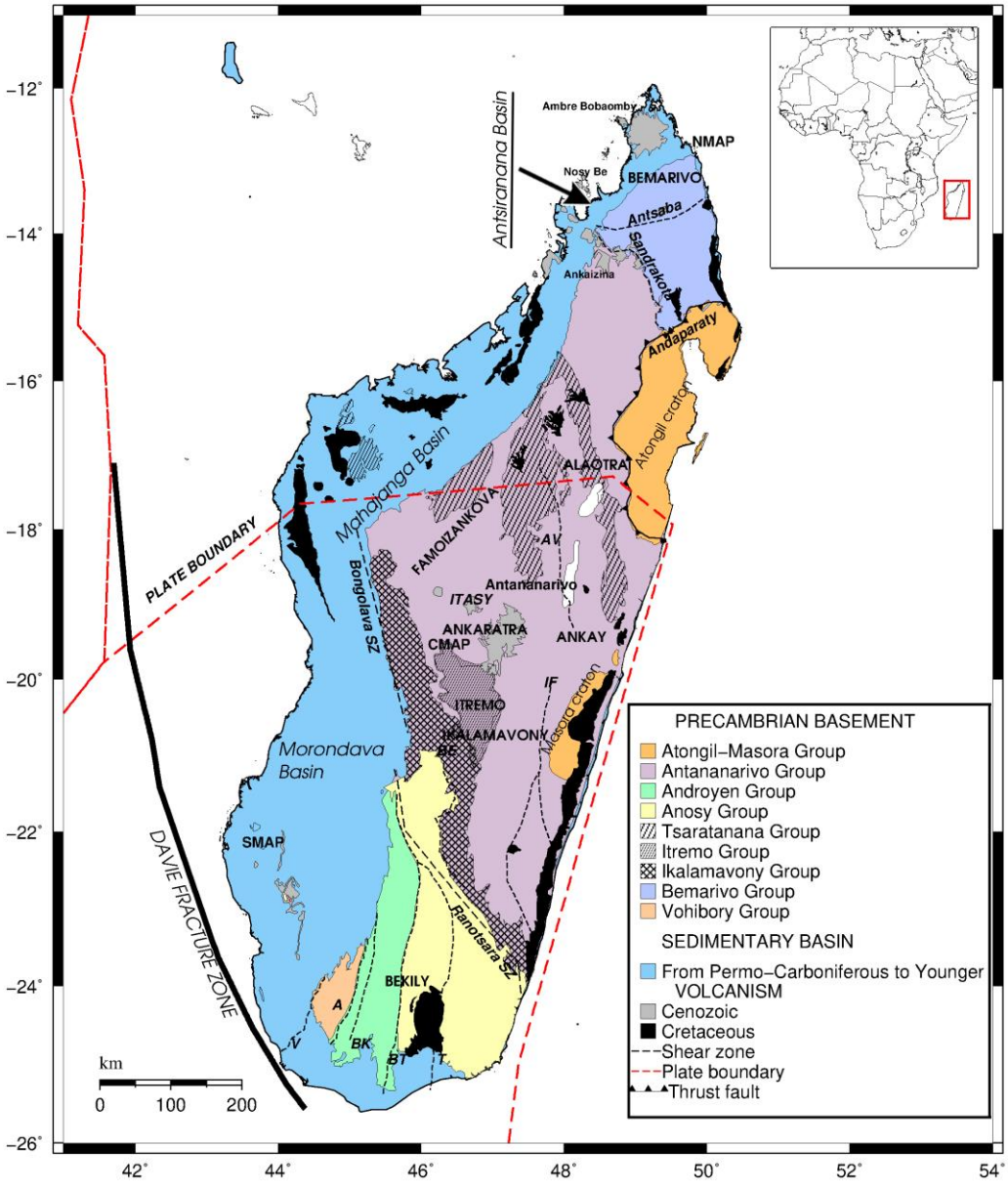

Figure 1. 3: Geological and tectonic map of Madagascar. Precambrian rocks and younger volcanics characterize the eastern and central parts of Madagascar, while sedimentary basins occupy the western third (after Bésairie, 1964). Dashed lines represent the shear zones: A - Ampanihy, AV - Angavo, BK - Bekily, BT - Betroka, BE - Betsileo, IF - Ifanadiana, T - Tranomaro, V - Vohibory. The red dashed line is the proposed plate boundary from Saria et al. (2014).

1.5.2 Sedimentary cover

The sedimentary cover consists mostly of Karoo Supergroup rocks (Bésairie 1971, 1973; Hottin, 1972; See Figure 1. 3). The Palaeozoic-Cenozoic sedimentary deposits cover the western third of the island (the Antsiranana, Mahajanga and Morondava basins) and several very small areas close to the east coast (Figure 1. 3). In areas of Precambrian basement, sediments are limited to Cenozoic grabens such as the Lake Alaotra region and the Ankay graben, both probably Neogene in age (Bésairie and Collignon, 1971).

1.5.3 Volcanic fields

Previous studies have shown that the island of Madagascar hosts two main volcanic fields (Besairie, 1973; Norton and Sclater, 1979) *viz.* Cretaceous-aged fields, which are mostly formed by tholeiitic basaltic lavas and Cenozoic-aged fields, formed by eruptions of alkali basalts.

Cretaceous volcanic rocks are found along the periphery of the island. They are related to the Mesozoic rifting (*ca*. 95-85 Ma), when basaltic magmas enveloped all surface area of Madagascar (Storey et al., 1995). The Cretaceous volcanic rocks are preserved in the western sedimentary basin, along the eastern coast, and in the Volcan de l'Androy in the southern part of Madagascar (Figure 1. 3) (*e.g.* Mahoney et al., 1991; Rasamimanana, 1996).

Three Cenozoic provinces are present (Figure 1. 3 and Figure 1. 4):

i. The **Northern Madagascar Alkaline Province** (NMAP) consists of several volcanic fields. The Ambre-Bobaomby field, in the extreme northern part of the island, consists of Miocene volcanics capped by very recent cones. Important features include the Ankaizina volcano, cinder cones, lava flows, and several crater lakes (Lakes Anakarefo, Beandrazina and Mantsaboramadio, the Nanilezana Marsh and two other unnamed lakes). Two groups of cinder cones (*viz.* Nosy Be and

the Ankaizina field) are also found in the northern part of the island. These volcanoes are thought to have been active during the Holocene, although the date of the most recent eruption is not confirmed. Nosy Be, a volcanic island off the NW of Madagascar, contains < 1 Ma basaltic lava flows from well-preserved cinder cones. Several large crater lakes are observed in the central part of the island (Tucker and Moine, 2012).

ii. The **Central Madagascar Alkaline Province** (CMAP) also consists of several fields. The Itasy field lies in central Madagascar (Figure 1. 4). The Kassigie volcano, situated about 100 km west of Antananarivo, is a prominent cone that covers an area of 100 km^2. It lies directly on the Precambrian migmatite and gneiss, and formed from the Pliocene to the Holocene. The Ankaratra volcanic field covers a 5000 km^2 area between Arivonimamo and Antsirabe (Figure 1. 3) and developed from the Miocene to the very recent Quaternary (Bésairie, 1973).

iii. The **Southern Madagascar Alkaline Province** (SMAP). The most important field, the Ankililoaka, lies near the southwestern coast and is aged *ca*. 12 Ma (Cucciniello et al., 2018).

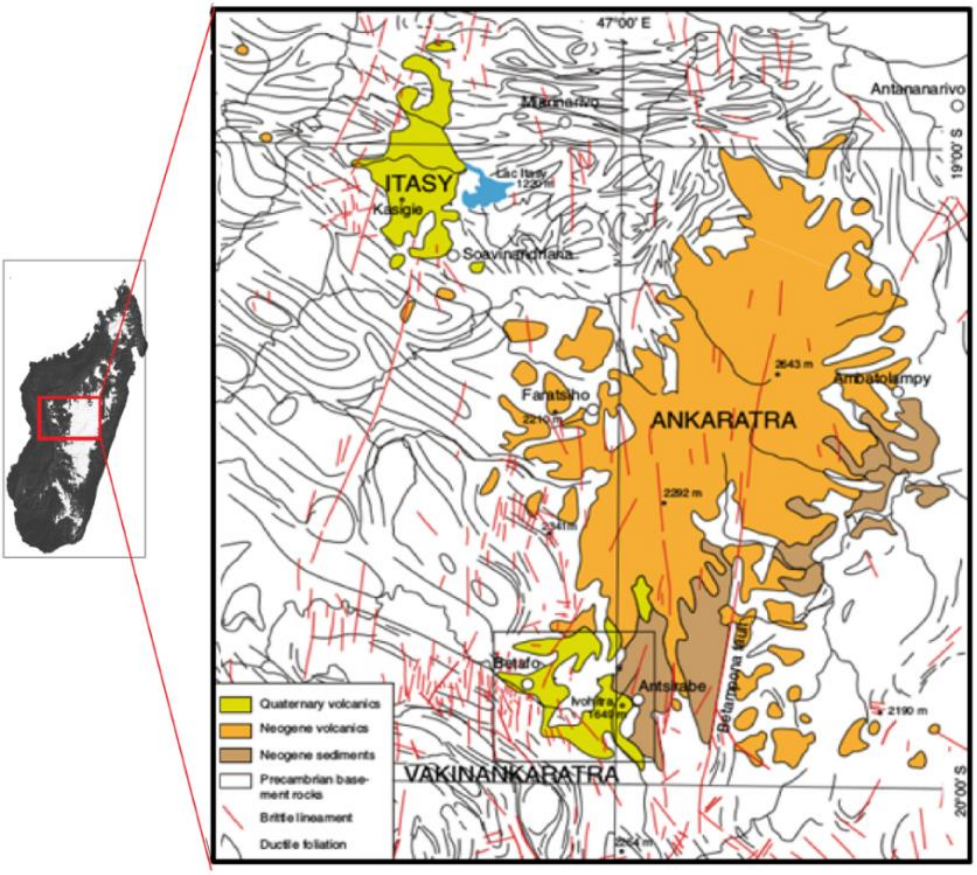

Figure 1. 4: Ankaratra and Lac Itasy volcanic fields in central Madagascar (after Bésairie, 1964).

1.6 Literature review: previous geophysical work

Seismic activity in Madagascar is generally described as 'moderate' as few destructive earthquakes have been reported (Rindraharisaona et al., 2013). It was only by the end of the 1900s, when seismographs were installed on the island, that earthquake and structural seismology studies could be conducted, for example by Rakotondrainibe et al. (1977), Rambolamanana (1989), Bertil and Regnoult (1998), Razafindrakoto et al. (2009), and Rindraharisaona et al. (2013). Various topics have been investigated, such as the seismic velocity structure of the central area of Madagascar, focal mechanism studies, seismotectonic studies, and seismic hazard assessment. These studies were conducted using data from a network of 11 permanent seismic stations (Figure 1. 5).

1.6.1 Seismicity studies of Madagascar

Historically, several large earthquakes have been recorded, notably an event with intensity VIII in the Itasy region in 1897, and with intensity VII in the Alaotra region in 1932. Earthquakes of magnitude M ≥ 5 recorded from 1897 to 1992 are listed in Table 1. 1.

Bertil and Regnoult (1998) used data from the *Institut et Observatoire de Géophysique d'Antananarivo* (IOGA) to study the seismicity of Madagascar. They found that earthquakes in the central part of the island had an east-west extension focal mechanism and suggested that seismic activity is related to the volcanic activity. Rindraharisaona et al. (2013) found high levels of seismic activity in the Ankaratra, Alaotra and Ankay regions (Figure 1. 5).

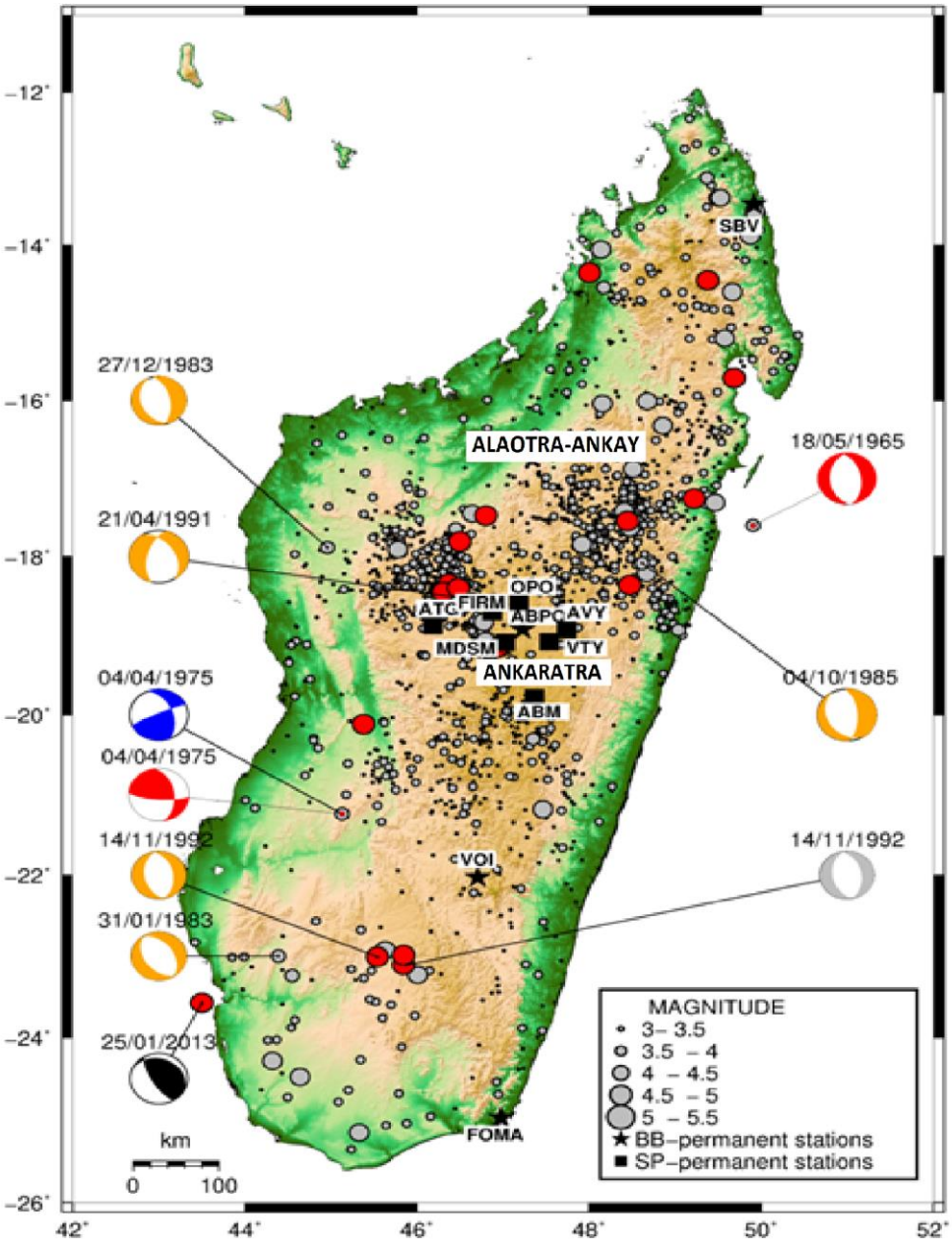

Figure 1. 5: Seismicity and focal mechanisms determined by earlier studies.Red circles are events in the ISC Bulletin with magnitudes M>4 http://www.isc.ac.uk/iscbulletin/citing.php. Grey circles are events with magnitude M≥3 compiled by Rindraharisaona et al. (2013) using the Madagascar National Data Central (NDC) catalogue between 1990 and 2011. Fault plane solutions are from the Global Centroid Moment Tensor (CMT) catalogue (orange) (https://www.globalcmt.org/CMTsearch.html), and from previous work by Shudofsky (1985) (blue), Grimison and Chen (1988) (red), Foster and Jackson (1998) (grey), and from this study, MACOMO bulletin (black).

Table 1. 1: Malagasy earthquakes with M≥5

NDC catalogue (1897-1992) : ISC (1964-1992), intensities from Poisson (1930).

DATE (dd/mm/yyyy)	LAT	LON	MAG	IMAX
03/11/1897	Itasy Region			VIII
04/09/1932	Alaotra Region			VII
29/03/1943	-18.6	44.2	M_L 6.0	
28/02/1945	Itasy Region			VII
18/05/1965	-17.6	49.9	M_B 5.4	
30/06/1974	-13.47	48.90	M_B 5.4	
04/04/1975	-21.24	45.12	M_B 5.3	
03/01/1983	-23.50	44.60	M_B 5.0	
27/12/1983	-18.30	45.10	M_B 5.1	
04/10/1985	-18.30	48.40	M_B 5.1	
21/04/1991	-18.35	46.37	M_B 5.8	
29/01/1992	-13.56	49.93	M_B 5.0	
20/02/1992	-23.24	44.55	M_B 5.0	
14/11/1992	22.87	45.74	M_B 5.1	

1.6.2 Magnitude scale

The earthquake magnitude scale for Madagascar was not well determined due to the shortage of earthquake data. The National Data Centre catalogue was compiled from a variety of sources. According to Rakotondrainibe (1977), the duration magnitude scale was developed using selected data recorded by the permanent short period stations and is in accord with the USGS m_b for M<5.0. It is defined by:

$$M_D = 2.04 \log \tau + 0.0004\,\Delta - 0.74 \tag{1.1}$$

where M_D represents the magnitude duration, $\boldsymbol{\tau}$ is the signal duration and $\boldsymbol{\Delta}$ the epicentral distance.

It was subsequently modified by Bertil and Regnoult (1998):

$$M_D = 2.04 \log \tau + 0.0004\,\Delta - 0.74 + (1.75 \text{ x } 10^{-7})\tau^2 \quad (1.2)$$

Magnitude duration M_D and local magnitude M_L were considered to be complementary for earthquakes having M<4.0, with a variance smaller than 0.2.

1.6.3 Velocity structure

Several structural seismology studies have been carried out since the late 1900s. Rakotondrainibe (1977) used the origin and arrival times of earthquakes to compute, using a least-squares method, the apparent velocities of P- and S-waves in Madagascar (Table 1. 2, model 1). Rambolamanana et al. (1997) studied the crustal structure in the central area of Madagascar applying the simultaneous inversion of earthquake source parameters (Table 1. 2, model 2). Rindraharisaona et al. (2013) studied the lithospheric structure and seismicity of Madagascar. They estimated the characteristics of the structure underneath the central area of Madagascar using jointly inversion of Rayleigh wave group velocities and receiver functions (Table 1. 2 - model 3) and concluded that the lithosphere beneath Madagascar is thinner than that beneath East Africa. They used their new velocity model to locate earthquakes and determine focal mechanisms.

We determined an 'average' 1D velocity model for Madagascar using results from Andriampenomanana et al. (2017) (Table 1. 2, model 4). The average 1D velocity model was derived from the V_S-depth functions at each of the MACOMO stations reported by Andriampenomanana et al. (2017) (Figure 1. 6a) which were weighted according to the emplacement of the earthquake stations and the mapped geology (shown in Figure 1. 3) to produce an 'average' V_S model for the whole island (See Appendix A). From the V_P/V_S ratios of 1.81 for the mantle and 1.75 for the crust, the corresponding V_P model (Figure 1. 6) was determined. The validity of using a ratio of 1.75 was confirmed by a Wadati plot, while the validity of applying 1.81 for the mantle is confirmed by a Pn tomographic study (Andriampenomanana, 2017; Andriampenomanana et al., 2020).

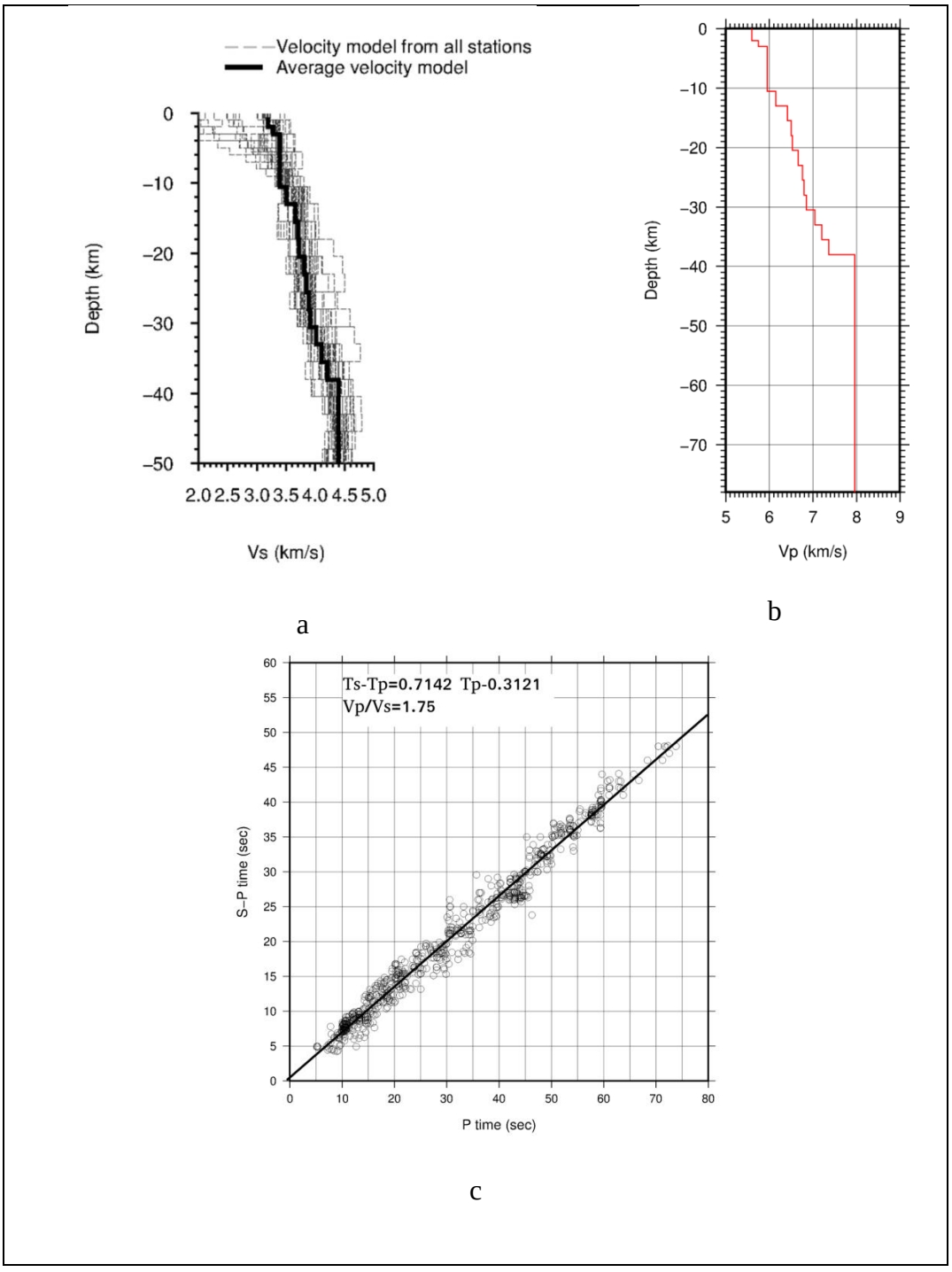

Figure 1. 6: (a) S-wave velocity model from all stations (Andriampenomanana et al. 2017), (b) Calculated vertical P-wave velocity structure for Madagascar using results from the (c) Wadati plot.

Table 1. 2: Crustal velocity models for Madagascar

Depth (km)	V_P (km/s)	V_S (km/s)
MODEL 1: Rakotondrainibe (1977)		
0	5.9	3.4
10	5.9	3.4
12.5	6.7	3.8
25	6.7	3.8
30	6.7	3.8
35	8.1	4.6
40	8.1	4.6
45	8.1	4.6
50	8.3	4.7
MODEL 2: Rambolamanana et al. (1997)		
0	5.9	3.4
10	6.5	3.7
20	6.7	3.8
30	6.3	3.6
35	6.3	3.6
42	8.1	4.6
50	8.1	4.6
MODEL 3: Rindraharisaona et al. (2013).		
0	5.4	3.1
5	5.6	3.2
10	5.9	3.4
20	6.5	3.7
25	6.7	3.8
35	6.7	3.8
42	7.9	4.5
50	7.7	4.4
MODEL 4: Derived from Andriampenomanana et al. (2017)		
0	5.6	3.2
10	5.9	3.4
13	6.4	3.6
16	6.5	3.7
30	7.0	4.0
33	7.2	4.1
40	7.9	4.4
55	7.9	4.4

1.6.4 Focal mechanisms

Focal mechanisms could only be determined once sufficient permanent stations had been installed. The earliest earthquake for which a mechanism has been determined occurred in 1965 and was found to be extensional (Grimison and Chen, 1988). The predominant normal faulting mechanism was confirmed by five mechanisms determined by the global CMT study and one by Craig (2011). A large number of extensional mechanisms were identified in the central area of the island, which is in accordance with the earlier findings of Bertil and Regnoult (1998). The most recent study by Rindraharisaona et al. (2013) concetrated on focal mechanisms determination for Madagascar, she used earthquake data recorded by the permanent stations. A large number of extensional mechanisms were identified in the central area of the island, which is in accord with the earlier findings of Bertil and Regnoult (1998).

Table 1. 3: Focal mechanism solutions for Malagasy earthquakes. Source: (1) Shudofsky (1985), (2) Grimison and Chen (1988), (3) CMT-Harvard (http://www.globalcmt.org/CMTsearch.html) and (4) Craig et al. (2011)

Source	Date dd/mm/yyy	Lat	Lon	Depth km	M_w	Strike	Dip	Rake
2	18/05/1965	-17.60	49.91	15	5.4	350	50	-95
2	04/04/1975	-21.24	45.13	13	5.6	95	75	44
1	04/04/1975	-21.24	45.13	11	5.4	245	85	140
3	31/01/1983	-23.00	44.39	15	5.1	326	45	-90
3	27/12/1983	-17.88	44.96	33	5.1	349	56	-84
3	04/101985	-18.08	48.62	10	5.5	357	61	-75
3	21/04/1991	-18.51	46.42	15	5.5	327	44	-128
3	14/11/1992	-23.01	45.54	15	5.0	350	45	-90
4	14/11/1992	-23.11	45.87	26	5.0	350	45	-90

1.6.5 Hazard studies

Seismic hazard studies began with the determination of the frequency-magnitude relationship. Earthquake data between the years 1979 to 1994 were used to establish an empirical relationship between magnitude (*M*) and the cumulative number of events greater than *M* for Madagascar *(N)* (Bertil and Regnoult, 1998).

$$logN = 9.23 - (1.65 \pm 0.10)M \tag{1.3}$$

The *b*-value of 1.65 value is high; values close to 1 are generally produced by natural tectonic seismicity (as opposed to induced seismicity, where values may range from 0.5 to 1.5). This may be due to the small number of earthquakes in the catalogue and also the fact that only short period permanent stations were used to calculate the magnitudes. This value could imply uncertainties of the interpretation results.

Razafindrakoto et al. (2009), using a neodeterministic approach which followed the calculation of realistic synthetic seismograms to estimate regional ground motion, calculated peak acceleration, velocity and displacement values of 0.03 g, 1.6 cm/s and 0.5 cm, respectively, for a site in Madagascar. They concluded that these values were below the damage threshold and consequently that the risk posed by earthquakes was low.

Chapter 2: Theory

In this chapter I describe the theory that underlies the techniques that I applied to achieve the main objectives stated in Chapter 1.

2.1 Seismic waves

Seismology is the study of earthquakes (and other sources of ground vibration), the propagation of the elastic waves that they generate and the shaking that they produce. Earthquakes may be caused by natural phenomena such as fault rupture and volcanic activity, as well as by human activities such as mining and the impoundment of large reservoirs. Seismograms may also be analysed to deduce the structure of the Earth's interior. Seismic waves produced by earthquakes are grouped into two principal categories: surface waves that are guided by the Earth's surface and body waves that travel through Earth's interior (Figure 2. 1).There are two types of body waves, *viz.* compressional waves (P-wave or primary wave), which consist of alternating expansion and compression pulses in the direction of the wave displacement; and shear waves (S-wave or secondary wave), whose displacement is perpendicular to the direction of movement of the wave (Figure 2. 1).

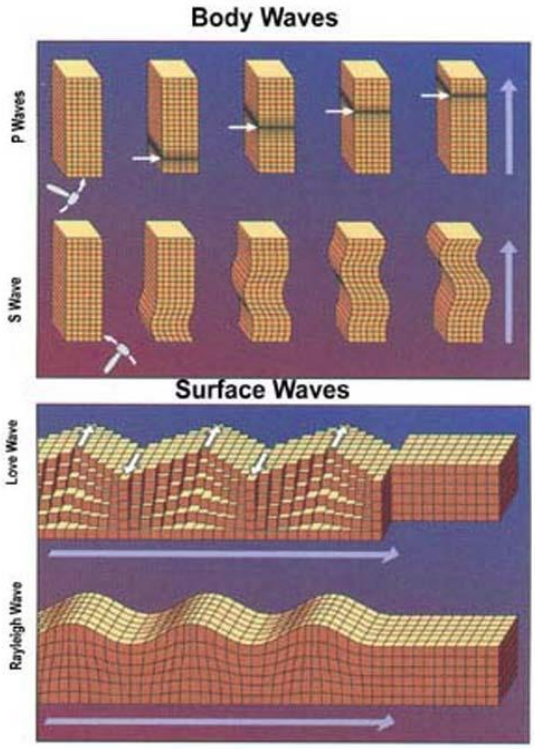

Figure 2. 1: Main types of waves produced by an earthquake. (https://courses.lumenlearning.com/geo/chapter/reading-studying-the-earths-interior)

Figure 2. 2 shows a seismogram recorded by the local permanent seismic station SBV of a magnitude 3.5 earthquake on 16 March 2012 to illustrate typical P and S waves as they were recorded.

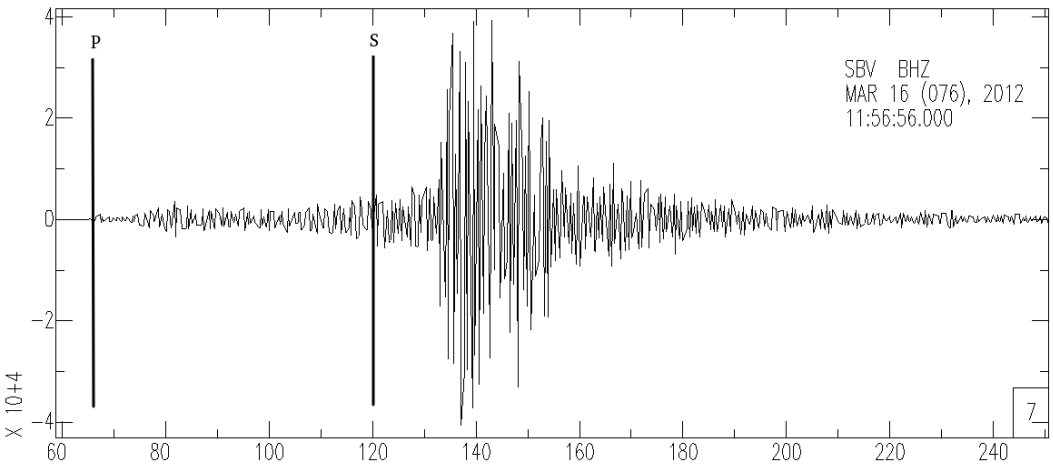

Figure 2. 2: Vertical component seismogram recorded at the SBV seismic station produced by a M3.5 earthquake on March 16th, 2012 at 11:56:55 UTC. P and S mark the onsets of the primary or P-wave and secondary or S-wave, respectively.

2.2 Source parameters and mechanisms

2.2.1 Location and origin time

The focus of an earthquake (also called the hypocenter) is the point within the Earth where the rupture initiates, while the epicenter is the point on the Earth's surface directly above it (Figure 2. 3). An earthquake is generally defined as 'shallow' if the focus is at a depth of <100 km from the ground surface, 'intermediate' if the focus is at depths between 100 km and 300 km, and 'deep' if the focus is >300 km. The greatest depth at which earthquakes occur is about 700 km.

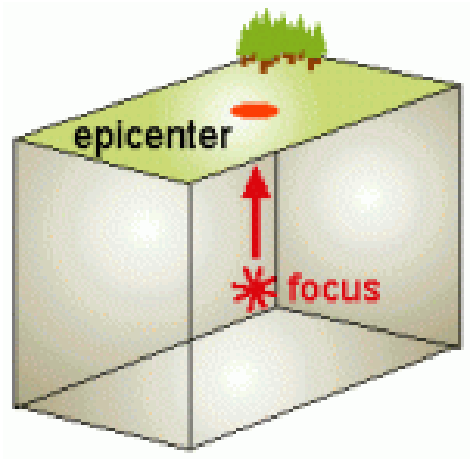

Figure 2. 3: Earthquake focus (hypocenter) and epicenter. The ground surface and subsurface are colored green and grey, respectively. (https://earthquakesandplates.files.wordpress.com/2008/05/epicenter.gif)

The first task in seismogram analysis is the identification and picking of the first phase arrivals, then measurement of the amplitude of ground motion, followed by the determination of the time, epicenter and depth of the point where the earthquake rupture initiated. In principle, the earthquake location can be estimated using three or more seismic stations using the 'triangulation method' (Figure 2. 4). Firstly, the distance from each station to the focus is calculated using the difference between the arrival times of the P- and S-waves and prior knowledge of the average P- and S-wave velocities. Secondly, circles with radii equal to the focal distance are drawn around each station. Lastly, the location is determined

from the intersection of these circles. The solutions are more accurate if the Earth's velocity structure is well-known and the refraction of waves is taken into account, and the stations are well-distributed.

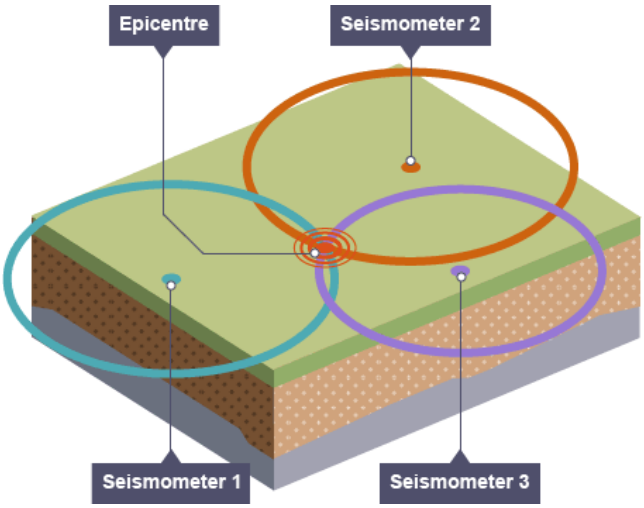

Figure 2. 4: Triangulation method to locate earthquakes. http://www.bbc.co.uk/education/guides/zq7ycdm/revision/2)

Several computer programs using different mathematical algorithms have been elaborated to determine earthquake locations. In this study SEISAN (Havskov and Ottemöller, 2010), HYPOELLIPSE (Lahr 1989, 1999), and HYPODD (Waldhauser, 2000, 2001) were used.

Many location methods use the iterative least square technique (Chiu, 2006), including the three codes that I used. An initial guess of the coordinates of the focus is made, usually the coordinates of the station that first recorded it and hence closest to it. The theoretical arrival times produced by an earthquake at this hypothetical location are then compared with the actual arrival times at each station. The difference is known as the travel time residual. The discrepancies between the theoretical and actual times are then used to adjust the location of the hypothetical focus. This process is repeated until there is no further reduction in the sum of the squares of the residuals.

Here we review the method developed by Geiger (1910, 1912). The coordinate of the ith station is (x_i, y_i, 0), representing that the station is on the surface, and the corresponding arrival time is t_j. Let $f_i(\boldsymbol{x})$ be the arrival time function at the ith station, and $\boldsymbol{x}$ represents the hypocentral parameters and T the transpose of the column vector:

$$\boldsymbol{x} = (x, y, z, t)^T$$

The value of $f_j(\boldsymbol{x_o})$ at a nearby location, $\boldsymbol{x_o}$, can be expressed by a first-degree Taylor polynomial:

$$f_j(\boldsymbol{x}) = f_j(\boldsymbol{x}_0 + \delta\boldsymbol{x}) = f_j(\boldsymbol{x}_0) + \frac{\partial f_j}{\partial x}\delta x + \frac{\partial f_j}{\partial y}\delta y + \frac{\partial f_j}{\partial z}\delta z + \frac{\partial f_j}{\partial t}\delta t \qquad (2.1)$$

with

$$x = x_0 + \delta x \qquad (2.2)$$

and

$$x_0 = (x_0, y_0, z_0, t_0)^T \qquad (2.3)$$

and

$$\delta x = (\delta x, \delta y, \delta z, \delta t)^T \qquad (2.4)$$

Equation (2.1) can be expressed in vector notation:

$$f_j(x_0 + \delta x) = f_j(x_0) + g_j^T \delta x \qquad (2.5)$$

where g_j^T is the transpose of the gradient vector g_j and defined as follows:

$$g_j^T = \nabla f_J(\boldsymbol{x}) = \left(\frac{\partial f_j}{\partial x}, \frac{\partial f_j}{\partial y}, \frac{\partial f_j}{\partial z}, \frac{\partial f_j}{\partial t}\right) \qquad (2.6)$$

$f_j(\boldsymbol{x}_0 + \delta\boldsymbol{x})$ represents the arrival time recorded at the jth station (the observed arrival time) and

$$\frac{\partial \mathrm{fj}}{\partial x}\delta x + \frac{\partial \mathrm{fj}}{\partial y}\delta y + \frac{\partial \mathrm{fj}}{\partial z}\delta z + \frac{\partial \mathrm{fj}}{\partial t}\delta t \tag{2.7}$$

Equation (2.7) is the correction value, which the partial derivatives function of the hypocentral parameters. For calculating a system of the Equation (2.5), it is important to find $\boldsymbol{x_0}$ such that the estimated arrival times will best fit the observed arrival times hence $\boldsymbol{x_0}$ can be defined as the hypocenter of the event. Equation (2.7) can be writen into the form:

$$\frac{\partial f_j}{\partial X}\delta x + \frac{\partial f_j}{\partial Y}\delta y + \frac{\partial f_j}{\partial Z}\delta z + \frac{\partial f_j}{\partial T}\delta t = r_j \tag{2.8}$$

where

$$r_j = t_{obs} - t_{calc} \tag{2.9}$$

$t_{obs} = f_j(x)$, $t_{calc} = f_j(x_0)$, and r_j is the residual

In matrix notation, Equation (2.8) can be written:

$$A\delta\boldsymbol{x} = \boldsymbol{r} \tag{2.10}$$

where;

$$\mathrm{A} = \begin{bmatrix} \frac{\partial f_1}{\partial X} & \frac{\partial f_1}{\partial Y} & \frac{\partial f_1}{\partial Z} & \frac{\partial f_1}{\partial Z} \\ \vdots & & & \\ \frac{\partial f_m}{\partial X} & \frac{\partial f_m}{\partial Y} & \frac{\partial f_m}{\partial Z} & \frac{\partial f_m}{\partial Z} \end{bmatrix}; \tag{2.11}$$

$$\delta\boldsymbol{x} = \begin{bmatrix} \delta x \\ \delta y \\ \delta z \\ \delta t \end{bmatrix}$$

and

$$\mathbf{r} = \begin{bmatrix} r_1 \\ \vdots \\ r_m \end{bmatrix}$$

The least squares solution to the system by Equation (2.10) satisfies (Strang, 1976)

$$A^T A\delta \boldsymbol{x} = A^T \boldsymbol{r} \tag{2.12}$$

or

$$\delta \boldsymbol{x} = (A^T A)^{-1} A^T \mathbf{r} \tag{2.13}$$

The total effect of the *m* mismatches between the observed and calculated arrival times is the event residual or simply residual; it is defined by the least-squares solution (Ge, 1995).

$$Res = \sqrt{\frac{r^T r}{m - q}} \tag{2.14}$$

where *m* is the number of equations and *q* is the degree of freedom.

The number of hypocentral parameters defined by the Equation (2.13) has degree of freedom 4. The correction vector, $\delta \boldsymbol{x}$, is determined and it can be introduced to the previous trial solution to form a new one. The iteration is carried out until the given error criterion was performed and the last trial solution is then considered as the solution for the hypocenter.

2.2.2 Correction for instrument response

Mathematically, a seismogram is the combined product of the signal produced by the earthquake with impulsive response from the equipment that recorded the signals (Havskov and Ottemōller, 2010). The signal recorded from a seismic station is represented by the equation:

$$x(n) = h(n) * [s(n) + z_1(n) + z_2(n)] \tag{2.15}$$

where *x(n)* represents the output of the seismograph, *h(n)* is the impulse response of the seismograph, *s(n)* is the actual ground motion produced by the earthquake, $z_1(n)$ is the natural noise, and $z_2(n)$ is the noise obtained from the acquisition system. After combining the different noises

$$z(n) = [h(n) * z_1(n)] + [h(n) * z_2(n)]$$

Equation (2.15) can be written as:

$$x(n) = h(n) * s(n) + z(n) \tag{2.16}$$

In the frequency domain, multiplication is the equal to the convolution operation. Thus Equation (2.16) can be written as:

$$X(f) = H(f).S(f) + Z(f) \tag{2.17}$$

where *X(f), H(f), S(f)* and *Z(f)* are the Fourier Transforms of the seismogram, impulse response, actual ground motion and noise, respectively.

It is therefore necessary to apply a deconvolution method to remove the effect of the instrument from the seismogram. Deconvolution can be carried out in either the time or the frequency domains. In the frequency domain

$$S(f) = \frac{X(f)}{H(f)} - \frac{Z(f)}{H(f)} \tag{2.18}$$

2.2.3 Fault geometry

When an earthquake occurs, the amplitude and polarity of the radiated seismic waves are a product of the fault geometry and the slip direction. The fault geometry is characterized by the strike angle (ϕ_f), dip angle (δ), and slip angle (λ). The strike direction is the intersection of the fault plane with the Earth's surface and varies from 0° to 360°, measured clockwise from North; the dip angle is the angle between the horizontal plane and fault plane and varies from 0° to 90°; and the slip angle varying from +180° to -180° from the horizontal on the fault plane. **d** is the slip direction, **n** is the normal to the fault plane, and x_1, x_2 and x_3 are the Cartesian coordinate system axes (Figure 2. 5; Figure 2. 6)**.**

The strike is characterized by the equation:

$$\tan\left[180° - \left(\phi_f + 90°\right)\right] = -\frac{x_2}{x_1} \tag{2.19}$$

where x_1, x_2 are defined in Figure 2. 14 and

$$\phi_f = \arctan\left(-\frac{x_1}{x_2}\right) \tag{2.20}$$

Dip angle is defined by:

$$\sin(90° - \delta) = \sin(\delta - 90°) = cos\delta = -\frac{x_3}{|n|} \tag{2.21}$$

with δ= arccos(-x_3)

Rake is defined by:

$$\sin(180° - \lambda) = -\sin(\lambda - 180°) = \frac{-\gamma_3/sin\delta}{|d|} \tag{2.22}$$

where $\boldsymbol{\gamma_3}$ **and** $\boldsymbol{\delta}$ are shown in Figure 2. 6, and

$$\lambda = \arcsin(-\frac{\gamma_3}{sin\delta}) \tag{2.23}$$

and

$$\begin{pmatrix} -\sin\delta \sin\phi_f \\ sin\delta cos\phi_f \\ -cos\delta \end{pmatrix} = \boldsymbol{n} \tag{2.24}$$

$$\begin{pmatrix} cos\,\lambda cos\phi_f + \cos\delta sin\lambda sin\phi_f \\ \cos\lambda\, sin\phi_f - \cos\delta \sin cos\phi_f \\ -\sin\delta\, sin \end{pmatrix} = \boldsymbol{\gamma} \tag{2.25}$$

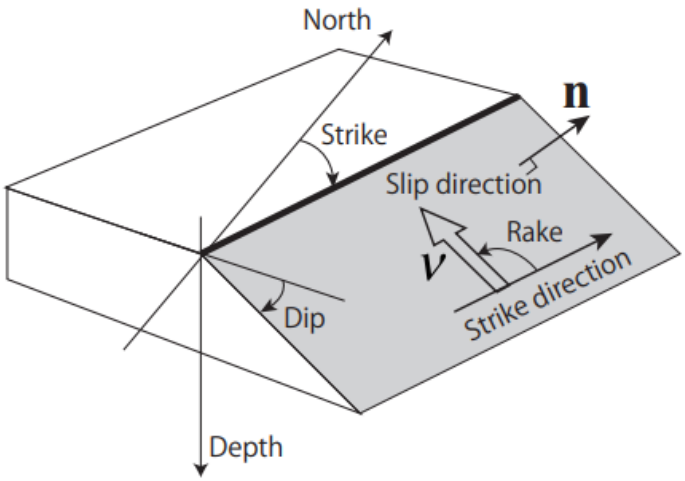

Figure 2. 5: Geometrical description of a fault plane $\boldsymbol{\gamma}$ is the rake direction and **n** is the normal to the fault plane (http://www.geol.tsukuba.ac.jp/~yagi-y/text/Source_meca_v0.7.pdf).

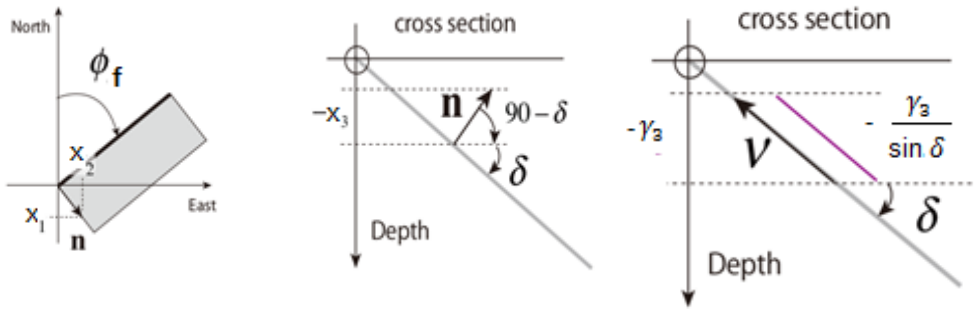

a) Strike b)Dip c)Rake

Figure 2. 6: Illustration of the method for calculating strike, dip, and rake angles (http://www.geol.tsukuba.ac.jp/~yagi-y/text/Source_meca_v0.7.pdf)

2.2.4 Focal mechanism solutions

Focal mechanism solutions use the ground motions produced by an earthquake and observed at many seismic stations to estimate the geometry of the fault plane (*i.e.* strike and dip) and the direction of the slip vector. Methods used to determine focal mechanism solutions include P-wave first motion polarity (Stein and Wysession, 2003), P/S amplitude ratios analysis (Kisslinger, 1980), polarization and amplitude of S-waves (Khattri, 1973), and moment tensor inversion.

In this study we determined focal mechanism solutions using the polarity of the first-motions of the P- and S-waves recorded at each station. The polarity (compressive or dilatational in the case of P-waves; or direction of the first motion of the S_V or S_H pulse, in the case of S-waves) is plotted on a stereogram at the point where the ray emanating from the focus pierces the focal sphere (a small imaginary sphere centered on the focus). The observed polarities are compared with those produced by a systematic search of all possible fault plane and slip vector orientations, and a set of plausible solutions is determined.

The position on the focal sphere where the polarity of ground motion is plotted depends on the azimuth (Φ) and take-off angle. The azimuth is simply the angle

describing the direction of the line joining the epicenter and station, measured clockwise from the North direction Figure 2. 7.

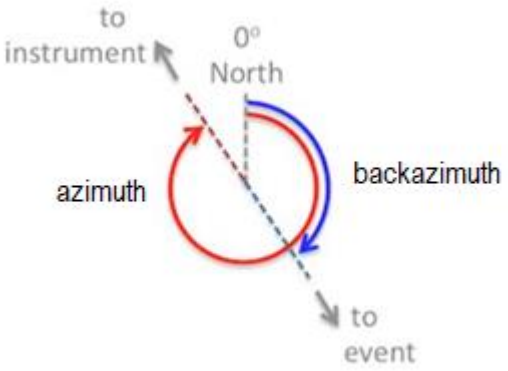

Figure 2. 7: Measurement of the azimuth angle
https://service.iris.edu/irisws/rotation/docs/1/help/

The take-off angle is the angle at which the seismic ray leaves the earthquake source during the signal's transference from the earthquake focus to the station through the Earth. It is more complicated to determine. Consider, for instance, two stations lying on the same azimuth but at different epicentral distances. The ray path to each station will differ, depending on the focal depth, the Earth's velocity structure, and the distance to the station. A standard Earth model is used to calculate the take-off angle (Figure 2. 8). It can also be determined from the gradient of the travel-time curve. In general, the greater the epicentral distance, the smaller the take-off angle.

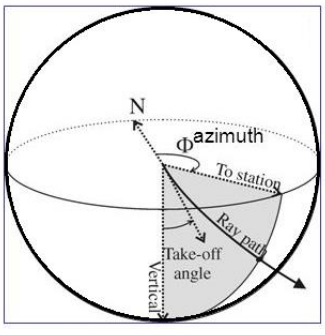

Figure 2. 8: Definition of the take-off angle
https://nctr.pmel.noaa.gov/education/ITTI/seismic/Focal_mech_USGS.pdf

In the P-wave polarity method, focal mechanisms are determined following three steps: (i) determine the location of the earthquake (latitude, longitude, depth),
(ii) Determine the azimuth and take-off angle values, and
(iii) Determine and plot first-arrival P-wave polarities (an upward inflection on the vertical component indicates a compression, while a downward inflection indicates a dilatation; (see Figure 2. 9), plot on the stereonet, and find the nodal planes that best separate the observations into quadrants.

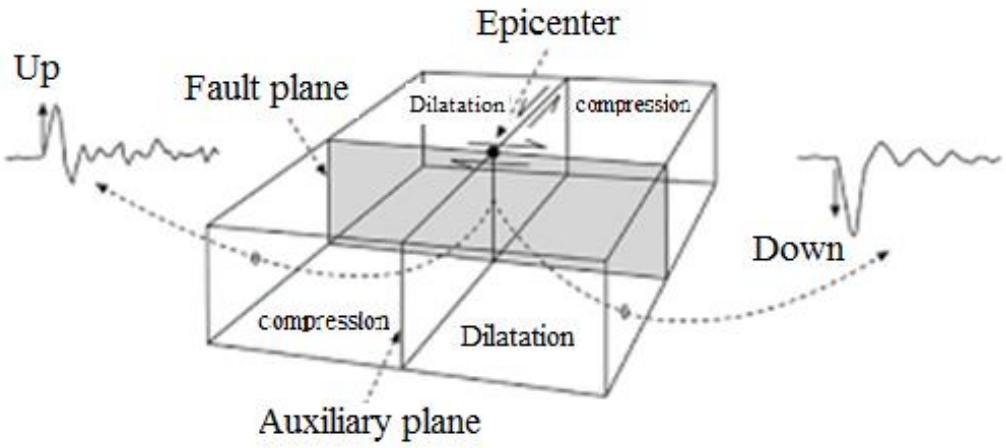

Figure 2. 9: Illustration of P-wave upward and downward first motions (Havskov and Ottemöller, 2010)

The picking of S-wave polarities is more complicated:

1. The two horizontal components (E-W and N-S) are rotated into radial (R) and transversal (T) components (Figure 2. 10 a).
2. A second rotation into the 3D LQT ray system is then performed Figure 2. 10 b). The R and T components are combined with the vertical (Z) component to determine the motion in the longitudinal (L) direction (along the ray path) and the Q-direction (perpendicular to the ray path in the vertical plane).
3. The polarities of the ground motion in the Q-direction (S_V) and the T-direction (S_H) are then determined.

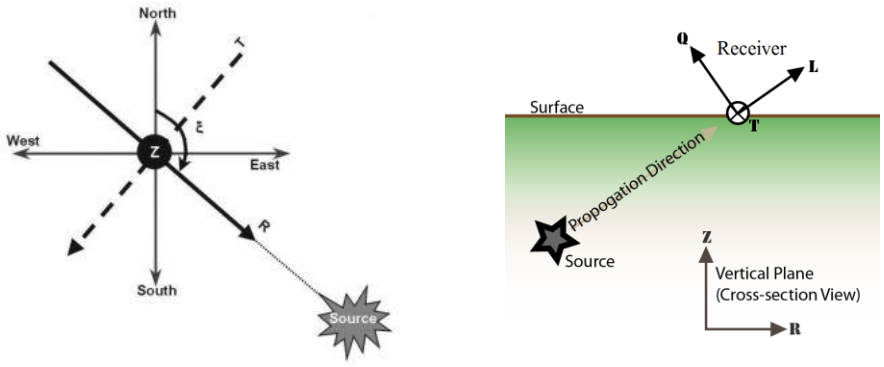

(a) (b)

Figure 2. 10: Transformation of ZNE to ZRT and LQT (https://service.iris.edu/irisws/rotation/docs/1/help/)

Transformation from ZNE to ZRT is as follows:

$$\begin{bmatrix} R \\ T \\ Z \end{bmatrix} = \begin{bmatrix} \cos\theta & \sin\theta & 0 \\ -\sin\theta & \cos\theta & 0 \\ 0 & 0 & 1 \end{bmatrix} \begin{bmatrix} E \\ N \\ Z \end{bmatrix} \text{ with } \theta = \frac{3\pi}{2} - \xi \qquad (2.26)$$

ξ is the back azimuth that represents the vector pointing from the seismic station to the epicenter, measured clockwise from the north (Figure 2. 10).

The transformation from ZNE to LQT is given by:

$$\begin{bmatrix} L \\ Q \\ T \end{bmatrix} = \begin{bmatrix} \cos\theta & \sin\delta\sin\xi & -\sin\delta\cos\xi \\ \sin\theta & \cos\delta\ \sin\xi & \cos\delta\cos\xi \\ 0 & -\cos\xi & \sin\xi \end{bmatrix} \begin{bmatrix} Z \\ E \\ N \end{bmatrix} \qquad (2.27)$$

with δ the angle of the incident wave from the vertical,

$\delta = 0^o$ for vertically incident wave

$\delta = 90^o$ for horizontally incident wave

Example of picks from P-wave and S-wave are presented in Figure 2. 11.

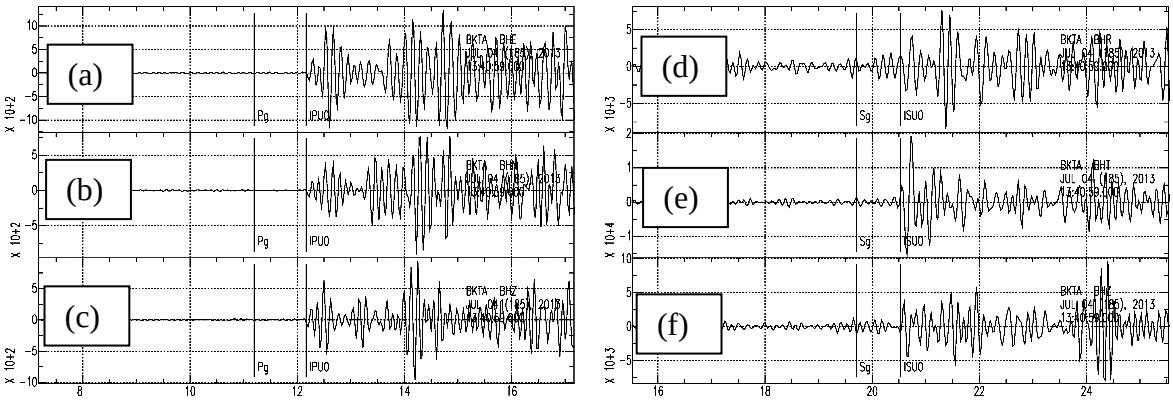

Figure 2. 11: Examples of polarity picking on a local M3.1 event recorded at station BKTA on 4 July 2013 at 13:40:59.08. P-wave picks on the (a) E-W, (b) (N-S) and (c) Z component; S-wave picks after rotating from ZNE to ZRT on the (d) R, (e) T and (f) Z component.

The advantage of picking both P- and S-wave polarities is to constrain the characteristics of the fault solutions better. In this work, we tried to pick both P- and S-waves polarities, although, due to the waveform characteristics some S-wave polarities were difficult to identify.

In general, faulting can be grouped into three types: strike-slip (left lateral or right lateral), normal and reverse (See Figure 2. 12). The P-wave first motions are divided by two nodal planes into four quadrants: two opposite quadrants that experience compressional first motions, and two opposite quadrants that experience dilatational first motion. One nodal plane is the fault plane, while the other is termed the auxiliary plane (Figure 2. 13). Other observations are needed to identify which nodal plane is the fault plane *e.g.*, surface rupture, aftershock distribution. By convention, the compressive quadrants are colored black (Figure 2. 14). The exact appearance of the stereogram will depend on the orientation of the planes and the slip vector. These diagrams are often referred to as ‘beach balls’.

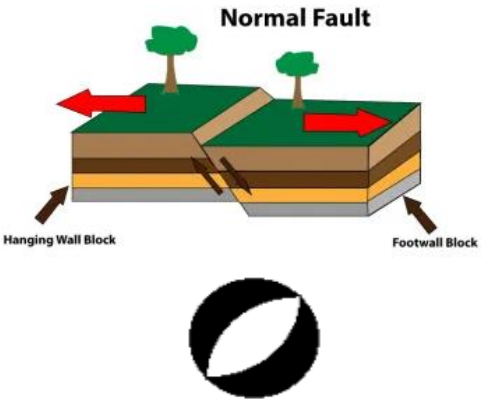

a) Normal faulting

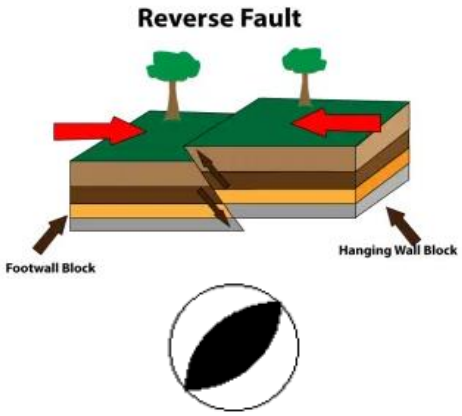

b) Reverse faulting

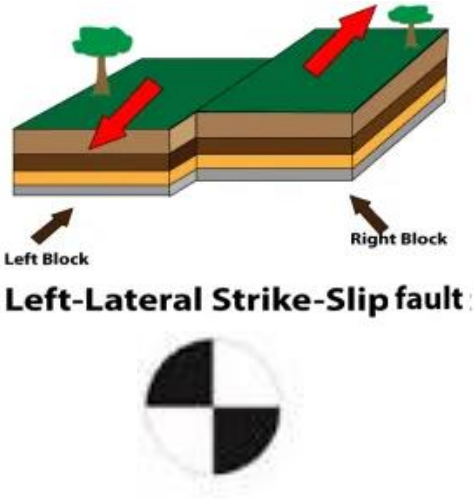

b) Left-lateral strike-slip

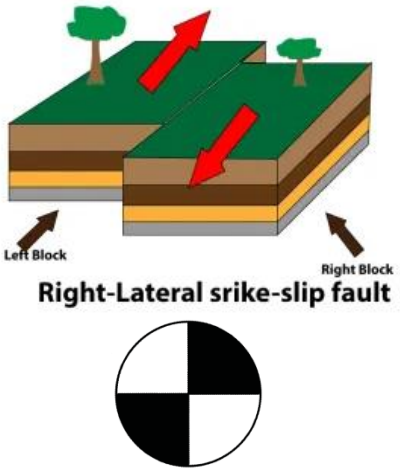

c) Right-lateral strike slip

Figure 2. 12: Fault mechanisms and 'beach ball' diagrams. Black and white represent the compressional and dilatational quadrants, respectively. https://inventionsky.com/normal-reverse-and-strike-slip-faults/

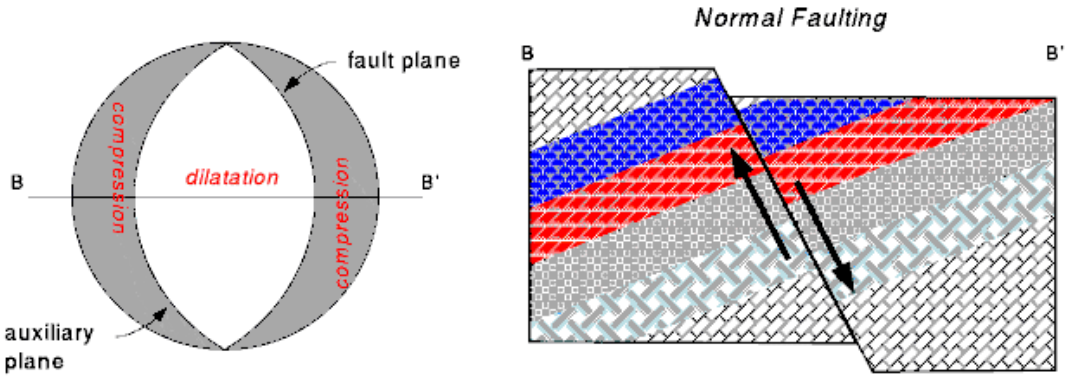

Figure 2. 13: Focal mechanism for a normal faulting earthquake with the actual fault plane and auxiliary plane in a section BB'. The two nodal planes are the auxiliary plane and the fault plane (http://www-udc.ig.utexas.edu/external/TXEQ/faq_basics.html)

From the focal mechanism, the orientations of the P-and T-axes that relate to the white and dark segments of the beach ball are determined (Figure 2. 14). P- and T-axes are geometric axes, not directly stress axes. They represent the average orientation of the quadrants in which the extensional and compressional stress axes lie. The P-axis, orthogonal to the B- and T-axes, is the pressure or compressional axis that bisects the dihedral angle between the two nodal planes. The T-axis is orthogonal to both B- and P-axes. The B-axis is the neutral axis, which is the intersection of the two nodal planes and is orthogonal to the P- and T-axes.

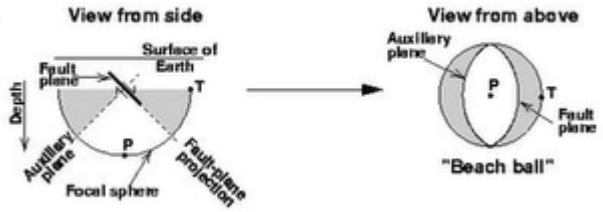

Figure 2. 14: Normal fault plane solution showing the P- and T-axes https://www.usgs.gov/natural-hazards/earthquake-hazards/science/focal-mechanisms?qt-science_center_objects=0#qt-science_center_objects.

Earthquake focal mechanisms can be displayed in a triangular diagram named the 'ternary diagram' (Frohlich, 1992; Frohlich and Apperson, 1992). The triangle

classifies the mechanisms as normal, thrust or strike-slip in terms of the dip angles or plunge of the P-, T-, and B-axes (Figure 2. 15).

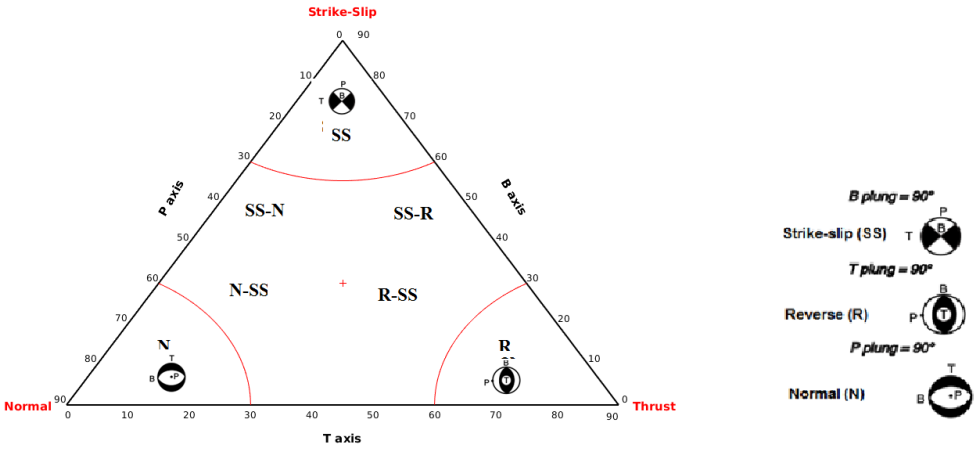

Figure 2. 15: Ternary diagram to display focal mechanisms (Frohlich, 1992)

The diagram displays the focal mechanism in terms of the plunge angles for the P-, T- and B-axes (Figure 2. 16). Angles are notated as dip-P (δ_P), dip-T (δ_T), and dip-B (δ_B.). These values satisfy the equation

$$sin^2\,\delta_T + sin^2\,\delta_P + sin^2\,\delta_B = 1 \tag{2.28}$$

By considering the vertical of the three axes,

$$\begin{aligned} x &= \sin\delta_T \\ y &= \sin\delta_P \\ z &= \sin\delta_B \end{aligned} \tag{2.29}$$

and the Equation 2.28 becomes;

$$x^2 + y^2 + z^2 = 1 \tag{2.30}$$

The horizontal h_G and the vertical distances v_G from the center of the triangle (G) are defined by:

$$\begin{aligned} h_G &= cos\delta_B sin\,\psi/[(sin\theta_0 \sin\delta_B + cos\theta_0 cos\delta_B cos\,\psi)] \\ v_G &= (cos\theta_0 sin\delta_B \\ &\quad - sin\theta_0 cos\delta_B \cos\psi)/[(sin\theta_0 sin\delta_B + cos\theta_0 cos\delta_B cos\psi)] \end{aligned} \tag{2.31}$$

where

ψ is defined by $\Psi = tan^{-1}\left(\frac{sin\delta_T}{sin\delta_P}\right) - 45^o$

$\theta_0 = 35.26°$ is the dip angle of the P- T- and B-axes for the source mechanism that plots in the exact centre of the ternary diagram

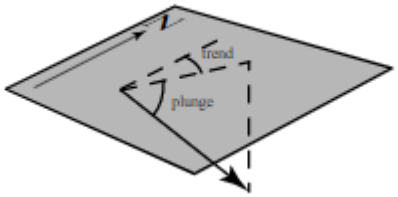

Figure 2. 16: Difference between trend angle and plunge angle, N represents North.

In this study, the ternary diagram plot was implemented in MATLAB using the Frohlich (1992) algorithm.

2.3 Stress field

2.3.1 Basic concepts

Stress describes the force acting on body and is expressed as the force per unit area. The stress vector may be decomposed into the component acting normal to a plane, which may be either compressive or tensile; and the component acting parallel to a plane, known as the shear stress.

The stress state within a body is often described in terms of a set of orthogonal 'principal stresses' that act on orthogonal planes such that they do not produce any shear stress on them. They are designated σ_1, σ_2 and σ_3, indicating the maximum, intermediate and minimum stress, respectively. The stress field may also be described in terms of the vertical, minimum, and maximum horizontal stresses σ_V, σ_{Hmin}, and σ_{Hmax} respectively.

An earthquake may occur if the shear stress acting on a geological weakness exceeds its shear strength (Figure 2. 17). High horizontal stresses (*i.e.* σ_1 sub-

horizontal; $\sigma_{Hmax}>\sigma_{Hmin}>\sigma_V$) will generally cause folding, reverse or thrust faulting, and the crust may thicken. If the horizontal stresses are relatively low (*i.e.* σ_1 sub-vertical; $\sigma_V>\sigma_{Hmax}>\sigma_{Hmin}$), the dominant mode of faulting will be normal and the crust may thin. The third case (*i.e.* σ_1 sub-horizontal; $\sigma_{Hmax}>\sigma_V>\sigma_{Hmin}$) will likely give rise to strike-slip faulting. There are, of course, many intermediate cases, which give rise to oblique-slip.

Knowledge of the stress field is useful when analyzing the distribution of seismicity, the kinematics of continental deformation and assessing seismic hazard. The stress field may be analysed using knowledge of fault plane geometries, Mohr circle diagram, and tensor calculus.

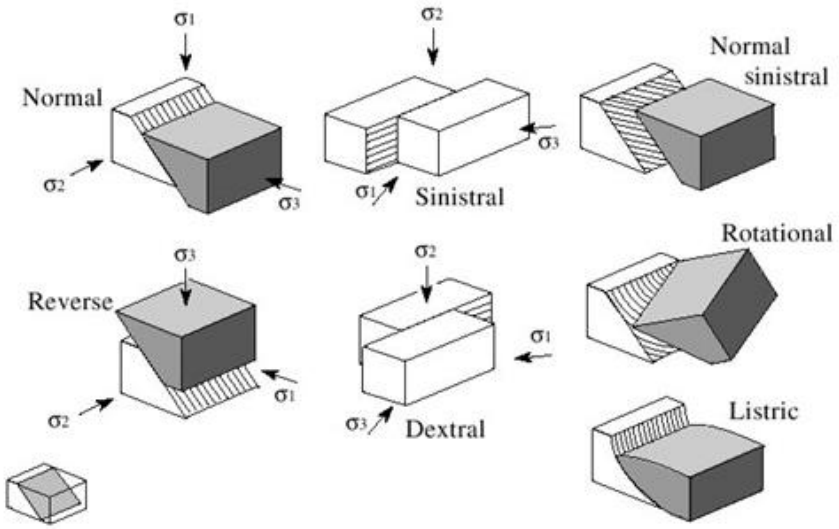

Figure 2. 17: Stress and fault mechanisms.
http://www.geosci.usyd.edu.au/users/prey/Teaching/Geol-3101/Strain/stress.html

2.3.2 Mohr's circle of stress

The Mohr circle diagram gives the relationship between the orientation of any plane and the values of the normal and shear stress acting on it (Holtz et al., 1981). This diagram can show the stress in two and three dimensions. In this study, Mohr's circle diagram is presented into three dimensions. According to Cauchy's

law and with respect to the principal direction 1, 2, and 3; the normal stress is defined by:

$$\sigma_{N\,=}\; t^{(n)}.n = (\sigma_n).n \tag{2.32}$$

where $t^{(n)}$ is the traction vector, σ_n represents the normal stress on the plane with normal *n*.

In term of matrix calculus, this can be written:

$$\sigma_N = \left\{\begin{bmatrix}\sigma_1 & 0 & 0\\ 0 & \sigma_2 & 0\\ 0 & 0 & \sigma_3\end{bmatrix}\begin{bmatrix}n_1\\ n_2\\ n_3\end{bmatrix}\right\}\begin{bmatrix}n_1\\ n_2\\ n_3\end{bmatrix} = \sigma_1 n_1^2 + \sigma_2 n_2^2 + \sigma_3 n_3^2 \tag{2.33}$$

Since $n_1^2 + n_2^2 + n_3^2 = 1$ with $\sigma_1 \geq \sigma_2 \geq \sigma_3$

$$\sigma_1 = \sigma_1 (n_1^2 + n_2^2 + n_3^2) \geq \sigma_1 n_1^2 + \sigma_2 n_2^2 + \sigma_3 n_3^2 = \sigma_N \tag{2.34}$$

Similarly,

$$\sigma_N = \sigma_1 n_1^2 + \sigma_2 n_2^2 + \sigma_3 n_3^2 \geq \sigma_3 (n_1^2 + n_2^2 + n_3^2) \geq \sigma_3 \tag{2.35}$$

As a result, the maximum normal stress occurring in a point is the maximum principal stress and the minimum normal stress is the minimum principal stress.

The shear stress occurring on the plane is given by:

$$\sigma_s^2 = (\sigma_1^2 n_1^2 + \sigma_2^2 n_2^2 + \sigma_3^2 n_3^2) - (\sigma_1 n_1^2 + \sigma_2 n_2^2 + \sigma_3 n_3^2)^2 \tag{2.36}$$

As $n_1^2 + n_2^2 + n_3^2 = 1$, we can write

$$\sigma_s^2 + \sigma_N^2 = \sigma_1^2 n_1^2 + \sigma_2^2 n_2^2 + \sigma_3^2 n_3^2 \tag{2.37}$$

So we have the system of equations:

$$\begin{gathered}\sigma_s^2 = (\sigma_1^2 n_1^2 + \sigma_2^2 n_2^2 + \sigma_3^2 n_3^2) - (\sigma_1 n_1^2 + \sigma_2 n_2^2 + \sigma_3 n_3^2)^2\\ n_1^2 + n_2^2 + n_3^2 = 1\\ \sigma_s^2 + \sigma_N^2 = \sigma_1^2 n_1^2 + \sigma_2^2 n_2^2 + \sigma_3^2 n_3^2\end{gathered} \tag{2.38}$$

Solving these equations produces:

$$\begin{gathered}n_1^2 = \frac{(\sigma_N - \sigma_2)(\sigma_N - \sigma_3) + \sigma_s^2}{(\sigma_1 - \sigma_2)(\sigma_1 - \sigma_3)}\\ n_2^2 = \frac{(\sigma_N - \sigma_3)(\sigma_N - \sigma_1) + \sigma_s^2}{(\sigma_2 - \sigma_3)(\sigma_2 - \sigma_1)}\end{gathered} \tag{2.39}$$

$$n_3^2 = \frac{(\sigma_N - \sigma_1)(\sigma_N - \sigma_2) + \sigma_s^2}{(\sigma_3 - \sigma_1)(\sigma_3 - \sigma_2)}$$

By taking $\sigma_1 \geq \sigma_2 \geq \sigma_3$with the condition that the squares of the normal components must be positive, one has that

$$\begin{aligned} (\sigma_N - \sigma_2)(\sigma_N - \sigma_3) + \sigma_s^2 &\geq 0 \\ (\sigma_N - \sigma_3)(\sigma_N - \sigma_1) + \sigma_s^2 &\leq 0 \\ (\sigma_N - \sigma_1)(\sigma_N - \sigma_2) + \sigma_s^2 &\geq 0 \end{aligned} \tag{2.40}$$

and we can get

$$\begin{aligned} \sigma_s^2 + [\sigma_N - \frac{1}{2}(\sigma_2 + \sigma_3)]^2 &\geq [\frac{1}{2}(\sigma_2 - \sigma_3)]^2 \\ \sigma_s^2 + [\sigma_N - \frac{1}{2}(\sigma_1 + \sigma_3)]^2 &\geq [\frac{1}{2}(\sigma_1 - \sigma_3)]^2 \\ \sigma_s^2 + [\sigma_N - \frac{1}{2}(\sigma_1 + \sigma_2)]^2 &\geq [\frac{1}{2}(\sigma_1 - \sigma_2)]^2 \end{aligned} \tag{2.41}$$

Considering the coordinates (σ_N,σ_S), a plot of circles in (σ_N,σ_S) is defined (see Figure 2. 18). The stress on a plane is presented in each point (σ_N,σ_S) in the stress space. Acceptable pairs (σ_N,σ_S) are given by the Equation (2.61) and all of these points have to fall inside a circle having center $(\frac{1}{2}(\sigma_1 + \sigma_3), 0)$ and radius $\frac{1}{2}(\sigma_1 - \sigma_3)$, the large circle in Figure 2. 18. The two smaller circles are the points which lie outside the circles with center $(\frac{1}{2}(\sigma_1 + \sigma_2), 0)$ and radius$\frac{1}{2}(\sigma_1 - \sigma_2)$. In conclusion, acceptable points in the stress space fall in the shaded region of Figure 2. 18.

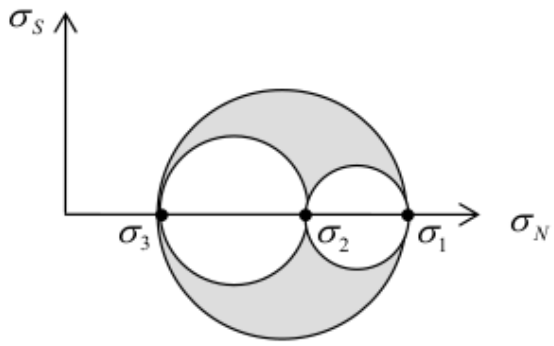

Figure 2. 18: Mohr diagram in 2-D with appropriate points in stress space https://courses.eas.ualberta.ca/eas421/lecturepages/stress.html

2.3.3 P- and T-axis

Using the method of first polarities of the P-arrivals for focal mechanism determination, four quadrants are created in which two are dilatational and two are compressional. The P- and T-axes lie in the center of the compressional and dilatational quadrants, respectively. The tension (T) and the pressure (P) axes are the axes of maximum extension (σ_3) and the maximum compression (σ_1), respectively. The intersection between the fault and the auxiliary planes is the B-axis. It is important to note that the P- and T-axes are geometric axes that describe the state of stress at the earthquake source and the average orientation of the quadrants in which the extensional and the compressional stress axes lie.

2.3.4 Stress inversion

The objective of stress inversion is to minimize the difference among the determined shear stress and the slip directions that has been determined from focal mechanism data set in order to estimate the orientation of the principal stress and the stress ratio value. It can be estimated from the faults' geometries or from fault plane solutions using different methods (Angelier, 1984; Gephart and Forsyth, 1984; Gephart; 1990, Rivera and Cisternas, 1990; Delvaux and Sperner, 2003).

Stress field inversion can be performed using several different methods.

1. Angelier (1984): This method uses earthquake focal mechanisms to distinguish successive fault events in a heterogeneous stress environment. A least squares method takes errors in the strike and dip of the plane into account.
2. Gephart and Forsyth (1984): This method determines the best fit for the principal stress axes using a grid search that compares the observed slip directions and those predicted by hypothetical stress fields in the source region.
3. Michael (1987): This linear inversion method finds the single uniform stress tensor assuming that the dimension of the tangential traction vector on the fault is equal to unity. This method was used for this study and is illustrated in greater detail in section 2.3.4.1. This method helped us to give smooth distribution of stress inversion from different region as it applied a method based on a bootstrap resampling and extended using simultaneous inversion calculation.
4. Arnold and Townend (2007): This method determines the tectonic stress from seismological data using a Bayesian approach.
5. Lund and Townend (2007) describe a method to transform the principal stresses into horizontal stress orientations.

2.3.4.1 Michael's method

Michael's method (Michael, 1984, 1987) seeks to determine the direction and magnitude of the stress driving earthquake activity in a region using a set of focal mechanism solutions. A grid search algorithm (Gephart and Forsyth, 1984) was used to search over all combinations of stress tensors in all sub-regions. The inversion minimizes the misfit between the predicted and observed slip directions. This method is quite fast and can be run repeatedly. The uncertainty in the solution is determined using the standard bootstrap method.

During the inversion, a minimization between the resolved shear stress vector and the slip vector on the fault plane was done as explained in the following equation:

$$Gm = d \tag{2.42}$$

$$m = \begin{pmatrix} \sigma_{11} \\ \sigma_{12} \\ \sigma_{13} \\ \sigma_{22} \\ \sigma_{23} \end{pmatrix} \tag{2.43}$$

and the vector d is defined as the *3*K* data vector for the *K* focal mechanisms

$$d = \begin{pmatrix} S_{11} \\ S_{12} \\ S_{13} \\ \dots \\ S_{g2} \\ S_{g3} \end{pmatrix} \tag{2.44}$$

where s_{ki} represents the ith component of the unit slip vector for k^{th} earthquake.

The matrix *G* is defined by:

$$G = \begin{pmatrix} n_{11} - n_{11}^3 + n_{11}n_{13}^2 & n_{12} - 2n_{21}n_{11}^2 & n_{13} - 2n_{13}n_{11}^2 & -n_{11}n_{12}^2 + n_{11}n_{13}^2 & -2n_{11}n_{12}n_{13} \\ -n_{12}n_{11}^2 + n_{12}n_{13}^2 & n_{11} - 2n_{11}n_{12}^2 & -2n_{11}n_{12}n_{13} & n_{12} - n_{12}^3 + n_{12}n_{13}^2 & n_{13} - 2n_{13}n_{12}^2 \\ -n_{13}n_{11}^2 - n_{13} + n_{13}^3 & -2n_{11}n_{12}n_{13} & n_{12} - 2n_{11}n_{13}^2 & -n_{13}n_{12}^2 + n_{13}n_{31}^3 & n_{12} - 2n_{12}n_{13}^2 \\ \dots & \dots & \dots & \dots & \dots \\ -n_{g2}n_{12}^2 - n_{g2} + n_{g2}^3 & -2n_{g1}n_{g2}n_{g2} & n_{g2} - 2n_{g1}n_{g2}^2 & n_{g2} - 2n_{g1}n_{g2}^2 & n_{g2} - 2n_{g2}n_{g2}^2 \\ -n_{g3}n_{g3}^2 - n_{g3} + n_{g3}^3 & -2n_{g1}n_{g2}n_{g3} & n_{g2} - 2n_{g1}n_{g3}^2 & n_{g2} - 2n_{g1}n_{g3}^2 & n_{g2} - 2n_{g2}n_{g3}^2 \end{pmatrix} \tag{2.45}$$

where n_{gi} is the ith component of the normal vector for k^{th} earthquake.

The solution of the least square inverse (Menke, 1989) is defined by:

$$G^T Gm = G^T d \tag{2.46}$$

and solved by Gaussian elimination (Heath et al., 1984). A bootstrap method was used to estimate the uncertainty by selecting the one of the two focal mechanism nodal planes. The solution to the damped least squares problem is given by the equation

$$\{G_{ALL}^T G_{ALL} + e^2 D^T D\} m_{ALL} = G_{ALL}^T d_{ALL} \tag{2.47}$$

where

$$G_{ALL} = \begin{pmatrix} G_{11} & & & \cdots & & \\ \vdots & G_{12} & & \ddots & 0 & \vdots \\ & & \cdots & \cdots & & \\ & & & G_{22} & & \\ & 0 & & & \cdots & \\ & & & \cdots & & G_{IJ} \end{pmatrix} \tag{2.48}$$

and

$$m_{ALL} = \begin{pmatrix} m_{11} \\ m_{12} \\ m_{13} \\ \cdots \\ m_{22} \\ m_{23} \\ \cdots \\ m_{IJ} \end{pmatrix} \tag{2.49}$$

and

$$d_{ALL} = \begin{pmatrix} d_{11} \\ d_{12} \\ d_{13} \\ \cdots \\ d_{22} \\ d_{23} \\ \cdots \\ d_{IJ} \end{pmatrix} \tag{2.50}$$

with I, J being the number of points on an I*J two-dimensional spatial grid. The scalar damping parameter is defined by ***e***, which controls the relative weighting of the data misfit and the model length in the minimization.

2.3.4.2 Shape ratio and friction

The relative stress magnitude of stress axes, also known as the 'shape ratio' is defined by the following equation:

$$R = \frac{(\sigma_2 - \sigma_3)}{(\sigma_1 - \sigma_3)} \tag{2.51}$$

where σ_1, σ_2, σ_3 are defined above. The stress shape ratio describes the nature of the strike-slip deformation (Figure 2. 19) and for the normal fault and thrust faulting deformation.

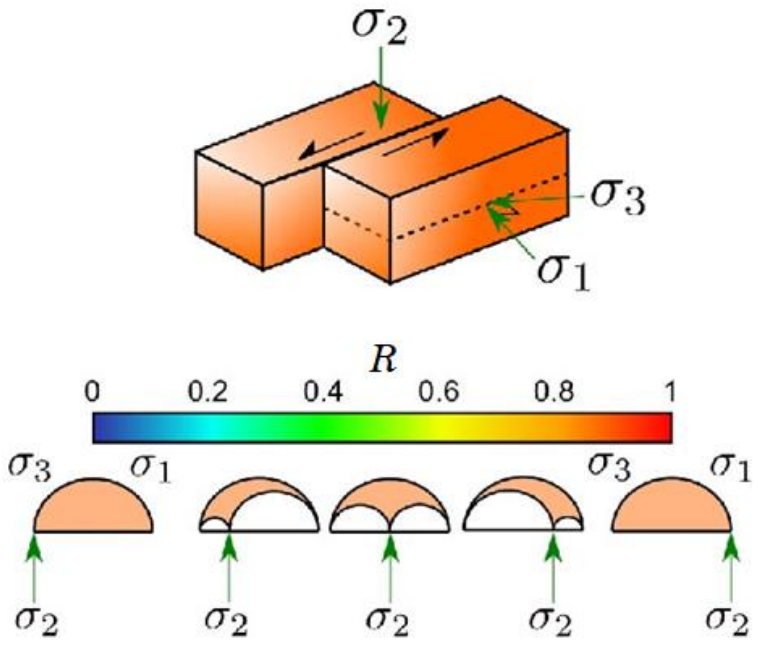

Figure 2. 19: An example of Mohr circle within its associated stress shape ratio values (R) in an overall strike-slip regime. R = 0 represents uniaxial compression, R = 0.5 for pure strike slip and R = 1 shows uniaxial extension. Transpression and transtension are bounded by those values, respectively. https://www.researchgate.net/publication/317620174_States_of_stress_and_slip_partitioning_in_a_continental_scale_strike-slip_duplex_Tectonic_and_magmatic_implications_by_means_of_finite_element_modeling/figures?lo=1.

The friction coefficient value controls the strength or fragility of the Earth's crust for deformation caused by faults (Katsushi, 2016) and is the ratio of a frictional force to normal force as shown in (Figure 2. 20) and does not have units.

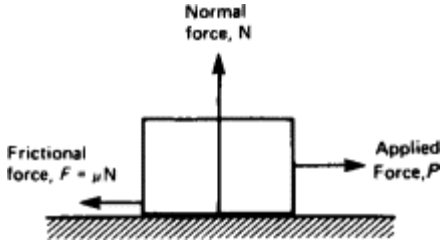

Figure 2. 20: Different forces that give definition of friction.

https://www.sciencedirect.com/topics/engineering/coefficient-of-friction?fbclid=IwAR0OzgBscqjOL-LlSAfnjn63XZblMLqnM6x6ANYsdjCfXWJLo0S-yIHFwaM#:~:text=The%20coefficient%20of%20friction%2C%20%C2%B5,coefficient%20of%20friction%20is%20high

This coefficient is determined from the Mohr Coulomb diagram as define in (Figure 2. 21) by the following formula:

$$\mu = tan\Phi \tag{2.52}$$

where μ is the the static coefficient of the friction value, Φ is the internal friction angle

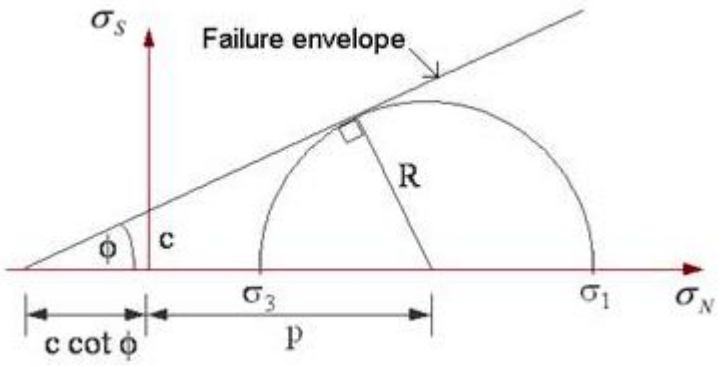

Figure 2. 21: Determination of the friction value from Mohr Coulomb failure criterion. σ_1, σ_3 are the principal stresses, ***c*** is the cohesion or the inherent shear strength, ***R, σ_S, σ_N*** and ***p*** are radius of the Mohr circle, the shear stress direction, the normal stress direction and the distance from the original axis and the Mohr circle center.

2.3.4.3 Uncertainties

Uncertainties of the obtained stress directions, the shape ratio and the overall friction on faults are calculated by the bootstrap method (Michael, 1987). Bootstrap processing is performed by randomly selecting a set of focal mechanisms with the same number of elements as the original data set. This means that some focal mechanisms could be selected more than once and others not at all. The nodal plane for each selected focal mechanism was again randomly selected from the two options. The new data set will get the same characteristics of errors that are observed in the original set, and this new data set is then inverted for the stress field. This is repeated many times, and the variation in the output is used as a measure of the uncertainty.

2.4 Earthquake magnitudes

The ‘magnitude’ is a characteristic of the ‘size’ of the earthquake. The different types of magnitude used in this study are briefly reviewed, *viz.* local, duration and moment magnitudes.

2.4.1 Local magnitude

Richter (1935) developed the local magnitude M_L scale. He determined the amplitudes of earthquakes registered by Wood-Anderson seismographs (Anderson and Wood 1925) and identified that the peak amplitudes reduce with distance from an earthquake (Figure 2. 22). The following formula was applied to determine the relative size of regional earthquakes, and is known as the ‘local magnitude scale’.

$$M_L = \log A \ - \log A_0(\Delta) + S \tag{2.53}$$

A is the maximum amplitude (zero to peak) in millimeters recorded on the Wood-Anderson seismograph for an earthquake at an epicentral distance of Δ in kilometers; $A_0(\Delta)$ is the amplitude of ground motion at Δ km produced by a standard earthquake; and S is the station correction. The earthquake location and the peak ground- motion measurement are needed for the estimation. Richter's original scale was applied for California and has become commonly used because of its simplicity. Richter’s method is focused on three choices:

1. The use of a standard Wood-Anderson seismograph,
2. The use of common logarithms to base 10, and
3. The definition of a standard earthquake (*i.e.* with M_L = 0) as one that produced a deflection of 0.001 mm on a Wood-Anderson seismograph at an epicentral distance of 100 km. Hence $-log\, A_0$=*3* at a distance Δ= 100km. Thus, an earthquake with A=1 mm recorded on a standard Wood-Anderson seismograph at 100 km has M_L=3.0. In general, calculation of M_L requires the table of $-log\, A_0$ as a function of earthquake source – station distance in kilometers.

In practice, the estimated distance source-station of an earthquake must be generalized, which can be calculated from S-P time. Since there are two

components (EW and NS) of Wood-Anderson seismograph, the average of the two magnitude values can be considered as the station magnitude. Then the average magnitude value from all stations that would have recorded the event is an estimate of the local magnitude M_L for the earthquake.

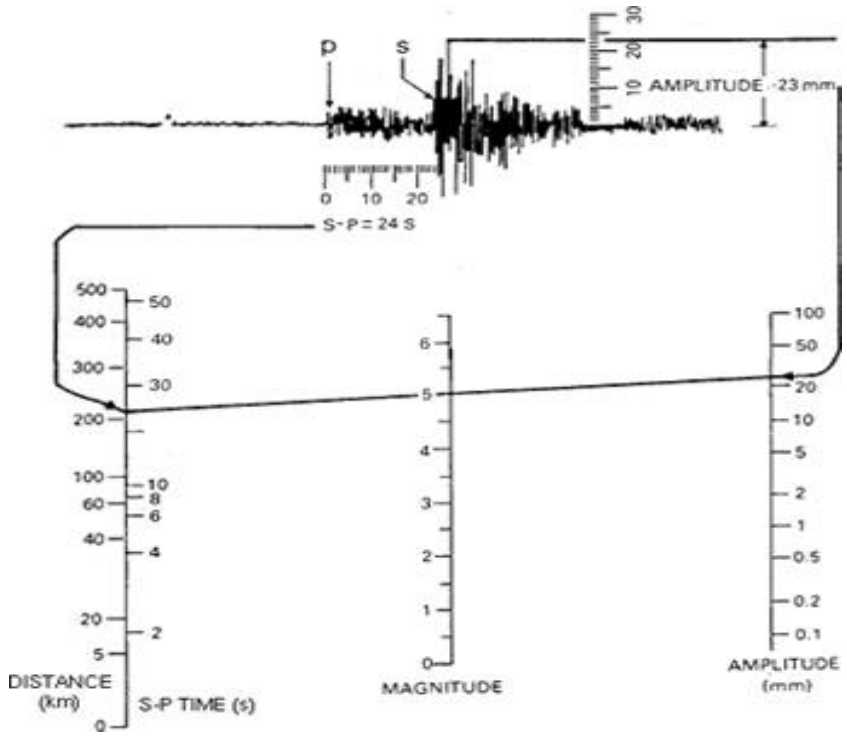

Figure 2. 22: Estimation of local magnitude using the Richter method. The P-S time and the maximum trace amplitude on the seismogram. Taken from
http://scecinfo.usc.edu/education/k12/learn/eq8.htm

The distance correction ($-log\ A_0$) is given by:

$$-logAo\ = n.log\ (r/100)\ + k(r-100)\ +\ 3.0 \qquad (2.54)$$

where n, k, and r are coefficients that account for geometrical spreading, the anelastic attenuation, and the hypocentral distance, respectively (Richter, 1935). Richter's formula was based on a small database of Wood-Anderson seismograph records in southern California, and did not separate the two terms in Equation (2.54). Hutton and Boore (1987), using a very large database for central and

southern California with more reliable focal depths, derived new attenuation terms. Alsaker et al. (1991) generalised the Hutton and Boore (1987) formula:

$$-logA_0 = n.log\left(\frac{r}{R_{ref}}\right) + k(r - R_{ref}) + k(R_{ref}) \tag{2.55}$$

where R_{ref} is a reference distance that could be different from 100 km, and $k(R_{ref})$ is a constant to be defined (could be at least 3).

Combining Equation (2.54) and (2.55):

$$logA_{ij} = -a\ log\left(\frac{R_{ij}}{R_{ref}}\right) - b(R_{ij} - R_{ref}) - \sum_{k=1}^{N_e} M_k\delta_{ik} + \sum_{l=1}^{N_S} S_l\delta_{ij} - k(R_{ref}) \tag{2.56}$$

with A_{ij} the amplitude of earthquake i at station j; R_{ij} the hypocentral distance for the events; δ_{ij} is the Kronecker delta (1 if $i = j$, otherwise 0), and N_s,and N_e are number of stations and seismic events, respectively. Parameters a, b, M_k, and S_l are the parameters that must be determined and represent the geometrical spreading, anelastic attenuation, magnitude, and station correction, respectively. According to Alsaker et al. (1991), Equation (2.56) can be written in matrix form:

$$\begin{pmatrix} 1 & 0 & 0 & \dots & 0 & 1 & 0 & 0 & \dots & 0 & r_{11} & u_{11} \\ 1 & 0 & 0 & \dots & 0 & 0 & 1 & 0 & \dots & 0 & r_{12} & u_{12} \\ \vdots & \vdots & \vdots & \ddots & \vdots & \vdots & \vdots & \vdots & \ddots & \vdots & \vdots & \vdots \\ 1 & 0 & 0 & \dots & 0 & 0 & 0 & 0 & \dots & 1 & r_{1Ns} & u_{1Ns} \\ 0 & 1 & 0 & \dots & 0 & 1 & 0 & 0 & \dots & 0 & r_{21} & u_{21} \\ 0 & 1 & 0 & \dots & 0 & 0 & 1 & 0 & \dots & 0 & r_{22} & u_{22} \\ \vdots & \vdots & \vdots & \ddots & \vdots & \vdots & \vdots & \vdots & \ddots & \vdots & \vdots & \vdots \\ 0 & 0 & 0 & \dots & 1 & 0 & 0 & 0 & \dots & 1 & r_{NeNs} & u_{NeNs} \end{pmatrix} \cdot \begin{pmatrix} M_1 \\ \vdots \\ M_{Ne} \\ S_1 \\ \vdots \\ S_{Ne} \\ -a \\ -b \end{pmatrix} = \begin{pmatrix} y_{11} \\ y_{12} \\ \vdots \\ y_1 N_e \\ y_{21} \\ y_{22} \\ \vdots \\ yN_eN_S \end{pmatrix} \tag{2.57}$$

or $\boldsymbol{Ax} = \boldsymbol{y}$ a system of at least $Ne + Ns + 2$ linearly independent equations.

In Equation (2.56), we define:

$$r_{ij} = log(\frac{R_{ij}}{R_{ref}});\ u_{ij} = (R_{ij} - R_{ref}) \text{ and } y_{ij} = log\ (A_{ij}) + k(R_{ref}).$$

The unknown vector $\boldsymbol{x}$ can be found by inversion of $\boldsymbol{A}$, under the constraint that $\sum_{k=1}^{N_S} S_k = 0$. The coefficients a and b determine the form of the $-log\ A_0$ curve in accordance with Equation (2.56).

The relationship with Richter's local magnitude scale is obtained by anchoring the ($-logA_0$) values to those of Hutton and Boore (1987), as defined in the following relation:

$$k(R_{ref}) = 1.110\, log\left(\frac{R_{ref}}{100}\right) + 0.00189\,(R_{ref} - 100) + 3.0 \quad (2.58)$$

This gives local magnitude values of 2.0 for 17 km and 3.0 at distance of 100 km. At these attributed distances, the similar amplitude will conform to the magnitude value in Norway and California.

After using data from 1979 to 1994, the empirical relationship by the Gutenberg and Richter (1949) was estimated from a linear regression for events with $M \geq 3.9$, hence the final equation (Bertil and Regnoult, 1998)

$$\log(N) = 9.23 - (1.65 \pm 0.10)M \quad (2.59)$$

2.4.2 Duration magnitude

Duration magnitude is estimated from the waveform duration. Duration is considered as the measured time between the P-wave arrival and the time when the S-wave coda amplitude decreases to, say, 10% of the maximum recorded amplitude (Sole' vev, 1965). The signal duration measurement is shown in Figure 2. 23.

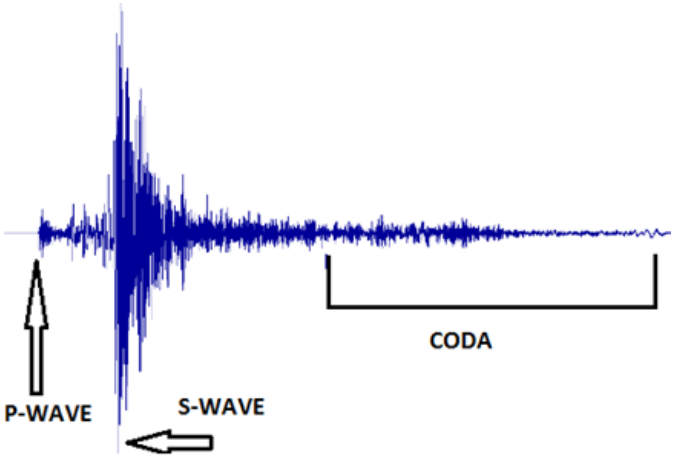

Figure 2. 23: Illustration of the earthquake coda, which is normally used to estimate duration magnitude

For Madagascar the duration magnitude formula was established by Rakotondrainibe (1977)

$$M_d = 2.04 \log(duration) + 0.0004\ distance - 0.74 \tag{2.60}$$

Duration is in seconds and the distance in kilometers

Equation (2.60) was updated by Bertil and Regnoult (1998)

$$M_d = 2.04 \log(duration) + 0.0004\ distance - 0.74 + (1.75 * 10^{-7}) duration^2 \tag{2.61}$$

2.4.3 Moment magnitude

The moment magnitude is derived from the seismic moment, defined as:

$$M_0 = \mu AD \tag{2.62}$$

where A is the area rupture along the geological fault, D is the mean value of displacement on A (meters) and $\boldsymbol{\mu}$ is the rock's shear modulus (Scordilis, 2006). The seismic moment generally represents the relationship between the size of an earthquake to the area of the rupture and the co-seismic displacement. Seismic signals can be expressed in either the time or the frequency domains. Seismic moment is calculated using the spectra of seismic signals from P- and S- waves or from the waveform inversion. In this study, we used the waveform inversion method after measuring the maximum amplitude of P-wave on the vertical component because the vertical component is less affected by the soil amplification and is available on all stations. The moment is measured in two steps:

1. The level of the low-frequency plateau of the P-wave displacement spectrum $\Omega(P)$ is obtained for each recorded event, following the determination of the decay slope and the corner frequency (Figure 2. 24).
2. The seismic moment and moment magnitude are calculated

$$M_0 = \Omega(P) 4\pi\rho D a^3 / cF \tag{2.63}$$

where $\Omega(P)$ is the low-frequency spectral level of the vertical ground displacement of P-wave (m*s), ρ is the density (2700 kg/m^3), a is the average P-wave velocity (6200 m/s), D is the distance correction, c is the surface amplification and F is the P-wave radiation pattern correction factor (F=0.64, Baumbach and Bormann, 2002).

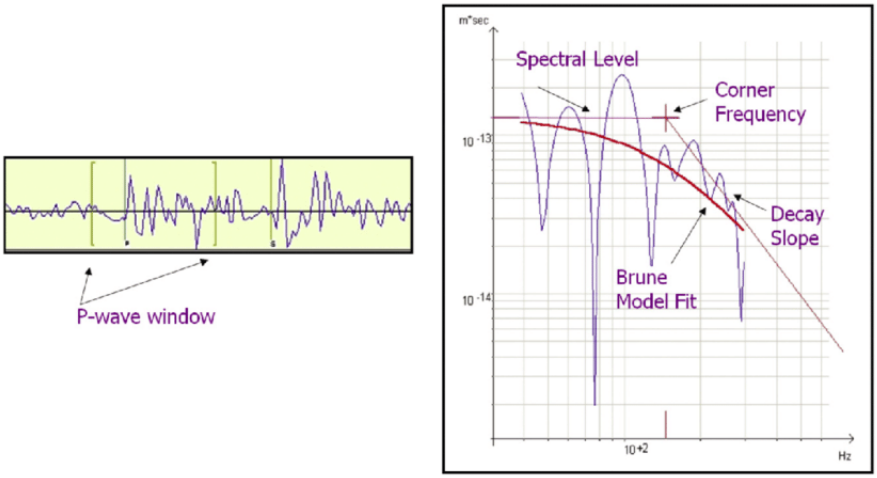

Figure 2. 24: Frequency-domain transformation of the ground displacement wave. https://www.researchgate.net/profile/T_Urbancic/publication/267969854/figure/fig1/AS:654373227085848@1533026143817/A-P-waveform-and-its-displacement-spectrum-based-on-the-shown-P-wave-window-The.png

The amplitude spectrum has different shapes for displacement, velocity and acceleration domains. According to the Brune model (Brune, 1970), the source displacement spectrum is defined as:

$$S(f) = \frac{M_o}{(1 + \left(\frac{f}{f_o}\right)^2)4\pi\rho v^3} \tag{2.64}$$

where ρ is the density in kg/m^3 ,the seismic moment is M_o in Nm, v is the velocity in m/s at the source (V_p or V_s depending on the spectrum), and f_o is the corner frequency. Radiation pattern is excluded in this expression.

The displacement spectrum at the receiver is the source spectrum affected by attenuation and geometrical spreading. If we correct for attenuation at an epicentral distance (Δ) and depth (h), the observed displacement spectrum at the receiver is

$$S(f) = \frac{M_o R_{\theta\varphi} 2G(\Delta, h)}{(1 + (\frac{f}{f_o})^2) 4\pi\rho v^3} \quad (2.65)$$

where G(Δ, h) is the geometrical spreading parameter, $R_{\theta\varphi}$is the radiation pattern effect and 2 corresponds to the free surface effect assuming a vertically incident ray. The attenuation-corrected spectrum is used to observe the corner frequency f_o, and the spectral flat level Ωo (Figure 2. 24). Thus, the seismic moment can be described as:

$$M_O = \frac{4\pi\rho v^3}{R_{\theta\varphi} 2G(\Delta, h)} \ [Nm] \quad (2.66)$$

Spectral analysis is usually performed on the vertical component because it relates to the P-wave spectrum. This is due to the near–surface site amplification, which mainly influences the horizontal components and therefore the S-wave spectrum (Sabetta and Pugliese, 1996). Another main difference between P- and S- wave spectra is the exception in the corner frequency value.

The relationship between seismic moment M_o (in Nm) and the moment magnitude M_w is described by Kanamori (1977), Hanks and Boore (1984) and Joyner (1984). The Hanks and Boore (1984) relationship is:

$$M_w = \frac{2}{3}(logM_0 - 9.1) \quad (2.67)$$

where M_o is expressed in Nm (kg m^2 s^{-2}). The relationship between moment magnitude and local magnitude is affected by source properties such as the stress and stress drop (Ristau, 2009).

In this study, moment magnitude values for Madagascar will be estimated by inserting updated information about the collected earthquake data from ISC bulletin.

2.4.4 Relation between M_W, M_L, M_S, m_B and m_b

The 'broad band' body wave magnitude scale (denoted as m_B) is used for P-waves with periods up to about 10 s recorded by medium to long period instruments, while the 'short period' body wave magnitude (denoted as m_b) is computed for periods of about 1 s. The m_B value was was originally determined from the ratio of amplitude to period for P or S waves according to the relation:

$$m_B = \log A/T + q(h) \tag{2.68}$$

where A is the maximum amplitude observed, T is the amplitude period and $q(h)$ is a calibration function that is given in tables for shallow earthquakes (Gutenberg, 1945b) and in charts for all depths of earthquake foci (Gutenberg, 1945c; Gutenberg and Richter, 1956).

In general, the magnitude m_B included in the ISC and NEIC bulletins is estimated using the recordings of the first 5 s of short period (T ≤ 3 s) P waves by short period instruments, following the procedure proposed by Gutenberg and Richter (1956), by applying the formula:

$$m_B = \sum_{i=1}^{n} \frac{[\log\left(\frac{A_i}{T_i}\right) + Q(i,h_i)]}{n} - 3 \tag{2.69}$$

where $Q(i,h)$ represents the depth–distance factor, n is the number of stations (recordings) used and A_i and T_i are the amplitude of the ith station in nanometers and its respective period in seconds.

The use of the different recordings resulted in differences between m_B and m_b scales that, in some cases (i.e. earthquakes produced by large faults or earthquakes with complicated rupture process), can be considered as important (Abe, 1981; Kanamori, 1983). Abe (1981) proposed the following equation:

$$m_B = 1.5m_b - 2.2 \tag{2.70}$$

which presents the relationship of m_B with m_b estimated by ISC.

The M_S magnitudes reported in ISC and NEIC bulletins are calculated using amplitudes and respective periods of Rayleigh waves with periods ranging between 10 s and 60 s at epicentral distances 20°–160°, using the Prague formula (Vanek et al., 1962):

$$M_S = \log\frac{A}{T_{max}} + 1.66\ \log\Delta + 3.3 \tag{2.71}$$

where A is the maximum ground amplitude, in μm, observed on horizontal components, T its respective period and Δ the epicentral distance in degrees. The focal depths of the earthquakes for which the M_s is estimated must not exceed 60 km.

Following Gutenberg and Richter (1956), the relations that connect the M_L, m_B and M_S magnitude scales is presented by the equations

$$m_B = 0.63\ M_S \tag{2.72}$$

$$M_S = 1.27\ (M_L - 1) - 0.016\ {M_L}^2 \tag{2.73}$$

According to Scordilis (2006), the distribution of M_W versus M_S for shallow earthquakes i.e., < 70 km is expressed by the equation:

$$M_W = 0.67(\pm 0.005)M_S + 2.07(\pm 0.03) \tag{2.74}$$

where $3.0 \leq M_S \leq 6.1$.

2.5 Seismic Hazard Assessment

2.5.1 Basic concepts

Seismic Hazard Assessment seeks to evaluate the magnitude and likelihood of future strong ground motion due to earthquakes. There are two main approaches, *viz.* Deterministic Seismic Hazard Assessment (DSHA) and Probabilistic Seismic Hazard Assessment (PSHA). In this study, we use the latter approach, as it is better suited to our data set.

2.5.1.1 Deterministic approach

In the deterministic approach, the strong motion parameters are calculated for the maximum reasonable earthquake at the closest possible distance to the site of interest. This method estimates the greatest possible strong earthquake ground motion at a site (Reiter, 1991; Anderson and Brune, 1999; Anderson et al., 2000). Thus, the seismic sources, the structure of the fault near a site and the geological structure of the area are all important factors.

The steps required to apply the deterministic method for seismic hazard assessment are presented in (Figure 2. 25). Firstly, an identification of the seismic sources that may create significant ground motion at the site of interest. Secondly, determination of the shortest distance from each potential source (*e.g*. a fault) to the site. Thirdly, the characteristics of the Peak Ground Acceleration (PGA) values from the attenuation relation from each source which is expected to produce the highest level of movement. Finally, determination of the PGA values for the most significant earthquake (the 'controlling' earthquake). The DSHA method is based on characterizing the maximum ground motion from single or set of earthquakes, and is often regarded as presenting a plausible 'worst case' scenario.

2.5.1.2 Probabilistic approach

The probabilistic approach, developed by Cornell (1968), quantifies the probability of exceeding different levels of ground motion at a site. A Poisson model of earthquake occurrence is used for the assessment *i.e*. each earthquake in the catalogue is considered an independent random event, meaning that no earthquake has any influence on the size, timing, and location of any other earthquake. Consequently, fore- and aftershocks must be removed from the catalogue. Uncertainties, such as the location, rate of recurrence, size and the effect of the earthquakes, are also taken into account. The four main steps required for PSHA are shown in (Figure 2. 26).

1. Source zones are defined based on the tectonic characteristics and past seismicity of the region.

2. A recurrence model is estimated for each source zone based on the frequency-magnitude distribution and an assessment of the maximum credible magnitude.
3. The attenuation of ground motion is estimated.
4. The likelihood of ground motion exceeding certain threshold values is expressed as a probability.

Different methodologies can be used. For example, the classic Cornell-McGuire approach (Cornell, 1968; McGuire, 1976), which is the most commonly used for Probabilistic Hazard Analysis; and the parametric-historic approach of Kijko and Graham (1998, 1999), which takes the incompleteness of the catalogues and the epicentral location uncertainties into account.

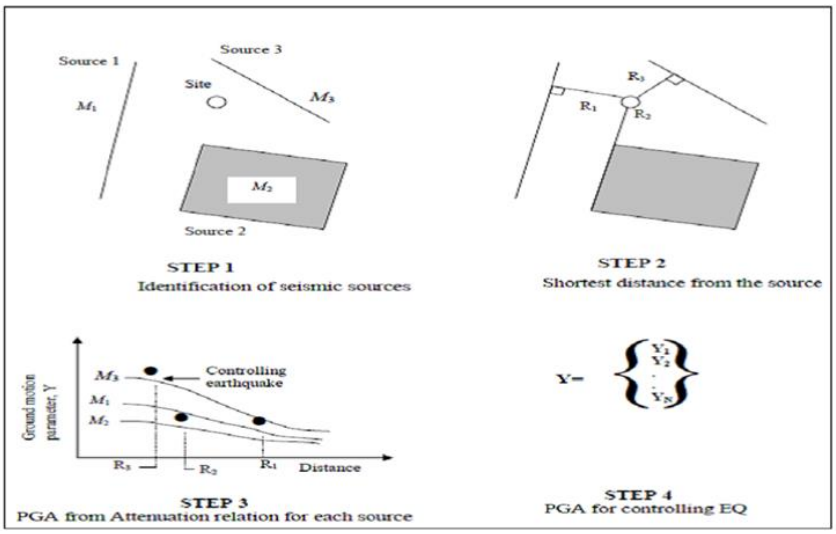

Figure 2. 25: Deterministic seismic hazard analysis (Kramer, 1996) (https://www.researchgate.net/figure/Different-steps-for-deterministic-seismic-hazard-analysis-Kramer-1996_fig5_303724910).

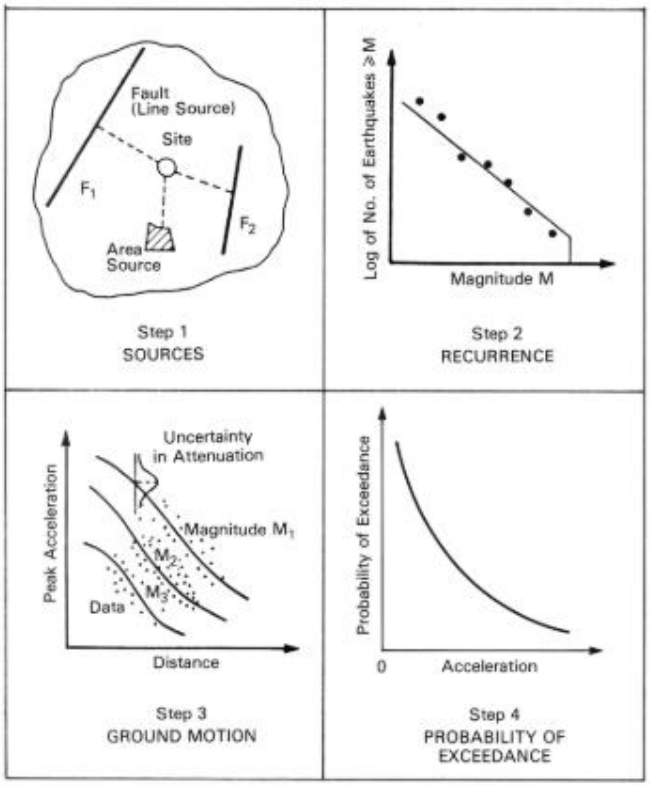

Figure 2. 26: Probabilistic seismic hazard analysis. (https://www.researchgate.net/figure/Basic-steps-of-probabilistic-seismic-hazard-analysis-after-Reiter-1990_fig4_228990134)

2.5.2 Cornell-McGuire approach

PSHA is often defined to as the 'Cornell approach' (Cornell, 1968, 1971) or the 'Cornell-McGuire approach' (Cornell, 1968; McGuire, 1976) for seismic hazard assessment. It is based on three fundamental assumptions:

1. That the earthquake catalogue consists only of independent events *i.e.* it follows a Poisson model.
2. An earthquake is equally likely to occur anywhere in a seismic source zone, be it an area source or a line source, and
3. Average occurrence rate of earthquakes is statistically stable.

2.5.2.1 Source zone

The characteristics of the earthquakes occurring in an area, as well as geological, tectonic and geophysical information, are used to define the type of source zone,

viz. line source, area source or volume source (Figure 2. 27). The choice of the source area type is based on the characteristics of the faults, the seismicity distribution and the geological structure.

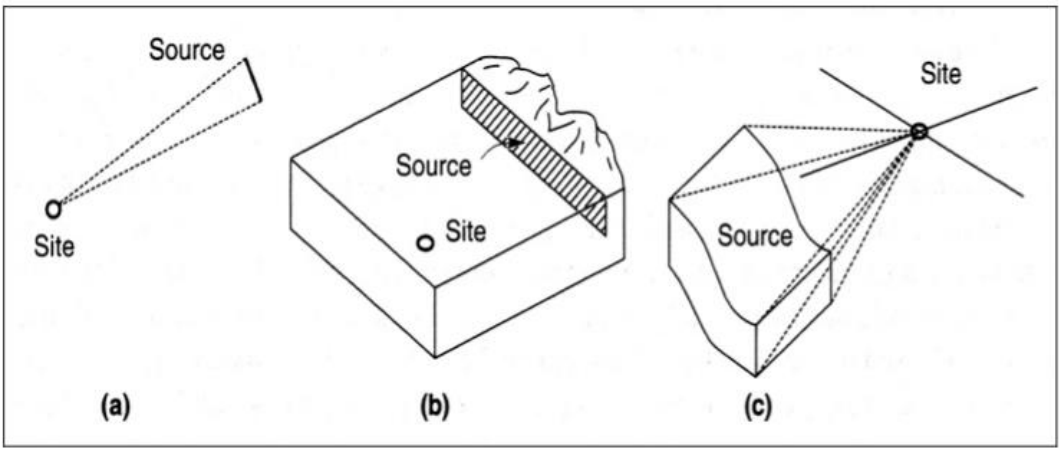

Figure 2. 27: Source zone geometries (a) point source *e.g.* from a short fault, (b) linear source defined as shallow fault modeled, c) a three-dimensional source zone (Kramer, 1996).

In probabilistic seismic hazard, identification of source to site distance is important (Figure 2. 28) because from a site, a projection of the rupture onto earth surface could probably be determined.

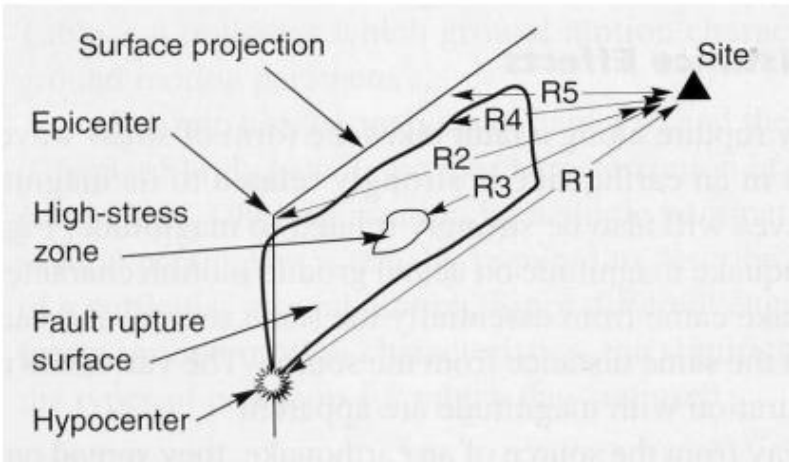

Figure 2. 28: Methods of source to site distance measurement. R1 indicates the hypocentral distance (dh); R2 the epicentral distance (de); R3 the distance to energy zone; R4 is the distance to slipped fault and R5 is the distance to surface projection of fault (dt) as defined Shakal and Bernreuter (1980). From http://biblioteca2.ucab.edu.ve/anexos/biblioteca/marc/texto/AAT6366.pdf (p. 9)

2.5.2.2 Recurrence model

The recurrence relation is calculated using all previous earthquake events that are included into the seismic hazard calculation in order to apply the probabilistic method. The recurrence relation is the most important for studying seismic hazard and depends on the uniformity of the seismic earthquake events.

For probabilistic seismic hazard studies, the catalogue completeness periods that are used to determine the recurrence relation are important for defining the appropriate seismic source models. In general, the recurrence relation is shown by a curve that represents the relation between the magnitude and number of earthquake (Figure 2. 29). It is modeled using the Gutenberg-Richter (G-R) relation:

$$\log N = a - bM \tag{2.75}$$

where N is the number of seismic events of magnitude greater than M, and a, b are parameters which measure the seismicity level, and the ratio among the number of small and large events, respectively. Equation (2.75) expresses the fractal and/or power law magnitude distribution of earthquakes in a specific area and in the defined time interval.

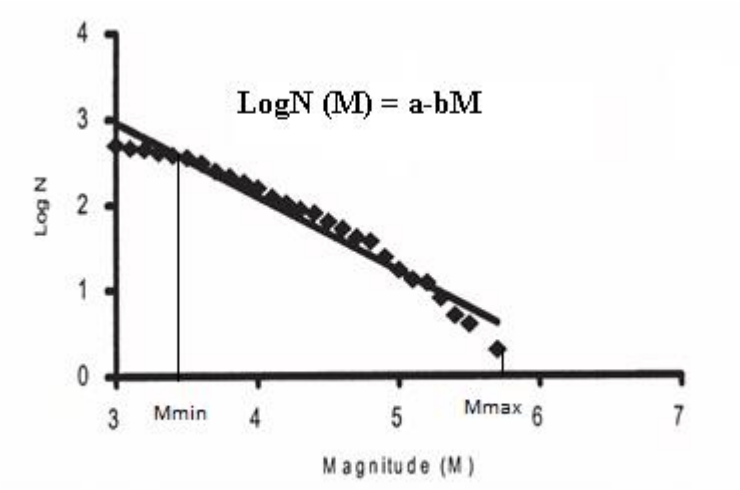

Figure 2. 29: An example of curve showing the Gutenberg-Richter relation (https://www.researchgate.net/figure/Gutenberg-Richter-relation-that-describes-the-relationship-between-the-logarithm-of-a_fig1_330979632)

The level of completeness $m_{min,}$ the maximum earthquake magnitude m_{max}, the Gutenberg-Richter parameter *b* and the seismic activity *a* are all important parameters used for seismic zone evaluation. They are generally estimated from instrumental, historical and paleo-seismic data.

2.5.2.3 Ground Motion Prediction Equation (GMPE)

In general, attenuation is the reduction in amplitude caused by the physical characteristics of the transmitting system. In seismology, attenuation causes the amplitude of ground motions to reduce with increasing distance from the source. Thus ground motion prediction equations (GMPE) are important when assessing the likely severity of strong ground motion.

To evaluate the peak acceleration values, a model of ground motion parameter is needed. In the majority of the cases, the GMPE is given by:

$$F_{source}(M)=C_1+C_2M+C_3M^2+f_{mech} \tag{2.76}$$

where C_1, C_2, C_3 are the regression coefficients, M is the magnitude value and f_{mech} varies according to the normal, strike-slip or reverse source mechanism. The GMPE equation varies from author to author and depending on the seismotectonic features of the site. Estimation of the coefficients used to predict earth movement correlates on the quality and quantity of the seismic data that has been measured in a region.

The GMPE depends strongly on the geological structure of the study area. Boore and Atkinson (2008) developed a GMPE for the central and eastern United States, which is characterized as an ‘intraplate’ or ‘stable continental’ region. Chiou and Youngs (2008, 2014) developed GMPEs, known as the ‘next generation attenuation’ equations (NGAs) that are appropriate for predicting ground motion due to shallow crustal earthquakes in active tectonic regions.

2.5.2.4 Estimation of ground motion parameters

The probability P that earthquake-induced ground motion at a site (arising from all possible earthquake sources) will exceed a certain level in a given time period can be expressed by Equation 2.77 (McGuire, 1977):

$$P[Z \geq z] = \int_{m_{min}}^{m_{max}} \int P[Z \geq z|m,r]\, f_M(m) f_{R|m}(r|m) dr dm \qquad (2.77)$$

where

Z is the characteristic of a particular ground motion parameter, *e.g.*, peak ground acceleration, peak ground velocity, spectral acceleration.

m is a given magnitude at an epicentral distance r;

$f_M(m) = f_M\left(\mathrm{m}\middle|m_{min}, m_{max,}\right)$ and $f_{R|m}\ (r|m) = F_M\left(m_0\middle|m_{min}, m_{max,}\right)$ are the Probability Density Function (PDF) of earthquake magnitude and the conditional Density Function (CDF) of the epicentral distance, respectively; and

$m_{min}, m_{max,}$ are the minimum and maximum regional magnitude.

If the magnitude of earthquakes conform to a Gutenberg-Richter (G-R) relation, (Gutenberg and Richter, 1942), defined in the next part below, we can write

$$f_M(m) = \frac{\beta\ exp[(-(m - m_{min})]}{1 - exp[(-\beta(m_{max} - m_{min})]} \qquad (2.78)$$

with $\beta = b\ ln\ 10$.

If the earthquake occurrence follows a Poisson distribution in all seismic sources, the probability can be written as follows:

$$P[Z > z; t = 1] = 1 - \exp\,[-t.\lambda] \qquad (2.79)$$

From Equation (2.79) above, if $t = 1$, the annual rate of exceedance of the ground motion parameter z, which determines the hazard curve, is defined. λ is the rate of occurrence of earthquakes greater than $m_{min.}$

2.5.3 Kijko and Sellevoll approach (KS)

The Kijko and Sellevoll (1989, 1992) method takes into account incomplete catalogues and inaccuracies in magnitude and epicentral location. This method

does not require the delineation of the seismic active zones. The KS approach was useful to assess the recurrence parameters and the maximum regional magnitude for seismic hazard study for Madagascar because some stations were out of operation during the period 1975-2016.

Maximum magnitude is an important parameter in seismic hazard assessment. Three different definitions of maximum magnitude are used (Reiter 1991):

1. Maximum magnitude from historical earthquakes associated with the seismotectonic source,
2. Maximum magnitude used in deterministic approach that are based on the largest plausible earthquake in the given tectonic setting, and
3. Maximum magnitude, which is the maximum possible earthquake that is likely to occur in a given time interval and tectonic setting.

In this present study, we applied the third definition of maximum magnitude. The main steps in selecting a maximum magnitude are:

1. Consideration of the largest magnitudes reported in historical data,
2. Consideration of earthquake catalogues, particularly gaps and changes in the magnitude of completeness,
3. Inclusion of cases with uncertain magnitude determination.

The completeness of the earthquake data is obtained using the historical data that contained the largest event only, and the instrumental complete data that have different stages of completeness (see Figure 2. 30). From this, the complete part of the catalogue is divided into s sub-catalogues ($i = 1, 2, \ldots . s$) and each is defined to be completed for event magnitudes that exceeding $m_{min}^{(i)}$during a period of time t_i. Values of $m_{min}^{(i)}$represented the magnitude of completeness for each sub catalogue. Description of the temporal distribution of earthquakes within a specific area is obtained from a Poisson model (Cornell, 1968; Lomnitz, 1973; Gardner and Knopoff, 1974).

2.5.3.1 Likelihood estimation

The likelihood estimation of seismic hazard involves the evaluation of the maximum amplitude of ground motion based on the activity rate and the Gutenberg-Richter *b* parameter using historical and instrument data. This method focuses on estimating the parameters of probability distributions by maximizing a likelihood function.

By considering the assumption of the doubly truncated Gutenberg-Richter method of earthquake magnitude x (Kijko et al., 1993), the cumulative probability distribution (CDF) of x is represented by:

$$fR\backslash M(r|m) = F_M(m_0|m_{min}, m_{max}\ ) = \Pr(X \leq x) = \frac{A_1 - A(x)}{A_1 - A_2} \qquad (2.80)$$

where the magnitude x ranges from $< m_0, m_{max} >$ with m_0 the threshold magnitude; m_{max} and m_{min} the maximum and minimum regional magnitude, respectively; X the observed magnitude; $A_1 = \exp(-\beta m_0)$; $A_2 = \exp(-\beta m_{max})$; $A(x) = \exp(-\beta x)$; and $\beta = b \ln(10)$ where b is the slope of the Gutenberg-Richter relation.

For earthquakes that have magnitude greater than x, a Poisson process can be applied with the mean rate of occurrence $\lambda[1 - F(x)]$, where λ is the activity rate corresponding to the threshold magnitude m_0 (Benjamin and Cornell, 1970). The probability that X the largest magnitude for a period t years is defined by:

$$G(x \mid t) = \Pr(X \leq x) = \exp\left[-\upsilon_0 t\left(\frac{A_1 - A(x)}{A_1 - A_2}\right)\right] \qquad (2.81)$$

where $\upsilon_0 = \lambda[1 - F(m_0)$. From the definition of the probability density function (PDF) and from equation 2.81, the PDF of strongest earthquake within a period t, standard deviation σ_M and with apparent magnitude $m \geq m_o$ is defined as:

$$f_M^{max}(m_{0i}|m_0, m_{max,}t_{0i}, \sigma_{M0i}) = \frac{\widetilde{\lambda_o} t\, \widetilde{f}_M(m\backslash m_0, m_{max,}t, \sigma_M) \exp[\widetilde{\lambda_o} tc\widetilde{F}_M(m\backslash m_0, m_{max,}t, \sigma_M)]}{1 - \exp(-\widetilde{\lambda_o} t)} \qquad (2.82)$$

where

$$c\widetilde{f_M}(m\backslash m_0, m_{max,}t, \sigma_M) = 1 - \widetilde{F_M}(m\backslash m_0, m_{max,}t, \sigma_M);\ \tilde{\lambda} = \lambda \exp(\chi^2),$$

and $\chi = \frac{\beta\sigma_M}{\sqrt{2}}$

After introducing the function in 2.82, the likelihood function can be defined as

$$L_o(\lambda, \beta) = const \prod_{i=1}^{n_0} f_M^{max}\left(m_{0i} \middle| m_0, m_{max,} t_{0i}, \sigma_{M0j}\right) \tag{2.83}$$

where m_{0i} ($m_{0i} \geq m_{min}^{(i)}$) the apparent magnitude of the strongest earthquake that occurred during the time interval t_{0i}; σ_{M0j} is its standard deviation, *j = 1,...*, n_o, where n_o denotes the number of earthquakes in the extreme part of the catalog and '*const'* is a normalizing factor.

According to Figure 2. 30 the entire catalogue can be divided into *s* sub-catalogues and each of the catalogues has a time span *Ti* and is complete that starting from the known magnitude $m_{min}^{(i)}$. For each sub-catalogue *i*, m_{0i} is the apparent magnitude in which $m_{0i} \geq m_{min}^{(i)}$. While numbers of seismic events are independently linked to their size, the likelihood function of earthquake magnitudes present in each complete sub-catalogue *i* is equal to $L_i(\lambda,\beta) = L_i(\beta)\, L_i(\lambda)$, which is the product of the function of β, $L_i(\beta)$, and the function of λ, $L_i(\lambda)$. Following the definition of the likelihood function of a set of independent observations, the function $L_i(\lambda)$ is given by

$$L_i(\lambda) = \text{const} \prod_{j=1}^{n_i} \widetilde{f_M}\left(m_{ij} \mid m_{min}^{(i)}, m_{max,}, \sigma_{Mij}\right) \tag{2.84}$$

where n_i represents the number of earthquakes in each complete sub-catalogue and i = 1,...,s. The hypothesis that the earthquake numbers per unit time is a Poisson random variable gives a form of $L_i(\lambda)$ equal to

$$\text{const}(\check{\lambda}_i t_i)^{n_i} \exp\left(-(\check{\lambda}_i t_i)\right) \tag{2.85}$$

where 'const' is a normalizing factor, $\check{\lambda}_i$ the apparent mean activity rate for the complete sub-catalogues. The true mean activity rate for the total for the ith sub-catalogue is

$$\check{\lambda}_i = \lambda(m_{min}^{(i)}) = \lambda c \mathrm{F}_M(\, m_{min}^{(i)} \mid m_{min}, m_{max}\,) \tag{2.86}$$

The two functions $L_i(\beta)$ and $L_i(\lambda)$, for i = 1,...,s, define the likelihood functions for each complete sub-catalogue and the joint likelihood function of all data in the catalogue is given by:

$$L(\lambda, \beta) = \prod_{i=0}^{n_i} L_i(\lambda, \beta) \tag{2.87}$$

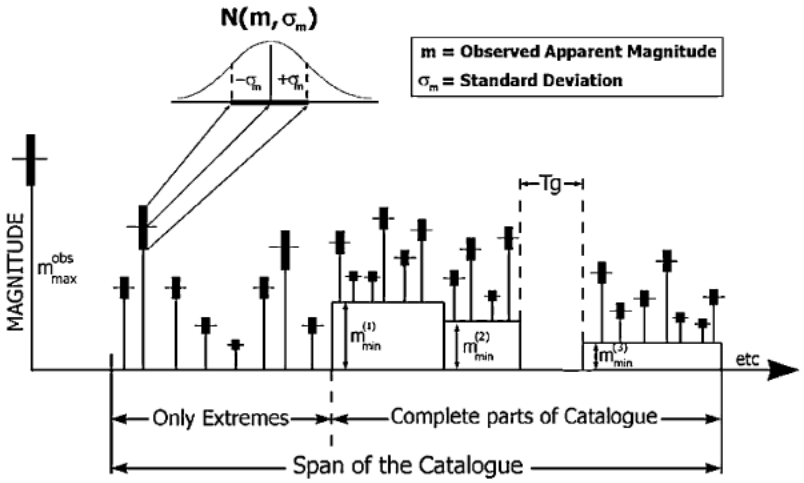

Figure 2. 30: Kijko and Sellevoll (1992) method to obtain seismic hazard parameters. m_{max}^{obs} is the largest observed earthquake and Tg the defined gaps. During the calculation, the procedure evaluates the area-specific parameters and then computation of the distribution of ground motion parameters (PGA values) in a specific area.

2.5.3.2 Computation of PGA values

The computation of the PGA values is the second step of the parametric historic procedure; it assesses seismic hazard at a site by taking the attenuation of the selected ground-motion parameter into account. For a given earthquake, PGA at a site is primarily a function of magnitude, hypocentral distance and the quality of the rock along the path between source and site. In general, the attenuation law of PGA is calculated as follows:

$$ln\,(PGA) = \, c_1 + c_2\, m \, + \, \Phi(r) + \varepsilon \tag{2.88}$$

where c_1, c_2 are the empirical coefficients and m is the earthquake magnitude, $\Phi(r)$ the function of the hypocentral distance and ε the random error.

The seismic hazard in terms of PGA is obtained from the calculation of the conditional probability that an earthquake of random magnitude that occurred at a random distance from a site. It will create the value of PGA_{min}, which is the threshold value at the site. The random value of m is in the range $m_{min} \leq m \leq m_{max}$, which is distributed according to the G-R relation.

The frequency-magnitude from the G-R relation is related to the cumulative distribution function of earthquake magnitude and given by:

$$F_M(m) = \frac{\exp(-\beta m_{min}) - \exp(-\beta m)}{\exp(-\beta m_{min}) - \exp(-\beta m_{max})} \tag{2.89}$$

where m_{min} and m_{max} are the minimum and maximum value of magnitudes;
$\beta = b \ln(10)$, with b the parameter of G-R which is the relative frequency of occurrence of earthquakes of different magnitudes (slope of G-R relation).

By selecting Equation (2.88) as a model of PGA, it assumes that

$$\log N(x) = c - d.x \tag{2.90}$$

where $N(x)$ is the number of earthquakes registered at the site with PGA equivalent to $x = ln(PGA)$, c and d values are parameters with $d = b/c$ the coefficient relative to the attenuation relation in (2.88).

From Equation (2.89), the cumulative distribution function (CDF) can be written as:

$$F_x(x) = \frac{\exp(-\zeta x_{min}) - \exp(-\zeta m)}{\exp(-\zeta x_{min}) - \exp(-\zeta x_{max})} \tag{2.91}$$

with $x_{min} = ln(PGA_{min})$, $x_{max} = ln(PGA_{max})$, and PGA_{max} is the maximum possible of PGA and $\zeta = b/c_2$ and $\beta = b \ln(10)$.

From Equation (2.75), if the *b-value* represents the slope of the G-R relation, the parameter d characterizes the slope of the distribution of $x = ln(PGA)$ and equal to $\frac{b}{c_2}$.. Consequently, the probabilistic seismic hazard is the probability of a specific value of PGA (the threshold value PGA_{min}). This value is being exceeded at least once at the source during an interval time *t* as defined by:

$$\mathrm{H}\left(\frac{\mathrm{x}}{\mathrm{t}}\right) = 1 - \exp\{-\lambda\, \mathrm{t}[1 - \mathrm{Fx(x)}]\} \tag{2.92}$$

with λ the site-specific rate of earthquakes that created the PGA value at the site and exceeding the PGA_{min}. The distribution in Equation (2.92) is obtained after considering that the earthquakes, which created $PGA \geq PGA_{min}$ at the site that follows the Poisson relation with mean value of $\lambda(x) = \lambda[1 - Fx(x)]$, where $x = ln\,(PGA)$.

2.5.4 Logic tree

A logic tree is a way to perform seismic hazard assessment by taking into consideration the uncertainties that are due to the improper knowledge about the process involved in earthquake events and algorithms used to model them. The epistemic uncertainties can be reduced after integrating the distribution of the ground motion parameter (GMPE) and then the seismic hazard should be assessed using a logic tree approach. A choice of GMPE parameter was set for the logic tree by reason of the lack of knowledge of the appropriate region-specific models of wave propagation.

For estimating the ground shaking and the hazard values in a particular region, ground motion prediction equations should be used. Numerous ground GMPEs are applicable for different regions for estimating the PGA values. So that the GMPEs will be inserted to the logic tree as different models will be applied for the seismic hazard assessment. An example of logic tree is presented in Figure 2. 31.

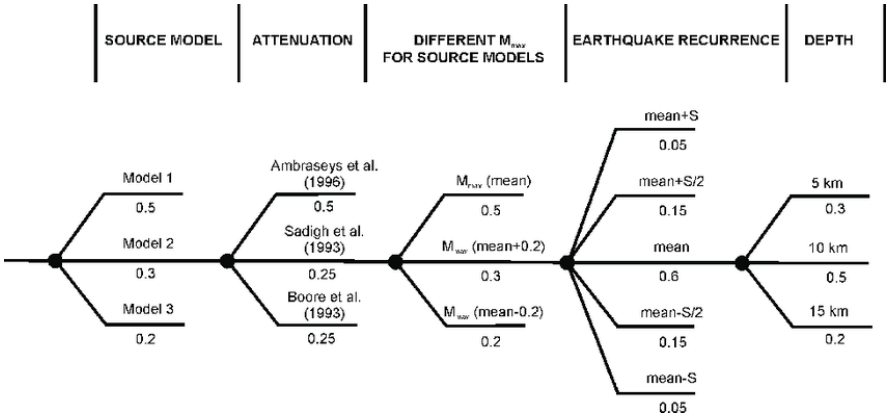

Figure 2. 31: An example of logic tree in which different parameters are inserted for computing seismic hazard.

The logic tree method is based on weighting factors and presented as a Venn diagram of the attenuation model (See Figure 2. 31). Within the logic tree, distinct nodes from the different options of the input choice and each branch that allow a weight factor are presented. So that, quantification of the epistemic uncertainty is obtained by taking into consideration the different branches of the logic tree based on the b-value calculated, the source models, the magnitude of completeness, the maximum magnitude, and the suitable GMPE.

The calculation of the hazard followed all branches throughout the logic tree and the analysis produced a hazard curve that presents the relation between the ground motion and the annual frequency of exceedance.

2.6 Computational packages

2.6.1 ANTELOPE software

Antelope is an automated software package that generates earthquake locations and magnitudes in real-time. It is a commercial package developed by Boulder Real-Time Technology (BRTT 2004) with root (www.brtt.com) and running under UNIX and Mac OS. The use of the Antelope program is described in the Antelope New Users Guide (Lockridge et al., 2012). The software is composed of various sub-programs, such as:

- *dbdetect* uses a short-term/long-term amplitude algorithm to detect bursts of energy that may be arrivals from a seismic event in continuous waveforms.
- *dbpick* picks the P-arrivals and S-arrivals in the waveforms.
- *dbwfmeas* convolves the horizontal displacement with a Wood-Anderson instrument response (Kanamori and Jennings, 1978) and measures the maximum amplitude.
- *dbml* processes the magnitude calculation after editing the parameter file *dbevproc.pf* that allows us to calculate the local magnitude.
- *dbloc2* locates the earthquake using arrivals from the *dbpick* program.

The earthquake location calculation (*dbloc2* program) uses either the Gauss-Newton inversion method (GNM) (Lee et al., 1981), which was used in this study, or a pseudo inverse and the Levenberg-Marquardt algorithm (Pavlis et al., 2004).

2.6.2 HYPOELLIPSE

This package, developed by Lahr (1989; 1999), is one of the programs that were used to refine the event locations. This software is an extension of the HYPO71 program that was written in FORTRAN in the late 1980 and runs in an interactive UNIX environment. This program applies Geiger's method (Geiger, 1910; 1912) to reduce the root-mean-square (RMS) of the travel time residuals and iteratively improve the location accuracy (Lahr, 1989; 1999) (See section 2.2.1). The main steps in HYPOELLIPSE are:

(a) Input a first guess of the hypocenter location coordinates (here called the 'theoretical' hypocenter) and origin time (x_o, y_o, z_o, t_o)

(b) Calculate the travel-time, *Tcalc*, using the theoretical location of the seismic event and station coordinates.

(c) Calculate the residual travel-time Res_i at each station *i*, which is the difference between the calculated travel time and the observed arrival-time, $Tcalc_i$ and $Tobs_i$, of the P- or S- arrival at the station.

(d) x_o, y_o, z_o, t_o are iteratively corrected until the sum of the squares of the travel-time residual is small by applying the iterative least-square technique of Geiger (1912).

The quality of the earthquake location is quantified by the SHE and SEZ values, which are related to the error estimate in the horizontal and vertical directions, respectively. Values of SEH and SEZ are defined in (Figure 2. 32).

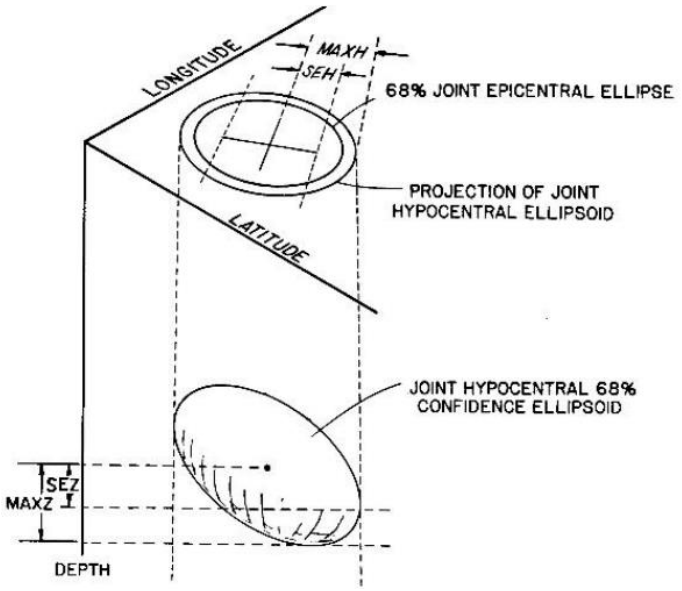

Figure 2. 32: Hypoellipse error ellipsoid relationships with SEH= MAXH/1.87, and SEZ=MAXZ/1.87. MAXZ is the radius of the 68% confidence ellipsoid (after Lahr, 1999).

Table 2. 1 shows the quality rating based on SEH and SEZ values (the vertical and horizontal errors). SEH indicates the greater uncertainties in the epicentral locations of the two horizontal components (68% confidence estimates), while SEZ is based on the uncertainties in source depth (single variable 68% confidence estimate). The relation between error estimates at the error ellipsoid is shown in Figure 2. 32.

Table 2. 1: Hypocentre quality factors based on the SEH and SEZ values (the vertical and horizontal errors)

Quality	a	b	c	d
Larger of SEH and SEZ in km	≤ 1.34	≤ 2.67	≤ 5.35	> 5.35

2.6.3 HYPODD

HYPODD uses a double-difference algorithm to determine the relative location within clusters of earthquake events (Waldhauser and Ellsworth, 2000; Waldhauser, 2001). If the distance between two earthquakes is small compared to the event-station distance, the ray paths may be considered to be virtually identical. The residual travel time is defined by the difference in observed and calculated travel times for the two earthquakes. The 'double-difference' of the travel times of two events is defined by:

$$dr_k^{ij} = (t_k^i - t_k^j)^{obs} - (t_k^i - t_k^j)^{calc} \tag{2.93}$$

where dr_k^{ij} is the residual between observed and calculated differential travel times, and *i, j* represents the number of the two events for any phase *k* (P- or S-phase). Consequently, Equation (2.93) can be simplified as:

$$dr_k^{ij} = \frac{\partial t_k^i}{\partial m}\Delta m^i - \frac{\partial t_k^j}{\partial m}\Delta m^j \tag{2.94}$$

where *d* and *m* are the change in location and origin time. Equation (2.94) is a system of linear equations that may be written:

$$\boldsymbol{WGm} = \boldsymbol{Wd} \tag{2.95}$$

$\boldsymbol{G}$ is the (*M* x *4N)* matrix containing the partial derivatives, where *M* is the number of double-differences observed and *N* is the number of seismic events,

d is the data vector containing the double-differences,

m is a vector of length 4N, and

$\boldsymbol{W}$ is a diagonal matrix to weight each equation

The goal is to find the weighted least squares solution of equation (2.95),

$$\boldsymbol{m}' = (\boldsymbol{G}^T W^{-1}\boldsymbol{G})^{-1}\boldsymbol{G}^T W^{-1}\boldsymbol{d} \tag{2.96}$$

where $\boldsymbol{m}'$ is the least square estimate of $\boldsymbol{m}$ (Waldhauser, 2001).

The main steps in running HYPODD are:

1. Forming event pairs to neighboring seismic events using the *ph2dt* program. This program links an event pair to a number of neighboring events (MINLNK) and creates a continuous chain of event-pairs. Different

constant values are involved such as the maximum distance between the station and the event pairs (MAXSEP), the velocity model (1-D), the number of neighbors per event (MAXNGH), and the maximum and the minimum number of links per pair saved events (MAXOBS and MINOBS, respectively).

2. Forming the grouped events from the event pairs created.
3. Determination of the double-difference relocation after inserting parameters in the file described in Table 2. 2

Table 2. 2: Parameters for double difference relocation using hypoDD.inp

PARAMETERS	CHARACTERISTICS
IDAT: data type	1: cross correlation only 2: catalogue data only 3: cross correlation and catalogue data
IPHA: Phase identification	1: P-wave 2: S-wave 3: Both P and S-waves
OBSCC, OBSCT:	Minimum number of cross correlation data, catalogue links per event pair 0: no clustering performed
ISTART: Initial locations	1: Start from cluster centroid 2: Start from catalogue locations
ISOLVE:	1: Singular value decomposition (SVD) 2: Conjugate gradients (LSQR)
MSET: Number of sets of iteration	N

The HYPODD program performs the relocation of the seismic events by minimizing errors; the calculation depends on the choice of an initial velocity model (Bondar et al., 2003). Two different choices are presented during the computation, *viz.* singular value decomposition (SVD) and the least square conjugate gradient method (LSQR) (Waldhauser, 2001). The SVD method is more appropriate for small clusters and well-conditioned seismic events (*i.e.*, surrounded by the seismic stations); while the LSQR method is more robust.

After using the HYPODD program, six output files are created such as: the initial location files *hypoDD.loc*, the relocation results *hypoDD.reloc*, the residual of the station travel time *hypoDD.sta*, the residual from the double difference *hypoDD.res*, the source characteristics *hypoDD.src*, the take-off angles of the ray joining hypocenter and station and the summary of the input *hypoDD.log*.

2.6.4 FOCMEC

FOCMEC was developed by Snoke (1984) to determine fault plane solutions. This program performs a grid search over all possible fault strikes, dips, and rake angles to find the solutions that minimise the misfit between possible nodal planes and the observed data set. The FOCMEC program was written in FORTRAN 77. The program can use data input from P, S_H, S_V wave phases, and S_H/P and S_V/P amplitude ratios of each station.

2.6.5 STRESSINVERSE program

STRESSINVERSE program is one of the software tools used to conduct the inversion in order to determine the stress field from fault plane solutions data. (https://www.ig.cas.cz/en/stress-inverse). It is written in MATLAB by Vavryčuk (2014). This program needs as input the file that contains the strike, dip and rake values that defined the fault geometry. The file *stressinverse.m* is the main executable file that runs with the *input_parameter.m* file, to get output files such as the shape ratio plot, the stress plot, the T- and P-axis plots, and the Mohr plot.

STRESSINVERSE applies Michael's method (1987), which is based on iterative stress inversion. The main steps are:

1. Definition of the optimum damping parameter,
2. Use of all grid points to determine the best stress-tensor orientation and relative stress magnitude,
3. Bootstrap resampling of the original full set of focal mechanisms, and
4. Determination of the confidence intervals.

2.6.6 HA3 program

HA3 program stands for Hazard program (Kijko and Smit, 2014), a program based on selected area. This program is written in MATLAB. It calculates the Gutenberg-Richter- *b*-value when the seismic catalogue is divided into sub-catalogues with particular levels of completeness. The HA3 program considers the incompleteness of the seismic catalogues and the temporal variation of seismicity. An area is characterized by:

(a) m_{max}, the maximum regional earthquake magnitude,

(b) λ, the mean activity rate, and

(c) the Gutenberg-Richter b-value

2.6.7 CRISIS software

Several software packages have been produced for the probabilistic assessment of earthquake hazard. For example, EQRISK (Anderson, 1978), SEISRISK (Bender and Perkins, 1987), OpenSHA (Field et al., 2003) and CRISIS (Ordaz et al., 2013), which was used in the investigation in this study. CRISIS is the seismic hazard module of CAPRA (Comprehensive Approach to Probabilistic Risk Assessment). The CRISIS software is a useful tool to perform PSHA using a catalogue containing all known earthquakes, including clustered seismic events. The software is based on the Esteva-Cornell approach (Cornell, 1968; Esteva, 1970) to PSHA. This software produces an evaluation of the probability of exceedance of the intensity values. Computation of the acceleration exceedance rate due to the *i*-th single source can be defined from the equation:

$$\gamma_{i(a)} = \sum_{j} W_{ij} \int_{M_0}^{m_{max}} \left(\frac{-d\lambda(M)}{dM} \right) \Pr\left(A > a \middle| M, R_{ij}\right) dM \qquad (2.\ 95)$$

where M_o and m_{max} are the threshold and maximum magnitudes, respectively; $\Pr\left(A > a \middle| M, R_{ij}\right) dM$ is the probability that the acceleration exceeds a certain value a at the site at a distance R_{ij} for an earthquake with magnitude M; and W_{ij} is the weight of each sub element.

The CRISIS software implements two methods to consider the local site effects:

1. The CAPRA method, which uses a special set of files to construct the spectral transfer functions.
2. A method (which we used) based on an approach proposed by Chiou and Youngs (2014). It requires a grid file for V_{S30} values at different locations and depends on the GMPE model used. V_{S30} is the average seismic S-wave velocity from the surface to a depth of 30 meters

Chapter 3: Data and Methodology

This chapter describes the characteristics of the data and methodology used to investigate the research questions posed in the introduction.

3.1 Data

3.1.2 Permanent seismic network

The permanent seismic stations in Madagascar comprise both short-period and broadband stations. Seven short-period stations were functional during the period of the MACOMO experiment (Figure 3. 1, Table 3. 1).

The first short-period seismic station (TAN) in Madagascar was installed in 1898 by the Jesuits at the IOGA in Ambohidempona. The second short-period station (AVY) was deployed in 1971 in Angavokely (Central Madagascar); and the third and fourth stations (VTY and VDA, respectively) in 1972. In 1978 the OBY and the FRR stations were installed. FRR was later renamed OPO, which recently was affiliated to the Comprehensive Nuclear Test-Ban Treaty Organization (CTBTO) network. The IOGA and the Département Analyse, Surveillance, Environnement, France (DASE; http://www-dase.cea.fr/public/dossiers_thematiques/alerte_aux_forts_seismes/description_en.html) are the main administrators of the short period data (FDSN Code RD). The ABM station was installed in Ambohimiarambe in 1982; MDSM was installed in Mandiavato in 1995; and ATG and FIRM in Ambohiby and Firavahana, respectively, in 2001. All these stations are equipped with 1 Hz vertical component short-period seismometers (ZM500).

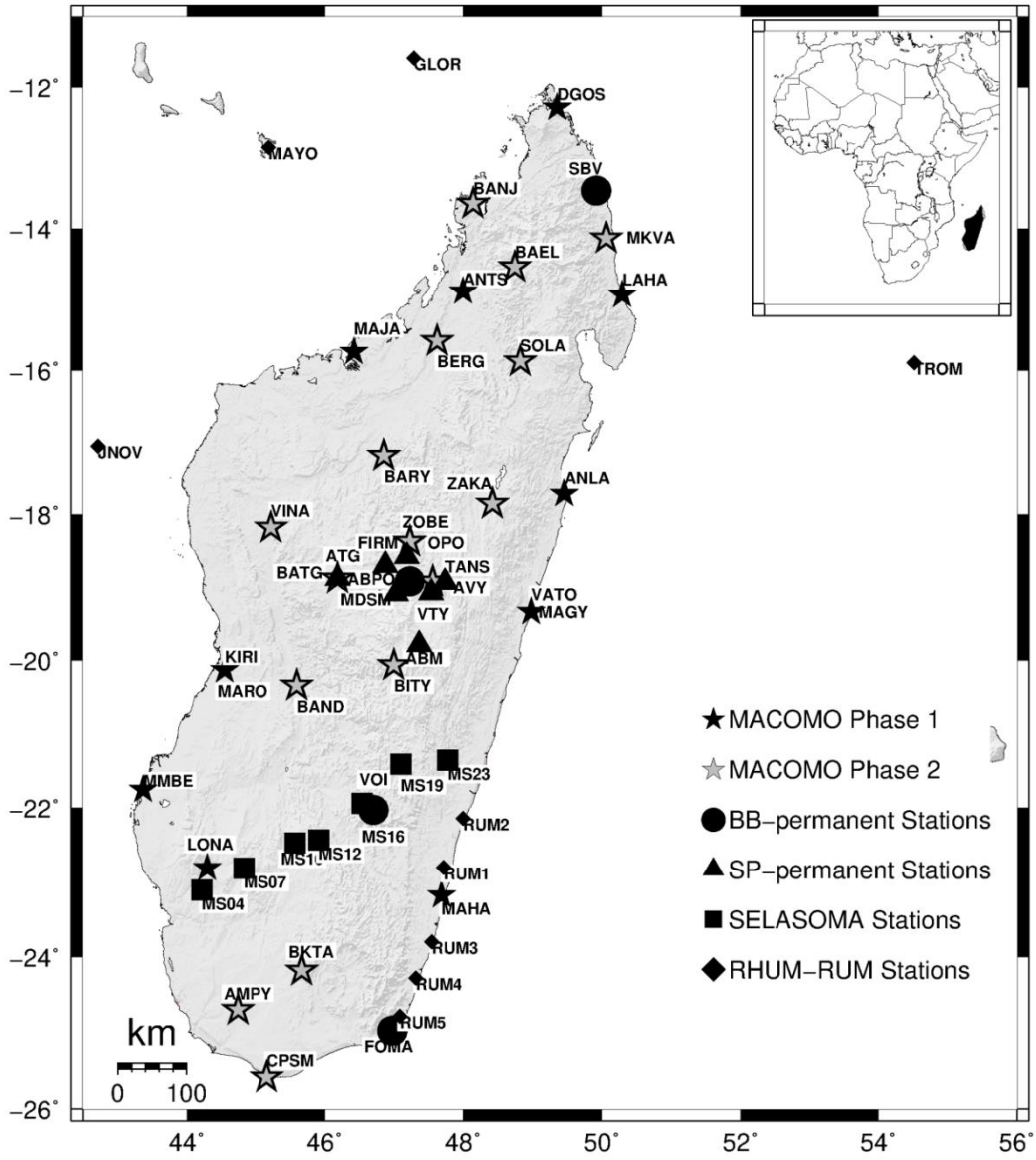

Figure 3. 1: Seismic stations in Madagascar

Four of five permanent broadband seismic stations that were operational in Madagascar were used in this study (Table 3. 1). Most of the permanent stations are in central Madagascar. The ABPO station is part of the International Deployment of Accelerometers (IDA) and equipped with Streckeisen STS-1H/VBB and STS-2 triaxial seismometers. This station has been operational since 2007 (FDSN Code II; http://ida.ucsd.edu/?q=station/abpo). The FOMA broadband station was installed in Fort-Dauphin in 2008. This station is part of the global seismological network GEOSCOPE (FDSN Code G; http://geoscope.ipgp.fr). It is

equipped with a Streckeisen STS-2 seismometer, EE08 Temperature + Humidity Sensor and Vaisala PTB110 Analog Barometer. The third and fourth broadband stations are SBV and VOI, both deployed in Vohemar and Vohitsaoka, respectively, in 2009. Both stations are equipped with Streckeisen STS-2 seismometers (FDSN Code GE; http://geofon.gfz-potsdam.de/). The most recent broadband seismic station is SKRH station, which was deployed in Sakaraha in 2014. It is equipped with a Trillium compact seismometer. It is part of the AfricaArray network (FDSN code AF; http://www.africaarray.psu.edu/). It was not used in this study.

Seismic data are transferred directly to the Madagascar National Data Central (NDC) at the IOGA by radio or internet for processing. The JADE and ONYX softwares, developed by DASE (France), detect the preliminary arrival time of the body waves and compute the earthquake locations, respectively. Data are available at IOGA by request. Data from ABPO and FOMA stations can be requested online through the IRIS website (http://www.iris.edu), while those from the VOI and SBV stations are available online from GEOFON (http://geofon.gfz-potsdam.de/).

3.1.3 Temporary seismic networks

3.1.3.1 MACOMO Project: a deployment between 2011 and 2013

I participated in the installation and the maintenance of the stations that were installed in Madagascar between 2011 and 2013, as part of the PASSCAL MAdagascar COmoros and MOzambique (MACOMO) network (FDSN Code XV; https://doi:10.7914/SN/XV_2011). The objective of the project was to determine the origin of intraplate volcanism in the region (Wysession et al., 2012). This project was conducted in collaboration with the AfricaArray program (http://www.africaarray.psu.edu/). Michael Wysession and Douglas Wiens of Washington University and Andrew Nyblade of Penn State University (http://epsc.wustl.edu/seismology/michael/web/research.html) were the principal investigators. Teams from the University of Antananarivo, Madagascar (including myself and Fenitra Andriampenomanana), from Saint Louis, Washington University, Missouri, USA (including Michael Wysession, Patrick Shore, Ghassan

Aleqabi and Martin Pratt) carried out the field work. All equipment (32 PASSCAL broadband seismic stations) was borrowed from the Instrument Centre of the Institute of Mining and Technology in Socorro, New Mexico (IRIS/PASSCAL).

.

The network operated from September 2011 to September 2013. Stations were deployed at 28 sites (Table 2.1); two stations (MARO and VATO) were shifted to new sites (KIRI and MAGY, respectively) after three months. Each seismic station was composed of:

- A three-component broadband seismometer. Three types were used (See Table 3. 2): Streckeisen STS-2, Guralp CMG-3T, or Nanometrics Trillium 120.
- A data logger. Two types were used:
    - Reftek 130 Digital Acquisition System (DAS). It is a high-resolution data logger composed of three or six channels. It records seismic data onsite and receives accurate timing from the GPS. Two internal storages drivers (Compact flash cards) are used to record the data. The DAS is commanded during installation by loading a file from a Clié palmtop computer.
    - Quanterra Q330. It is a three or six channel high-resolution data logger. It has a data storage system (on site) with external balers. Four different receiving systems are linked with the Quanterra simultaneously, such as the control of the sensor, re-center of the equipment, calibration of the functions and writing data. This datalogger is controlled by “Willard” a Windows program and programmed by the Pam OS program from the Clié palmtop computer during the on-site field work.
- Clié tool programmed by PASSCAL for transferring and retrieving parameters or configurations, editing the name of the station, changing IP address, and transfering commands to Quanterra Q330 and Reftek 130 and data loggers.
- Breakout box for Guralp seismometers.
- GPS antenna used for timing and location
- Batteries (12V) for supplying the system.
- Solar panels for charging batteries.

- Two big barrels to cover the sensor, DAS, batteries and power box.
- Log sheet, which records the characteristics of the station.
- Cables, PVC tubes, concrete, rocks.

The solar panels and GPS antenna are exposed at the surface; all other components are housed inside the two plastic barrels buried at a depth of up to 1.75 m (Figures 3.3 and 3.4).



Figure 3. 2: Seismometers (1) CMG-3T, (2) STS-2, and (3) Trillium-120

The MACOMO array was designed to study the seismicity and structure of the crust and mantle beneath Madagascar using body wave imaging, as deep as the mantle transition zone, and extending into the lower mantle (Pratt et al., 2017). The station spacing was about 250 km. Factors that were considered when selecting geographical locations of the seismic station were the geology, accessibility, characteristics of the seismic-noise sources in the region (noise level), the land proprietorship, the security and the safety of the site.

A preparatory survey to identify suitable sites for the broadband seismograph stations was conducted in May 2011. Most of the MACOMO seismic stations were installed on government ground (*e.g.*, military areas, national parks, etc.) or private properties. The stations were installed in two consecutive deployments:

1. The first array comprised 10 stations that were deployed mostly along the coast of Madagascar between September 2011 and September 2013. The station codes are ANLA, ANTS, DGOS, LAHA, LONA, MAHA, MAJA, MARO (shifted to KIRI after three months), MMBE, and VATO (shifted to MAGY after three months).

2. The second array comprised 16 seismic stations, mainly deployed in the Precambrian basement between September 2012 and September 2013 (Table 3. 1). The stations codes are AMPY, CPSM, BAEL, BAND, BANJ, BARY, BATG, BERG, BITY, BKTA, MKVA, SOLA, TANS, VINA, ZAKA, and ZOBE.

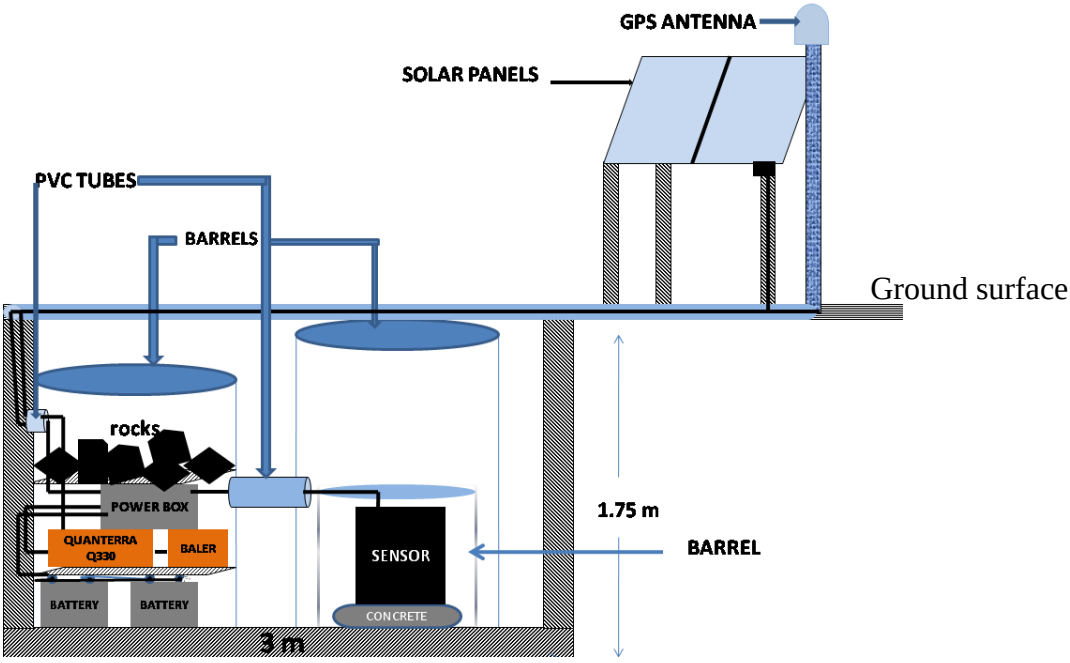

Figure 3. 3: Schematic of a typical MACOMO seismic station.



Figure 3. 4: Installation of Vatomandry (VATO) station. The team is Patrick Shore (Washington University, USA), grey shirt and black hat; Tsiriandrimanana Rakotondraibe (Madagascar), blue hat and black shirt; Fenitra Andriampenomanana (Madagascar), green hat and grey shirt; and the driver.

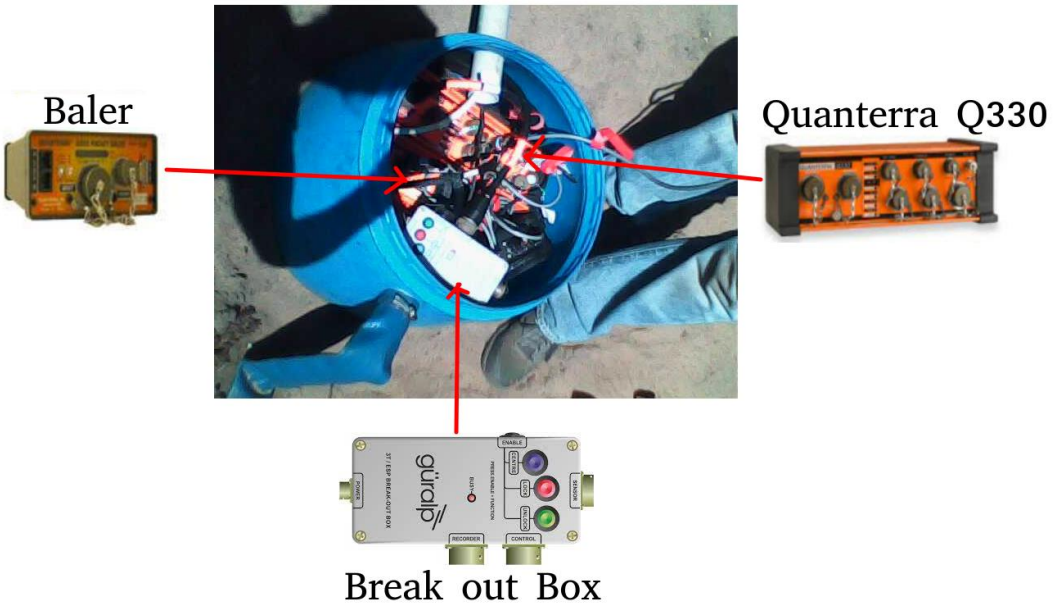

Figure 3. 5: A set of equipment inside the blue barrel (DAS – Power box-Batteries- Cables-PVC tube)

Table 3. 1: Seismic stations used in the study (Shown in Figure 3. 1).

Code	Start	End	Site	Latitude (deg)	Longitude (deg)	Altitude (m)	Station correction β (sec)
BROADBAND PERMANENT SEISMIC STATIONS ***GSN***							
ABPO	2007/04/04		Ambohimpanompo, Madagascar	-19.018	47.229	1528	0.043
GEOSCOPE							
FOMA	2008/09/01		Fort Dauphin, Madagascar	-24.9756	46.978	28	0.187
GEOFON							
SBV	2009/11/19		Sambava, Madagascar	-13.4584	49.921	65	0.087
VOI	2009/11/26		Vohitsoka, Madagascar	-22.0260	46.705	993	0.079
SHORT PERIOD PERMANENT STATIONS ***Madagascar National Seismic Network***							
ABM			Ambohimiarambe	-19.780	47.360	1894	0.0
AVY			Angavokely	-18.930	47.740	1807	0.02
OPO			Fihaonana	-18.570	47.190	1463	0.05
VTY			Vatovaky	-19.080	47.540	1453	0.05
MDSM			Mandiavato	-19.090	47.030	1524	0.04
FIRM			Firavahana	-18.700	46.880	1748	0.03
ATG			Ambohiby	-18.89	46.19	1541	0.19
TEMPORARY SEISMIC STATIONS ***MACOMO***							
AMPY	2012/08/15	2013/12/31	Ampanihy, Madagascar	-13.46	44.7436	252.4	0.001
ANLA	2011/09/21	2013/12/31	Analava, Madagascar	-24.98	49.4599	33.3	0.229
ANTS	2011/09/26	2013/12/31	Antsohihy, Madagascar	-14.8843	47.9993	12.2	0.168
BAEL	2012/08/11	2013/12/31	Bealanana, Madagascar	-14.5397	48.7467	1147.8	0.047
BAND	2012/08/05	2013/12/31	Malaimbandy, Madagascar	-20.3428	45.5964	178.6	0.058
BANJ	2012/08/10	2013/12/31	Ambanja, Madagascar	-13.6426	48.4537	17.3	0.00
BARY	2012/08/05	2013/12/31	Antanimbary, Madagascar	-17.1845	46.8571	265.7	0.028
BATG	2012/08/20	2013/12/31	Tsiroanamandidy, Madagascar	-18.8786	46.1871	1552.2	0.01
BERG	2012/08/06	2013/12/31	Port Berge, Madagascar	-15.58	47.6277	67.8	0.02
BITY	2012/08/04	2013/12/31	Ibity, Madagascar	-20.0608	47.0001	1566	0.07
BKTA	2012/08/11	2013/12/31	Beraketa, Madagascar	-24.1822	45.673	576	0.04
CPSM	2012/08/13	2013/12/31	Cap Ste. Marie, Madagascar	-25.5358	45.15	172.8	0.03
DGOS	2011/09/27	2013/12/31	Deigo Suarez, Madagascar	-12.2825	49.3606	33.5	0.20
LAHA	2011/10/06	2013/12/31	Antalaha, Madagascar	-14.9344	50.2911	11.1	0.06

LONA	2011/09/25	2013/12/31	Analavelona, Madagascar	-22.8057	44.2959	416.6	0.09
MAHA	2011/10/04	2013/12/31	Mahabo, Madagascar	-23.1714	47.6899	31	0.35
MAJA	2011/09/24	2013/12/31	Mahajanga, Madagascar	-15.7323	46.4263	35.7	0.14
MARO (replaced by KIRI	2011/10/01	2013/12/31	Marofandilia, Madagascar Kirindy, Madagascar	-20.1331 -20.0676	44.5515 44.5515	32.9 27	-0.01
MKVA	2012/08/23	2013/12/31	Makirovana, Madagascar	-14.1368	50.0608	19.6	0.03
MMBE	2011/09/28	2013/12/31	Morombe, Madagascar	-21.7501	43.3721	32	0.30
SOLA	2012/08/12	2013/12/31	Mandritsara, Madagascar	-15.8636	48.8263	316.8	0.08
TANS	2012/09/06	2013/12/31	Antananarivo, Madagascar	-18.9176	47.5511	1397.9	0.002
VATO (Replaced by MAGY)	2011/09/20	2012/01/18	Vatomandry, Madagascar	-19.3314 -19.3179	48.9824 48.9785	48.98 48.98	-0.36
VINA	2012/08/22	2013/12/31	Beravina, Madagascar	-18.1769	45.2247	293.8	0.05
ZAKA	2012/08/17	2013/12/31	Ambatondrazaka, Madagascar	-17.8471	48.423	814	0.001
ZOBE	2012/08/02	2013/12/31	Ankazobe, Madagascar	-18.1369	47.2289	1614.2	0.04
SELASOMA							
MS04	2012/04/28	2014/12/31	Madagascar	-23.1050	44.2199	439	0.46
MS07	2012/04/28	2014/12/31	Madagascar	-22.8124	44.8289	663	0.14
MS10	2012/05/04	2014/12/31	Madagascar	-22.4735	45.5668	972	0.23
MS12	2012/05/03	2014/12/31	Madagascar	-22.4374	45.9150	1038	0.17
MS16	2012/05/01	2014/12/31	Madagascar	-21.9357	46.5430	772	0.21
MS19	2012/05/07	2014/12/31	Madagascar	-21.4093	47.1028	1140	0.07
MS23	2012/04/27	2014/12/31	Madagascar	-21.3542	47.7780	254	0.12
RHUM-RUM							
EURO	2011/04/06	2013/12/09	Europa	-23.3440	40.3401	10	
GLOR	2011/04/08	2013/12/11	Grande Glorieuse	-11.5824	47.2895	4	
JNOV	2011/04/11	2013/12/09	Juan De Nova	-17.0543	42.7125	8	
MAYO	2011/04/15	2014/01/14	Mayotte	-12.8456	45.1868	41	
RUM1	2012/09/25	2014/08/31	Vohimasina-Madagascar	-22.8022	47.7175	45	
RUM2	2012/09/23	2014/08/31	Manakara-Madagascar	-22.1367	48.0022	11	
RUM3	2012/09/27	2014/08/30	Manambondro-Madagascar	-23.7988	47.5459	8	
RUM4	2012/09/28	2014/08/29	Manenterina-Madagascar	-24.2767	47.3157	15	
RUM5	2012/09/30	2014/08/27	Mahatalaky-Madagascar	-24.7852	47.0851	21	
TROM	2011/04/23	2013/12/16	Tromelin	-15.8885	54.5218	6	

The data from all MACOMO stations were manually collected. Fenitra Andriampenomanana and I made a field trip to service all operational seismic stations every six months. Three main functions were performed during the visit to each station:

1. The signals recorded since the previous service were retrieved,
2. Any problems or damage were identified and fixed, and
3. Consumables such batteries and DAS data cards were replaced.

The following equipment was taken on the service trip:

- Spare sensors, data loggers, and solar panels,
- Serial cable for Q330,
- Clié palmtop computer,
- New memory card or baler,
- Hot-timing cable,
- Power supply, and
- Serial cable for RT-130.

The first task on arrival at a site was to check the voltage of the solar panels and batteries. An example of service visit is shown in Figure 3. 6. Raw data stored in the baler (orange box) are then transferred into an external disk using a laptop. These data were recorded under seismic network code "XV". The six stations that malfunctioned or were vandalized are listed in Table 3. 2. All stations were serviced prior to removal at the end of the experiment in 2013. Researchers from the USA and Madagascar were divided into two demobilization teams; I worked with the team that serviced stations in northern Madagascar.



Figure 3. 6: Field servicing by Tsiriandrimanana Rakotondraibe and Fenitra Andriampenomanana in the SOLA station in northern Madagascar. This station had a problem with the data acquisition system (DAS). We tested the Quanterra and replaced it.

Table 3. 2: Stations that failed or were vandalized, 2011-2013.

STATION	SITE CONDITION	SERVICE DATA & ACTION
VATO	Solar panels stolen	2012; moved to MAGY
MARO	One solar panel stolen	2012; moved to KIRI
ANTS	Sensor broken, covered by water	May 2013; replaced sensor.
ANLA	Sensor broken	June 2012; replaced sensor.
SOLA	Q330 broken	June 2013; replaced data logger.
BANJ	Solar panels stolen	June 2013; removed station.

3.1.3.2 SELASOMA and RHUM-RUM projects

From 2012 to 2014, the SEismological signatures in the Lithosphere/ Asthenosphere system of SOuthern MAdagascar (SELASOMA) project deployed 25 temporary broadband seismic stations along a linear array that stretched coast-to-coast across the Ranotsara shear zone (the profile trends in a SW-NE direction across the southern part of the island, (Figure 3. 1) and 23 short-period stations distributed in the southeastern part of Madagascar (Tilmann et al., 2013) (Table 3. 1) (http://www.gfz-potsdam.de/en/section/seismology/projects/madagascar/). Only

seven of the 25 SELASOMA broadband stations were used for this work (*viz.* MS04, MS07, MS10, MS12, MS16, MS19 and MS23). In addition to these stations, 10 stations deployed by the Réunion Hotspot and Upper Mantle – Réunions Unterer Mantel (RHUM-RUM) project (Barruol and Sigloch, 2012) were also used in this present study (TROM, GLOR, EURO, MAYO, JNOV, RUM1, RUM2, RUM3, RUM4, and RUM5) (Figure 3. 1).

In conclusion, data from a total number of 56 temporary and permanent seismic stations were used in this study: four broadband permanent stations, seven short-period permanent stations, 28 from the MACOMO project, seven from the SELASOMA project, and 10 from the RHUM-RUM project (Figure 3. 1, Table 3. 1). The periods during which they operated are summarized in Figure 3. 6.

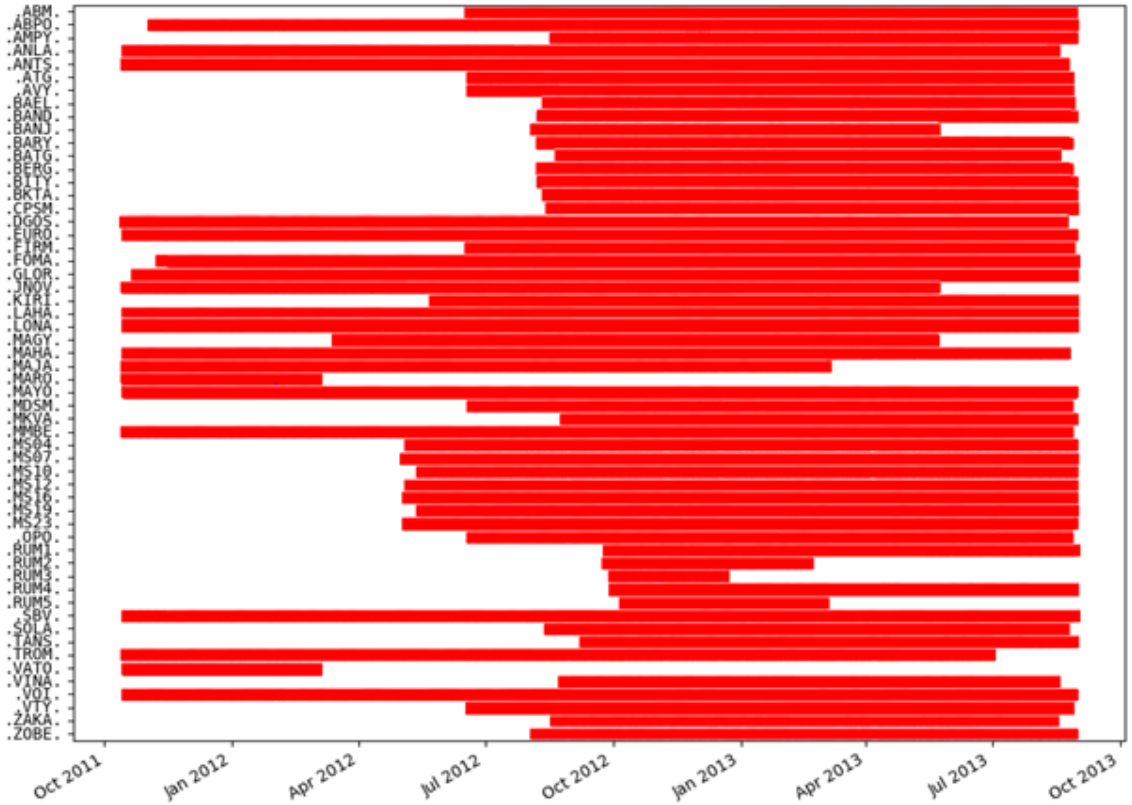

Figure 3. 7: Histogram showing data collected from MACOMO, local permanent, SELASOMA, and RHUM-RUM seismic stations.

3.2 Methodology

3.2.1 Completeness of the catalogue

The determination of the completeness of a catalogue is a typical problem for seismic hazard study. A method developed by Stepp (1972) was used. The completeness is estimated from the earthquake catalogue by plotting the cumulative number of events of a certain magnitude range versus time. In each magnitude bin, the cumulative number of events is evaluated for various time windows, and then the variation (sigma) is calculated. Then the period during which the data follows the trend parallel to the $1/T^{1/2}$ line is the completeness period of that magnitude class.

3.2.2 Declustering method

In seismic hazard calculation, declustering analysis is very important to ensure that earthquakes are independent of any other. The declustering method aims to remove earthquakes that occur in clusters such as foreshocks, aftershocks and swarms. Calculation of the declustering effect was done using statistical analysis in which earthquake clusters are grouped by their proximity in space and time.

In this work, we applied the declustering calculation using the ZMAP program (Wiemer, 2001). Declustering method is used in this study in order to remove seismic events from a sequence and to divide earthquakes catalogs into dependent and independent events and also the declustering method is considered as a potential source of bias in seismic hazard studies. Foreshocks and aftershocks were removed in order to underestimate the annual rates of the earthquake events which associate with the low seismic hazard.

Several approaches are developed to apply the declustering method. For example

- The Gardner and Knopoff (1974) method was proposed to identify aftershocks and foreshocks within seismicity catalogues based on the distances inter-event in time and space. The method consists of providing

specific space-time distances as a function of the mainshock magnitude in order to identify the aftershocks

- The approach that applies Reasenberg (1985) algorithm to eliminate all events that fall within specified space and time interval of main shocks and the approach that applies the Gardner and Knopoff (1974) algorithm that uses predefined windows in space and time to identify independent and dependent seismicity.

The Reasenberg (1985) approach required the following parameters to be set:

- Minimum and maximum look-ahead time (TAUMIN and TAUMAX).
- Probability of detecting the next event as dependent to the sequence (P_1).
- Increase of lower cut-off magnitude (XK).
- Effective lower magnitude cut-off for the earthquake catalogue (XMEFF).
- Number of crack radii surrounding each earthquake for new events to be considered part of the cluster (RFACT); and
- Epicenter and depth errors

(http://terra.geociencias.unam.mx/~ramon/ZMAP/chap7.htm).

We introduced all raw data from the catalog into a text file and used it as input for the program; then we ran the program by selecting “Decluster the catalog” from the “Tools” in ZMAP. In this study, we applied both declustering methods, Gardner and Knopoff, and Reasenberg, as these are the most frequently used approaches for seismic hazard studies.

The CRISIS software comprises several modules, *viz*:

1. Inclusion of the earthquake recurrence model such as Gutenberg-Richter model or Poisson model, earthquake characteristics model, the non-Poisson model and the gridded seismicity model.
2. Geometry of the source
3. Models of the attenuation
4. Measure of the spatial integration:

The spatial integration is determined by considering the source as comprised of area sources, and the seismicity is distributed by unit of area. This spatial integration is based on subdividing the original source in order to get accurate hazard value.

The Poisson model is widely used to describe the earthquake probability distribution. It is used to determine the likelihood that an earthquake greater or equal to a given magnitude will occur in a given time period. In this study a Poisson process was applied to establish the seismic hazard assessment in order to fit the frequency-magnitude distributions.

A discrete probability distribution for number of earthquakes in a determined interval of time is called Poisson distribution (Ranganathan, 1940) and defined by the following formula:

$$P(X = x) = e^{-\lambda}\frac{\lambda^x}{x!} \tag{3.1}$$

with X is the number of events in a given interval, λ the distribution parameter or the expected number of events in the interval and $x = 0, 1, 2, 3, 4, \ldots$

3.2.3 Seismic source zone

Seismic area source zones are regions with similar levels of earthquake activity, which is described by the earthquake frequency-magnitude distribution. Generally, area source zones are defined by taking account of the lithospheric structure, tectonic history, and instrumental, historical and paleoseismic studies of seismic activity. In the central areas of Madagascar (Ankaratra, Alaotra, Famoizankova) the study of the lithosphere of Andriampenomanana et al. (2017) was very useful, while in the northern and southern areas we used various published geological maps.

3.2.4 Earthquake catalogue

The catalogue of 18,970 events used in this study was compiled from historical data, instrumental data listed in the bulletins of the Madagascar National Data

Centre (1975-2016, 18,275 events) mostly derived from a network of short-period seismometers concentrated in the center of the island, and earthquakes recorded by the MACOMO temporary array (2011-2013, 695 events). The data in the catalogue included information on the origin time (year, day, hour, minute and second), epicentral coordinates and magnitude of each seismic event.

All duplicate and dependent seismic events such as seismic swarms and aftershock sequences, were removed after using ZMAP software package (Wiemer, 2001) by following the declustering algorithm developed by Reasenberg (Reasenberg, 1985).

3.2.5 Magnitude homogenization

The size of an earthquake can be measured in various ways. For example, observations of damage are indicators of the intensity of shaking of the Earth's surface that can be applied to deduce the size of the earthquake. The length and throw of the earthquake rupture are indicators of the work done by the earthquake, and seismograph measurements of the duration of shaking and the distance-corrected amplitude of the ground motion can be used to estimate the amount of energy released by the earthquake.

Various magnitude scales are used to report the 'size' of earthquakes depending on the instrument used, the vintage of the recording, and the distance from the focus *e.g*. local magnitude M_L, body wave magnitude m_b, moment magnitude M_w. In order to accurately analyse seismicity data to produce recurrence parameters, it is necessary to convert the reported magnitudes to a single magnitude scale. The M_w scale (Hanks and Kanamori, 1979) was usually chosen as it is also compatible with the GMPEs for the earthquake hazard assessment, and it does not saturate at large magnitudes.

Numerous studies have investigated the conversion of various magnitude scales to moment magnitude. For example, Das et al. (2012) determined relationships

between m_b and M_s with M_w using linear regression based on data acquired in northeast India between 1978 and 2006; Grünthal et al. (2009) used Chi-square maximum likelihood regression techniques to determine magnitude relationships and quantified errors and uncertainties by calculating the 68% confidence bounds; while Hussein et al. (2008) used orthogonal regression to account for uncertainties in the various magnitude measures and Scordilis (2006) who described a relation between M_s and m_B with M_w (See section 2.4.4).

In this work, we applied the method developed by Scordilis (2006) (see Chapter 2) for the conversion of M_s and m_B to the moment magnitude M_W. While for the conversion of M_L to M_w, we applied the amplitude spectra measurement method from some earthquakes that have clear signals from the recorded data (See Appendix H)

M_w and M_L relation from GSN, GEOSCOPE, GEOFON and MACOMO data

Ideally, we would like to calibrate and homogenise the Malagasy NDC bulletin using earthquake magnitudes validated by the International Seismological Centre (ISC). Earthquakes in the Malagasy NDC bulletin are described in terms of local, surface wave and body wave magnitude types, which depend on the characteristics of the seismic stations used to determine the magnitude *e.g.*, temporary, permanent, short period and long period stations.

To homogenize the identified magnitude into moment magnitude, we decided to apply the following steps:

a. We first selected seismic events during the period 1975-2016 that are recorded at the ISC bulletin (http://www.isc.ac.uk/cgi-bin/web-db-v4?request=COMPREHENSIVE&out_format=CATCSV&searchshape=RECT&bot_lat=-26&top_lat=-12&left_lon=42.5&right_lon=50&ctr_lat=&ctr_lon=&radius=&max_dist_units=deg&srn=&grn=&start_year=1975&start_month=1&start_day=01&start_time=00

%3A00%3A00&end_year=2016&end_month=12&end_day=31&end_time=00%3A00%3A00&min_dep=&max_dep=&min_mag=&max_mag=&req_mag_type=Any&req_mag_agcy=&include_links=on). This contributed about 70 seismic events. Events from the MACOMO bulletin were added (See Table 6. 1). The ISC bulletin included m_b, M_S, M_L magnitude values, so it was necessary to transform all these values to M_W using the global relations between Mw and m_b and Mw, M_S developed by Scordilis (2006) as mentioned previously (See Chapter 2).

b. Then we selected 11 earthquakes from the MACOMO bulletin in order to determine the moment magnitude values using the spectral amplitude method of Hanks and Kanamori (1979) (See Chapter 2 and Appendix H).

d. Finally we determined a linear regression that gives the final relation between M_w and M_L. Data from about 80 earthquakes were used to establish a reliable relation between moment magnitude and local magnitude values. Characteristics of the data are shown in Table 6. 1. The following criteria were used to select the events for the calculation:

1. The distance between the event and stations was not excessive, with a signal-to-noise ratio that allowed reliable measurements of the peak amplitude (Figure 3. 8) and the spectral plateau for estimates of M_L and M_w, respectively.
2. Earthquakes with magnitude (M_L, m_b, M_S) between 4 and 5 recorded at the ISC bulletin, including data from the National Data Center in Madagascar between 1975 -2016 (Figure 3. 9).
3. For the 11 selected events from MACOMO bulletin, earthquakes were recorded at least five widely-distributed stations (including MACOMO, permanent broadband and short period), providing good azimuthal coverage (Figure 3. 10).

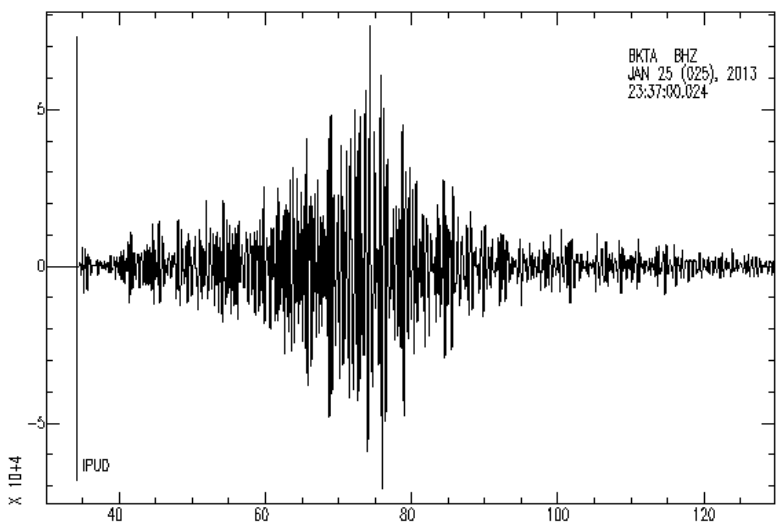

a.Recorded waveform in the station BKTA for the event on 01 January 2013

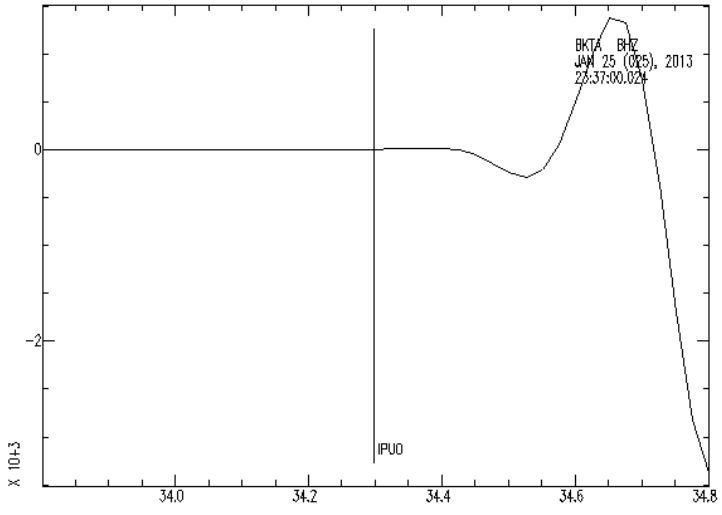

b. Cut waveform from 0.5 s before the P-arrival (IP0) and 0.5 after the arrival

Figure 3. 8: Characteristics of the waveform from signal-to-noise ratio that allowed reliable measurements of the peak amplitude and the spectral plateau for estimates of M_L and M_W

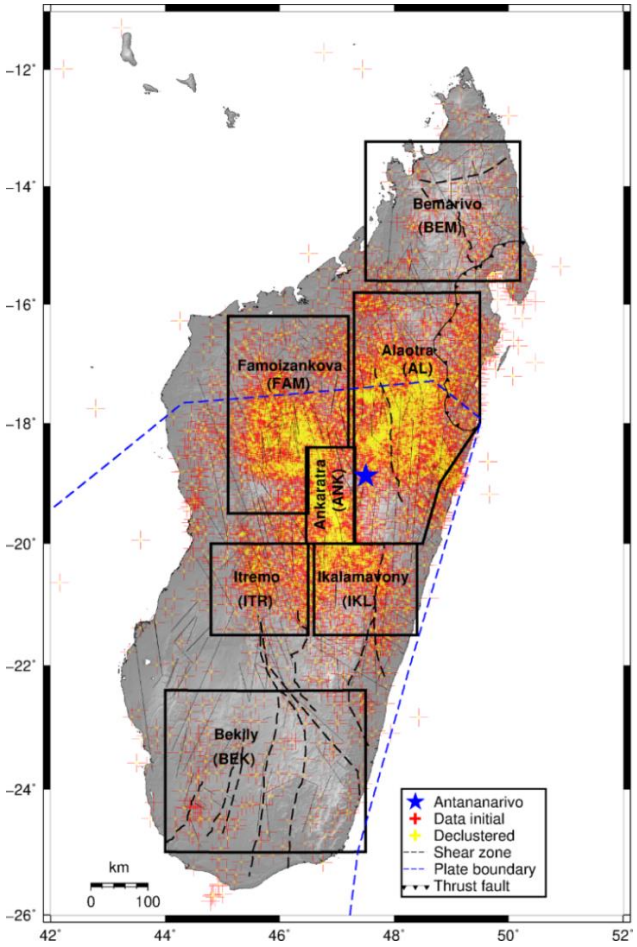

Figure 3. 9: Topographic map of Madagascar with 18,970 earthquakes from the combined MACOMO and Madagascar NDC catalogue between the time periods 1975-2016 (red + symbol) and the 11,950 events after declustering (yellow + symbol) and the blue star shows the main town of Madagascar.

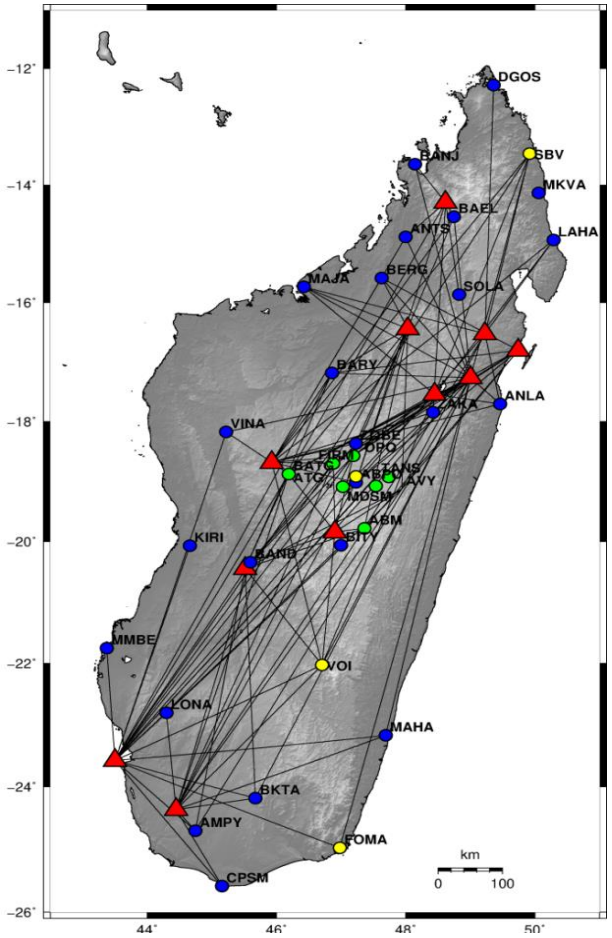

Figure 3. 10: Earthquakes and seismic stations used to determine M_W. Blue circles - temporary MACOMO stations; yellow circles - permanent broadband GSC, GEOFON and GEOSCOPE stations, green circles permanent short period stations; red triangles - selected large earthquakes used to determining M_W. Solid lines represent event-station paths joining the events and stations.

Chapter 4: Seismotectonics of Madagascar

4.1 Introduction

Previous seismotectonic studies of Madagascar were carried out using earthquake data recorded by the few local permanent stations (*e.g.*, Poisson, 1924, 1930; Bertil and Regnoult, 1998; Rindraharisaoa et al., 2013). Central Madagascar is relatively well studied, mainly because it is more seismically active than the rest of the island and that the seismic station distribution in this region is reasonably good. An extensional faulting regime was found to exist in the central region (Bertil and Regnoult, 1998). Some studies sought to explain how Madagascar experienced magmatic events during the Cenozoic Era, even though it is remote from active plate boundaries. Mantle upwelling was recently identified beneath the Central, Northern and Southern Madagascar Alkaline Provinces (CMAP, NMAP and SMAP, respectively), and likely contributes to the seismicity, especially in the central region of the island (Pratt et al., 2017).

The work in this study contributes to the development of the seismotectonic model of the whole of Madagascar. Data obtained from recent deployments of MACOMO, some SELASOMA temporary stations and the existing permanent stations between 2011 and 2013 were used. Additional data from seismic station from the RHUM-RUM project and from the National Data Center were also used. Results from this thesis yield a new seismicity map for Madagascar, with new information particularly in the southern and northern regions. Fault plane solutions were determined where the azimuthal coverage and signal to noise ratio was adequate. The relationship between earthquake epicenters, fault plane solutions, and known faults and shear zones was explored.

This chapter shows the brief results of the earthquake spatial distribution including focal mechanism solutions and the magnitude calibration for Madagascar. Discussion and conclusions of the results are also presented. Findings in this chapter have been published in Tectonophysics (see Appendix A) as:

Tsiriandrimanana Rakotondraibe, Andrew A. Nyblade, Michael E. Wysession, Raymond J. Durrheim, Gérard Rambolamanana, Ghassan I. Aleqabi, Patrick J. Shore, Martin J. Pratt, Fenitra Andriampenomanana, Georg Rümpker, and Elisa Rindraharisaona. *The seismicity and seismotectonics of Madagascar revealed by 2011-2013 island-wide broadbdand seismic networks. Tectonophysics*, 2020, vol. 790, p. 228547.

4.2 Seismicity

4.2.1 Location of earthquakes

The HYPOELLIPSE program (Lahr, 1979) was used to determine the hypocenters of 695 seismic events in Madagascar (Figure 4. 1) recorded by the MACOMO network (Figure 4. 1). Thereafter, the HYPODD software (Waldhauser and Ellsworth, 2000) was used to relocate and to identify clusters of seismic events after grouping seismic events according to regions. Four hundred and twenty-two events were relocated using HYPODD. A model of the average velocity structure, calculated using the results from Andriampenomanana et al. (2017), was used for both HYPOELLIPSE and HYPODD computations. Examples of an input file for HYPOELLIPSE and HYPODD are shown in APPENDIX A.

The distribution of the depth from the 695 local earthquakes was investigated. It was identified that nearly 85% of the earthquakes were in the middle crust *i.e*., at depths between 10 and 25 km (Figure 4. 2 a). The estimated average error from HYPOELLIPSE is less than 5 km. HYPODD double-difference relocation of 422 events (Figure 4. 2 b) reduced the average error to less than 1 km.

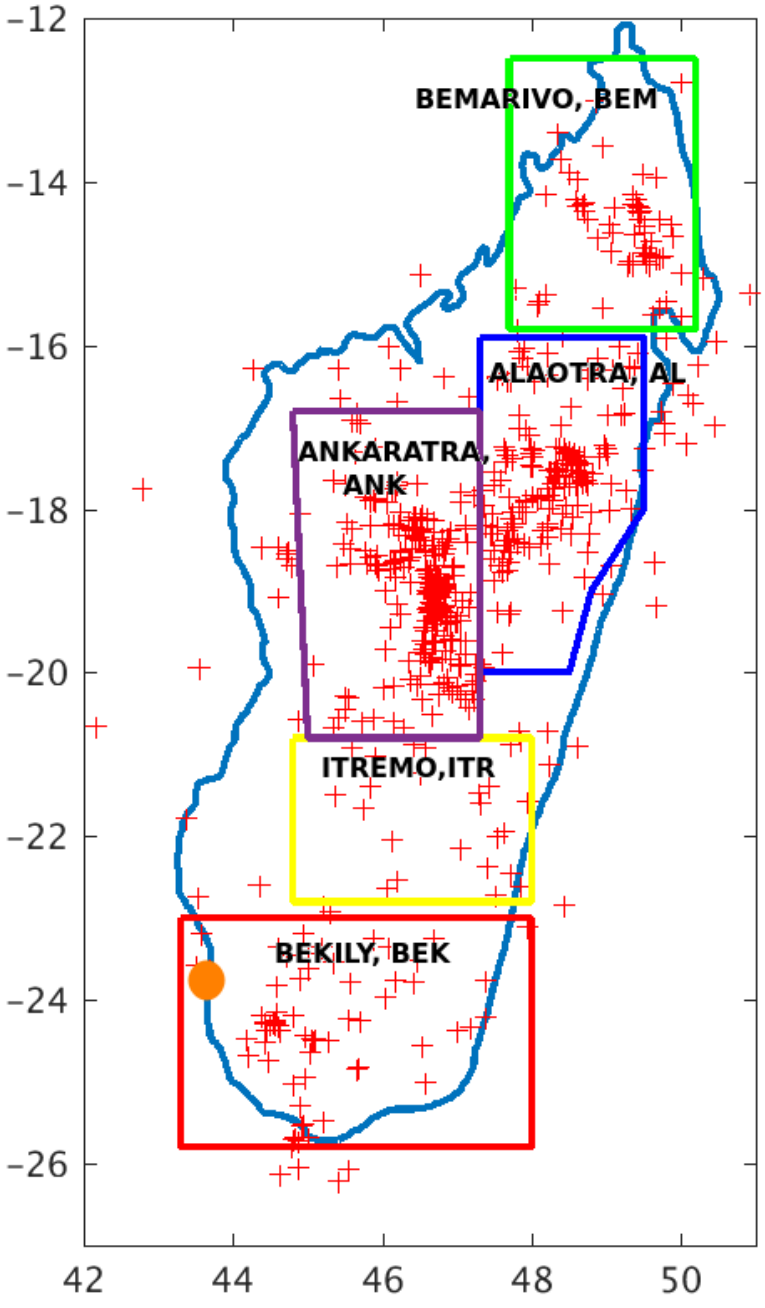

Figure 4. 1: Seismicity map for Madagascar using data from the MACOMO project. Red plus symbols (+) represent the location of all 695 earthquakes; rectangles the area source zones; and the orange circle an offshore earthquake with M5.3 on 25 January 2013.

(a)

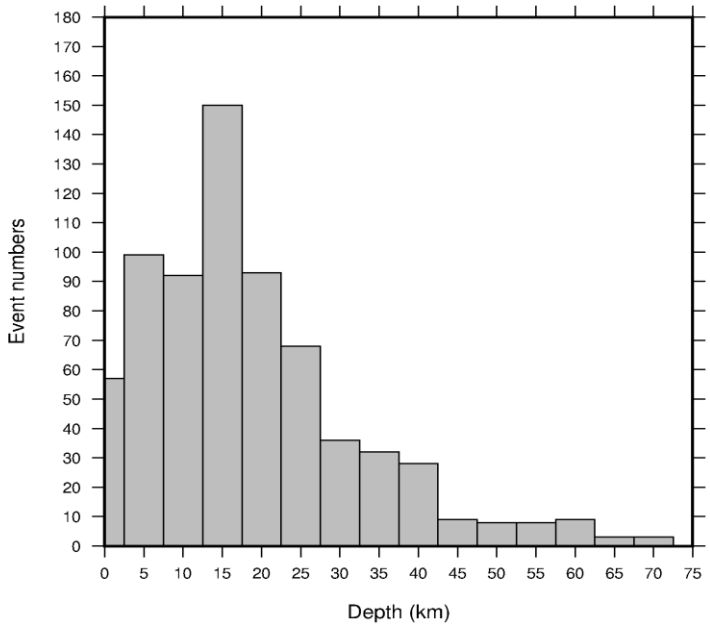

(b)

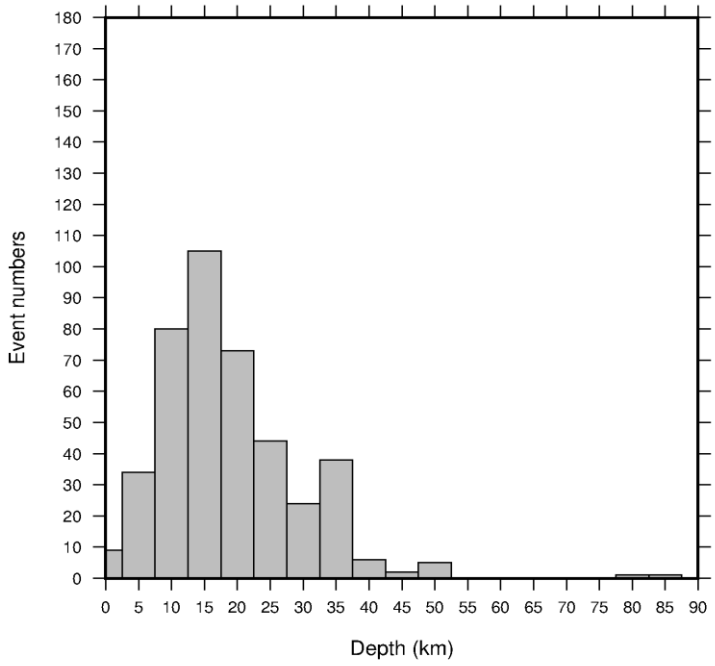

Figure 4. 2: Computed depth distributions from (a) HYPOELLIPSE program (for 695 events) and (b) HYPODD program (for 422 events)

In addition, to assist in efforts to improve the determination of earthquake source parameters, earthquake magnitude calibration was conducted following the Gutenberg-Richter method (Gutenberg and Richter, 1942) to obtain a local magnitude relation for Madagascar. The magnitude calibration is presented in section 4.4 below. The results of the analysis of seismicity in each region of Madagascar are presented below, and the earthquake catalogues are presented in APPENDIX C.

4.2.2 Northern region

The northern part of Madagascar, referred to as the Bemarivo region, has a low level of earthquake activity (Figure 4. 3). A total number of 67 events were identified and analyzed using the HYPOELLIPSE program, and 34 of them were relocated using the double difference method.

Correlation between the seismic distribution and existing tectonic features is observed (Figure 4. 3), with several seismic events located near the Sandrakota shear zone in the Ankaizina zone and Andaparaty thrust zone in the northernmost part of Antananarivo block, which are indicated as the two blocks BEM1 and BEM2 in Figure 4. 3. The BEM1 zone has 9 events while the BEM2 has 25 events. Relocation using HYPODD shows a shift from west to east of the epicenters in BEM1 compared to those obtained using the HYPOELLIPSE program (Figure 4. 3). Three seismic events with magnitude between M3 and M4 are observed, whilst the remaining events have magnitude values less than M3. Seismic event depths are shallow, not exceeding 45 km after the relocation calculation.

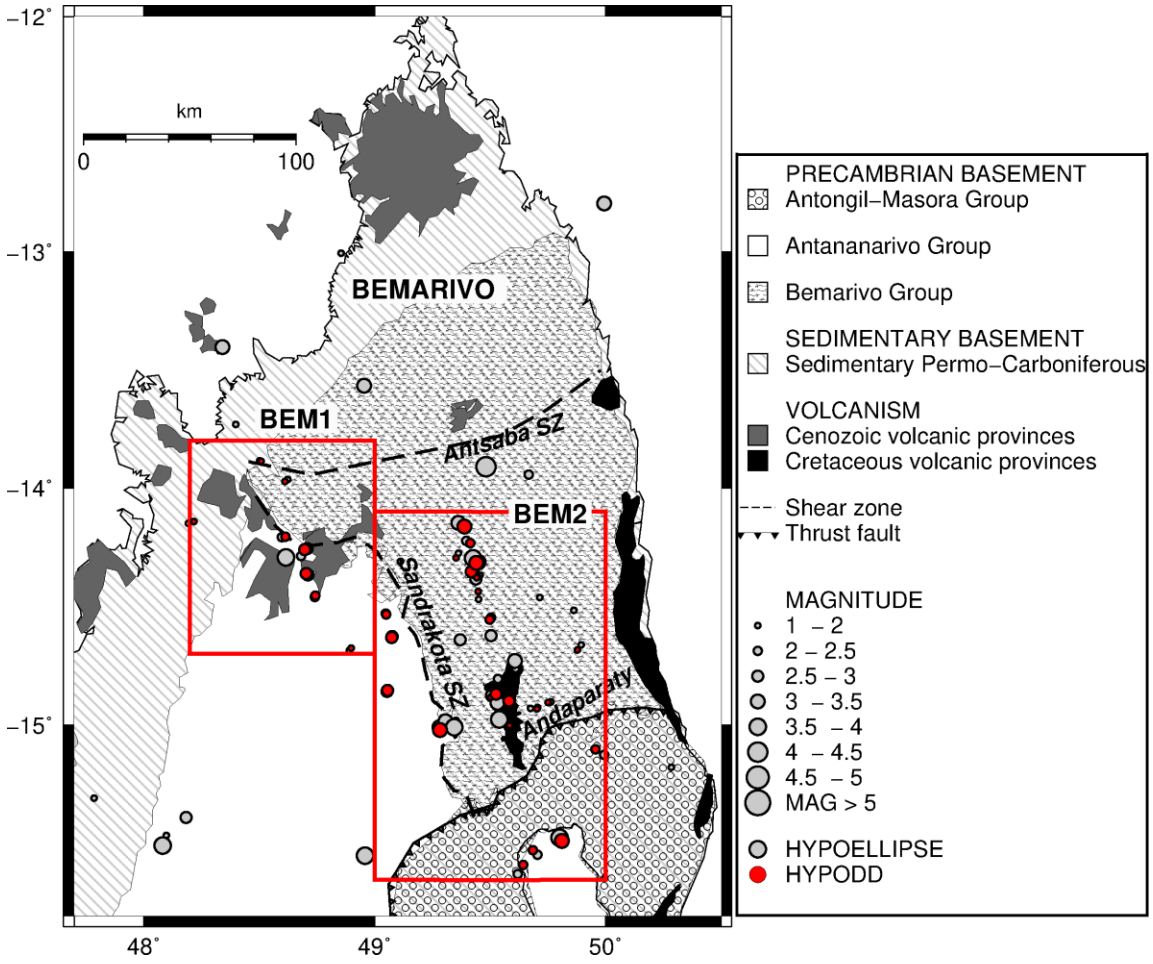

Figure 4. 3: Earthquake distribution in Bemarivo area. Locations by HYPOELLIPSE (grey circles) and the HYPODD double-difference relocation method (red circles).

4.2.3 Central region

Central Madagascar is the most seismically active area in the island, particularly in Alaotra, Ankaratra and Itremo areas, which are discussed below.

4.2.3.1 Alaotra area

From this present study, seismic clusters are observed in the Alaotra region (see Figure 4. 4); 204 earthquakes are concentrated around the known faults. Earthquake

magnitudes ranged from M1 to M4.3 (see Figure 4. 4). After applying the double difference relocation using HYPODD program, 123 events were relocated (See Figure 4. 4). Relocation from HYPODD program is based on minimizing the residual between observed and theoretical travel time measurements for pairs of earthquakes at each station that link together all observed event station pairs. The effect of relocation is the formation of several clusters and a reduction in the average horizontal and vertical errors and uncertainty values. Four clusters of earthquakes are observed after the relocation (Figure 4. 4). The first cluster (AL1) is in the Cretaceous volcanic zone; the second and fourth clusters (AL2 and AL4) are parallel to the direction of the known existing faults; and the third cluster (AL3) is closely associated with known faults. From the observed earthquake location, seismic activities occurred far from the fault zones which could be explained as a possibility of unmapped or even new fault zones (See AL2 and AL4)

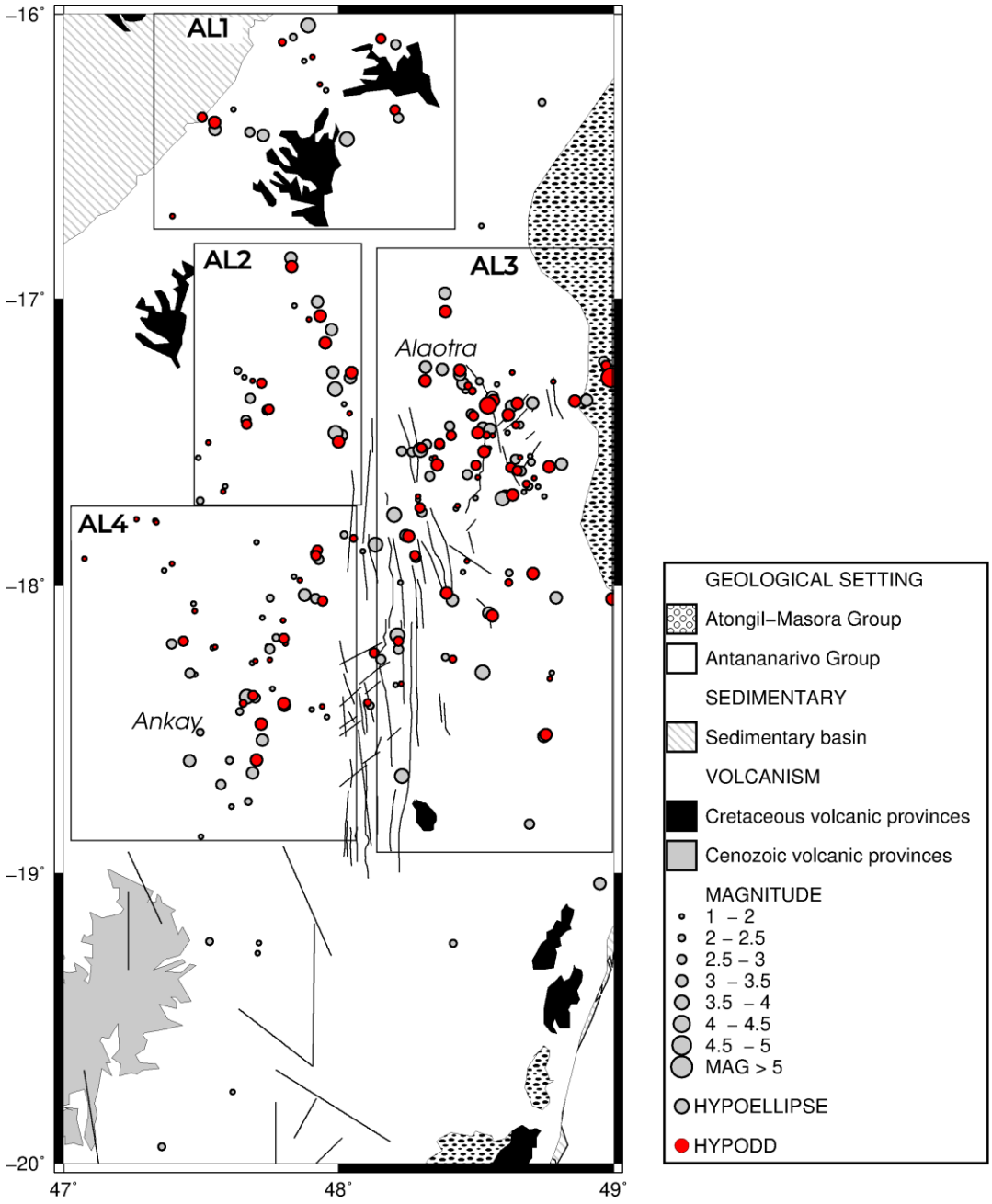

Figure 4. 4: Earthquake distribution in Alaotra area. Grey circles are earthquake locations obtained from HYPOELLIPSE, and red circles are obtained from HYPODD double-difference relocation method. AL indicates the Alaotra region. Grey squares highlight the four subzones for double difference relocation.

4.2.3.2 Ankaratra - Famoizankova area

Lake Itasy and the main volcanic zone of Ankaratra are found in this region. The Lake Itasy is located at about 58 km from the main town of Antsirabe (Figure 4. 5). From the results of this present work, this region appears to be the most active area in the country. A total number of 313 earthquakes were identified and located using HYPOELLIPSE; 228 of them were relocated using the HYPODD program. Two main clusters were identified: the first cluster (ANK1) lies NW of the Lake Itasy, and the second cluster (ANK2) is mostly aligned in a NS direction which is parallel to the main Cenozoic volcanic feature of Ankaratra.

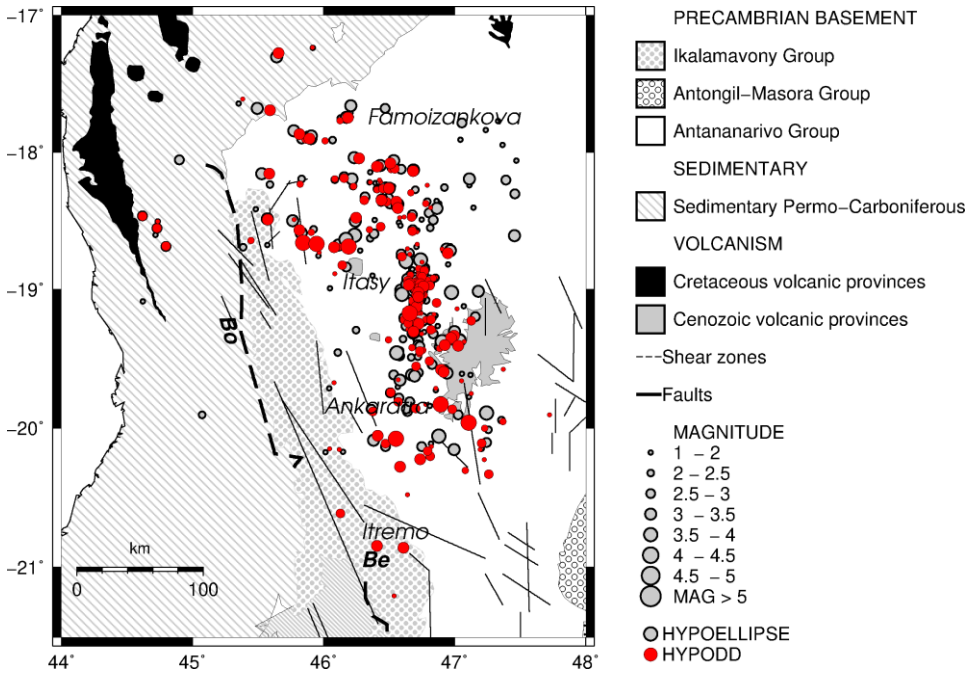

Figure 4. 5: Earthquake distribution in the Ankaratra area. Locations from HYPOELLIPSE (grey circles) and the effects of event relocation by the HYPODD double-difference relocation method (red circles).

4.2.3.3 Itremo area

Our study recorded only 26 earthquakes in the Itremo region (Figure 4. 6). They were located using HYPOELLIPSE. Their epicentres are scattered and hence not amenable to relocation using the double difference method.

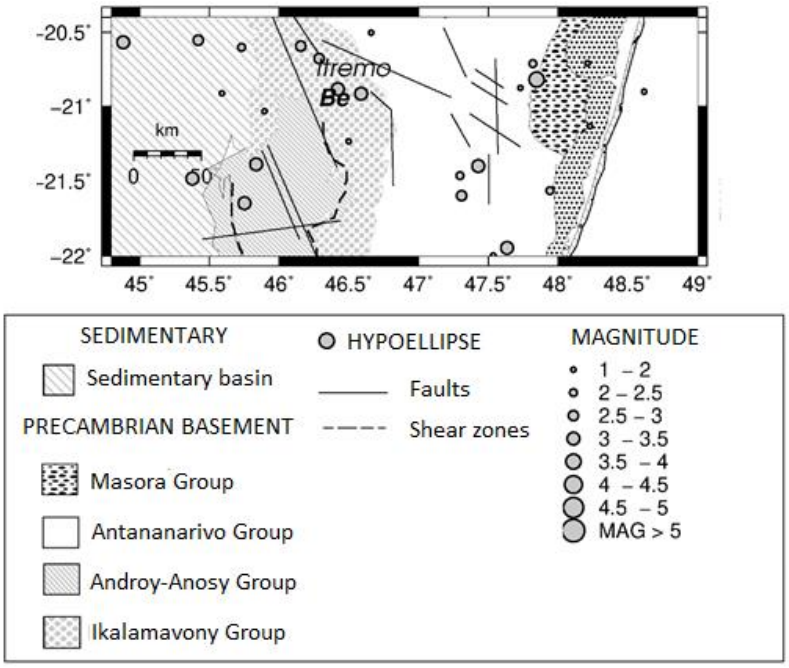

Figure 4. 6: Earthquake distribution in the Itremo area (ITR). Locations from HYPOELLIPSE (gray circles). Be indicates the Bekily shear zone

4.2.4 Southern region

In this current study, earthquake activity appears lower in southern Madagascar when compared to the other regions. Most of the 83 detected seismic events have magnitudes less than M5.3. Three clusters are observed, *viz.* BEK1, BEK2, and BEK3 (Figure 4. 7) and composed of 37 relocated earthquake events. The HYPODD program located some events along the Ampanihy shear zone (about four earthquakes), and three of them moved far from the individual location while some are grouped inside the selected zone. Other seismic events were also observed within the Bekily, the Vohibory and Anosy groups. The magnitudes range from M1.2 to M4.2, except for a M5.3 offshore event on 25 January 2013 (Figure 4. 7).

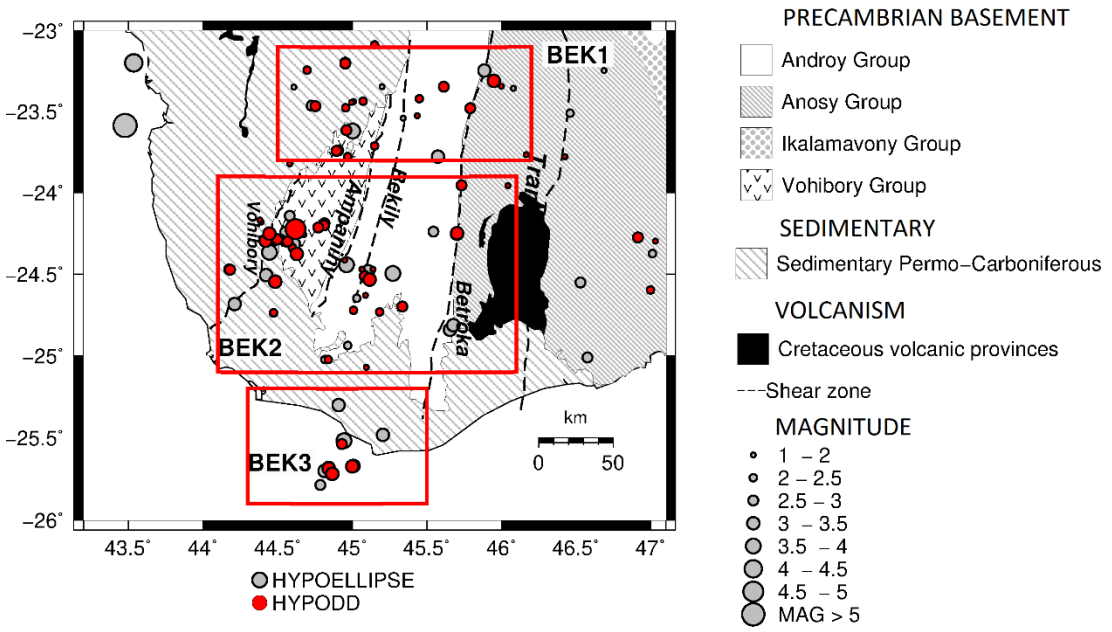

Figure 4. 7: Map showing the earthquake distribution in Bekily area (BEK) from HYPOELLIPSE (grey circles) and the effects of event relocation by the HYPODD double-difference relocation method (red circles). Red squares show the zones of the clustered events for the three sub-zones (BEK1, BEK2, BEK3) for the HYPODD relocation.

4.3 Focal mechanisms

4.3.1 Computation

The FOCMEC program (Snoke, 1984), described in Chapter 2, section 2.6.4, was used to compute the fault mechanisms. FOCMEC conducts a grid-search of the solution space to find all acceptable solutions. The fault plane solution for each selected earthquake is described in terms of the strike and dip of the nodal planes (one the fault plane, the other the auxiliary plane); and the rake of the slip vector. Examples of an input file and a summary of all steps used to obtain the focal mechanism are contained in APPENDIX D.

Fault plane solutions were determined for 23 local earthquakes that had at least eight clear P-wave and S-wave first motion polarities and good coverage of the focal sphere. Earthquake depth is an important parameter for the computation of the focal mechanism as it is used to calculate the take-off angle and hence the position of the station on the focal sphere. Thus, a great deal of effort was devoted to assessing the reliability of the depth calculation. HYPOELLIPSE was run for a range of fixed depths and the residual error plotted to confirm the reliability of the solutions (Figure 4. 8). In some cases, the depth is very well constrained (*e.g.*, events 1 and 17), while in other cases (events 13 and 21) only the shallower depth limit was well constrained.

The 23 focal mechanism solutions are shown in Figure 4. 9 and discussed in the next section.

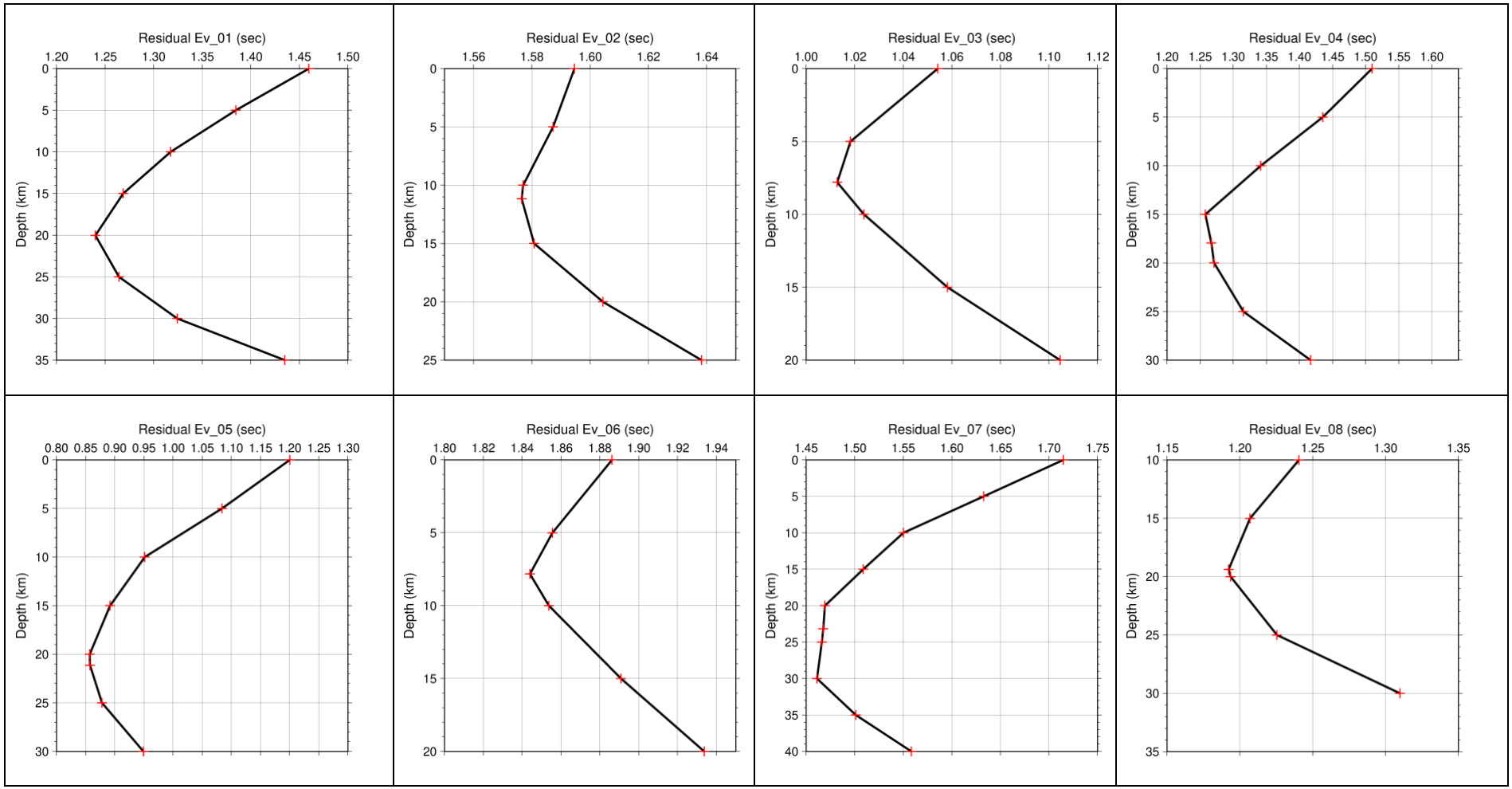
Residual Ev_01 (sec)
1.20 1.25 1.30 1.35 1.40 1.45 1.50
Depth (km)
0 5 10 15 20 25 30 35
Residual Ev_02 (sec)
1.56 1.58 1.60 1.62 1.64
Depth (km)
0 5 10 15 20 25
Residual Ev_03 (sec)
1.00 1.02 1.04 1.06 1.08 1.10 1.12
Depth (km)
0 5 10 15 20
Residual Ev_04 (sec)
1.20 1.25 1.30 1.35 1.40 1.45 1.50 1.55 1.60
Depth (km)
0 5 10 15 20 25 30
Residual Ev_05 (sec)
0.80 0.85 0.90 0.95 1.00 1.05 1.10 1.15 1.20 1.25 1.30
Depth (km)
0 5 10 15 20 25 30
Residual Ev_06 (sec)
1.80 1.82 1.84 1.86 1.88 1.90 1.92 1.94
Depth (km)
0 5 10 15 20
Residual Ev_07 (sec)
1.45 1.50 1.55 1.60 1.65 1.70 1.75
Depth (km)
0 5 10 15 20 25 30 35 40
Residual Ev_08 (sec)
1.15 1.20 1.25 1.30 1.35
Depth (km)
10 15 20 25 30 35

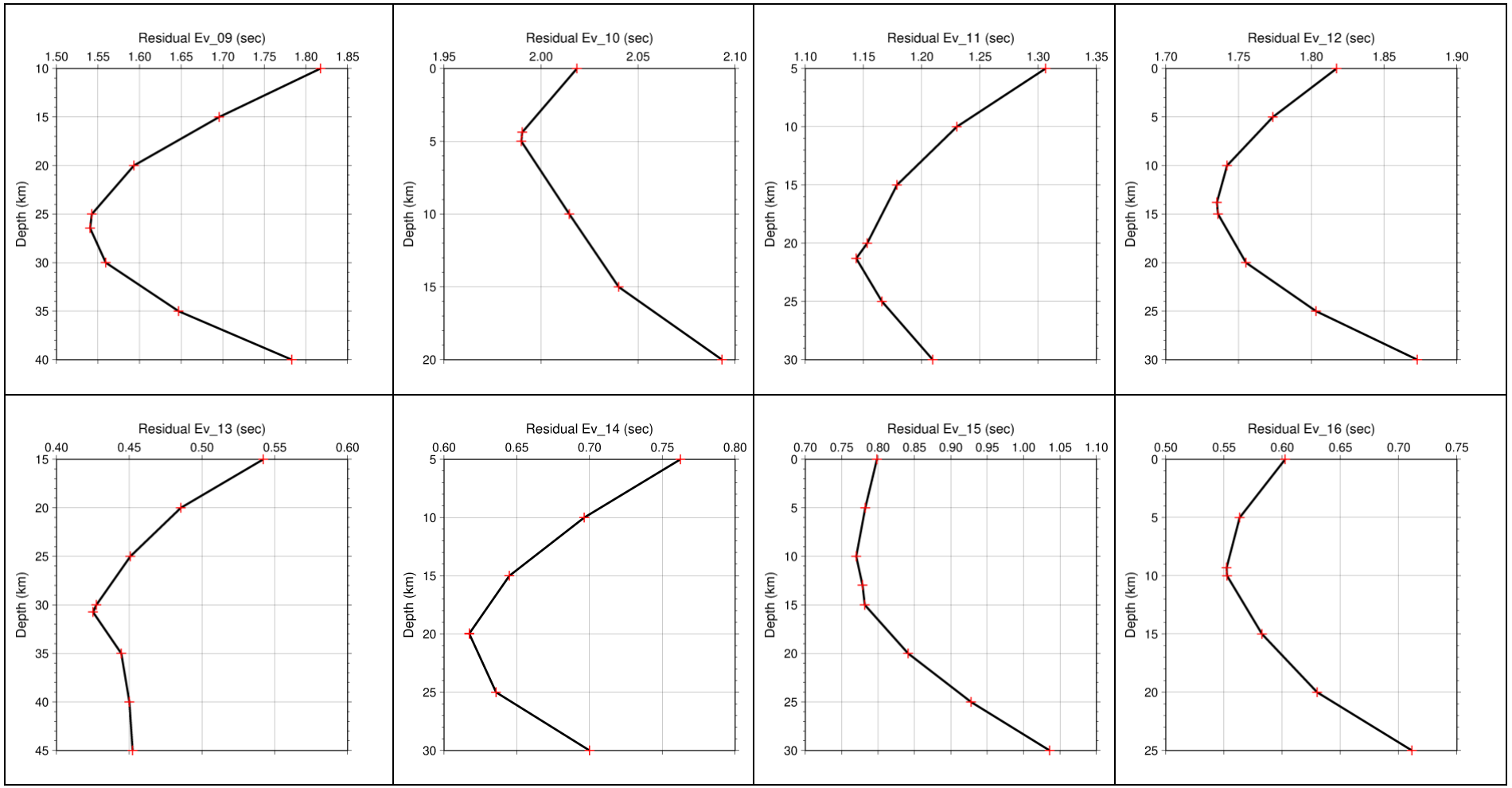
Residual Ev_09 (sec)
1.50 1.55 1.60 1.65 1.70 1.75 1.80 1.85
10 15 20 25 30 35 40
Depth (km)
Residual Ev_10 (sec)
1.95 2.00 2.05 2.10
0 5 10 15 20
Depth (km)
Residual Ev_11 (sec)
1.10 1.15 1.20 1.25 1.30 1.35
5 10 15 20 25 30
Depth (km)
Residual Ev_12 (sec)
1.70 1.75 1.80 1.85 1.90
0 5 10 15 20 25 30
Depth (km)
Residual Ev_13 (sec)
0.40 0.45 0.50 0.55 0.60
15 20 25 30 35 40 45
Depth (km)
Residual Ev_14 (sec)
0.60 0.65 0.70 0.75 0.80
5 10 15 20 25 30
Depth (km)
Residual Ev_15 (sec)
0.70 0.75 0.80 0.85 0.90 0.95 1.00 1.05 1.10
0 5 10 15 20 25 30
Depth (km)
Residual Ev_16 (sec)
0.50 0.55 0.60 0.65 0.70 0.75
0 5 10 15 20 25
Depth (km)

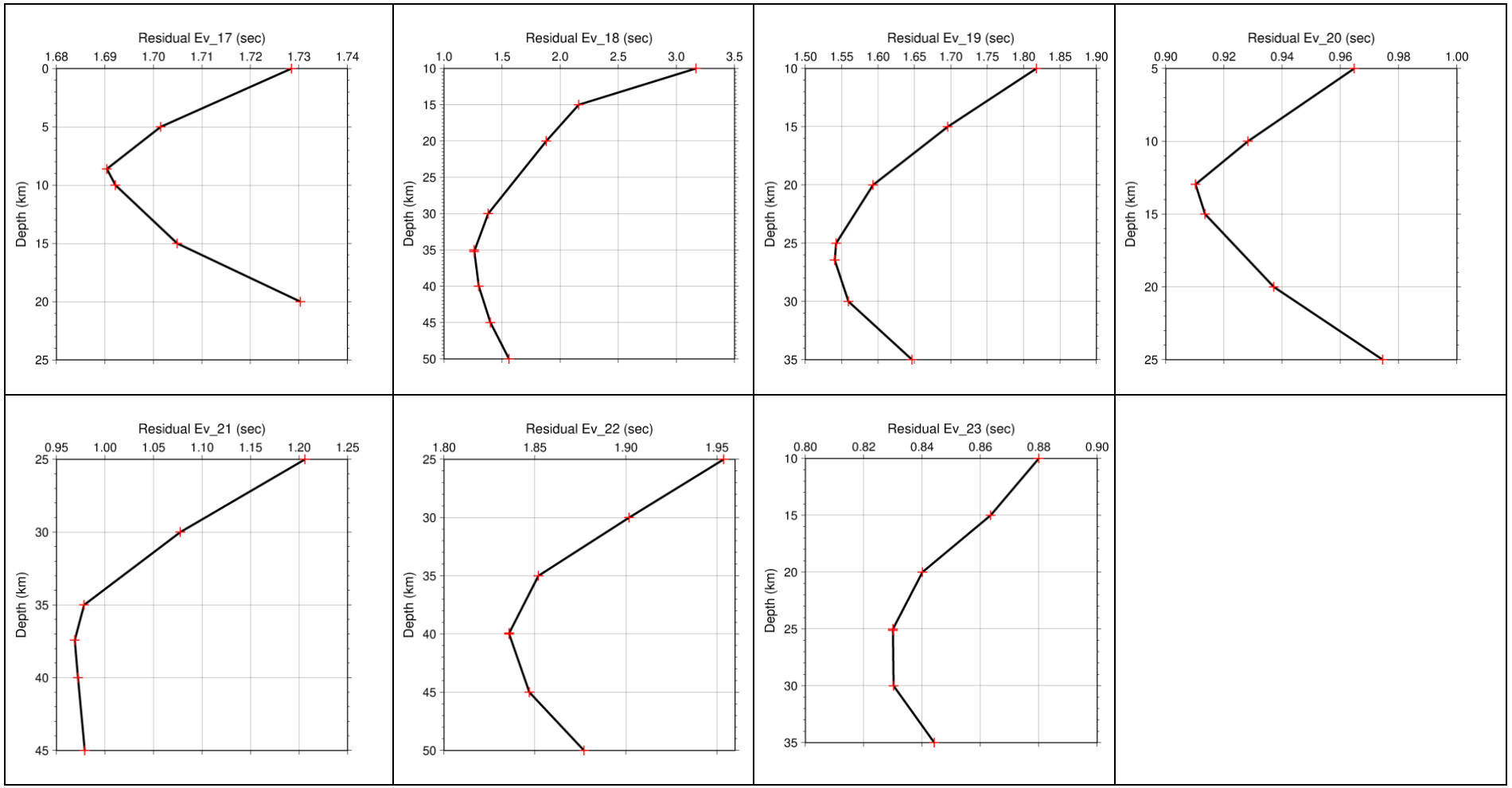

Figure 4. 8: Depth constraints for the 23 focal mechanisms, plotting the RMS travel-time residuals vs depth at intervals of 5 km.

4.3.2 Discussion

Figure 4. 9 shows the island-wide distribution of the 23 new focal mechanisms, and Figure 4. 10 shows the coverage of the focal sphere for each mechanism; at least eight reliable polarity measurements were used to conduct the calculations. The calculated focal mechanism solutions vary from strike-slip, to normal faulting (Figure 4. 10).

The two focal mechanisms in the northern part of Madagascar (Bemarivo region) show normal (mechanism 1) and oblique-slip (mechanism 2) motion.

Seventeen focal mechanisms were estimated for the central region of Madagascar (five in the Alaotra region, nine in the region of Ankaratra, and three in the Itremo regions). The dominant mechanism is normal faulting (mechanisms 4, 9, 10, 19, 20, 21, 22), often with part of strike-slip motion (mechanisms 3, 5, 6, 7, 8, 11, 23). Five mechanisms were determined for the Alaotra region (19, 20, 22, 22 and 23): 19 and 22 have NW-SE striking nodal planes, 20 and 21 have significantly different orientations, striking NE-SW, while 23 displays transtensional oblique slip. Nine mechanisms were estimated for the region of Ankaratra (3-11, inclusive). The three focal mechanisms for the Itremo region (16, 17, 18) show strike slip (16), normal slip (18) and reverse faulting as the nodal plane dips at 45 degrees (17).

The four obtained fault plane solutions for events in the southern part of the island (mechanisms 12, 13, 14, 15) show a range of mechanisms (extensional and strike-slip motion) and nodal plane orientations. Three are predominantly normal faulting (12, 14, 15), and one is considered to be strike slip faulting (13).

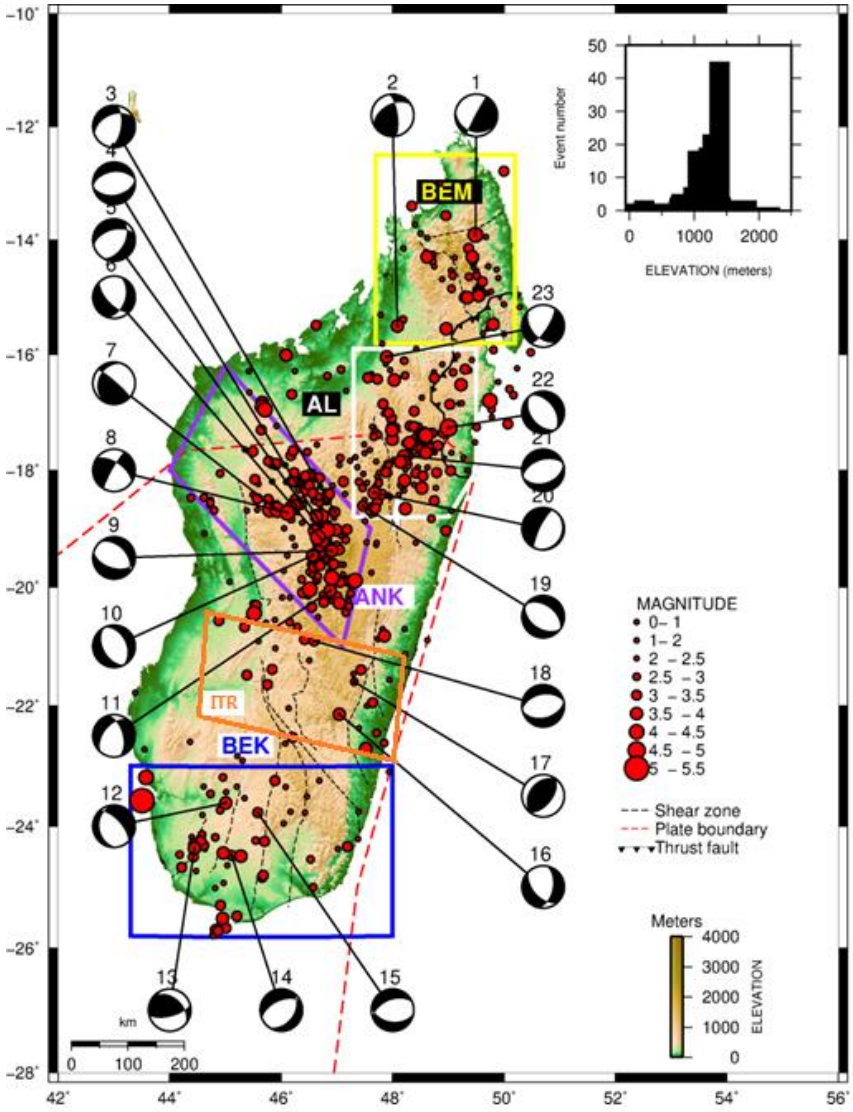

Figure 4. 9: Focal mechanisms of 23 earthquakes in Madagascar. Yellow - Bemarivo zone (BEM), white - Alaotra zone (AL), purple - Ankaratra zone (ANK), orange - Itremo zone (ITR), and blue - Bekily zone (BEK).

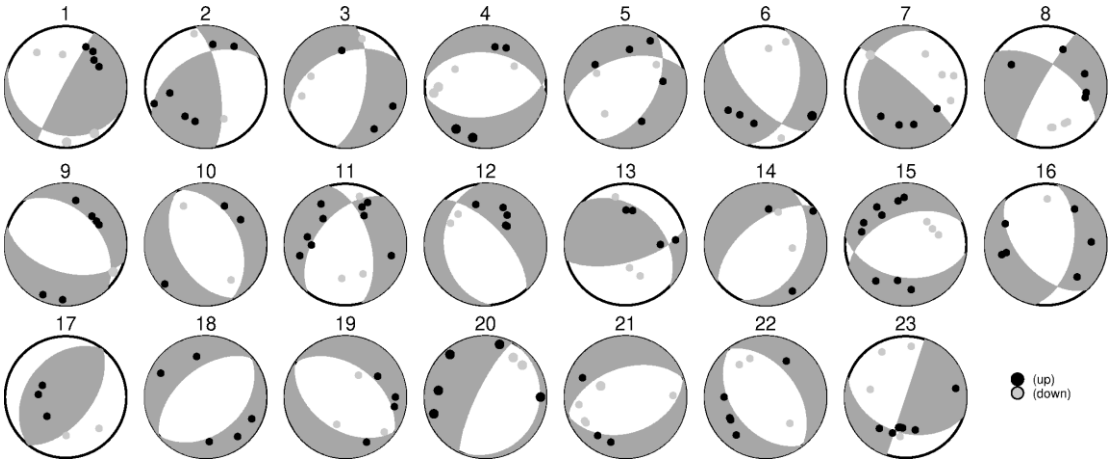

Figure 4. 10: Focal mechanism solutions, constructed using P-wave first polarities and S-wave polarities, for 23 Madagascar intraplate earthquakes with good station coverage. Events numbers are the same as those shown in Figure 4. 9 and listed in Table 4. 1.

Table 4. 1: Focal mechanism solutions for 23 Madagascar intraplate earthquakes

ID	Date	hh/mm/ss	Lon (deg)	Lat (deg)	Depth (km)	Nodal plane 1			Nodal plane 2			MAG M_L
						Strike1 (deg)	Dip1 (deg)	Rake1 (deg)	Strike2 (deg)	Dip2 (deg)	Rake2 (deg)	
1	2012-05-29	01:50:37 PM	49.4832	-13.9112	20.02	208	87	68	215	77	67	4.0
2	2012-08-11	11:32:13 PM	48.0825	-15.5058	11.16	351	71	46	12	65	33	3.5
3	2012-09-03	12:40:31 PM	47.8897	-16.0392	7.8	246	43	-41	256	45	-40	3.5
4	2012-08-02	11:42:42 PM	46.9673	-18.7167	17.95	277	43	-78	265	46	-90	3.3
5	2012-09-27	11:17:37 PM	46.7393	-18.9652	21.14	254	51	-58	264	40	-58	3.4
6	2012-12-21	11:47:33 PM	46.6923	-19.0032	7.82	18	46	-38	0	36	-38	3.5
7	2012-09-01	11:31:13 PM	46.7475	-19.2175	23.17	311	82	65	150	72	-64	3.9
8	2013-01-13	01:24:55 PM	45.9278	-18.6833	19.37	210	82	-31	187	62	-31	4.2
9	2013-05-17	06:39:54 AM	46.1083	-18.7277	26.45	316	42	-67	322	52	-77	4.0
10	2012-09-29	04:13:56 PM	46.9052	-19.3782	4.38	334	42	-89	321	25	-66	3.5
11	2013-03-06	05:46:55 PM	46.5587	-19.4585	21.31	219	50	-48	45	89	52	3.5
12	2012-09-22	06:21:37 AM	46.8805	-20.0595	13.84	175	32	-56	160	21	-56	3.9
13	2012-07-30	04:45:51 PM	45.0037	-23.62	30.73	75	66	57	66	46	54	3.9
14	2013-03-26	09:48:40 AM	44.4453	-24.3653	19.95	232	57	-74	46	44	-88	3.9
15	2013-07-04	01:40:59 PM	45.1075	-24.4833	12.96	98	44	-68	125	34.	-68	3.2
16	2013-01-28	11:54:35 PM	45.5752	-23.7787	9.31	10	52	-52	225	88	41	3.3
17	2013-01-19	04:19:04 AM	47.0463	-22.1437	8.61	38	55	90	225	45	90	3.5
18	2013-05-14	03:43:12 PM	47.31	-21.5973	2.04	230	52	-90	53	36	-88	2.9
19	2012-10-01	11:47:44 PM	46.5893	-20.9137	24.6	306	46	-89	120	46	-88	3.2
20	2012-10-10	04:11:29 AM	47.4588	-18.6092	12.96	206	78	-90	66	32	-80	3.4
21	2013-07-10	07:43:11 PM	47.6657	-18.3877	37.42	252	50	-90	60	45	-90	3.5
22	2012-08-30	07:02:52 AM	48.2025	-17.7543	39.92	323	47	-90	318	37	-87	3.8
23	2012-11-01	12:19:28 AM	49.0033	-17.2653	25.12	199	90	49	21	83	-47	4.6

4.4 Magnitude calibration

To calibrate the magnitude scale for Madagascar, the size of each earthquake was determined using the local magnitude scale proposed by Richter (1935). Earthquake data from broadband stations, including the temporary stations from MACOMO and the permanent stations ABPO, FOMA, SBV and VOI were used. The peak amplitude (zero to peak) on the vertical-component signal obtained by each located seismic event was determined at every station, corrected for the response of the instrument and the frequency response of a standard Wood–Anderson seismograph applied (Kanamori and Jennings, 1978).

Different steps were achieved for calibrating the local magnitude for Madagascar such as:

a. Determination of the reference amplitude after measuring the maximum amplitude (zero-to-peak) on the vertical seismogram-component that are recorded from the local earthquake by using the frequency response of a standard Wood-Anderson torsion seismograph by Kanamori and Jennings (1978), and application of the Richter method (1935) which is based on the definition that an event with M_L = 3.0 produces a motion with a peak amplitude of 1 mm on a Wood-Anderson seismogram recorded at a station located 100 km away. So that the expression of the amplitude reference

$$-\log Ao = n\log\left(\frac{r}{100}\right) + k(r - 100) + 3.0 \quad (4.1)$$

where n is the geometric spreading coefficient, k is the anelastic attenuation coefficient, and r is the hypocentral distance in kilometers.

b. Calculation of the difference between the log of the measured amplitudes from the recorded signals on a particular seismograph ($log\ A$) and the log of a reference amplitude ($log\ A_o$).

$$M_L = \log A - \log Ao + \beta \quad (4.2)$$

where β represents the station correction and *Ao* is a value obtained from an empirically-determined amplitude-distance curve,

c. Determination of the observed amplitude at some station j after combining equations (4.1) and (4.2), and after using by least squares inversion of 5304 amplitude measurements on the 695 located events, yielding the distance-correction function which is defined by:

$$\log A_j = -n\log\left(\frac{r_j}{100}\right) - k(r_j - 100) - 3.0 + \mathrm{M}_L - \beta_j \qquad (4.3)$$

So that the distance-correction function was observed to be:

$$log\ A_0 = 0.7314 \log\left(\frac{r}{100}\right) + 0.0005\ (r - 100) + 3.0 \qquad (4.4)$$

After measuring the maximum amplitude values described previously (see section 4.4 paragraph a), the new M_L scale for Madagascar is given by:

$$M_L = log\ A + 0.7314\ \log\left(\frac{r}{100}\right) + 0.0005(r - 100) + 3.0 + \beta_j \qquad (4.5)$$

where *A* is the maximum amplitude (mm), *r* is the hypocentral distance (km), and the station corrections (β_j) were determined in the regression analysis and are listed in Table 4. 1

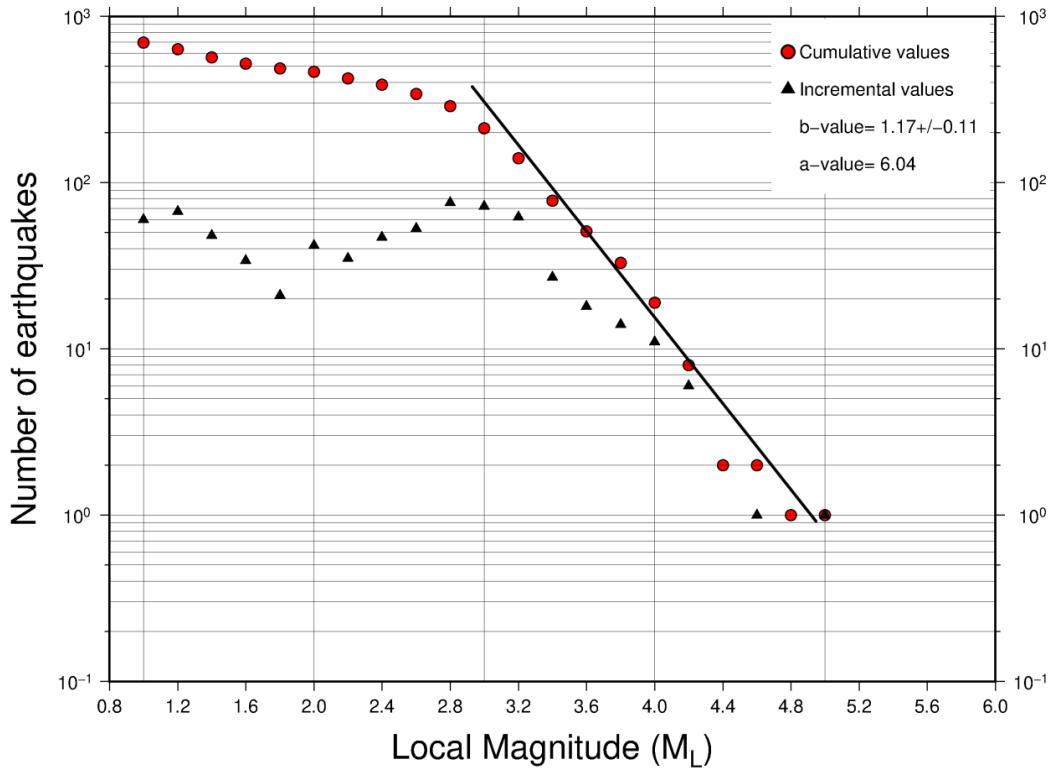

Figure 4. 11: Frequency-magnitude analysis of the 695 intraplate Madagascar earthquakes. The horizontal scale shows local magnitudes in 0.2-unit bins (See Figure 4. 2). The vertical axis shows the log of the cumulative number of earthquakes of that magnitude and above. The solid line shows a linear regression through the bins from M_L 2.8 to M_L 5.4.

The frequency-magnitude analysis for these 695 events is shown in Figure 4. 11. The triangles represent the number of events in each magnitude bin, while the circles are the cumulative number equal to or exceeding each magnitude. We found that the magnitude of completeness of the 695 seismic events is 3.0, and the frequency – magnitude distribution *a*- and *b*- values for Madagascar using the MACOMO data are 6.04 and 1.17, respectively. This indicates that Madagascar is, generally speaking, a region of low stress characterized by relatively small earthquakes.

Table 4. 2: The numbers of earthquakes in the different binned M_L magnitudes. The bins used to calculate the *b*-value from the linear regression shown in Figure 4. 11

BIN	EQ	CUM	MAG	Log_{10}(CUM)
$1.0 < M_L \leq 1.2$	60	695	1.0	2.842
$1.2 < M_L \leq 1.4$	67	635	1.2	2.803
$1.4 < M_L \leq 1.6$	48	568	1.4	2.754
$1.6 < M_L \leq 1.8$	34	520	1.6	2.716
$1.8 < M_L \leq 2.0$	21	486	1.8	2.687
$2.0 < M_L \leq 2.2$	42	465	2.0	2.667
$2.2 < M_L \leq 2.4$	35	423	2.2	2.626
$2.4 < M_L \leq 2.6$	47	388	2.4	2.589
$2.6 < M_L \leq 2.8$	53	341	2.6	2.533
$2.8 < M_L \leq 3.0$	76	288	2.8	2.459
$3.0 < M_L \leq 3.2$	72	212	3.0	2.326
$3.2 < M_L \leq 3.4$	62	140	3.2	2.146
$3.4 < M_L \leq 3.6$	27	78	3.4	1.892
$3.6 < M_L \leq 3.8$	18	51	3.6	1.708
$3.8 < M_L \leq 4.0$	14	33	3.8	1.519
$4.0 < M_L \leq 4.2$	11	19	4.0	1.279
$4.2 < M_L \leq 4.4$	6	8	4.2	0.903
$4.4 < M_L \leq 4.6$	0	2	4.4	0.301
$4.6 < M_L \leq 4.8$	1	2	4.6	0.301
$4.8 < M_L \leq 5.0$	0	1	4.8	0.000
$5.0 < M_L \leq 5.2$	0	1	5.0	0.000
$5.2 < M_L \leq 5.4$	1	1	5.2	0.000

4.5 Discussion

Seismic data from the recent MACOMO deployment (2011-2013), together with the SELASOMA, RHUM-RUM, and the National Data Center (NDC) stations were used to perform a comprehensive study of the earthquake distribution within the Madagascar area. A new seismicity map, fault plane solutions for 23 earthquakes, and magnitude calibration were produced. The new seismicity map

comprises 695 earthquakes located using HYPOELLIPSE, 422 were re-located using the HYPODD double difference method, and fault plane solutions obtained for 23 events with each having at least eight clear polarities and good azimuthal coverage.

Occasional seismic events were detected beneath the Paleozoic sedimentary basins that occupy the western third of Madagascar. The seismicity map for Madagascar shows that seismic activity is concentrated in five regions within the Precambrian shield that comprise the eastern two-thirds of the island (Figure 4. 1). The level of seismic activity is highest in the central region, especially in the Antananarivo Block. Activity in northern and southern Madagascar is comparatively low compared to the central region. The higher level of seismic activity in the central part of Madagascar might be caused by the extensional deformations from the immense topography within the uplifted regions of the island.

Earthquake clusters observed along the northern part of Madagascar are mostly in the southern end of the Bemarivo zone (box BEM1, Figure 4. 3), in the south of the Antsaba shear zone, around the Sandrakota shear zone, and in the northernmost part of the central block (box BEM2, Figure 4. 3). Additionally, most of the central and northern part of the Bemarivo area, as well as the volcanic regions in the north of Madagascar, display almost no earthquakes. This is difficult to understand given the high level of seismicity that was reported in the previous studies (Bertil and Regnoult, 1998), which included a m_b 5.4 earthquake that occurred on 30 June 1974 in the central Bemarivo area and a m_b 5.0 earthquake on 29 January 1992 near the northeast coast (Bertil and Regnoult, 1998).

It has been suggested that the high level of seismicity in the central Alaotra zone is related to the intrusion of sub-volcanic material (Rechenmann, 1981). Two large historical earthquakes with a maximum Mercalli intensities of VII (no reported magnitude values) were located in this region: one in Mantasoa on 14 September 1932 and the other near the Alaotra rift on 10 November 1955 (Bertil and Regnoult, 1998).

In general, the Ankay and Alaotra zones are defined by normal faults that trend north-south and dip towards the east (Bertil and Regnoult, 1998). These extensional structures are considered as very seismically active structures within Madagascar. Rindraharisaona et al. (2013) gave results of focal mechanisms for six earthquakes in the Alaotra zone, and which indicated dominant normal faulting. Two large earthquakes with normal-faulting occurred close to the east of the Ankay region, along the coast: a M_w5.4 event on 18 May 1962 (Grimison and Chen, 1988) and M_w5.5 event on 4 October 1985 (http://www.globalcmt.org/CMTsearch.html).

This study observed the highest seismic activity in the Ankaratra and Itasy zones, with a total of 313 earthquakes (Figure 4. 5) and predominantly normal fault mechanisms (Figure 4. 9). These results are in accord with previous work by Bertil and Regnoult (1998) who identified a high level of seismic activity in the central area of Madagascar; and by Rindraharisaona et al. (2013) who showed that the mechanisms of about 45 earthquakes that occurred between 1990 and 2011 was predominantly normal faulting. The seismicity trends roughly north-south, but is concentrated in the eastern part of the Ankaratra and Itasy zones (Figure 4. 5). The observed seismic activity can be explained as a tectonic regeneration of ancient normal faults, generated in part by the thermal anomalies similar to the latest magma emplacement (Pratt et al., 2017).

In the southern area of Madagascar, this study shows that most of the earthquake data were localized around the existing thrust of Ampanihy, Bekily, Betroka and Tranomaro (Figure 4. 1). The results further revealed that the southern area of Madagascar has a moderate characteristic of distributed seismicity that is mostly divided the island to two sections north and south, by the Bongolava-Ranotsara shear zone, as mentioned previously. A combination of thrust and slip faulting were also observed in the southern area of Madagascar by Rindraharisaona et al. (2013).

We attribute the variety of fault plane solutions determined by this work to the complex tectonic structures in Madagascar. Also, fault plane solutions in the north and south are sparse because of the lack of seismic stations that have quality waveform signals and clarity in polarity identification for optimum fault plane solution characteristics.

After using the original Richter (1935) method, we determined a new local magnitude scale for Madagascar. The additional temporary seismic stations from the MACOMO project helped us to improve the local magnitude scale for Madagascar. Earthquake frequency numbers obtained from this study suggested that about 180 earthquakes with $M_L \geq 3$ occur annually; 12 above $M_L \geq 4$; and one or two with $M_L \geq 5$. An earthquake with $M_L \geq 6$ is expected every 18 years, on average. The results differ considerably from previous research work. For example, Rindraharisaona et al. (2013) reported 1221 earthquakes with $M_L \geq 3$ in a 22-year period, or about 55 earthquakes per annum, on average. Note that Rindraharisaona et al. (2013) only used the permanent seismic stations that are mainly located in the middle part of Madagascar, in their study. Bertil and Regnoult (1998) reported 104 $M_d \geq 3$ earthquakes per year, which is closer to this study. However, they found only a few events from the southern and northern parts of Madagascar, compared to the current study.

4.6 Conclusion

Seismicity, magnitude calibration and fault plane solutions were determined in this study using data recorded by 56 seismograph stations. Various techniques were applied, including absolute location using HYPOELLIPSE, relative relocation using HYPODD, the Richter method to calibrate earthquake mangitudes, and determination of fault plane mechanism using P-wave and S-wave polarities.

The volcanic area of Ankaratra and the high seismic activity zone of Alaotra are the most active regions. The fault plane solution results were improved due to the high density of seismic stations used compared to the previous research done in

Madagascar. New focal mechanism results were determined in the northern, northwest, and southern areas of Madagascar.

In terms of seismicity, a good correlation is observed between the earthquake location from this present study and the previous research. However, new seismic activities were seen in the northern and southern part of Madagascar that correlate well with known geological features. The results of the calculated focal mechanisms revealed an extensional faulting in the central area of Madagascar, which shows a close relationship between focal mechanism and the sub-regional structures. Comparatively few solutions were determined for the southern and northern parts of the island, the Bemarivo and Bekily zones, respectively, owing to the low density of seismograph stations.

Chapter 5: Stress field inversion

The contents of this chapter will be submitted for publication in a peer-reviewed journal.

Determining the stress field in Madagascar using focal mechanism data by Tsiriandrimanana Rakotondraibe, Raymond Durrheim, Andrew A. Nyblade, Michael E. Wysession, Gérard Rambolamanana, Fenitra Andriampenomanana, and Elisa Rindraharisaona.

A draft of the manuscript is presented in APPENDIX E.

5.1 Introduction

The present-day stress field Madagascar is investigated by combining focal mechanism results from the MACOMO project and focal mechanisms determined using events that occurred between 2000 and 2016 and are listed in the NDC (National Data Center) database (Figure 5. 1). The directions of the minimum and maximum principal stresses are mapped by inverting 182 focal mechanisms.

5.2 Focal mechanisms

The major drivers of seismicity in Madagascar are volcanic activity and the reactivation of ancient tectonic features by present-day tectonic forces (Bertil and Regnoult, 1998). The major tectonic features of Madagascar (Figure 1. 3) are various shear and thrust zones that are thought to be associated with the separation of Madagascar from Africa and India during the breakup of Gondwana (Rabinowitz et al., 1983).

Suitable earthquakes were selected from the combined MACOMO and NDC (National Data Center) bulletins between 2000 and 2016 (Figure 4. 1). Boundaries were inserted to the map (Figure 5. 1) in which are important for determining characteristics of the stress within the different areas, the choice of these boundaries based on the earthquake distributions and the historical earthquake activities that were recorded from the existing seismic stations. For the zone of Alaotra, subdivision of the area depended on the geological structures and the numbers of seismic events.

All events were relocated using the HYPODD double difference method and 182 events were selected for further analysis based on the following three criteria (Figure 5. 2):

1. The event was recorded by more than six stations.
2. The polarity of the first motion was clear for all three components at all considered stations.
3. The local magnitude values of the events were larger than magnitude 2.5.

We separated the Famoizankova zone from the Ankaratra zone because the numbers of events in each zone in the extended catalogue (2000 to 2016) were sufficient.

Focal mechanisms were determined using the method described in Chapter 4. P- and S-wave polarities were picked and introduced into the FOCMEC program (Snoke et al., 1984). The focal mechanisms results were classified into six zones, according to the locations of the events. All 182 focal mechanisms were quantified in terms of the direction of the slip vector using a ternary diagram plot program (Figure 4. 3). Distributions and classifications of the selected focal mechanisms are shown in Figure 5. 2 and Figure 5. 3 and their characteristics are listed in APPENDIX F. Figure 5. 3 shows the ternary diagrams that classified the focal mechanism inserted for the inversion depending on their characteristics (normal, strike-slip or reverse faulting). The number of focal mechanisms that are visible in some diagrams is fewer than the number of calculated solutions (especially in the Alaotra area) as some solutions overlap.

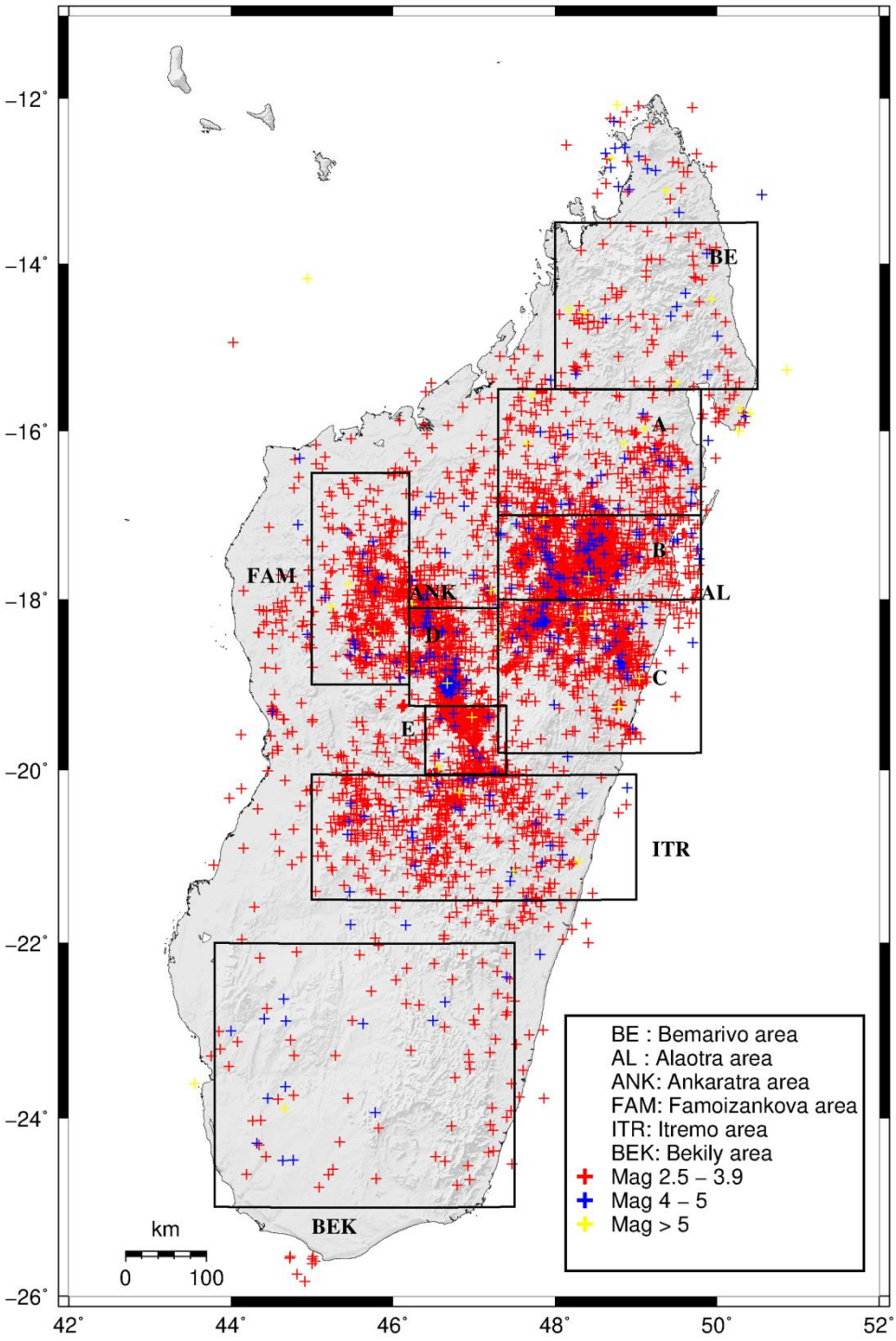

Figure 5. 1: A total of 12,727 earthquakes with M_L>2.5 in Madagascar (2000-2016) from the MACOMO bulletin and Madagascar NDC including all 182 earthquake events used for stress field inversion. The rectangles represent the boundaries of the various source zones; the Alaotra zone was divided into five sub-zones (A to C) and Ankaratra into two sub-zones (D, E).

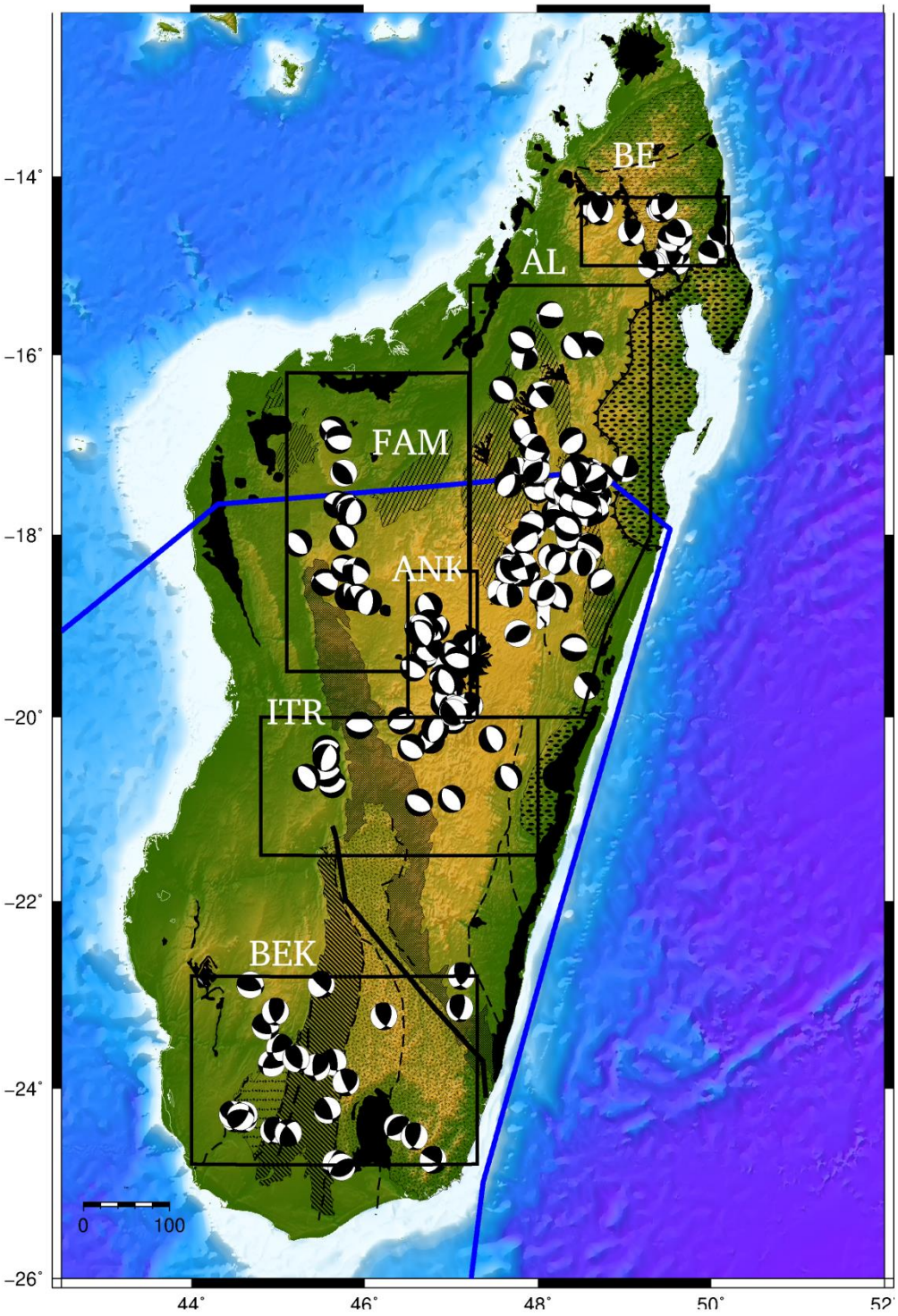

Figure 5. 2: Focal mechanisms for 182 earthquake events BE - Bemarivo region, AL - Alaotra region, ANK - Ankaratra region, FAM - Famoizankova region, ITR - Itremo region, BEK - Bekily region. Geological units as obtained from Figure 1.2.

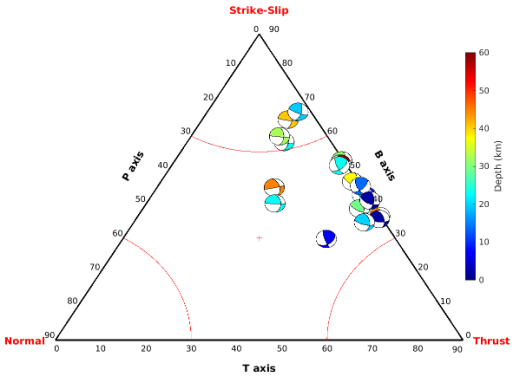

A. BEMARIVO

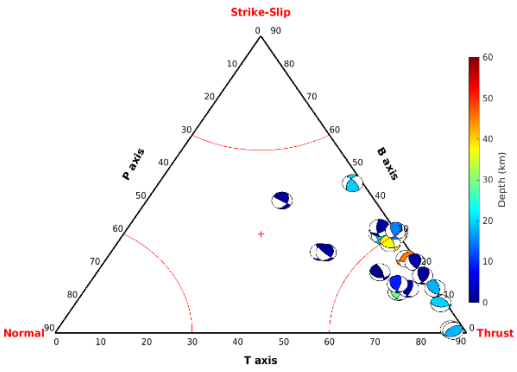

B. BEKILY

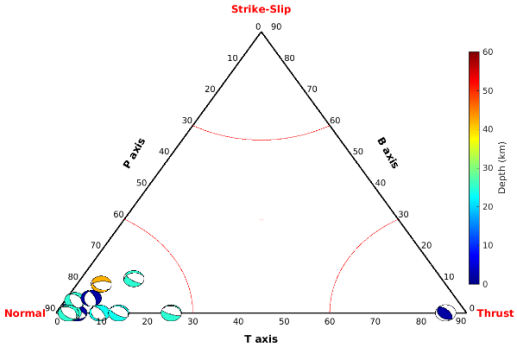

C. FAMOIZANKOVA

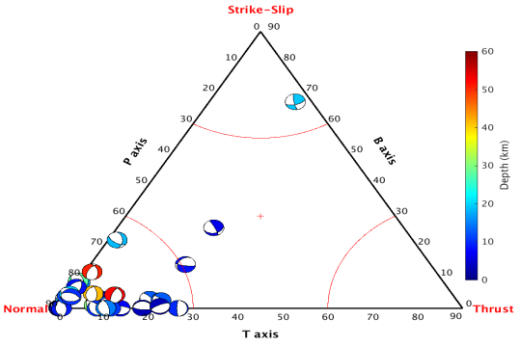

D. ALAOTRA

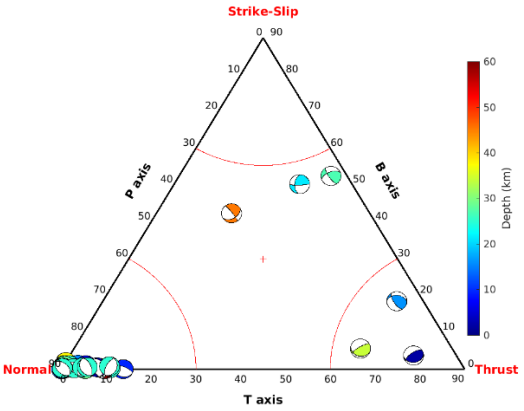

E. ANKARATRA

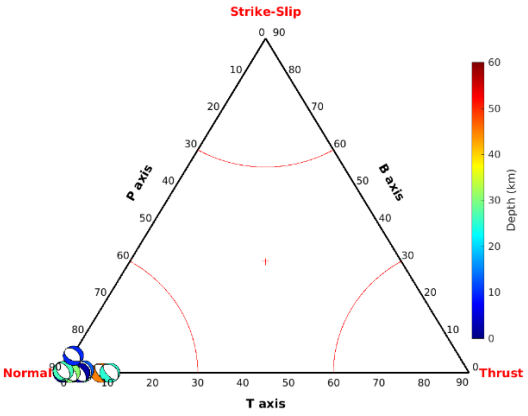

F. ITREMO

Figure 5. 3: Ternary diagram showing the classification of the focal mechanisms used for the stress inversion calculation

5. 3 Stress Inversion

The 182 focal mechanisms were inverted using the STRESSINVERSE program (Vavryčuk, 2014) in order to assess the stress field directions. Calculation was done using Michael's method (Michael, 1984) which is based on the linearized stress inversion method and iterative joint inversion (see Chapter 2: section 2.6.5 STRESSINVERSE program). A grid search for five-degree steps in the stress direction and with a shape ratio equal to 0.1 was applied. The angles of the slip vector and the resolved shear stress on the fault from each fault plane solution were determined. A relatively large increment (5°) was used because the accuracy of the direction of the fault-dip azimuth is limited by the number of focal mechanisms, which is relatively small. The inversion was performed for 15 iterations with damping parameters of 300 and 400 for the central region and a damping parameter of 400 for the northern and southern areas in order to apply the relative weighting between the misfit data and the model length in minimization or to form a balance between excessive misfit and unnecessary model length.

A 2000 bootstrap resampling was applied for the focal mechanisms data (Hardebeck and Michael, 2006). The bootstrap calculation is based on the reproduction of the original data set using a random selection of focal solutions from the catalogue. The choice could be repetitive, but the sample of the bootstrap and the original data supposed to have equal number of elements. As example, assuming a data set X comprising N elements, where N is the number of fault plane solutions we can write:

$$X = \{x_1, x_2, x_3, \ldots, x_N\}$$

The first bootstrap sample, X^*_1 (the number 1 represents that this is the sample primary bootstrap), is calculated by randomly selecting N focal mechanisms from X. The process is repeated until the required number of sets is generated, in this case 2000.

5.4 Results of inversion

As described previously, the inversion was run for 15 iterations, which gave an average RMS error of 0.28. Damping parameters of 300 and 400 were used following the grid search selection. The results are presented in four different formats (example)

1. Stereographic plot of P-axes (blue + symbol) and T-axes (red o symbol), which represent the directions of the P- and T-axes of the focal mechanisms.
2. Histogram of the shape ratio (R), which defines the shape of stress ellipsoid.
3. Mohr-Coulomb plot showing a quantitative assessment of the distribution of earthquake focal mechanisms.
4. Stereographic plot of the principal stress from each region that summarized the stress orientation from sets of focal mechanisms.

In addition, friction coefficient values were obtained for each region, as summarized in Table 5. 1. After applying Michael's method, the bootstrapping method (See Chapter 2) was used to estimate the confidence interval in terms of the standard deviation.

Results of the regional variation of stress from the inversion of 182 focal mechanisms with depth between 1 km and 45 km distributed across Madagascar were grouped in six zones: Bemarivo (BE); Alaotra (AL), sub-divided into three zones (A, B, C); Ankaratra (ANK), subdivided into two zones (D, E); Famoizankova (FAM); Itremo (ITR); and Bekily (BEK) (see Figure 5. 1). The definition of these zones was based on the number of focal mechanisms and the characteristics of the geology and seismotectonics. The inversion determined the orientations of the principal stress axes, *i.e.*, the azimuth and plunge of the maximum stress (σ_1), the intermediate stress (σ_2), and the minimum stress (σ_3). Values of the shape ratio and the friction coefficient were also determined; they

define the relative stress magnitude and control the brittle strength beneath the earth during the fault movement, respectively.

5.4.1 Bemarivo

From the inversion of 20 focal mechanisms in the northern Bemarivo zone (Figure 4. 3 A), the average for the azimuth and plunge of the maximum stress (σ_1) are 247° and 7° from the horizontal, respectively. The intermediate stress trends 151° and plunges 40°. For σ_3, the minimum stress direction trends 345° and 49° from the horizontal (See Figure 5. 4, Figure 5. 5). The average value of the shape-ratio is 0.5 and the friction value is equal to 0.7.

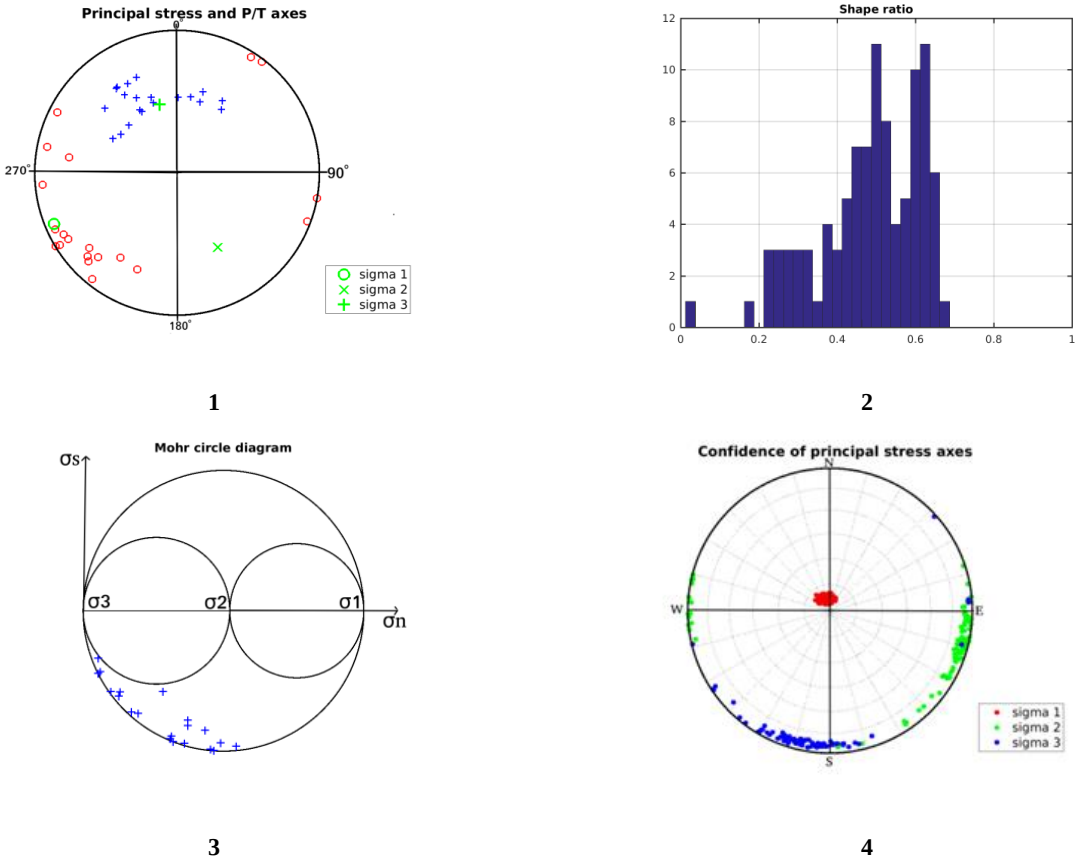

Figure 5. 4: Stress field inversion for 20 earthquakes in the Bemarivo zone (1) Stereographic plot showing orientations of P-axes (red circles), T-axes (blue crosses), (2) Histogram plot of the shape ratio R values, (3) Mohr Coulomb plot, (4) Plot of high confidence level to determine the best stress directions of σ_1, σ_2, and σ_3 interpreted as shear stress regime of a slight dip-slip displacement (red, blue and green dots).

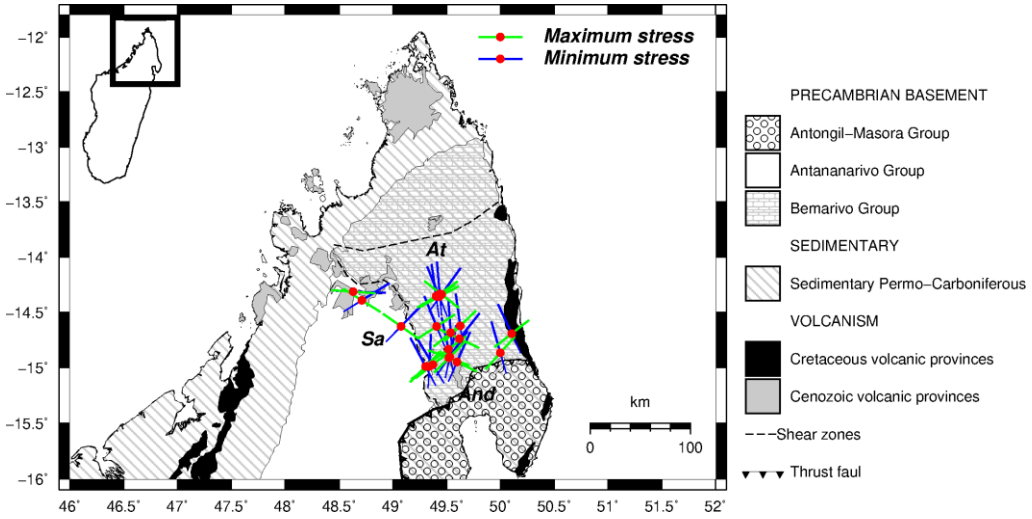

Figure 5. 5: Stress direction results for the Bemarivo area.

5.4.2 Bekily

In the southern region of Madagascar, the stress field results were obtained from 23 focal mechanisms (Figure 5. 3 B). Stress directions are presented in Figure 5. 6 and Figure 5. 7. The σ_1-axis direction for the maximum principal stress trends 309° and plunges 4° from the horizontal. The intermediate stress (σ_2) trends 218° and plunges 3°, while the minimum stress (σ_3) trends 100° and plunges 83° from the horizontal. The average value of the shape ratio is equal to 0.36 whilst the friction value is equal to 0.5.

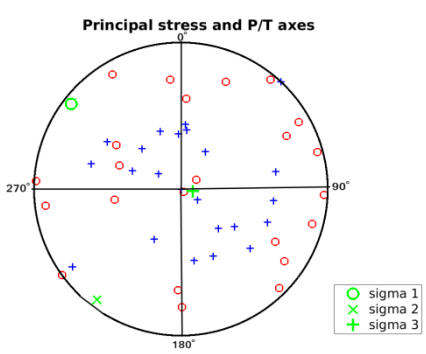

1

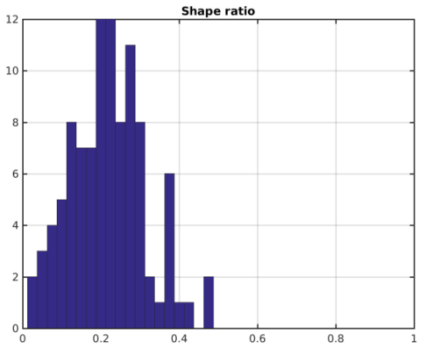

2

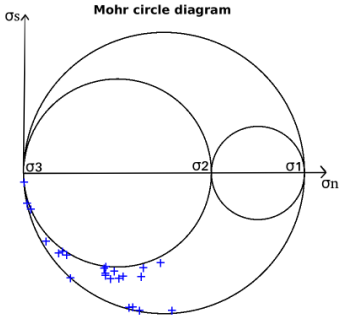

3

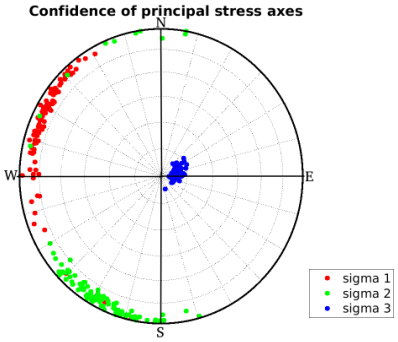

4

Figure 5. 6: Same as Figure 5. 4 but for 23 events in Bekily zone.

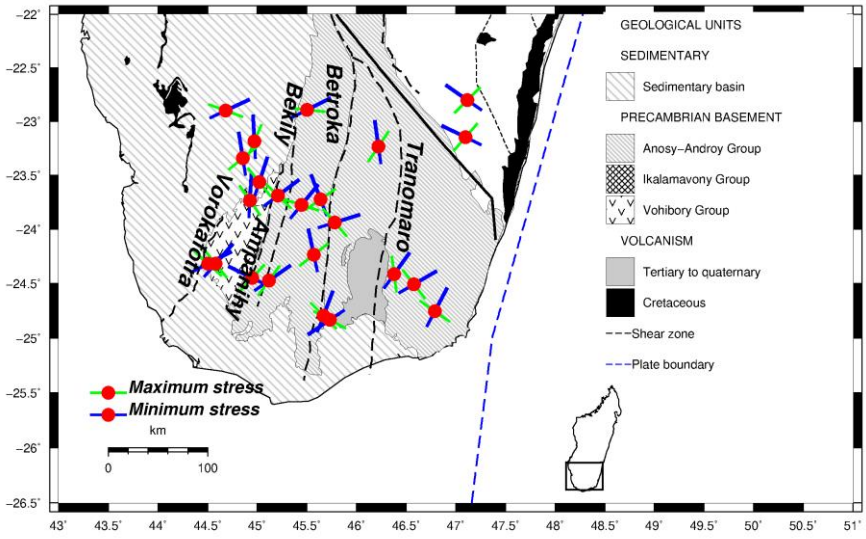

Figure 5. 7: Stress direction results in the Bekily area.

5.4.3 Famoizankova

Domination of normal faulting was observed in the Famoizankova region according to the results of the inversion of the 15 fault plane solutions for this region (Figure 5. 8). The directions of the P- and T- axes were found to be mostly uniform (Figure 5. 9). The orientation of the principal stress (σ_1) trends from 195° and plunges 79° down from the horizontal. For the intermediate stress (σ_2), the direction trends 306° and plunges 4°. For σ_3, the direction trends from 37° horizontally with plunge 10°. Values of the shape ratio and the friction are 0.9 and 0.6, respectively.

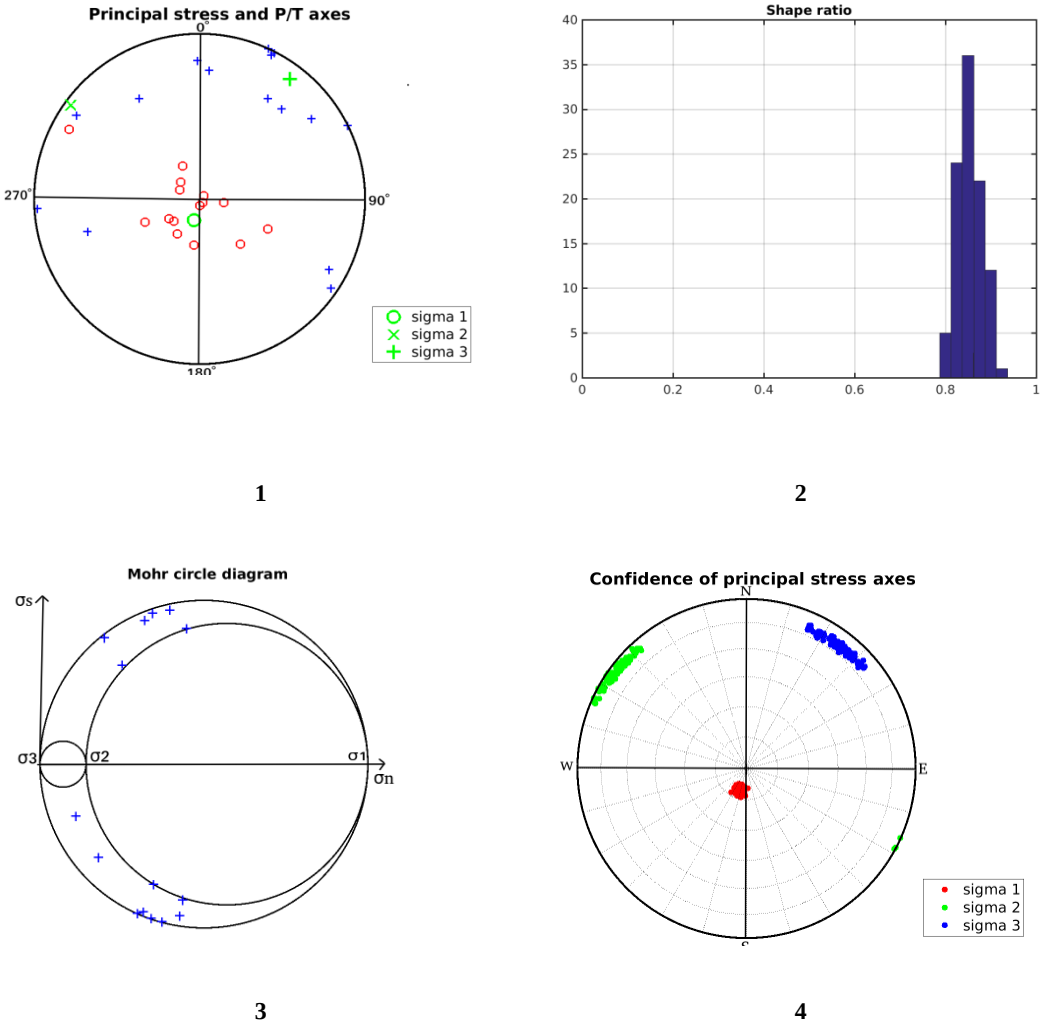

Figure 5. 8: Same as Figure 5. 4 but for the Famoizankova zone.

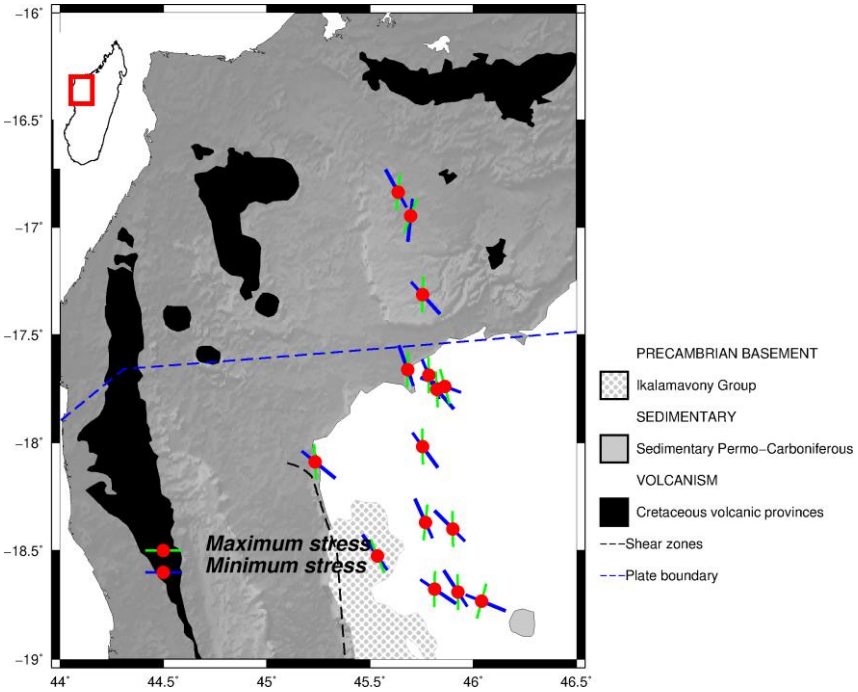

Figure 5. 9: Stress direction results in the Famoizankova region

5.4.4 Alaotra

The regional results of stress in Alaotra region were obtained from the 78 inverted focal mechanisms after subdividing the region into three sub-zones (A, B, C). The quality of the results varies according to the sub-zone. In sub-zone A (Figure 5. 10), the maximum stress (σ_1) is mostly in a vertical direction trending 221° and plunging 83°, while the minimum stress (σ_3) trending 66° and plunges 6°. The intermediate stress (σ_2) trends and plunges 335° and 3°, respectively. The shape ratio and friction values are 0.8 and 0.4, respectively.

In sub-zone B (Figure 5. 11), the average direction of the maximum stress (σ_1) trends 259° with plunge 77° down from the horizontal. The intermediate stress (σ_2) direction trends 114° and plunges 11°, and the average minimum stress direction (σ_3) trends 22° and plunges 7.2°. The values of shape-ratio and friction are 0.9 and 0.8, respectively. In sub-zone C (Figure 5. 12), the maximum stress (σ_1) trends 246° with plunge 77° down from the horizontal; the intermediate stress (σ_2) trends 131° and plunges 6°, and the minimum stress trends 40° with a plunge of 12°. The shape ratio value is 0.9 and the friction is 0.7.

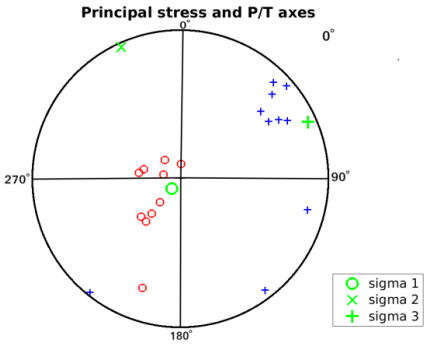

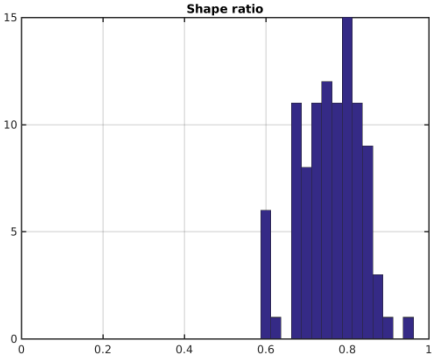

1 **2**

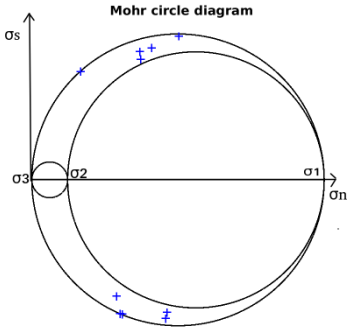

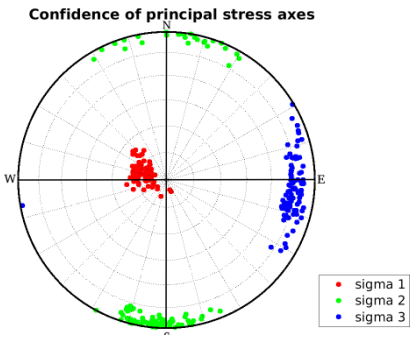

3 **4**

Figure 5. 10: Same as Figure 5. 4 but for the events in the sub-zone A of Alaotra

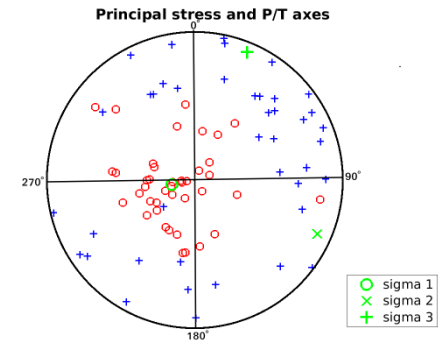

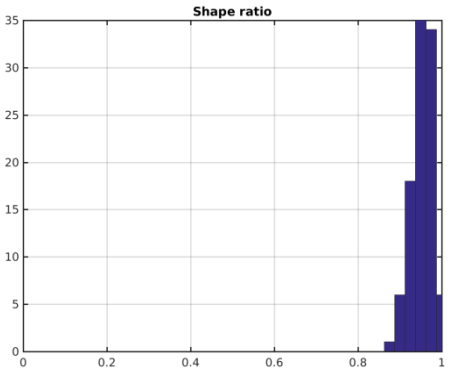

1 **2**

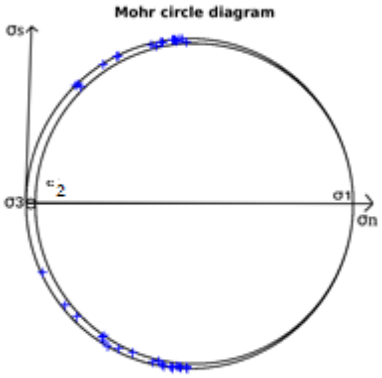

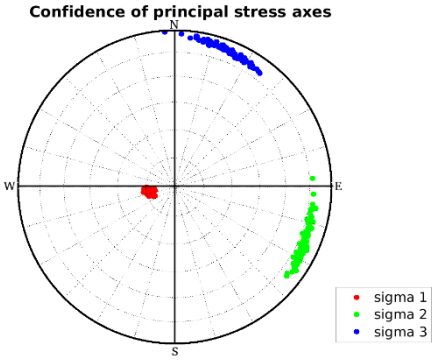

3 **4**

Figure 5. 11: Same as Figure 5. 4 but for the events in the sub-zone B of Alaotra

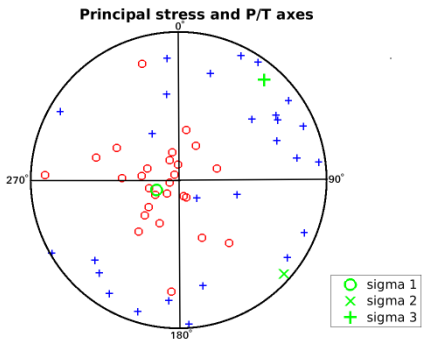

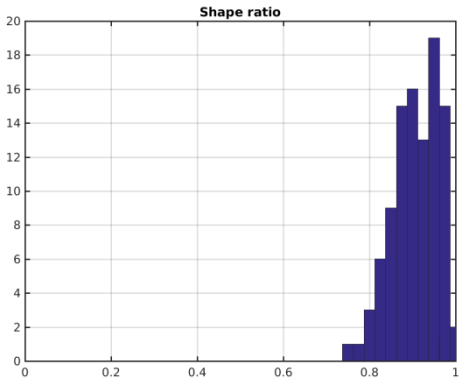

1 **2**

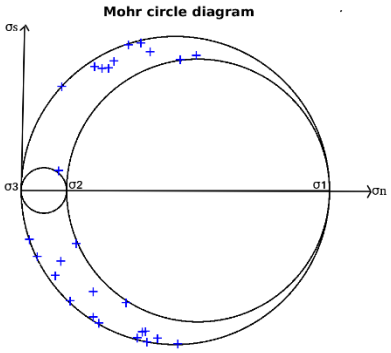

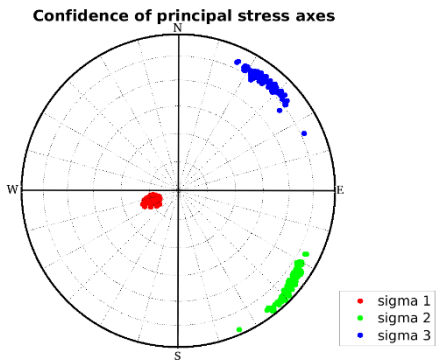

3 **4**

Figure 5. 12: Same as Figure 5. 4 but for the events in the sub-zone C of Alaotra

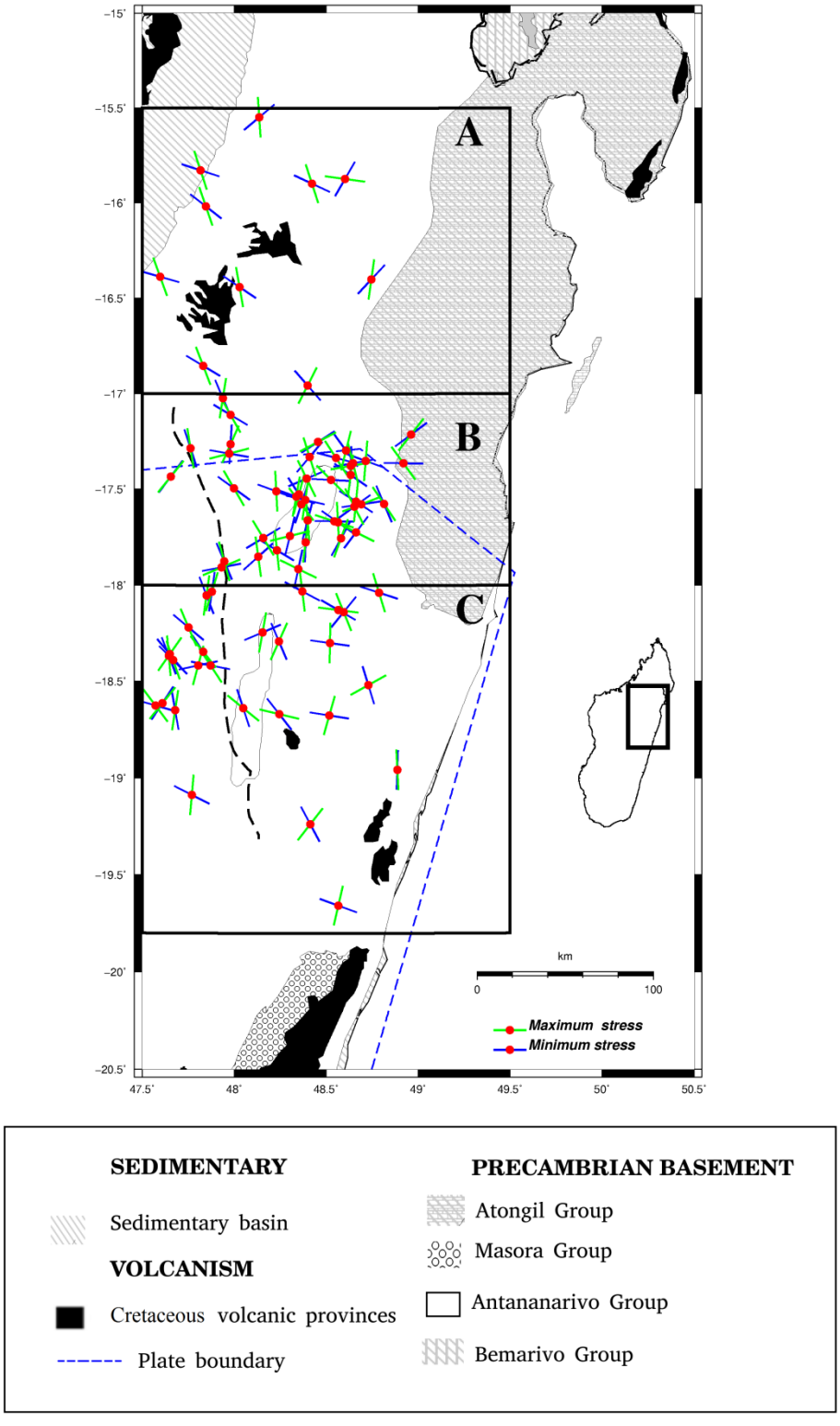

Figure 5. 13: Stress direction results in the Alaotra region

From Figure 5. 13, significant deviation of the maximum stress is shown within the subzones A and C, while it has quite similar directions in the subzone B.

5.4.5 Ankaratra

From a total of 30 mechanisms (Figure 5. 2), results of the inversion are presented in Figure 5. 14 and Figure 5. 15 for both zone D and zone E. Fewer observed results of the maximum stress (σ_1) and minimum stress (σ_3) are seen in zone D than in zone E. Predominant extension faulting and its scatter are projected into a scatter of the P- and T- axes, which form clusters of a specific shape and presented in Figure 5. 14.

In the zone D, the average maximum stress direction (σ_1) trends 268° and plunges 74°, whilst for the intermediate stress (σ_2) the direction trends 136° and plunges 6°. The average minimum stress direction (σ_3) trends 45° and plunges 14°. Shape ratio value and friction values are 0.89 and 0.5, respectively

In the zone E, the maximum stress (σ_1), the intermediate stress (σ_2) and the minimum stress (σ_3) direction trend 269°, 138° and 38°, respectively and plunge 81°, 2° and 8°, respectively. The shape ratio value is 0.92 while the friction value is 0.45.

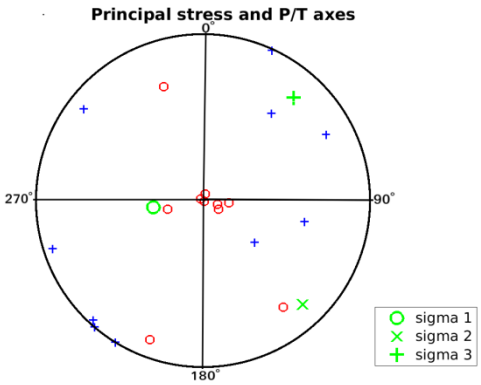

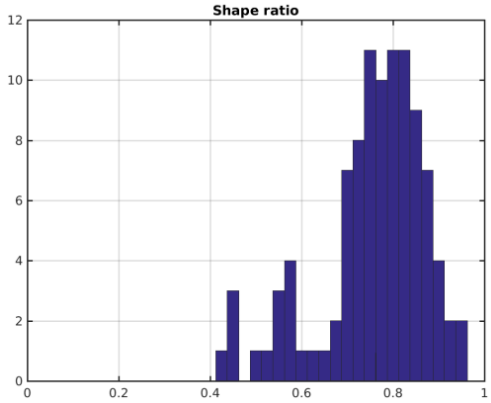

1 **2**

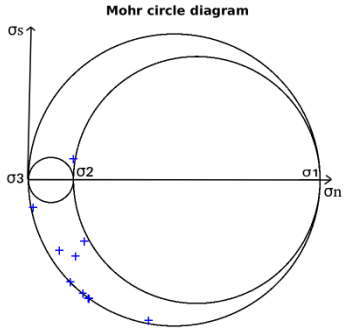

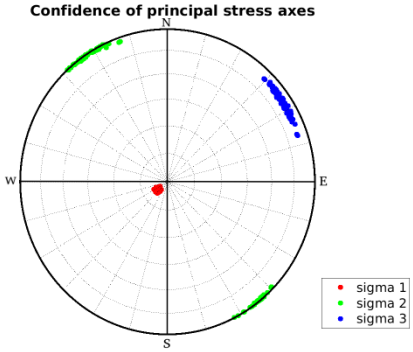

3 **4**

Figure 5. 14: Same as Figure 5. 4 but for the events in the sub-zone D of Ankaratra

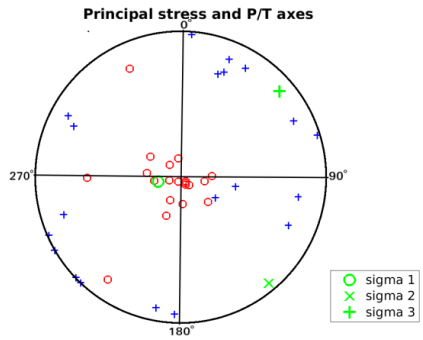

1

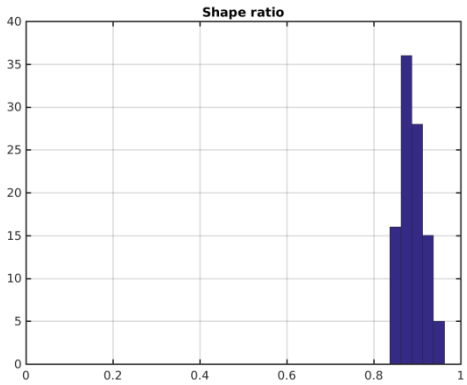

2

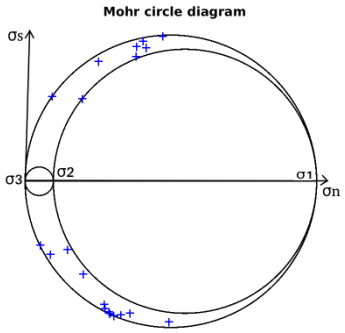

3

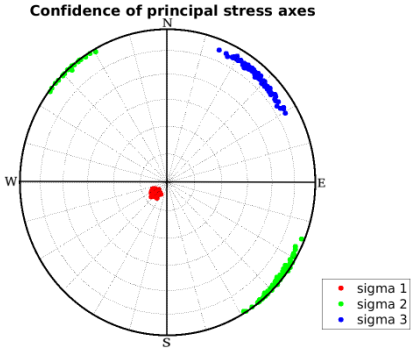

4

Figure 5. 15: Same as Figure 5. 4 but for the events in the sub-zone E of Ankaratra

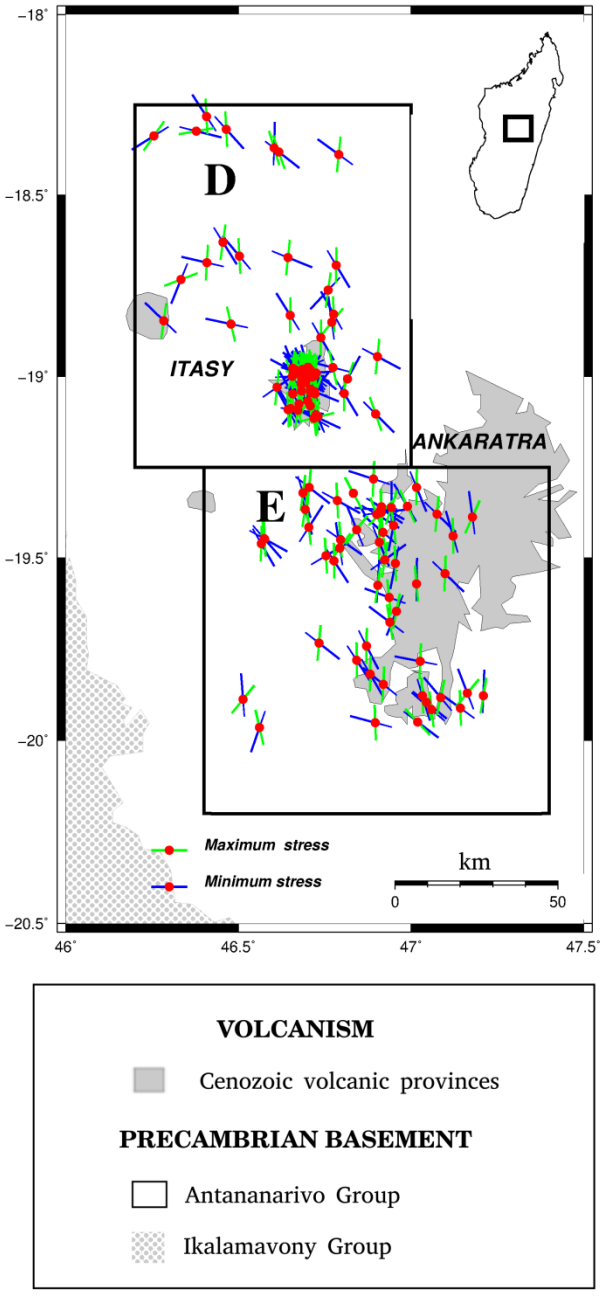

Figure 5. 16: Stress direction results in the Ankaratra region

Results from the inversion in the Ankaratra zone show constant direction of the maximum stress that follows the direction NW-SE except for some events (See Figure 5. 16).

5.4.6 Itremo

Results of stress inversion in Itremo zone are obtained using 16 focal mechanisms and are dominated by normal faulting (Figure 5. 17). The orientation of the principal stress (σ_1) trends 226° and plunges 78° from the horizontal and considered as consistent to the average dip of the P-axis. The intermediate stress (σ_2) trends 117° and plunges 6°. For the σ_3, the minimum stress-axis direction trends from the azimuth 16° and plunges 10°. Values of the shape ratio and friction are 0.9 and 0.5, respectively.

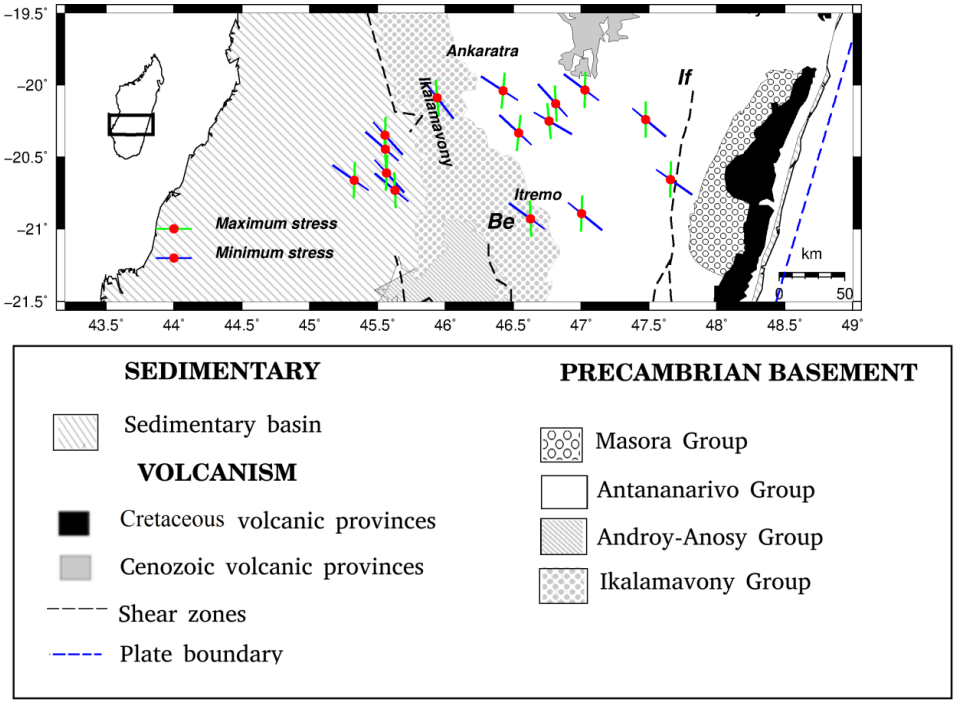

Figure 5. 17: Stress direction results in the Itremo region

Table 5. 1: Stress inversion results for 182 events recorded from 1 January 2000 - 31 December 2016 in Madagascar.

AZ and PLG indicate Azimuth and Plunge. AZ is measured clockwise from the north and PLG downwards from the horizontal plane.

Magnitude range (M_L)							**2.5 -5.8**							
Latitude Range (deg)	**Longitude Range (deg)**	**Depth Range (km)**	**Average Strike, Dip, Rake (S,D,R) from the two nodal planes**						**Stress direction (AZ/PLG)in (º)**			**R**	**Friction**	**RMS error**
			S_1	**D_1**	**R_1**	**S_2**	**D_2**	**R_2**	**σ_1**	**σ_2**	**σ_3**			
Bemarivo zone: 20 events														
-16.0/-14.0	48/50	2/59.6	18	70	19	225	80	46	247/7	151/40	345/49	0.48	0.71	0.51
Bekily zone: 23 events														
-26/-22	43/49	2/34	185	63	61	160	46	54	309/4	218/3	100/83	0.36	0.50	0.54
Famoizankova zone: 15 events														
-19.2/-16.8	45.2/47.3	2/42	168	46	-72	263	43	-51	195/79	306/4	37/10	0.90	0.60	0.21
Alaotra zone: total of 78 events with 3 sub-zones (A, B, C)														
-19/-17	47/48	1/42	257	3	-90	320	50	-68	221/83	335/3	66/6.4	0.84	0.40	0.12
-17.75/-17	48.25/49.5	1/25	149	8	84	223	80	40	259/77	114/11	22/7.2	0.90	0.80	0.18
-19.5/-18.5	48.1/49.5	1.34	176	41	-89	230	40	-68	246/77	131/6	40/12	0.90	0.70	0.20
Ankaratra zone: total of 30 events with 2 sub-zones (D, E)														
-19.25/-18.30	46.2/47.3	1/35	222	53	-28	277	40	-90	268/74	136/6	60/14.2	0.89	0.5	0.19
-20/-19.5	46.30/47.4	1/25	181	45	77	220	56	-90	269/81	138/2	38/8	0.92	0.45	0.20
Itremo zone: 16 events														
-21.8/-20.2	44/48	2/58	162	48	-89	231	41	-90	226/78	117/6	16.3/10	0.90	0.50	0.30

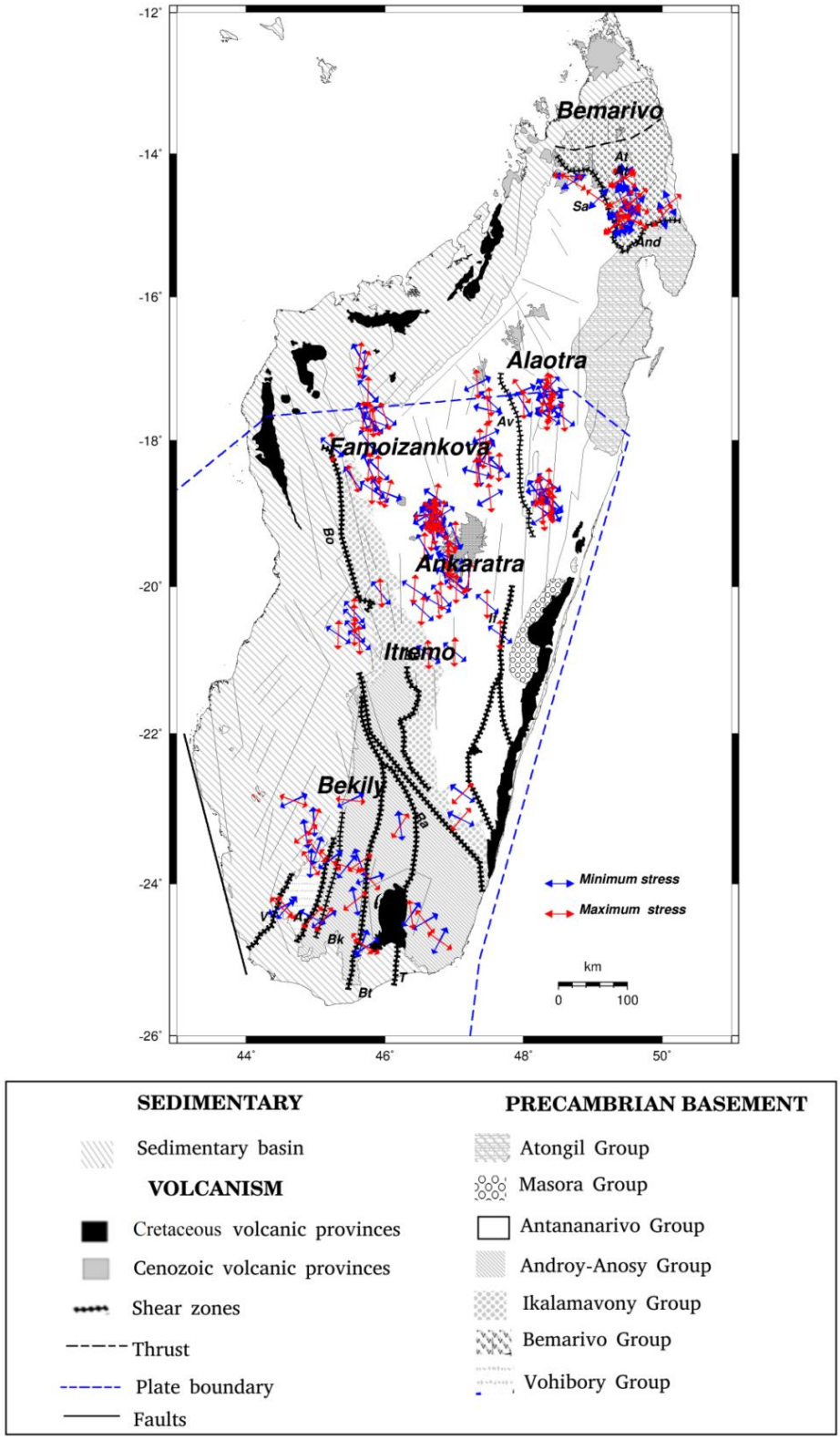

Figure 5. 18: Map showing the results of the minimum (blue) and maximum (red) stress direction after the inversion from each selected region.

5.5 Discussion

Reliable fault plane solutions from 182 well-covered earthquakes, spanning the period from 2000 to 2016, are used to estimate stress field directions in the northern, central and southern areas of Madagascar. According to Hardebeck and Hauksson (2001), the stress field orientation can be well-resolved using focal mechanism solutions. Hence, after inverting 182 focal mechanisms stress field orientations were estimated. Results show variation of the maximum tensile stress (σ_1) and the minimum compressional stress (σ_3) and reveal various stress directions that are classified into six regions.

Stress inversion estimation for the whole country of Madagascar has not been estimated previously, though Bertil and Regnoult (1998) determined the fault directions using focal mechanism solutions. In addition, Collins et al. (2000) conducted a study of the tectonics of Madagascar, which helped to elucidate the characteristics of faulting in the country.

In this study, the regional stress field is computed and studied for the northern, central, and southern parts of Madagascar. The stress field results obtained in the central area of Madagascar are consistent with those of previously conducted studies on fault structures *i.e.*, mainly extensional (Rindraharisaona et al., 2013). They were computed for the first time for the northern and southern parts of Madagascar. The stress field results reveal many extensional structures in the central part of Madagascar, which are consistent with the fault plane solutions obtained by Rindraharisaona et al. (2013). Some of the stress field directions observed in the northern and southern part of Madagascar correlate well with the existing thrust and shear zones in the regions (Figure 5. 5 and Figure 5. 6).

5.5.1 Northern region

Deformation processes in the area can be explained by combining the shape ratio (R) and force directions with the existing fault structure and thermal regime (Bott,

1959; McKenzie, 1969). Stress directions calculated in the northern part of the island show that the compressional stress axis is generally orientated NE-SW, although poorly constrained. R is about 0.5, which suggests strike slip faulting in this area (*e.g.*, Rakotondraibe et al., 2020, Figure 5. 5). The compressional stress σ_1 is not consistently vertical, unlike the central area of Madagascar. Prominent geological and tectonic features are the Andaparaty thrust (Figure 1. 3), the metasedimentary and (younger) volcano-sedimentary rocks in the southern and northern parts of the Bemarivo Belt, respectively (Tucker et al., 1999; Figure 1. 3); and strike-slip faults in the Antsaba and Sandrakota shear zones (Figure 5. 18). Thus, various structures are capable of slip.

5.5.2 Central region

The tectonic structure of central Madagascar is dominated by extensional faulting, formation of volcanic massifs, and the thermal bulge associated with Cenezoic magmatism (Chorowicz et al., 1990, Bertil and Regnoult, 1998, Rindraharisaona et al., 2013). Large numbers of grouped seismic events occur annually in the Famoizankova, Alaotra and Ankaratra regions. Focal mechanism solutions across this region have been reported in previous studies (Bertil and Regnoult, 1998; Rindraharisaona et al., 2013), however, no studies of stress field directions have been conducted.

For the purpose of this discussion, the central Madagascar was divided into the Alaotra, Ankaratra, Famoizankova and Itremo regions. Focal mechanism results computed in this study show that the regions are characterized by a mixture of reverse, strike-slip and normal faults. The occurrence of normal faulting is observed to be higher than that of reverse faulting (a few reverse fault mechanisms were found in the central area and strike slip faulting (see Figure 5. 2).

The stress field in the central part of Madagascar is largely extensional with the maximum compressive axis-oriented NW-SE, which is consistent with the normal faults observed in the Ankaratra and Alaotra zones. The σ_1 axis is near-vertical,

except for one subzone in the Alaotra regime where it dips at 80° (Figure 5. 13). The σ_3 axis trends 45° to the strike of the pre-existing faults. The observed stress direction can be interpreted as a reactivation of a pre-existing fault, because the principal stress values within their direction relate to the existing fault in the area study (Célérier, 1988).

In the Ankaratra zone, a volcanic area where the most recent eruption occurred during the Quaternary (de Wit, 2003*)*, the stress direction aligns with the dominant geological features, indicating the exceedance of the lithostatic pressure in the rocks beneath the area study (LeRiche et al., 2017).

Friction coefficient values estimated from the inversion revealed a range between 0.5 and 0.8. From Vavryčuk (2014), these values most often range between 0.2 and 0.8, but it is necessary for the future to test different values in order to characterize the fault strength beneath the areas.

Estimated results show that both σ_2 and σ_3 are similar to the lithostatic stress in the central region of Madagascar around the existing faults of the Angavo and the seismically active area of Alaotra, Ankaratra, and Famoizankova.

5.5.3 Bekily region

Inversion of the observed focal mechanism solutions from some of the events revealed that the direction of maximum stress trends NW-SE, while the direction of minimum stress is ENE-SWS next to the Ampanihy and Beraketa shear zones (Figure 5. 6). Next to the Ampanihy shear zone, σ_1 and σ_3 are almost horizontal, trending in the NW-SE and ENE-SWS directions. These results are in accord with strike-slip faulting on the N-S or E-W oriented vertical planes of the existing shear zone. On the other hand, the value of R is close to 0.5 around the southern active area of Madagascar. It can be interpreted as due to the small number of focal mechanisms introduced into the inversion.

The shape ratio R in the central area was generally 0.8 to 0.9, while in the northern and southern areas of Madagascar R varied from 0.3 to 0.5. The low values of R can be attributed to the variations in the horizontal compressive stress direction but may also be influenced by the small numbers of focal mechanisms used in the inversion.

5.6 Conclusion

Regional variation of stress in Madagascar and characteristics of the shape ratio including friction values were determined in this study by inverting 182 focal mechanisms of earthquakes that occurred between 2000 and 2016. The average direction of the stress field in central Madagascar is approximately NW-SE and trends W-E in the southern and northern part of the island. The shape ratio values indicate that the magnitude of stress in central Madagascar varies from 0.83 to 0.97 and the friction values range from 0.45 to 0.65.

The central part of Madagascar shows a dominant NW-SE main stress direction, which supports the link between the seismicity and volcanic activity in the Central Madagascar Alkaline Province (Andriampenomana et al., 2017). Around Lake Itasy, in the Ankaratra region, the directions of stress field are related to an extension of CMAP that shows a NW-SE direction of the mantle flow. The stress distributions in the northern and southern areas of Madagascar are consistent with the existing fault structure (*e.g.,* Andaparaty thrust, Ampanihy shear zone) observed in these two regions.

This work underlines the importance of knowing the level of the background seismic activity and the reason why clustered events are observed in the northern and southern areas. Based on this study, the main stress regime in Madagascar has been determined and was helpful in the seismic hazard studies, whose results are presented in the next chapter, and the geodynamics analysis.

Chapter 6: Seismic hazard analysis

The contents of this chapter will be submitted for publication in a peer-reviewed journal.

Probabilistic seismic hazard study for Madagascar
by Rakotondraibe, T., Durrheim, RJ, Nyblade, AA, Wysession, ME, Rambolamanana, G, Aleqabi, G, Shore, P, Pratt, MJ, and Andriampenomanana, F.

A draft of the manuscript is presented in APPENDIX G.

6.1 Introduction

Razafindrakoto et al. (2009) assessed the seismic hazard in several major Malagasy cities using the neo-deterministic approach and concluded that earthquake risk is only significant in the central part of the island. However, this could be explained by the fact that only data from permanent seismic stations, which are concentrated in the central region, were used (see Figure 3. 1). In this study we sought to overcome this spatial variation in the sensitivity of earthquake detection by using data recorded by a temporary array of stations that were widely distributed over the island.

The 41-year-long catalogue (1975-2016) of the Madagascar National Data Central (NDC, 18,275 earthquakes) was supplemented with data from the 23-month-long MAdagascar-Comoros-MOzambique (MACOMO, 695 earthquakes) project (see Chapter 3), as well as all historical events since 1897. Duplicate seismic events were removed; the catalogue was homogenized to moment magnitude (M_w) and then declustered to remove dependent earthquakes. The ZMAP (Wiemer, 2001), HA3 (Kijko and Smit, 2016) programs, and an updated version of the CRISIS 2015 software (Ordaz et al., 2013) were used to calculate the seismicity parameters for each area source zone (*viz*. the mean seismic activity rate (λ), the

Gutenberg-Richter *b*-value, and the maximum credible magnitude m_{max}) and to produce Peak Ground Acceleration (PGA) and Spectral Acceleration maps.

A probabilistic seismic hazard assessment (PSHA) was conducted using a logic-tree formalism that incorporated two ground motion prediction equations. The results are presented as maps showing the values of the peak ground acceleration (PGA) and spectral acceleration that have 2% and 10% probability of exceedance in 50 years.

6.2 Methodology

In order to determine the moment magnitude value, we first calculated the seismic moment M_o using the amplitude spectrum method described in section 2.4. Calculation was performed using the spectrum of the vertical component of the P-wave measured at five or more seismic stations (Brune 1970, 1971). The numbers of stations used for the measurement are described in Table 6. 1. The measured values of the amplitude spectra were used to compute the scalar seismic moment M_o

$$M_0 = \frac{\Omega(P) 4\pi\rho a^3 r}{cF} \text{ [N.m]} \tag{6.1}$$

where $\Omega(P)$ is the low frequency spectral level of the ground vertical displacement of the P-wave (m/s), ρ is the density (2700 kg/m^3), a is the average P-wave velocity (6200 m/s), r is the source-receiver distance (m), c is the surface amplification, and F is the P-wave radiation pattern correction factor (F=0.64, Baumbach and Bormann,2012). The measurement was performed using the *dbfmeas* module in the Antelope software. An example of the measurement is presented in APPENDIX H. The moment magnitude (M_w) was then calculated using the expression (Hanks and Kanamori, 1979) for magnitudes between 3< M<7.5:

$$M_w = \frac{2}{3}\log M_0 - 6.07 \tag{6.2}$$

After getting values of moment magnitude M_w, a relation between local magnitude M_L and moment magnitude M_w was established using a linear regression method from the 79 seismic events presented in Table 6. 1

$$M_w = 0.6927M_L \pm 1.0729 \quad (6.3)$$

Table 6. 1: Earthquakes used to determine the M_L-M_w relation. (A) Earthquakes from the MACOMO bulletin, (B) Earthquakes from the ISC bulletin; "σ" is the average uncertainty value for M_w in m.u. (magnitude units).

ID	Date	Time	Lat (deg)	Lon (deg)	Depth (km)	Number of stations	M_W calculated	σ [units]	M_L	Ms	mb
A – MACOMO Bulletin											
1	17/06/2012	10:11:35.55	-16.522	49.2278	16.94	7	**3.8**	0.42	**3.7**	x	x
2	22/08/2012	00:35:11.87	-14.2947	48.6165	11.46	9	**3.7**	0.23	**3.6**	x	x
3	18/10/2012	17:36:06.02	-19.8398	46.9042	16.82	12	**4.3**	0.13	**4.1**	x	x
4	18/10/2012	16:12:48.69	-16.804	49.7427	29.59	20	**4.1**	0.09	**4.0**	x	x
5	01/11/2012	00:19:28.21	-17.2653	49.0033	11.41	20	**4.8**	0.18	**4.6**	x	x
6	20/11/2012	00:00:51.88	-20.4418	45.5143	24.35	9	**4.5**	0.12	**4.3**	x	x
7	13/01/2013	13:24:54.51	-18.6833	45.9278	13.04	12	**4.4**	0.19	**4.2**	x	x
8	18/03/2013	21:50:52.25	-16.4393	48.0308	5.00	14	**3.7**	0.21	**3.6**	x	x
9	26/03/2013	09:48:39.60	-24.3653	44.4453	9.22	10	**4.0**	0.26	**3.9**	x	x
10	16/03/2012	11:56:55.31	-17.5436	48.4476	10.12	8	**4.0**	0.20	**3.9**	x	x
11	25/01/2013	23:37:26.10	-23.5760	43.5002	22.73	25	**5.4**	0.05	**5.2**	x	x
B – ISC Bulletin											
12	19/08/1981	21:35:30.39	-20.6244	47.3995	10.0	5	x	x	x	x	**3.8**
13	04/10/1982	00:50:59.75	-12.3790	47.2181	10.0	5	x	x	x	x	**4.9**
14	27/12/1983	00:39:06.20	-18.1941	44.6756	12.4	5	x	x	x	x	**5.2**
15	16/06/1986	05:41:26.49	-12.2811	43.6517	10.0	5	x	x	x	x	**4.8**
16	08/02/1996	15:32:15.32	-12.0438	43.9341	10.0	5	x	x	x	x	**4.2**
17	26/07/1996	19:54:44.60	-25.8200	46.3500	0.0	5	x	x	x	x	**4.0**
18	15/10/1999	11:35:06.97	-20.1722	45.8332	28.6	5	x	x	x	x	**4.1**
19	15/08/2005	00:44:05.30	-12.4197	43.2172	10.0	5	x	x	x	x	**4.4**
20	11/06/2006	00:04:53.95	-15.7449	49.7074	10.0	5	x	x	x	x	**4.0**
21	13/10/2006	21:31:02.90	-12.4284	43.3217	10.0	5	x	x	x	x	**4.5**
22	28/12/2006	10:02:22.92	-12.3042	46.4062	10.0	5	x	x	x	x	**4.2**
23	27/07/2008	17:47:24.61	-20.2209	44.4145	10.0	5	x	x	x	x	**3.8**
24	18/12/2009	08:05:26.57	-19.3590	45.0111	10.0	5	x	x	x	x	**3.6**

25	18/09/2011	06:28:38.65	-16.0901	43.3165	0.0	5		x	x	x	**3.7**
26	04/04/1975	17:41:16.17	-21.2314	45.1490	16.5	5	**5.6**	x	x	x	x
27	31/01/1983	17:37:49.45	-23.2150	44.0992	10.0	5	**5.1**	x	x	x	x
28	04/10/1985	15:17:09.68	-18.2948	48.4866	17.9	5	**5.5**	x	x	x	x
29	21/04/1991	23:12:22.86	-18.5510	46.4513	14.2	5	**5.6**	x	x	x	x
30	14/11/1992	05:54:48.10	-23.2313	45.8835	16.3	5	**5.0**	x	x	x	x
31	21/05/2000	02:58:45.14	-12.3331	43.6925	17.0	5	**5.2**	x	x	x	x
32	23/06/2007	11:54:54.66	-12.2689	46.4098	10.4	5	**5.1**	x	x	x	x
33	09/09/2011	13:25:04.17	-12.6705	44.8002	10.0	5	**5.0**	x	x	x	x
34	25/01/2013	23:37:02.99	-23.5456	43.6027	23.6	7	**4.9**	x	x	x	x
35	21/09/2016	01:08:45.17	-12.5798	43.2469	10.8	7	**5.2**	x	x	x	x
36	27/11/2016	16:13:53.48	-16.4369	42.9991	10.0	7	**4.8**	x	x	x	x
37	23/04/1993	16:35:43.00	-13.7273	45.0225	13.8	4	x	x	x	**4.2**	x
38	01/12/1993	22:04:24.29	-12.8529	44.7101	12.6	4	x	x	x	**4.9**	x
39	26/06/1996	02:04:03.94	-18.4544	48.4423	11.6	5	x	x	x	**4.7**	x
40	22/09/1998	19:27:33.81	-20.1456	45.3536	19.3	5	x	x	x	**4.4**	x
41	19/01/1999	01:03:36.36	-22.2088	47.1451	10.0	5	x	x	x	**3.7**	x
42	23/09/2001	17:57:48.38	-12.4446	45.4456	10.0	5	x	x	x	**3.4**	x
43	31/03/2004	09:27:11.62	-23.8339	46.4847	10.0	5	x	x	x	**4.2**	x
44	05/01/2005	14:06:27.26	-14.2579	47.9732	10.0	5	x	x	x	**4.9**	x
45	15/08/2005	00:44:05.30	-12.4197	43.2172	10.0	5	x	x	x	**3.7**	x
46	08/12/2007	15:58:17.56	-24.5803	44.6343	10.0	5	x	x	x	**2.8**	x
47	09/06/2008	12:19:59.56	-17.9393	45.9144	0.0	5	x	x	x	**2.8**	x
48	09/09/2008	18:23:30.55	-12.3286	46.1930	10.0	5	x	x	x	**3.4**	x
49	03/11/2008	08:41:24.34	-17.5206	46.8588	12.5	5	x	x	x	**3.3**	x
50	06/02/2010	01:53:24.77	-15.8630	49.8874	10.0	5	x	x	x	**2.9**	x
51	08/12/2010	02:45:55.73	-14.4152	48.7230	10.0	5	x	x	x	**3.0**	x
52	16/03/2012	11:56:55.31	-17.5436	48.4476	10.0	6	x	x	x	**3.3**	x
53	12/03/2014	20:43:32.13	-12.2028	44.0956	10.0	5	x	x	x	**4.2**	x
54	01/10/2015	21:47:08.86	-12.4683	44.4869	10.0	5	x	x	x	**3.6**	x
55	30/10/2015	02:19:38.17	-14.7956	49.9844	10.8	5	x	x	x	**3.9**	x
56	01/01/1995	11:57:03.30	-18.0800	46.4100	10.0	5	x	x	**4.5**	x	x
57	05/01/1995	01:02:04	-16.3900	49.0900	10.0	5	x	x	**4.1**	x	x

58	08/01/1995	06:48:51.10	-17.6400	46.4500	10.0	5	x	x	**5.4**	x	x
59	25/01/1995	11:55:04.90	-24.6800	44.9400	10.0	5	x	x	**4.3**	x	x
60	12/02/1995	12:56:50.50	-19.0700	46.8000	10.0	5	x	x	**4.7**	x	x
61	16/02/1995	10:24:01.30	-15.8400	48.5200	10.0	5	x	x	**4.2**	x	x
62	20/02/1995	11:00:38	-18.2500	49.3100	10.0	5	x	x	**4.0**	x	x
63	28/02/1995	23:28:23.70	-18.3500	48.5800	10.0	5	x	x	**4.3**	x	x
64	27/03/1995	01:18:40.70	-23.5600	45.5200	10.0	5	x	x	**4.0**	x	x
65	13/04/1995	02:49:31.33	-14.7300	45.1800	10.0	5	x	x	**2.9**	x	x
66	15/05/1995	04:58:06.50	-18.3100	45.4700	10.0	5	x	x	**4.2**	x	x
67	17/05/1995	01:34:28	-16.1400	42.5700	10.0	5	x	x	**4.9**	x	x
68	12/06/1995	15:40:53.70	-17.8500	49.6700	10.0	5	x	x	**4.3**	x	x
69	14/07/1995	19:23:42.20	-22.4000	46.8300	10.0	5	x	x	**4.4**	x	x
70	31/07/1995	05:33:38.40	-12.5700	46.3700	10.0	5	x	x	**4.8**	x	x
71	06/08/1995	03:53:22.70	-12.6300	45.7200	10.0	5	x	x	**4.0**	x	x
72	15/08/1995	12:18:44.10	-12.2300	47.6500	10.0	5	x	x	**5.0**	x	x
73	23/08/1995	01:13:13.90	-18.4300	46.2400	10.0	5	x	x	**5.3**	x	x
74	31/08/1995	07:13:24	-20.0400	47.1200	10.0	5	x	x	**4.1**	x	x
75	13/10/1995	19:23:08.40	-17.8300	46.5100	10.0	5	x	x	**4.1**	x	x
76	15/10/1995	16:02:32.90	-19.6400	46.9900	10.0	5	x	x	**4.3**	x	x
77	12/11/1995	00:37:56.80	-17.3800	48.3300	10.0	5	x	x	**4.2**	x	x
78	13/12/1995	11:26:47.70	-12.1800	43.9400	10.0	5	x	x	**4.8**	x	x
79	07/12/2016	01:02:07.70	-17.1030	46.7800	10.0	8	x	x	**3.4**	x	x

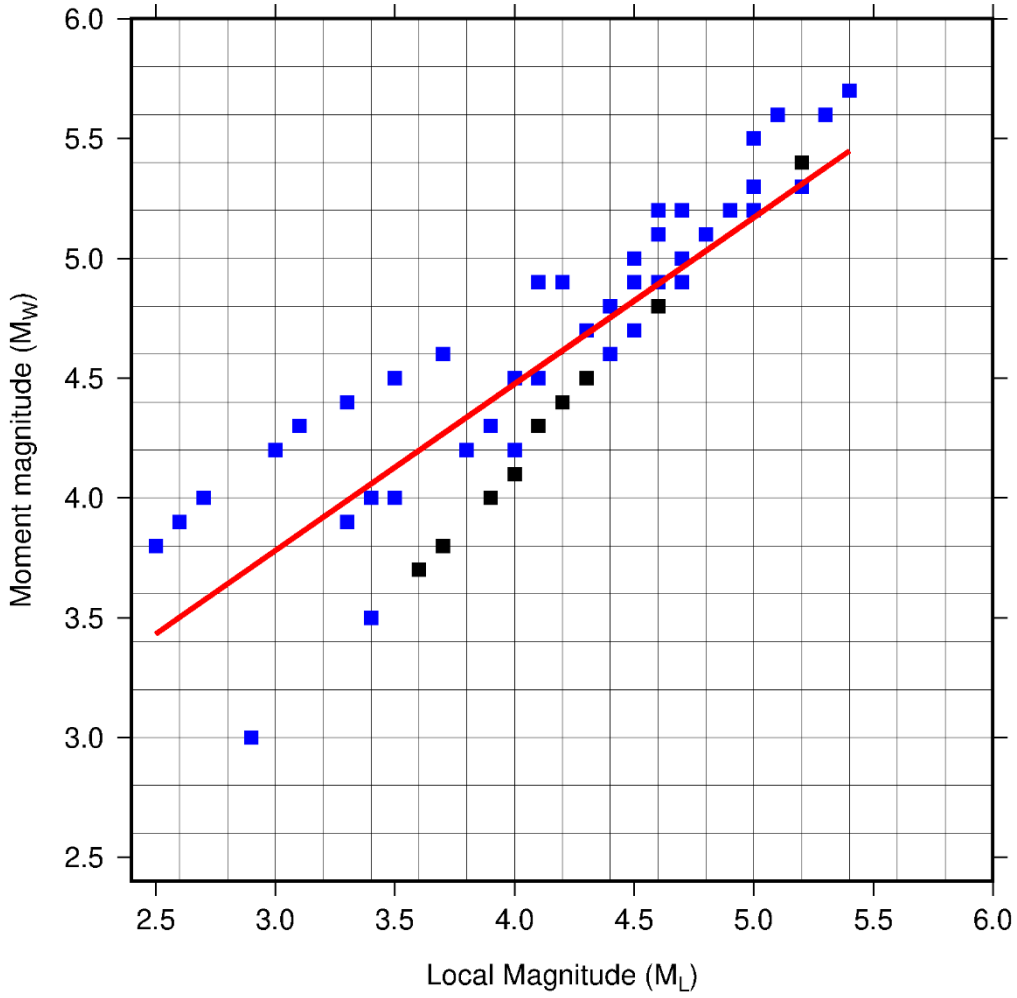

Figure 6. 1**:** Plot of the estimated relation between M_w and M_L for 80 eartthquakes reported in the MACOMO catalogue (black) and events derived from ISC bulletin (blue).

6.2.1 Declustering

In PSHA it is assumed that the events in the catalogue have a Poissonian distribution *i.e.*, that they are independent. Thus, it is necessary to identify and remove dependent events, such as fore- and aftershocks, from the catalogue (See Chapter 3, section 3.2.2).

Declustering was done using the ZMAP program (Wiemer, 2001). Two different approaches were set during the calculation. The approach that applies the Reasenberg (1985) algorithm to eliminate all events that fall within specified space and time intervals of main shocks; and the approach that applies the Gardner and Knopoff (1974) algorithm that uses predefined windows in space and time to identify independent and dependent seismicity (See Chapter 3, section 3.2.2).

We introduced all raw data from the catalog into a text file and take it as input for the program; then we run the program by selecting "Decluster the catalog" from the "Tools". From the criteria mentioned in section 3.2.2, we first tested the program by running the Reasenberg algorithm using different parameters presented in Table 6. 1. Unsurprisingly, different parameter values produced different numbers of declustered events (See Table 6. 2). TEST 1 used the default values except for RFACT, which was changed from 10 km to 15 km due to the characteristics of the repeated earthquakes that surrounding the area; while TEST 2 and 3 consist on setting all values to 5 and 20 for RFACT based on the characteristics of the seismic events in some areas which are not very seismically active and recorded by few seismic stations (*e.g.,* in the Northern part and Southern part of Madagascar). It was found that all tests produced a smaller catalogue than the default parameters (Table 6. 2)

Table 6. 2: Parameters set for the declustering method following Reasenberg (1985) method after inserting 18,970 seismic events.

Declustering parameters	**DEFAULT**	**TEST 1**	**TEST 2**	**TEST 3**
TAUMIN (days)	1	1	0.5	2.5
TAUMAX (days)	10	10	3	15
P_1	0.95	0.95	0.95	0.95
XK	0.5	0.5	0	1
XMEFF	1.5	1.5	1.5	1.5
RFACT (km)	10	15	5	20
Epicenter-Error (km)	1.5	1.5	1.5	1.5
Depth-Error (km)	2	2	2	2
RESULTS event numbers in the map after declustering	11,950	9,622	10,348	7,503

To apply the Gardner and Knopoff (1974) method, which is also called a “window method”, we used the same input catalogue as used to test the Reasenberg method and specified the maximum and minimum numbers of events and grid spacing in the parameter file (Table 6. 3).

The characteristics of the declustered events from Gardner and Knopoff method are shown in Figure 6. 2 as two cross sections which present the magnitude-time and magnitude-distance distributions for declustered events.

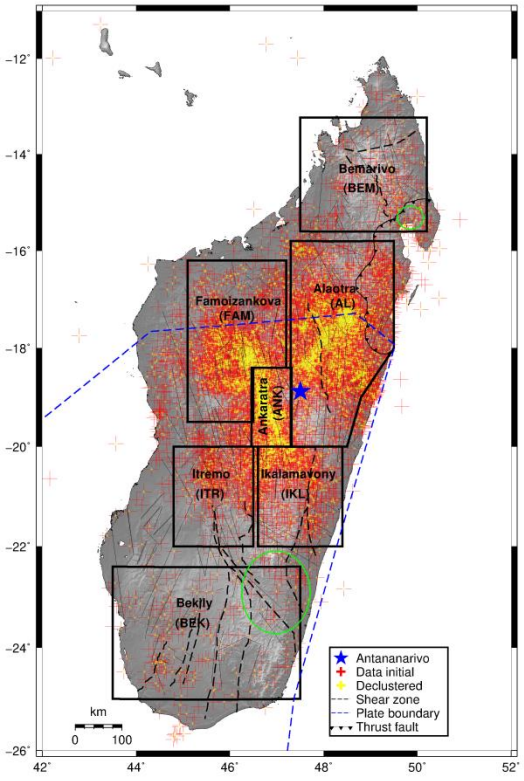

From the default values

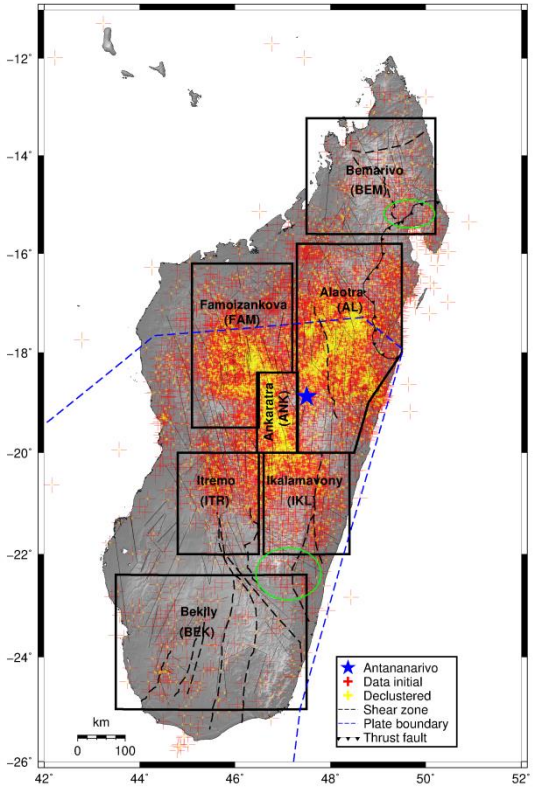

From TEST 1

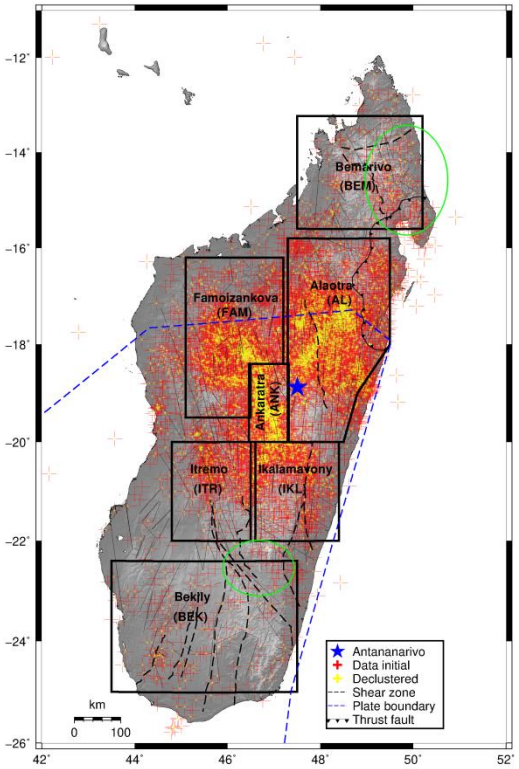

From TEST 2

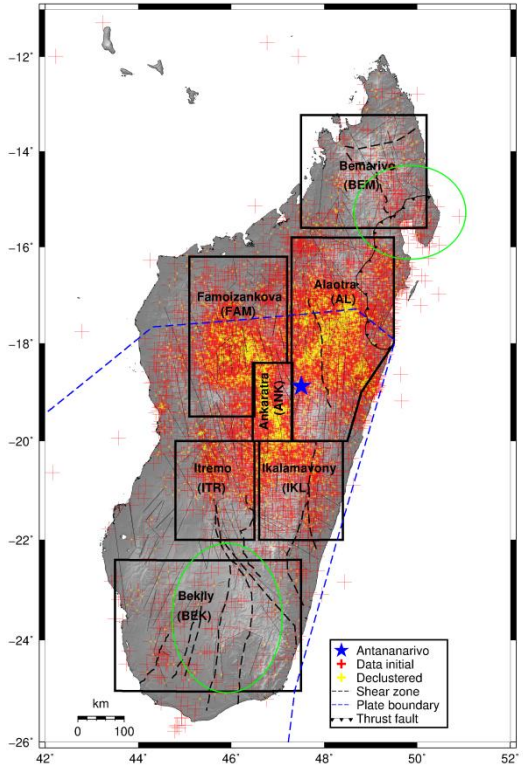

From TEST 3

Figure 6. 2: Declustering using the Reasenberg (1985) method after testing different values into the parameter files. The red plus symbols represent the main event in the catalogue and the yellow plus symbols represent events after declustering. Highlighted areas in black show the defined area sources in this study, green ellipses show the areas where some events were removed after

declustering.

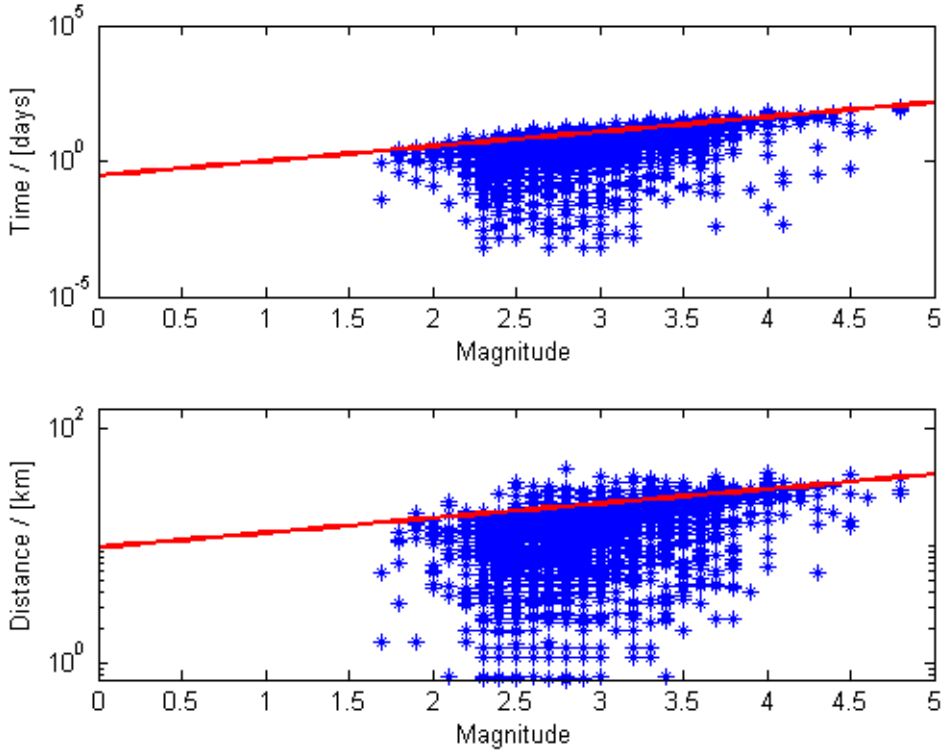

Figure 6. 3: Magnitude-time distribution and magnitude-distance distribution for declustered events in the whole area of Madagascar. The size of the time and space windows depends on the magnitude of the main shock. Blue stars represent all events, and the red line shows the calculated regression depending on time and the distance (best fit). Seismic events below the red line are potential members of clusters.

Table 6. 3: Parameter values inserted for declustering method using the Gardner and Knopoff (1974) approach. Max. Numb and Min. Numb are the maximum and minimum numbers of events to identify clusters, Max. radius is the maximum radius between two linked events.

Max Numb	Min. Numb	Max. radius (km)	Grid spacing (deg)
200	20	40	0.5
RESULTS Numbers of removed seismic events: Total numbers of seismic events after the declustering method:	2,740 11,950		

We decided to use Gardner and Knopoff (1974) (Table 6. 3) approach for the seismic hazard study for Madagascar. We considered that the window method gave better results as this method preserved events in the northern and southern parts of Madagascar that were removed by the Reasenberg (1985) method (Figure 6. 2).

6.2.2 Definition and characterization of source zones

The definition and characterization of fault and area sources are crucial steps in PSHA. The characterization of a fault source requires a dense seismic network that accurately locates the hypocenters of many events on a particular fault. This is not the case in Madagascar, where the network is too sparse to allow locations to be reliably attributed to any particular fault, and the duration of recording is too short to characterize fault behavior. Consequently, we had to rely on area sources. We defined regions that have similar seismotectonic characteristics by considering the factors such as spatial and temporal earthquake distributions, and the presence of faults that are known or suspected to be active (Rindraharisaona et al., 2013; Rakotondraibe et al., 2020). In this work we defined seven area source zones (Figure 3. 9):

Zone 1 (S1: BE), named the Bemarivo zone. The Andaparaty thrust is a prominent feature. The thrust zone is several hundred meters thick and dips northwards at a

low angle (Thomas et al., 2008). A total number of 300 events remained after declustering.

Zone 2 (S2: AL), named the Alaotra zone. The Alaotra area is seismically very active (Rindraharisaona et al., 2013). The zone includes both the Alaotra and Ankay basins. Both basins contain basal conglomerates, lake and swamp deposits (Bésairie, 1964) and are connected by a river that flows along the Alaotra-Ankay rift. The river course is considered to reflect re-adjustment of the land surface following recent tectonic activity (Bertil and Regnoult, 1998). The cluster of seismicity near the rift system has been attributed to extensional tectonic activity (Mougenot et al., 1986; Bertil and Regnoult, 1998; Rakotondraompiana et al., 1999). The Alaotra basin contains volcanic rocks that are considered to be a continuation of the Neogene-Quaternary Ankaratra magmatic field (Brenon and Bussiere, 1959; Bésairie, 1964; Laville et al., 1998). A total number of 4,954 events remained after declustering.

Zone 3 (S3: FAM), named the Famoizankova zone. It is characterized by relatively high seismic activity and relatively large events. The maximum observed magnitude is M5.6. A total number of 2,498 events remained after declustering.

Zone 4 (S4: ANK), named the Ankaratra zone. Lake Itasy lies within the zone. It is a relatively active zone associated with volcanic fields. Extensional source mechanisms were identified by Rindraharisaona et al., (2013). A total number of 2,546 events remained after declustering.

Zone 5 (S5: ITR), named the Itremo zone. The geology in this zone is characterized by volcano-clastic metasediments. A total number of 318 events remained after declustering.

Zone 6 (S6: IKL), named the Ikalamavony zone. The Ranotsara shear zone is an important feature in this area source zone. A total number of 1,224 events remained after declustering.

Zone 7 (S7: BEK), named the Bekily zone. Delimitation of this zone is based on the characteristics of earthquake data and the available tectonic constraints, including the tectonic orientation of the crustal stress field direction. Different zones were supposed to be set depending on the observed fault zones but due to the small amount of the earthquakes data observed around the different fault zones, it is better for this study to group the zone into one area source. This area is located in the extreme southern part of Madagascar. Several shear zones occur in this area source zone. A total number of 110 events remained after declustering. The MACOMO network added considerably to the knowledge of seismicity in this region. The largest observed earthquake is an M4.8 event.

In order to assess the seismic hazard of Madagascar, each seismic source area was characterized in terms of:

1. Magnitude of completeness of the earthquake catalogue (M_c),
2. Seismic activity rate (λ) for magnitude $\geq$ M2.9,
3. Maximum possible earthquake magnitude (m_{max}),
4. The *b*-value and β, and
5. Focal depth.

The listed parameters for each source area were estimated using a maximum likelihood approach using the HA3 program of Kijko and Smit (2016) (see section 2.6.6).

6.2.2.1 Magnitude of Completeness, M_C

The magnitude of completeness (M_c) is the smallest magnitude for which all the earthquakes that occurred in a certain region and in a given time window are recorded. The completeness of the earthquake catalog is an important consideration in seismic hazard studies as it affects the calculation of seismicity parameters. Completeness can be assessed using network- or catalogue-based

methods. The network-based strategies use waveforms and phase-pick data to calculate the probability that an earthquake will be detected, depending on the location and the susceptibility of the seismic stations (Mignan and Woessner, 2012). In this study, we used a catalogue-based method. It assesses the range over which cumulative frequency-magnitude distribution of Gutenberg and Richter (1942) is linear. The point of maximum curvature of the frequency-magnitude distribution underestimates M_c. Several catalog-based methods have been proposed to determine M_c more accurately *e.g.*, Stepp (1972), Wiemer and Wyss (2000), Beauval and Scotti (2003). M_c may also change with time as the density and sensitivity of the network changes. The Malagasy catalogue may be divided into two main periods:

1. 1897 to 31 December 1974. The catalogue comprises on nine earthquakes, one historical (1897) and eight that were instrumentally recorded (Table 6. 2)
2. 1 January 1975 to 31 December 2016. The catalogue can be split into sub-catalogues with diverse levels of completeness based on the location and number of stations.
    a. 01 January 1975 to 31 December 2008, where seismic stations were mostly located in the central area of Madagascar.
    b. 01 January 2009 to 31 October 2013, in which the number of seismic stations started to be improved after including the ABPO permanent station and all temporary station from MACOMO; and
    c. 01 November 2013 to 31 December 2016, in which all temporary stations were removed.

The time-magnitude distribution within color-coded M_w for each year is presented in Figure 6. 4, which shows that between 1990 and 2015 the number of earthquakes having magnitude below 4.0 are quite large. The selected Mc values for each zone are presented in Table 6. 4. The time-magnitude distribution within color-coded M_w for each year is presented in Figure 6. 4, which shows that between 1990 and 2015 the number of earthquakes having magnitude below 4.0 are quite large.

Table 6. 4: Mc values from the two bulletins NDC and MACOMO. (a) 1897-1974, (b) 1975-2008; (c) 2009-2013; (d) 2013-2016

Mc values	BEM	AL	FAM	ANK	ITR	IKL	BEK
a	2.4	2.6	2.5	2.1	2.6	2.3	2.7
b	2.8	2.5	2.8	2.3	2.4	2.5	2.9
c	2.6	2.4	2.6	2.4	2.3	2.5	2.6
d	2.6	2.4	2.4	2.1	2.5	2.1	2.8
Average	2.6	2.5	2.6	2.2	2.5	2.4	2.8

Table 6. 5: Largest earthquakes between November 1897 and December 1995

ID	d/m/y	Lat(deg)	Lon(deg)	Mag	Intensity	Region
1	11/03/1897				VIII	Itasy
2	09/14/1932				VII	Mantasoa
3	03/29/1943	-18.6	44.2	6	VII	West Coast
4	02/28/1945				VII	Itasy
5	04/29/1952	-15	44.5	6		Mozambique
6	04/16/1955				VII	Itasy
7	11/10/1955				VII	Alaotra
8	05/18/1965	-17.6	49.9	5.4		Ste Marie
9	06/30/1974	-13.47	48.9	5.4		Nosy Be
10	04/04/1975	-21.24	45.12	5.3		Morondava
11	01/31/1983	-23.5	44.6	5		Morondava
12	12/271983	-18.3	45.1	5.1		Bongolava
13	10/04/1995	-18.3	48.4	5.1		Ankay
14	04/21/1991	-18.35	46.37	5.8		Famoizankova
15	01/29/1992	-13.56	49.93	5		North Madagascar
16	02/20/1992	-23.24	44.55	5		Morondava
17	11/14/1992	-22.87	45.74	5.1		Betroka

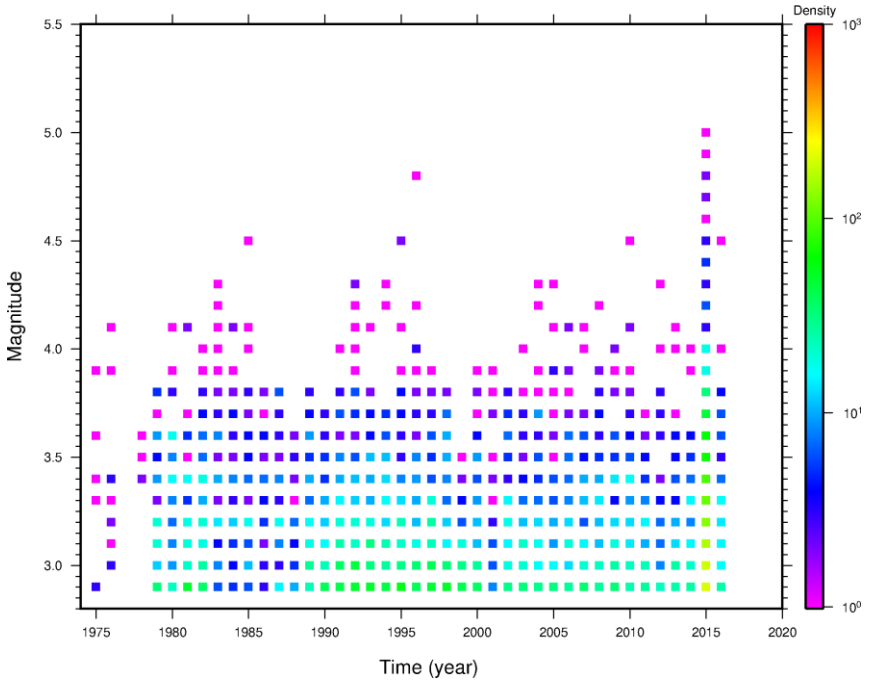

Figure 6. 4: Timeline showing the annual number of earthquakes as a function of magnitude in the period 1975-2016, $M_w \geq 2.9$

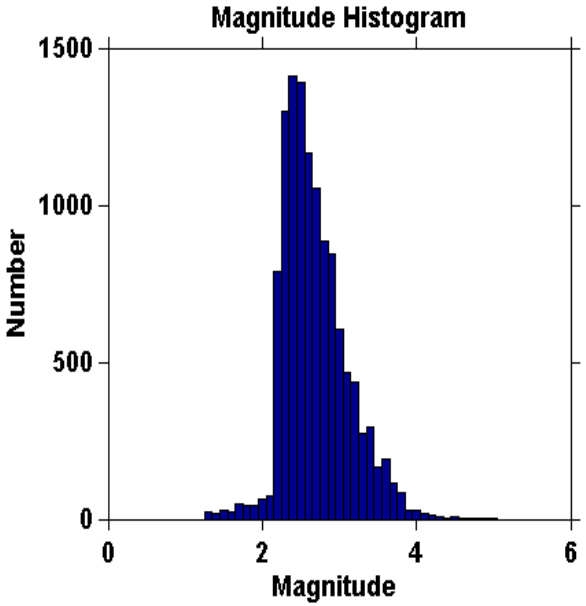

Figure 6. 5: Histogram showing the moment magnitude of all earthquakes in Madagascar, 1975-2016 inclusive.

The magnitude of completeness (M_C) for each source zone was estimated using the HA3 computer program (Kijko, 2016; Figure 6. 6). After determining all values of M_C for all seismic source zones, the completeness magnitude map (Figure 6. 7) was created using the output file from ZMAP program (Wiemer, 2001). Estimated MC map was done in single measurement for each source zone using ZMAP (ZTool) and input data from the bulletin were initialy inserted to the ZMAP program zone by zone so that combination of the results into one map using the Generic Mapping Tool (GMT program) is seen in Figure 6. 7. The observed map shows the spatial distribution of the magnitude of completeness (Figure 6. 7).

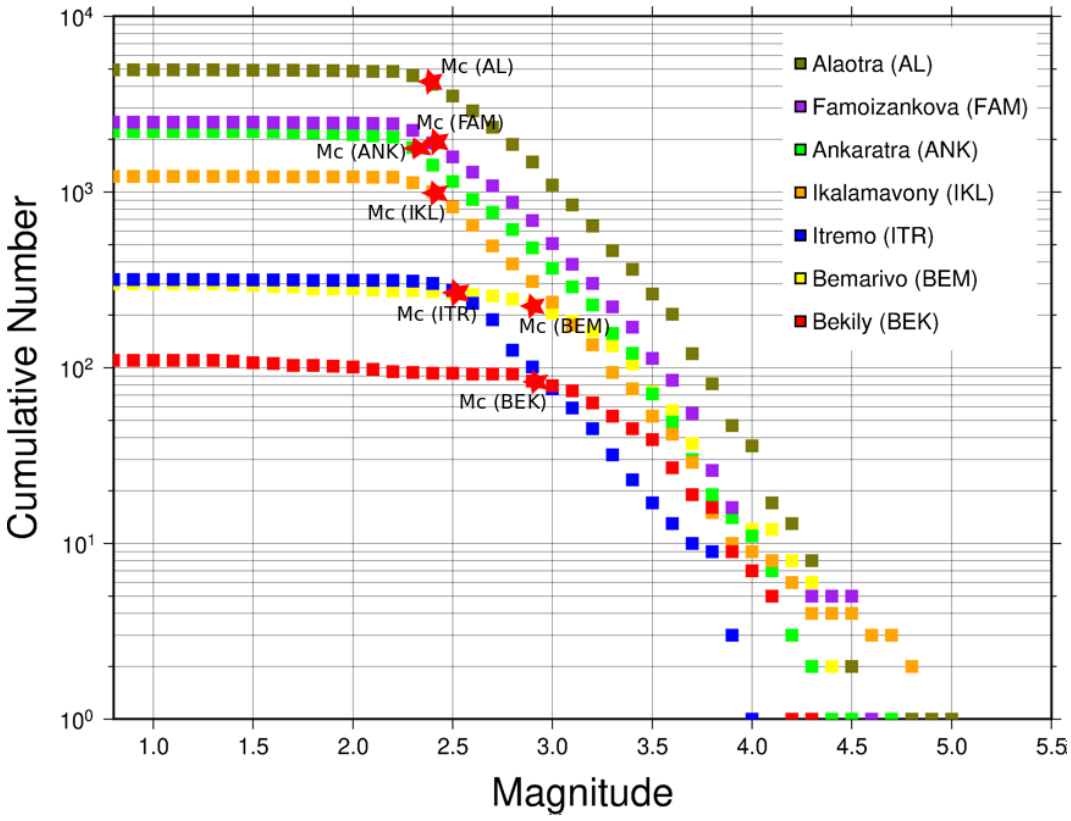

Figure 6. 6: Completeness estimation for all source zones for 42 years (1975- 2016, inclusive). Red stars indicate the M_C values.

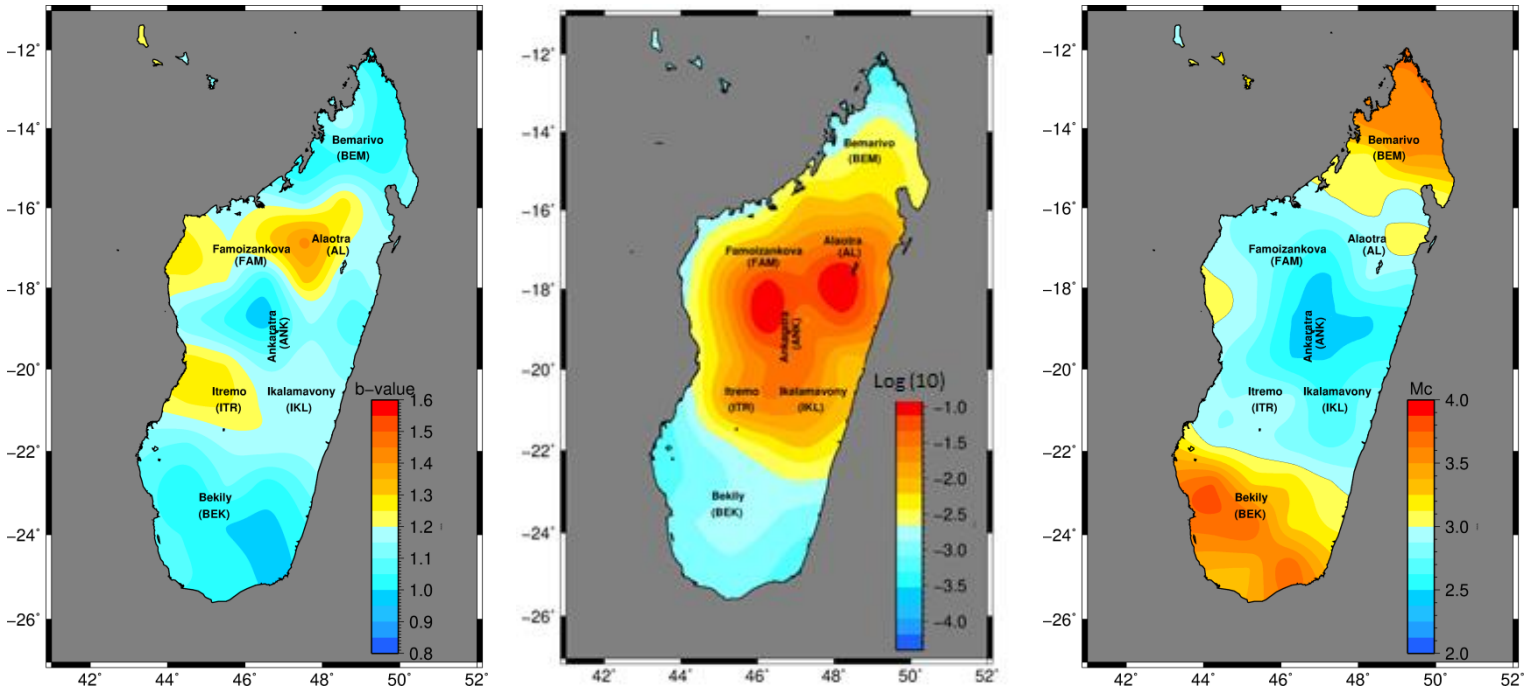

Figure 6. 7: Results from ZMAP using data from the combined two catalogues (NDC+MACOMO) but plotted using GMT (Wessel and Smith, 1998). Figures show: a) *b*-value distribution, b) the earthquake density (Tremors/area) and c) Magnitude of completeness distribution.

6.2.2.2 Recurrence parameters (*a* and *b*–values)

The *a*- and *b*-values of the Gutenberg-Richter relation (Richter 1935; Gutenberg and Richter, 1942) were calculated using the earthquake catalogues for each area source using Kijko and Sellevoll (1992) method (see Chapter 2, section 2.5.3). Distribution of the *b*-values is shown in Figure 6. 7 a. Earthquake activity is shown in Figure 6. 7 b and it clearly shows that the central area of Madagascar is the most active. The spatial distribution of the magnitude of completeness is shown in Figure 6. 7 c.

The frequency magnitude distribution for each source zones is shown in Figure 6. 6 and the seismicity parameters obtained for each area source are summarized in Figure 6. 7.

However, the m_{max} values that are considered as largest possible earthquake on faults were calculated from the estimated magnitude frequency relation mentioned previously (See Chapter 2). Values are presented in Figure 6. 7.

6.2.2.3 Focal Depth Values

Accurate focal depths are difficult to determine owing to the sparse station coverage. However, according to previous seismic studies (*e.g*. Rindraharisaona et al., 2013), earthquake foci are generally in the crust, shallower than 35 km. We selected values between 1-15 km and 15-35 km in the logic tree because about 66% of events have depths between 1-15 km while 34% have depths between 15 and 35 km according to the recorded seismic events in the catalog. During this work, range of the depth was applied for the seismic hazard calculation.

Table 6. 6: Characteristics of all seismic hazard parameters for all sources, where m_{max} is the maximum magnitude value, Beta (β) is equal to b*ln(10) a Gutenberg-Richter parameter.

	BEM	**AL**	**FAM**	**ANK**	**ITR**	**IKL**	**BEK**
***b*-value**	1.32	1.54	1.49	1.52	1.17	1.28	1.19
m_{max}	4.8	5.4	4.8	4.8	4.8	5	4.4
***a*-value**	6.69	167.45	81.23	129.30	8.26	34.97	2.52
Beta	3.04	3.55	3.43	3.50	2.69	2.95	2.74

6.2.3 Ground Motion Prediction Equations

The ground motion model plays an important role in seismic hazard assessment as it determines the anticipated level of the ground movement. This parameter relates to the ground motion of a geographical area. To the best of our knowledge, no strong ground motion data has been recorded in Madagascar and thus no GMPE has been developed specifically for Madagascar. In such cases researchers normally make use of models developed for other regions that have similar tectonics to the study region (Douglas, 2007). Madagascar is located in the southeastern part of Africa (Figure 6. 8) and in a stable intraplate region which has low seismic activity, randomly located in space and time. Consequently, we decided to use well-accepted attenuation models that have been developed for similar tectonic settings.

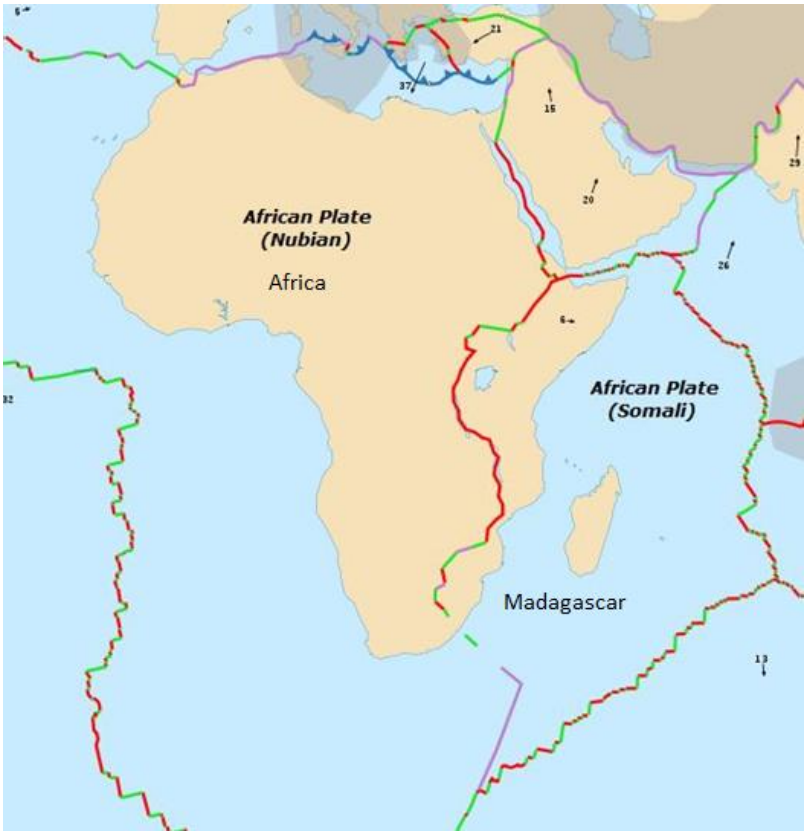

Figure 6. 8: Madagascar's location in the southeastern part of Africa https://platetectonicsafrica.weebly.com/cer.html

In general, it is standard practice to use the mean or median of multiple attenuation equations in assessing seismic hazard for an area by taking into consideration the geological structure statements of the area studies.

During this work, we selected the Next Generation Attenuation (NGA) models developed by Boore et al. (2014) and Chiou and Youngs (2014). Both models are for shallow (crustal) earthquakes. The Boore et al. (2014) model was developed for active tectonic region, considered to be similar to the volcanically-active regions of Madagascar; while the Chiou and Youngs (2014) model is applied for stable continental regions, which is similar to the rest of the island. Attenuation curves were plotted in a graph for a M3.5 seismic event at a distance range of 0 to 250 km (Figure 6. 7). The results are typical for a small felt earthquake. Records at station about 8 km from the epicenter were used for calibration.

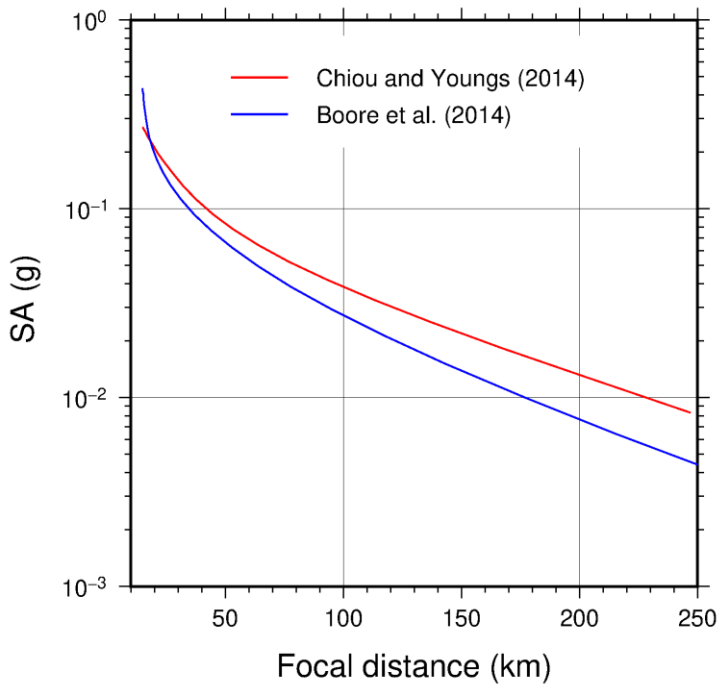

(a)

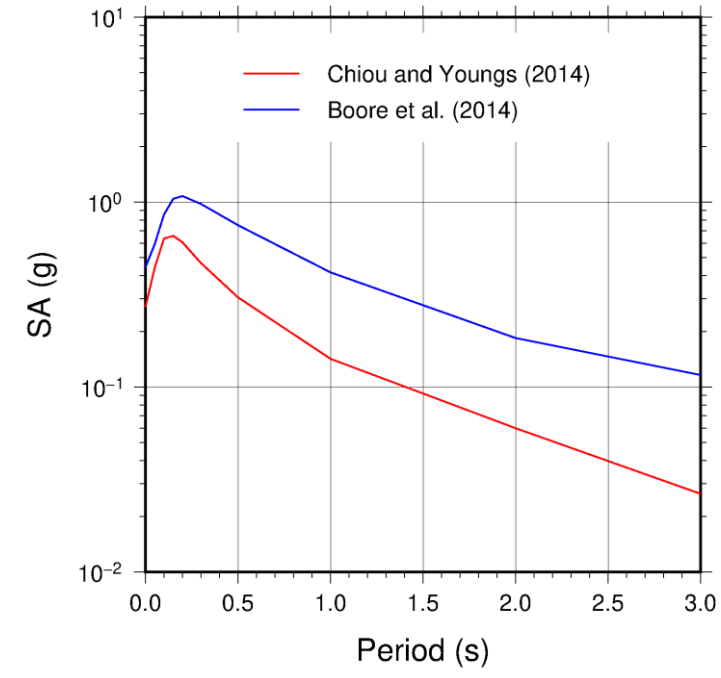

(b)

Figure 6. 9: Predicted ground motion for an M=3.5 earthquake with a 15 km focal depth calculated using the Chiou and Youngs (2014) and Boore et al. (2014) attenuation equations. (a) Attenuation curves, (b) Spectral acceleration at an epicentral distance of 8 km.

6.2.4 Seismic Hazard Computation

6.2.4.1. Ground motion parameter model

The CRISIS software (Ordaz et al., 2013), which was used to perform the hazard calculation for Madagascar, follows the Cornell (1968) approach (see Section 2.5.2). This software requires information about each seismic source area (see section 3.2.3) including the latitude and longitude defining the boundary; the activity rate (λ) for $M \geq 2.9$, the *b*-value derived from the Gutenberg-Richter frequency magnitude distribution; the minimum magnitude which is $m_{min=}$ 2.9 and the derived maximum earthquake magnitudes using the Kijko and Sellevol approach (K-S approach) (Kijko and Sellevol, 1989, 1992). In addition to these parameters the local site effect was considered by implementing the V_{S30} method as mentioned in section 2.6.7. Amplification induced from site effects has been recognized as the major cause of structural collapse. In this study, seismic amplification is measured with an amplification factor (AF), defined as the ratio of response spectra between soil surface and outcropping reference rock.

A 0.5° x 0.5° grid covering the whole of Madagascar was constructed, consisting of 510 nodes (Table 6. 7; Figure 6. 10). At each node, the contribution of each of the seven source areas to the hazard was calculated and summed. Prior to running CRISIS to calculate the PSHA map, two preliminary procedures had to be performed, *viz.* the choice of the spatial integration parameters, and the definition and assignation of weights to the various branches of the logic-tree. The spatial integration was carried out to assess the contributions of all possible focal locations (See Chapter 4). As Madagascar's dimension is about 1,580 km, high integration distance was set to 500 km which shows that, for each node over the grid, only sources situated within that distance are defined for the seismic hazard assessment.

Table 6. 7: Parameters used to create the grid for seismic hazard

Location	Longitude (degrees)	Latitude (degrees)
Origin	43	-26
Increment	0.5	0.5
Number of lines	18	30

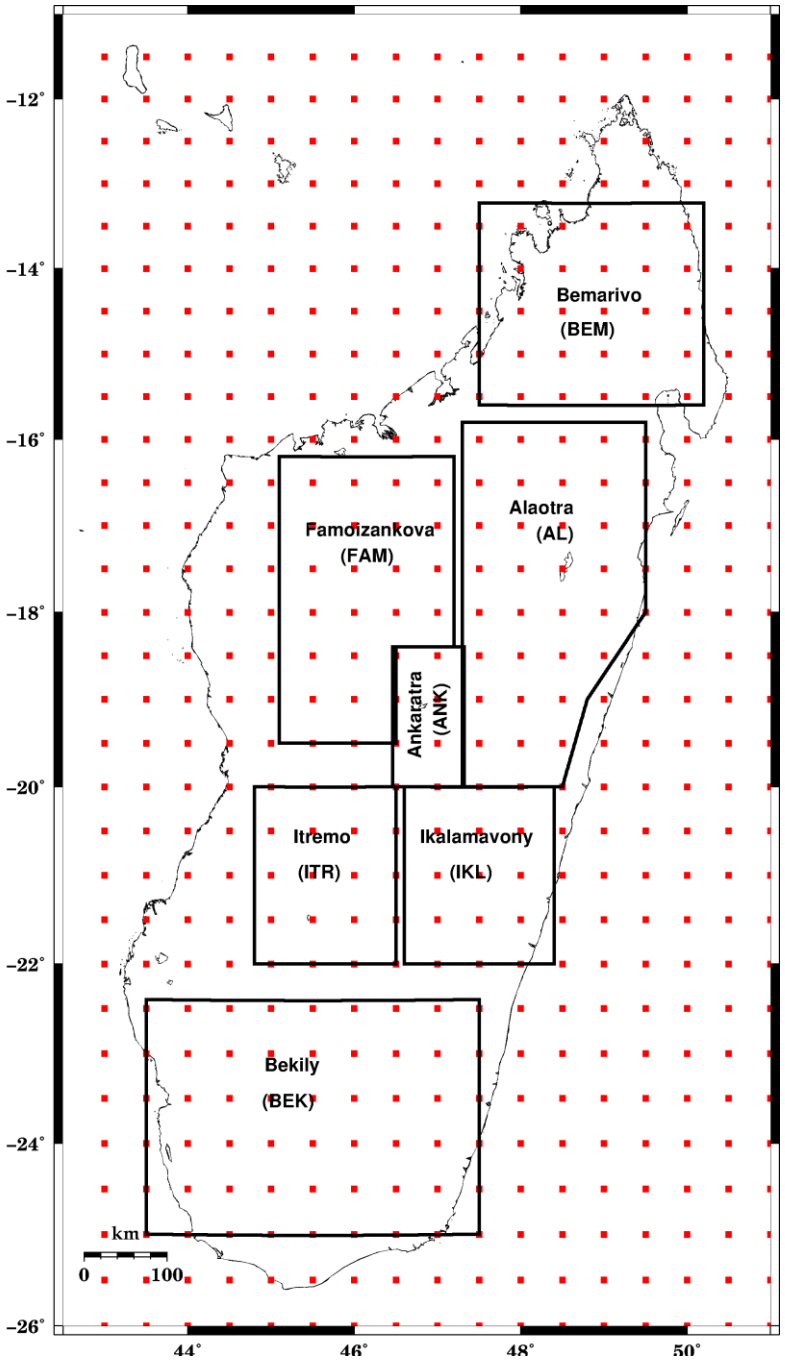

Figure 6. 10: Map of Madagascar showing the 510 nodes (red squares) and seismic source zones (black boxes) used to establish the seismic hazard studies for Madagascar. The nodes constitute a grid of 0.5°x0.5° distance.

6.2.4.2 Logic tree

As mentioned in chapter 2, intrinsic uncertainties in earthquake physics (*e.g.*, exactly when and where an earthquake will occur, and what size it will be) and limitations in knowledge (*e.g.*, incomplete catalogues, lack of local measurements of strong ground motion) pose a major challenge for seismic hazard assessment. A logic tree is used to take these aleatory and epistemic uncertainties into account after inserting alternative models during the analysis (Bommer and Scherbaum, 2008). The logic tree consists of different nodes and branches. Expert judgment is used to assign weights to each branch and the sum must be equal to the unity for all branches for a particular node. The sum of the weight of all branches that lead the logic tree gives the weight of each terminal branch of the logic tree. The logic tree used in this study considers, for each source area, two different ground motion prediction equations and two different magnitudes of completeness M_c 2.3 and M_c 2.9, selected to represent the average Mc values within the less active and more active areas, respectively.

Input parameters are introduced into the logic tree. The focal depths of 15 km and 35 km are assigned probabilities of 0.6 and 0.4, respectively. The two GMPE models (Boore et al., 2014; Chiou and Youngs, 2008, 2014) are assigned equal weight (see Figure 6. 9). As there are seven source areas, the logic tree has a total of 28 branches (which means 4 branches for each source, Figure 6. 11.

6.2.4.3 PSHA calculation

The probabilistic seismic hazard for Madagascar was calculated for 2% and 10% probability that exceeds in 50 years, which correspond to 2,475- and 474-year return periods, respectively. Spectral acceleration for 1.0 s and 3.0 s and Peak ground acceleration (PGA) were calculated.

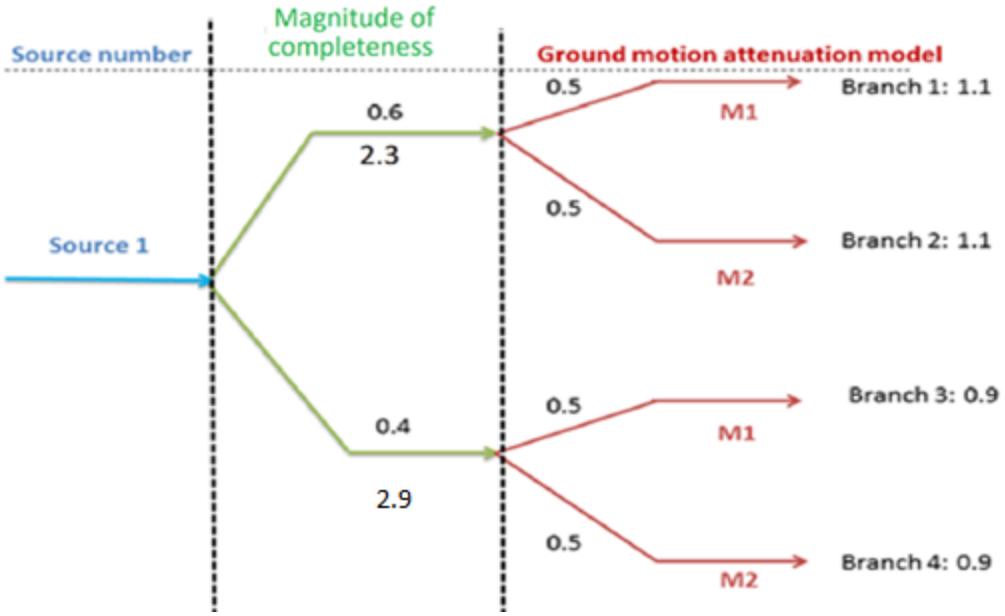

Figure 6. 11: Logic tree for median ground motions for determining the branches at the final branches. M2.3, and M3.0 are the Mc values using bulletin from the database MACOMO and from the database NDC; M1, M2 are the GMPE models proposed by Boore et al. (2014), and Chiou and Youngs (2008, 2014)

6.3 Results

6.3.1 Hazard maps in term of PGA

Results of probabilistic seismic hazard are shown for probabilities of exceedance of 10% and 2% in 50 years, equivalent to return periods of 474- and 2,475-years, respectively, and were produced for peak ground acceleration (PGA) and spectral acceleration of 1.0 s and 3.0 s, expressed in units of *g*. All results are shown in Figure 6. 12 and Figure 6. 13.

Most buildings in Madagascar are single story or low-rise and constructed of unreinforced masonry. It was considered that maps showing the expected PGA and the ground motion at 1 s and 3 s period would cover the range of frequencies expected to contribute most to the hazard.

The PGA maps show that the central area of Madagascar has the highest levels of seismic hazard in the country. In a global context, the levels of hazard may be characterized as “low”’.

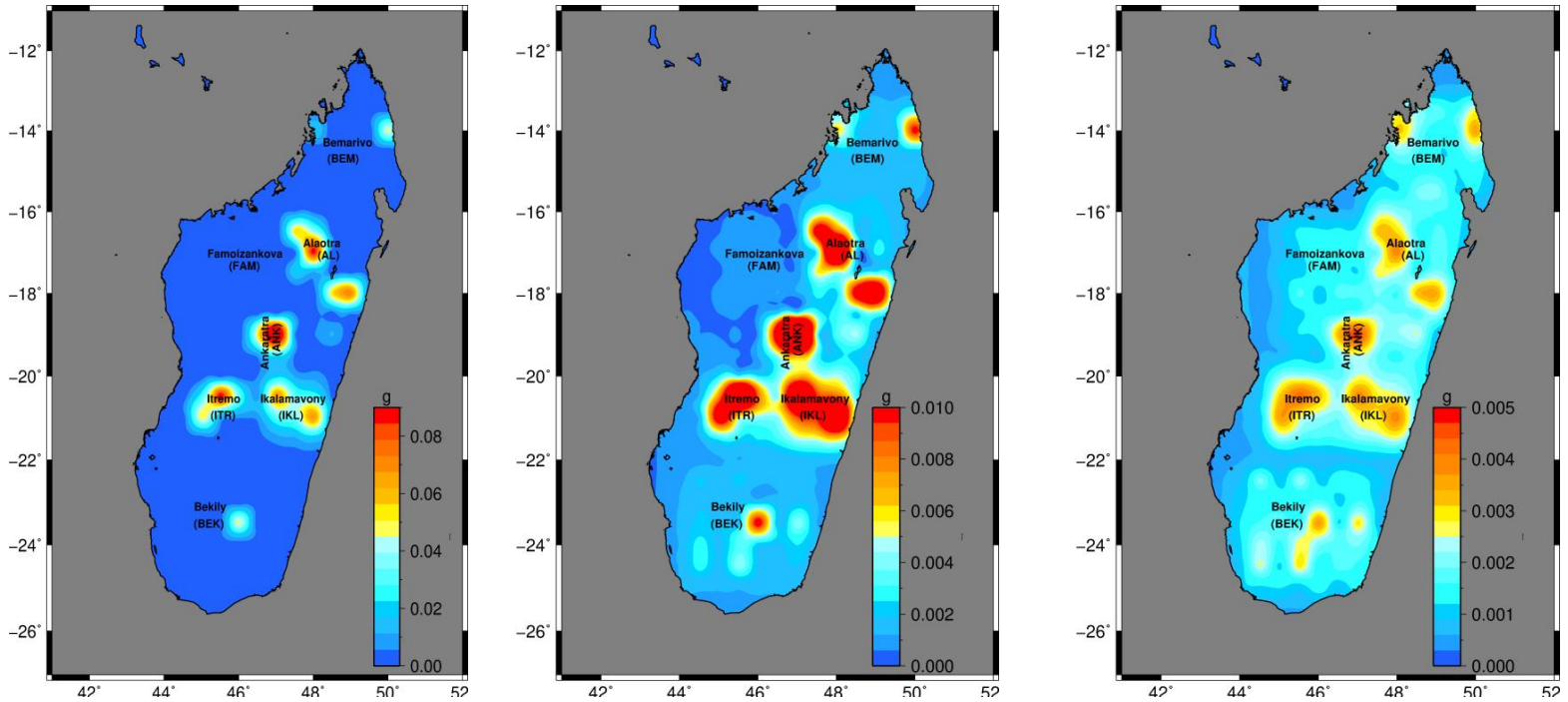

PGA in (g) **Hazard map for SA 1.0 s in (g)** **Hazard map for SA 3.0 s in (g)**

Figure 6. 12: Seismic hazard maps showing the expected PGA, estimated spectral acceleration for a period 1.0 s and 3.0 s at 10% probability of being exceeding in 50 year period (474-year return period).

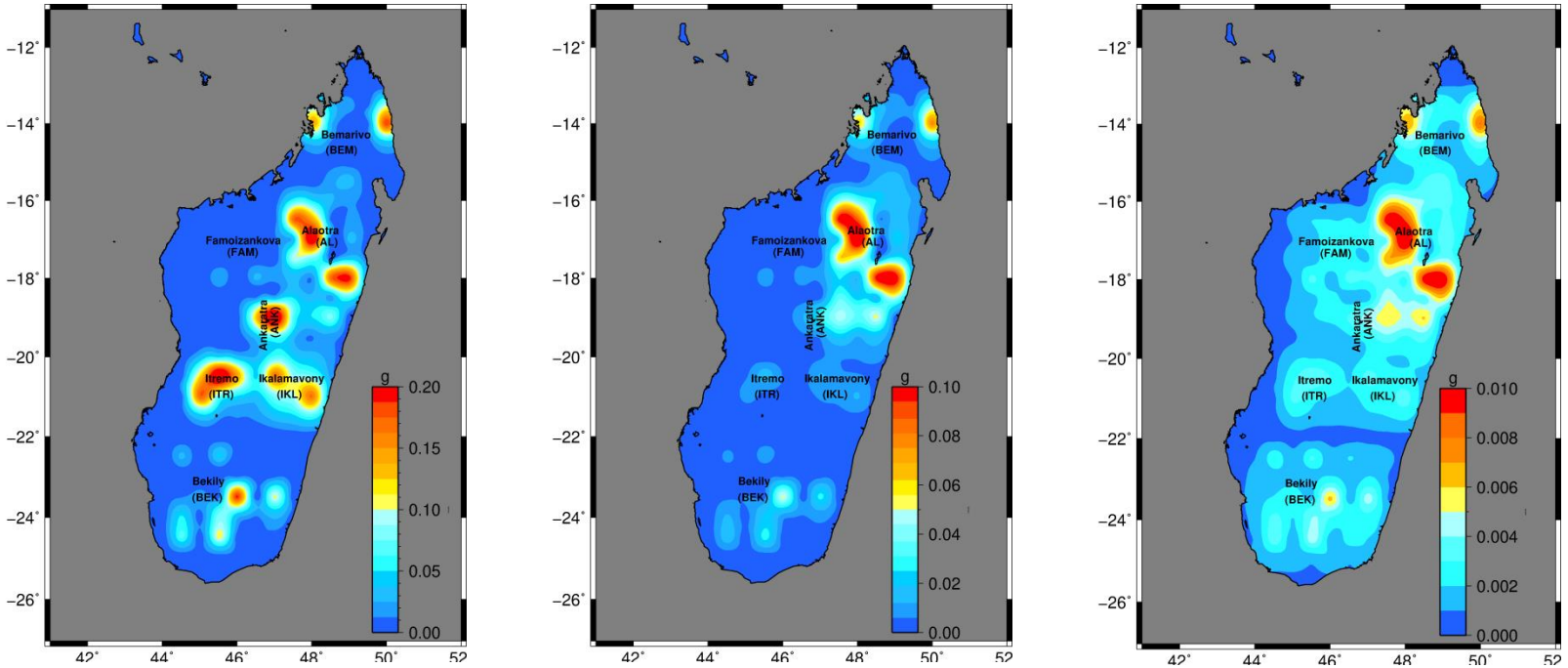

PGA **Hazard map for SA 1.0 s in (g)** **Hazard map for SA 3.0 s in (g)**

Figure 6. 13: Seismic hazard maps showing the expected PGA, estimated spectral acceleration for a period 1.0 s and 3.0 s at 2% probability of being exceeding in 50 year period (2,475-year return period).

6.3.2 Uniform hazard spectrum

In addition to the PGA- maps, spectral acceleration- maps (See Figure 6. 12 and Figure 6. 13) are used to generate uniform hazard spectrum for each point on hazard maps. Calculation was made for the range of periods that are important for common engineering structures. Figure 6. 14 shows that the highest ground accelerations occur around 0.15-0.2 s. From 1.0 s to 3.0 s the spectral acceleration values decreased from 0.02 g to 0.004 g.

Figure 6. 14 was selected as example for one city around the main town of Antananarivo, in Ankaratra.

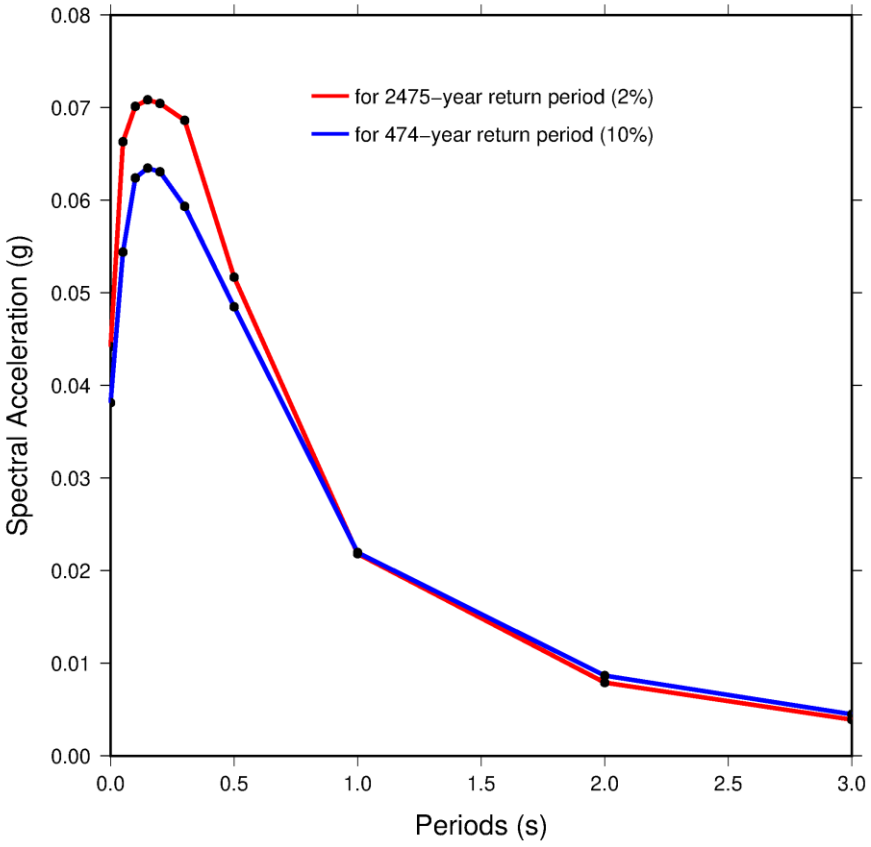

Figure 6. 14: Example of uniform hazard spectrum calculated for a site in the Ankaratra region in central Madagascar for a return period of 474- and 2,475-years (10% and 2% probability of exceedance in 50 years).

6.4 Discussions and conclusion

The seismic hazard for Madagascar was assessed using the CRISIS software (Ordaz et al., 2013) that is based on the probabilistic seismic hazard (PSHA) approach of Cornell (1968, 1971), McGuire (1977) and Kijko and Sellevoll (1989, 1992).

The bulletins of the NDC (1975-2016) and MACOMO (2011-2013) were merged producing a combined bulletin of 18,970 events. The seismicity catalogue for Madagascar was homogenized to M_w and then declustered, removing 7020 dependent events leaving a catalogue of 11,950 events. Seven source areas were defined Figure 6. 1 and the maximum magnitude, activity rate, and *b*-value were calculated for each source area (Table 6. 7). The estimated maximum magnitude in some source zones (about M5.6) is somewhat higher than the values used in a previous study (Razafindrakoto et al., 2009). CRISIS was used to calculate the likely ground motion at 10% and 2% likelihood of occurrence in 50 years on a 0.5°x 0.5° grid covering the island. Ground motion was defined as peak ground acceleration and spectral acceleration for the period of 1.0 s and 3.0 s (Figure 6. 12 and Figure 6. 13).

A logic tree formalism was used to take uncertainties into account, principally in the ground motion models and depth distribution. The attenuation models of Boore et al. (2014) and Chiou and Youngs (2008, 2014) were used as they were considered to be most compatible with the geological structure of Madagascar, the earthquake magnitude range, and the source-site distance range.

The highest levels of predicted ground motion are found to be in the most active areas, *viz.* central Madagascar. In global terms, the hazard in central Madagascar may be described as moderate, and elsewhere in the island as low. However, this does not mean that a moderate-sized and potentially damaging earthquake (M>5.5) cannot occur elsewhere in Madagascar, just that it is a lot less frequent.

We compared our results with Rindraharisaona and Rambolamanana (2007) who used the Kijko and Sellevoll (1989, 1992) method; Razafindrakoto et al. (2009) who used a neodeterministic approach; and Poggi et al. (2017) who used the GEM OpenQuake methodology. All these studies suffered from scarcity of data in the southern and northern regions. In general, in the central part of Madagascar, we found that PGA varied between 0.01g and 0.05g for 10% probabilities of exceedance in 50 years within the central area of Madagascar, close to the main town of the country. Our results correlate fairly well with Poggi et al. (2017), who found an average value of PGA between 0.05g and 0.08g for Madagascar (Figure 6. 16), while they are somewhat higher than the values determined by Razafindrakoto et al. (2009) of 0.01g to 0.03g (Figure 6. 16). The neodeterministic assessment of PGA from Razafindrakoto et al. (2009) was constrained using the 21 April 1991 earthquake, which caused minor damage to many buildings in nearby settlements in the Alaotra region (cracks were observed in 90% of the dwellings in Ambohimanarina, 33% in Beanana, 84% in Kiranomena, and 30% in Fenoarivo Be) (Rambolamanana and Ratsimbazafy, 1991).

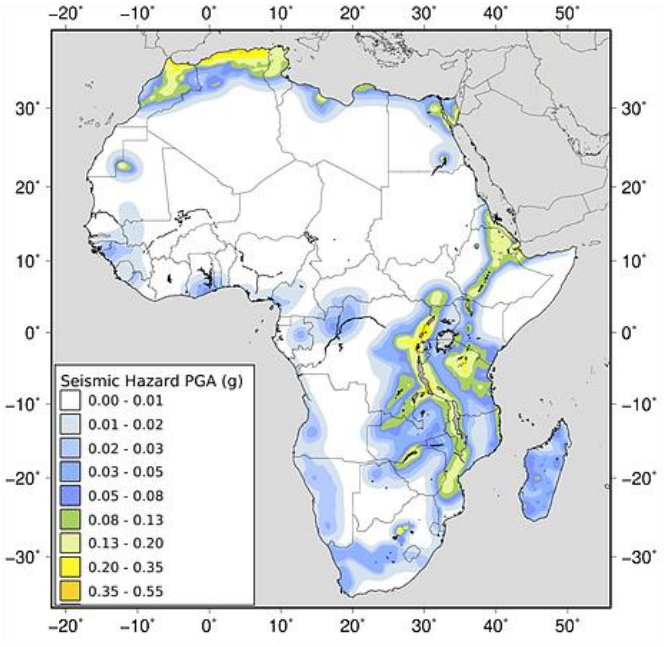

Figure 6. 15: Earthquake hazard map for Africa in units of g with a 10% probability of being exceeded in 50 years (Poggi et al., 2017)

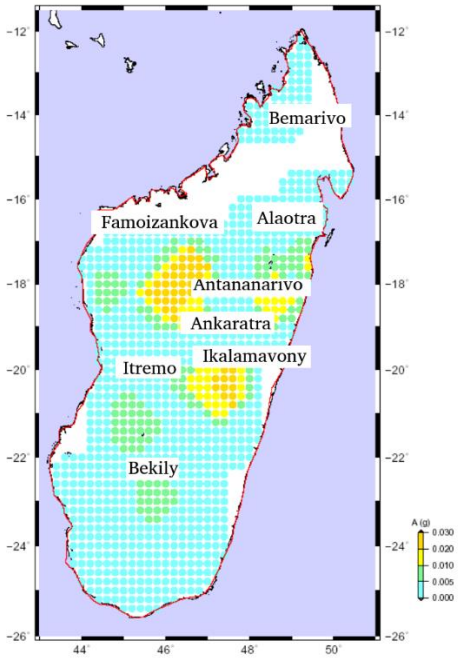

Figure 6. 16: Seismic hazard map showing PGA values in units of g with a 10% probability of being exceeded in 50 years (Razafindrakoto et al., 2009)

6.4.1 Northern and southern part of Madagascar

The seismic hazard values determined for northern and southern part of Madagascar, have similar PGA values *i.e.* Bemarivo and Bekily regions give maximum PGA values of 0.00g to 0.015g for 10% probability in 50 years and 0.00g to 0.025g for 2% probability in 50 years. The spectral acceleration SA values for 1.0 s vary between 0.00g and 0.025g for 10% probability and 0.00g to 0.05g for 2 % probability; and from 0.001g to 0.048g for both 10% and 2% probabilities for the period of 1.0 s and 3.0 s

The seismic hazard in these regions is thus characterized as ‘low’. We ascribe the difference between our results (Figure 6. 12, Figure 6. 13,Table 6. 7) and Razafindrakoto et al., 2009 (Figure 6. 16) to our use of data recorded by the MACOMO and other temporary arrays. While earthquake risk might be low, this does not mean that a damaging earthquake cannot occur, just that it is less likely. Furthermore, the threat posed by tsunamis such as the 2004 Indian Ocean tsunami must not be forgotten.

6.4.2 Central part of Madagascar

The highest levels of seismic activity are found in the middle part of Madagascar (Bertil and Regnoult, 1998, Rindraharisaona et al., 2013, Rakotondraibe et al., 2020). Consequently, moderate seismic hazard is present in the Central areas of the island (*i.e.*, around the Ankaratra, Famoizankova, and Alaotra regions).

Present-day seismicity is driven by the mantle upwelling that has produced recent Quaternary volcanic activity, as well as tectonic forces associated with distant plate boundaries acting on faults and shear zones that were active during the breakup of Gondwana (Storey et al., 1995; Torsvik et al., 1998) as discussed in Chapter 4 of the thesis.

This study made use of data from temporary deployments of broadband seismographs that greatly increased the coverage of the island, especially in the peripheral regions. However, the duration of the seismic catalogue is still short, the distribution of permanent stations is sparse, and there are no local strong motion data. The maximum magnitude of earthquakes is poorly constrained including Mc values. Agencies responsible for disaster management cannot be complacent.

To conclude, it is recommended that additional seismic stations are installed, especially in the north and south of the island, and that strong ground motion sensors are installed in the most seismically active regions so that it is possible to develop a local ground motion prediction equation.

Chapter 7: Discussion and Conclusion

7.1 Introduction

The geology of Madagascar is best understood by considering its paleoposition, at the heart of Gondwana, and the tectonic processes associated with the breakup of the supercontinent. Several previous studies have investigated the seismotectonics and evolution of fault structures in Madagascar (*e.g.*, Bertil and Regnoult 1998; Rindraharisaona et al., 2013), but were affected by the insufficient numbers of seismic stations in most parts of Madagascar. Thus, the studies were limited exclusively to the central region of Madagascar.

In addition to the local permanent broadband and short period stations in Madagascar, temporary seismic stations were installed between 2011 and 2013 as part of the MACOMO, SELASOMA and RHUM-RUM projects (Sigloch and Barruol, 2012; Wyssession et al., 2012; Tilmann et al., 2013;). In this study, seismic data collected by both permanent and temporary stations were used to investigate the seismotectonics of Madagascar.

Arrival times of P- and S-waves were first utilized to locate local and regional earthquakes using a least square technique. Then, a double difference program was used to refine the obtained earthquake locations in regions where events were clustered. Focal mechanisms were determined using the first P-wave and some clear S-wave polarities, which then used to conduct stress inversion studies. Finally, the seismic hazard was assessed following probabilistic logic tree formalism.

The major findings of this study include the characteristics of earthquake distributions in Madagascar, which are crucial in the assessment of the seismic hazard of the country. Fault plane solutions help us to understand the relationship between earthquake sources

and the existing faults. Results are generally focused on the main active sources existing in Madagascar and the estimation of the big seismic events that might create some damage.

In this chapter we seek to integrate the findings of the detailed investigations conducted as part of the PhD research programme.

7.2 General discussion and conclusion

7.2.1 Seismicity and magnitude

In general, Madagascar is a moderately seismically active island. Temporary seismic stations deployed by the MACOMO, SELASOMA and RHUM-RUM projects recorded 695 earthquakes with magnitude varying between M1 and M5.3 from 2011-2013.

The central region of Madagascar is the most seismically active region. Clusters of earthquakes aligned in NE-SW and NW-SE trends are observed in the Ankaratra and Alaotra regions, respectively. These are likely related to active faults in the crust and upper mantle and Cenezoic volcanism. Our findings are consistent with previously work (Bertil and Regnoult 1998; Rindraharisaona et al., 2013).

In northern Madagascar, earthquakes were observed along the Sandrakota and Andaparaty shear zones, as well as around the Vohibory and Bekily areas in the southern region (Figure 4. 3; Figure 4. 7). We observed new seismogenic zones in the northern and southern areas of the island related to prior studies by Bertil and Regnoult (1998) and Rindraharisaona et al. (2013) due to the greater number of stations deployed in the areas.

IRIS (https://www.iris.edu) reported the occurrence of a large offshore seismic event at a depth greater than 15 km, with magnitude of 5.3 on January 25th, 2013, in the south-

western coast of Madagascar. This seismic event is also observed in our results. The seismic event is related to strike slip faulting that occurred in the Davie Ridge.

The magnitude scale plays an important role in determining the seismotectonic of an area as it enables us to characterize the energy and co-seismic displacements of the earthquakes. The greater number of stations allowed us to develop a new local magnitude scale for Madagascar (Equation 4.5).

7.2 2 Focal mechanisms

In this study two different groups of focal mechanisms were observed:

(a) The first group of focal mechanisms is from the MACOMO, SELASOMA, RHUM-RUM and the national permanent stations. A total number of 23 focal mechanisms were determined. Of these, 85% are normal faulting, while the remaining 15% are a mixture of strike-slip and thrust faulting (Figure 4. 10). The majority of the normal faults trend in an N-S direction, suggesting an extension structure caused by the separation of Madagascar from the East African Rift. This is consistent with the findings of Bertil and Regnoult (1998). In addition, the strike-slip faulting that occurs in the southern and northern regions linked with the presented tectonic features in the regions.

(b) The second group of focal mechanisms is from previous studies (Rindraharisaona et al., 2013) using permanent local seismic stations. Data were relocated using Double-Difference method then reprocessed in order to get the fault plane solutions for about 182 mechanisms. The majority of the solutions are observed in the central region of Madagascar (Figure 4. 10).

The first group of focal mechanisms helps us understand the partition of the focal mechanisms and the evolution of the fault plane characteristics after improving the numbers of the seismic stations. The second group of focal mechanism helps us to evaluate the stress direction from the fault plane solutions. By analyzing the fault plane solutions, we realized that some fault plane solutions are connected to the existing

tectonic features in the southern and northern part of the island. The central region is mostly dominated by normal faulting, which is in accord with the results from previous studies (Bertil and Regnoult, 1998; Rindraharisaona et al., 2013).

The determination of the fault plane solutions performs an important aspect in seismic hazard in that they help to understand better the movement of the ground along active faults. The combination of the two groups of fault solutions helps us to understand more about the evolution of fault structure in Madagascar. The distribution of seismic events shows various mechanisms such as around the Alaotra, Bemarivo, Ankaratra, Itremo, Ikalamavony, Famoizankova and Bekily areas.

Clusters of focal mechanism solutions are observed in the central Alaotra and Ankaratra regions. These two regions are geologically linked as they are both underlain by upwelling asthenosphere that uplifts both regions (Pratt et al., 2017). The upwelling asthenospheric mass is thought to cause the increase in seismic events in the two regions and produces the extensional structure related to the normal fault.

The strike direction of the fault planes in the central part of Madagascar coincides with the E-W direction of the stress field, which suggests the dominance of an extensional stress field. The hypocenters are mostly located at depths between 10 km and 18 km depth. The orientation of most of the fault plane P-axis varies from 30 to 160 degrees, which means that these fault planes strike in the NE-SW direction.

Characteristics of focal mechanisms obtained in this study are more robust and accurate than those obtained in previous studies, because more well-distributed stations with good quality data were used.

The geodynamics of Madagascar is controversial. Many authors have emphasized the important role of E-W extension (Bésairie, 1964; Bertil and Regnoult, 1998; Hottin, 1972; Piqué et al., 1999, Rindraharisaona et al., 2013). Conversely, Arthaud et al. (1989) suggested an N-S extension. Kusky et al. (2003, 2007) proposed that the Ankay-Alaotra

rift has extension kinematics comparable to the East African rift. Saria et al. (2014) implied that a diffuse plate boundary cuts Madagascar over its central part from west to east and suggested that it is likely related to the formation of the Lwandle microplate. This model was not consistent with the results obtained from this study as we did not find clear W-E direction of seismicity anywhere in the island and most of the seismic events present normal faulting.

In conclusion, normal faulting dominates in the central area, whilst a mixture of all types, strike slip, thrust and normal faulting are observed in the southern and northern areas of Madagascar.

7.2.3 Stress field

In Chapter 4, after determining the seismic mechanisms from grouped seismic events in Madagascar, inversions of 182 clustered earthquake events were performed. The results showed that in Madagascar, a direction of NW-SE of principal stress is observed.

The study helped to identify which faults are most active and where the reactivation of fault zones might occur in the future. The Famoizankova, Ankaratra and Alaotra regions are most seismically active.

Unfortunately, focal mechanism solutions in the northern part are not sufficient to explore the mechanism in the whole region of the northern part of Madagascar, but results from this study will give information about how seismic intensities in this region will occur.

Several studies have looked at the relationship between stress direction and seismic hazard (*e.g.*, Hagos, 2006; Rebetsky et al., 2012; Rebetsky and Tatevossian, 2013). Kijko and Sellevol (1989) proposed that the use of stress direction results, along with structural information and earthquake source characteristics, improves the computation of seismic hazard. Thus, in this study, the earthquake sources, the stress direction, which

are mostly in the same direction (central area of Madagascar), and geological structure information were used to calculate seismic hazard.

The results that we obtained show that the orientation of active faults in the southern and northern areas of Madagascar is controlled by the existing shear zones, with small variations. The average stress direction in the northern and southern parts of Madagascar could not be predicted because the number of seismic events that occurred during the seismic station observation period (*i.e.*, 2011-2013) was low compared to the number recorded in the central region of Madagascar.

Our results show that the average direction of the stress field in the central part of Madagascar trends in the NE-SW direction, which means that the direction of extension is generally NW-SE. We think that the extensional nature of the stress field in the central part of Madagascar suggests that the stress direction observed in the region was largely influenced by the thermal bulge that correlated to Cenozoic volcanism in the center area of Madagascar (Besairie, 1959, Bertil and Regnoult, 1998; Rindraharisaona et al., 2013, Andriampenomanana et al., 2017)

In the central part of Madagascar, most seismic activity is observed in the Alaotra and Ankaratra regions. The stress field in Ankaratra, which is mainly a volcanic area, trends in the NE-SW direction, while the stress field in the Alaotra, which is mainly an extensional region, varies considerably between N and E (Bertil and Regnoult, 1998). Both the Alaotra and Ankaratra regions are dominated by normal tectonic mechanisms. This can be explained by the interaction between the direction of maximum horizontal stress and the direction of faults. The extensional regime might be the result of thermal uplift associated with Cenozoic volcanism. The stress tensor results that we obtained, with σ_1 and σ_3 in the horizontal and vertical directions, show an extensional regime trending NW-SE for both regions. Small variation of principal stress axis orientation (σ_3) presented from the two regions can be regarded as an influence of the uplifting structure in the central region dominated by the volcanic zone of Ankaratra (Bertil and Regnoult, 1998).

7.2.4 Seismic hazard

Razafindrakoto et al. (2009) suggested that, according to the numbers of earthquakes that occurred in the island, the central area of Madagascar has a high value of PGA. In this study, a seismic hazard assessment for Madagascar was carried out. Source zones were characterized using data from the combined earthquake catalogue from Madagascar National Data Center (NDC) and MACOMO (Madagascar - Comoros - Mozambique) catalogues.

In Chapter 6, earthquake magnitude values were homogenized using a new relation from the combined data recorded at the ISC, and MACOMO bulletin. The homogenized catalogue was then declustered before it was used to identify and characterize seismic source zones.

Seismic hazard maps were obtained for Peak Ground Acceleration (PGA) and Spectral Acceleration (SA, periods T=1.0s and T=3.0 s). We obtained higher ground motion values than Razafindrakoto et al. (2009). PGA values with 10% probability of exceedance in 50-years ranged from 0.001 g to 0.09 g in the central part of the island. Low PGA values (between 0.003 g to 0.004 g) were obtained in the northern and southern areas. High values of SA for T=1.0 s and T=3.0 s were also obtained in the central region, which are attributed to the high seismic activity for earthquakes of magnitude M2.9 and above.

The number of recorded earthquake events in the northern and southern part of Madagascar is less than in the central region because 1) the central part is more active and 2) the station coverage in both the northern and southern parts is low. Thus, the seismic hazard results for the southern and northern regions are influenced by the poor network coverage in those regions.

Seismic hazard parameters were estimated for the identified and delineated seismic zones *viz. the* Gutenberg Richter *b*-value, mean activity rate lambda, and the maximum magnitude m_{max}. The estimated m_{max} is around 5.6 for the Ankaratra and Alaotra zones, which is a little bit higher than the one reported from previous work (Razafindrakoto et al., 2009). Seismic hazard was assessed considering the rate of events with magnitude greater or equal to 3.0. This is far smaller than the commonly used value of magnitude 5.0, which is the threshold at which damage might occur. However, there are very few events in the earthquake catalogue for Madagascar that exceed magnitude 5.0, and we considered that the use of a lower value would be useful in showing regional differences in hazard.

We compared our results with prior work, especially Razafindrakoto et al. (2009). Our study used a different seismic source model (a total number of seven source areas) and different Ground Motion Prediction Equations (GMPE). The PSHA studies show that the central part of Madagascar is the most seismically active region. Our PGA and SA values are somewhat higher than those reported by Razafindrakoto et al. (2009).

According to the NDC of the Institute et Observatoire de Géophysique d'Antananarivo, the region of Ankaratra and Itasy has remained seismically active since 2016, producing about three felt events per day, on average. As an example, recent seismic events that occurred in these areas were on 11 January 2017 and 9 March 2017 with magnitude 5.6 and 4.9 respectively.

From this study, earthquakes in Madagascar occur mostly in the central area of Madagascar, around the Famoizankova, Alaotra and Ankaratra regions. These regions are influenced by various active faults and volcanic structures. In the Ankaratra region, the observed local earthquakes and fault plane solutions can be interpreted as the result of a hotspot or mantle upwelling that created the mid-plate volcanoes. In addition, various seismic activities are present in the Famoizankova and Alaotra regions where existing active faults are observed. It is possible that other faults might be reactivated.

According to the fault plane and the stress direction results from this study, fractures could be parallel to the Somalian and Nubian plate boundaries.

7. 3 Recommendations for future studies

The sparse station network coverage in the southern and northern part of Madagascar resulted in an incomplete catalogue of earthquakes as many earthquakes were not detected and recorded. In the future, it is hoped that there will be an improvement in the distribution of seismic stations in the country to enable better monitoring of all earthquakes in Madagascar. Certainly, additional permanent seismic stations are needed, especially in the southern and northern part of Madagascar.

To ensure that focal mechanism is determined confidently, it is necessary that stations are located at suitable, quiet locations to ensure good quality waveforms. A challenge encountered in this study was that though stations were distributed well in some parts of the country, the waveform records were of poor quality due to noise contamination making it difficult to identify P and S wave polarities.

The poor quality of some waveforms also provided a challenge in calculating earthquake magnitude. This reinforces the recommendation that permanent stations should be located at suitable places. Also, it is important to select the right type of sensor to be installed, preferably a three-component one to facilitate the identification of the real phases that are crucial to determine the moment magnitude.

In order to mitigate the risk posed by earthquakes to Malagasy society it is necessary to improve seismic monitoring and conduct new research work. Geophysical and geotechnical surveys should be combined with seismic hazard results in order to improve information in the very seismically active areas and formulate and implement building regulations. In particular, it is recommended that attention be given to the study of earthquake site effects. It is important to identify variations in ground shaking due to near surface geology and take this into account in urban planning and the formulation of building codes.

References

Abe, K., 1981. Magnitudes of large shallow earthquakes from 1904 to 1980. *Physics of the Earth and Planetary Interiors*, *27*(1), 72-92.

Alsaker, A., Kvamme, L.B., Hansen, R.A., Dahle, A. and Bungum, H., 1991. The M_L scale in Norway. *Bulletin of the Seismological Society of America*, 81(2), 379-398.

Anderson, J.G., 1978. Program EQRISK: A computer program for finding uniform risk spectra of strong earthquake ground motion. *Department of Civil Engineering, University of Southern California*.

Anderson, J.A. and Wood, H.O., 1925. Description and theory of the torsion seismometer. *Bulletin of the Seismological Society of America*, 15(1), 1-72.

Anderson, J.G. and Brune, J.N., 1999. Probabilistic seismic hazard analysis without the ergodic assumption. *Seismological Research Letters*, 70(1), 19-28.

Anderson, J.G., Sucuoglu, H., Erberik, A., Yilmaz, T., Inan, E., Durukal, E., Erdik, M., Anooshehpoor, R., Brune, J.N. and Ni, S.D., 2000. Implications for seismic hazard analysis. *Earthquake Spectra*, 16(S1), 113-137.

Andriampenomanana, F., Nyblade, A.A., Wysession, M.E., Durrheim, R.J., Tilmann, F., Julia, J., Pratt, M.J, Rambolamanana, G., Aleqabi, G.I., Shore, P.J. and Rakotondraibe, T., 2017. The structure of the crust and uppermost mantle beneath Madagascar. *Geophysical Journal International*, 210, 1525-1544.

Andriampenomanana F., Nyblade, A.A., Durrheim, R., Wysession, M.E., Durrheim, R.J., Tilmann, F., Barruol, G., Rambolamanana, G. and Rakotondraibe, T., 2020. Seismic velocity and anisotropy of the uppermost mantle beneath Madagascar from Pn tomography. *Geophysical Journal International*, 224, 290-305, https://doi.org/10.1093/gji/ggaa458.

Angelier, J., 1984. Tectonic analysis of fault-slip data sets. *Journal of Geophysical Research*, 89, 5835–5848.

Angelier, J., 1990. Inversion of field data in fault tectonics to obtain the regional stress—III. A new rapid direct inversion method by analytical means. *Geophysical Journal International*, 103(2), 363-376.

Arnold, R., and Townend, J. 2007. A Bayesian approach to estimating tectonic stress from seismological data. *Geophysical Journal International*, 170(3), 1336-1356.

Arthaud, F., Grillot, J.C. and Raunet, M., 1989. Mise en évidence d'une néotectonique en distention NS à Madagascar (Hauts Plateaux). Comptes rendus de l'Académie des sciences. Série 2, Mécanique, Physique, Chimie, Sciences de l'univers. *Sciences de la Terre*, 309(1), 125-128.

Atkinson, G.M. and Boore, D.M., 1995. Ground-motion relations for eastern North America. *Bulletin of the Seismological Society of America*, 85(1), 17-30.

Atkinson, G.M. and Boore, D.M., 1997. Stochastic point-source modeling of ground motions in the Cascadia region. *Seismological Research Letters*, 68(1), 74-85.

Barruol, G. and Sigloch, K., 2013. Investigating La Réunion hot spot from crust to core. *Eos, Transactions American Geophysical Union*, 94(23), 205-207.

Bauer, W., Walsh, G.J., De Waele, B., Thomas, R.J., Horstwood, M.S., Bracciali, L., Schofield, D.I., Wollenberg, U., Lidke, D.J., Rasaona, I.T. and Rabarimanana, M.H., 2011. Cover sequences at the northern margin of the Antongil Craton, NE Madagascar. *Precambrian Research*, 189(3), 292-312.

Baumbach, M. and Bormann, P., 2012. Determination of source parameters from seismic spectra. *IASPEI Manual of Seismological Observatory Practice*. GFZ Publication.

Beauval, C. and Scotti, O., 2003. Mapping b-values in France using two different magnitude ranges: possible non power-law behavior. *Geophysical Research Letters*, 30, SDE1-1 – SDE1-4.

Bender, B and Perkins, D.M., 1987. *SEISRISK III, a computer program for sesmic hazard estimation*. US Government Printing Office.

Benjamin, J. R. and Cornell, C. A., 1970. Solutions Manual to Accompany Probability. Statistics, and Decision for Civil Engineers. *McGraw-Hill*.

Berger, A., Janots, E., Gnos, E., Frei, R. and Bernier, F., 2014. Rare earth element mineralogy and geochemistry in a laterite profile from Madagascar. *Applied Geochemistry*, 41, 218-228.

Bertil, D. and Regnoult, J.M., 1998. Seismotectonics of Madagascar, *Tectonophysics*, 294, 57-74.

Bésairie, H., 1956. Carte géologique à 1 n 200; 000 de Sakoa (F.G 58-59)-Benenitra (H.I 58-59). *Service Géologique de Madagascar, Antananarivo*.

Bésairie, H., 1964. Carte géologique de Madagascar (1/1.000.000). *Service Géologique de Madagascar, Antananarivo*.

Bésairie, H., 1968–1971. Description géologique du massif ancien de Madagascar.

Bésairie, H., 1971. Madagascar, Tectonique de l'Afrique. *Science de la terre*, UNESCO, Paris, 6, 549-558.

Bésairie, H., 1973. Shema stratigraphique de Madagascar au 1/ 2. 000.000. *Service Géologique de Madagascar, Tananarive (Archive N0.2199).*

Bésairie, H. and Collignon, M., 1971. Géologie de Madagascar. 1 Les terrains sédimentaires. *Annales Géologiques de Madagascar. fasc. XXXV Tananarive*, 463.

Bondar, I., Myers, S.C., Engdahl, E.R. and Bergman, E.A., 2004. Epicentre accuracy based on seismic network criteria. *Geophysical Journal International*, 3, 483 – 496.

Boore, D.M. and Atkinson, G.M., 2008. Ground motion prediction equations for the average horizontal component of PGA, PGV, and 5% damped PSA at spectral periods between 0.01 s and 10.0 s. *Earthquake Spectra,* 24, 99-138.

Boore, D.M. and Joyner, W.B., 1984. A note on the use of random vibration theory to predict peak amplitudes of transient signals. *Bulletin of the Seismological Society of America*, 74(5), 2035-2039.

Bommer, J.J. and Scherbaum, F., 2008.The use and misuse of logic trees in probabilistic seismic hazard analysis. *Earthquake Spectra*, 24(4), 997-1009.

Bott, M.H.P., 1959. The mechanics of oblique slip faulting. *Geology Magazine,* 96, 109–117.

Boulanger, J.and Pavlovsky, R., 1954. Madagascar 1:100,000, (carte géologique). H 59, Ianapera. *Service géologique de Madagascar, Antananarivo.*

Brenon, P., and Bussiere, P., 1959: Le volcanisme à Madagascar. *Bulletin Volcanologique*, 21, 77-93.

BRTT (Boulder Real Time Technology), 2004. Evolution of the Commercial ANTELOPE Software, Open file Report, available at: http://www.brtt.com/docs/evolution.pdf (last access: 22 April 2013).

Brune, J.N., 1970. Tectonic stress and the spectra of seismic shear waves from earthquakes. *Journal of Geophysical Research*, 75(26), 4997-5009.

Brune, J.N., 1971. Correction to tectonic stress and the spectra of seismic shear waves from earthquakes. *Journal Geophysical Research,* 76(20), 5002.

Caen-Vachette, M., 1979. Le Précambrien de Madagascar. Radiochronométrie par isochrones Rb/Sr sur roches totales. *Revues de Géologie Dynamique et de Géographie Physique*, 21, 331-338.

Célérier, B., 1988. How much does slip on a reactivated fault plane constrain the stress tensor? *Tectonics,* 7(6), 1257-1278.

Chiou, B.J. and Youngs, R.R., 2008. An NGA model for the average horizontal component of peak ground motion and response spectra. *Earthquake Spectra*, 24(1), 173-215.

Chiou, B.S.J. and Youngs, R.R., 2014. Update of the Chiou and Youngs NGA model for the average horizontal component of peak ground motion and response. *Earthquake Spectra*, 30(3), 1117-1153.

Chiu, G., Lockhart, R. and Routledge, R., 2006. Bent-cable regression theory and applications. *Journal of the American Statistical Association*, 101(474), 542-553.

Chorowicz, J., Lavreau, J., Theunissen, K., Klerkx, J., Lepage, A.,Nanyaro, J., Roggeri, I., Rudant, J.P., Ruder, J., Tack, L., Temu, E.,Thouin, C., Trefois, P. and Yanda, P., 1990. The evaluation of satellite imagery and field spectro-radiometric data for the study of the lithology and the ancient and reactivation tectonics in the vicinity of the East African Rift. *ISPRS Journal of Photogrammetry and Remote Sensing*, 45, 355–381.

Coffin, M.F. and Rabinowitz, P.D., 1987. Reconstruction of Madagascar and Africa: evidence from the Davie fracture zone and western Somali basin. *Journal of Geophysical Research: Solid Earth*, 92(B9), 9385-9406.

Coffin, M.F. and Rabinowitz, P.D. (eds), 1988. Evolution of the conjugate East African-Madagascan margins and the western Somali Basin. *Geological Society of America*, 226.

Coffin, M.F. and Rabinowitz, P.D., 1992. The Mesozoic East African and Madagascan conjugate continental margins: stratigraphy and tectonics. *African and Mediterranean Margins*, 207-240.

Collins, A.S., 2006. Madagascar and the amalgamation of Central Gondwana. *Gondwana Research*, 9(1), 3-16.

Collins, A.S., Johnson, S., Fitzsimons, I.C., Powell, C.M., Hulscher, B., Abello, J. and Razakamanana, T., 2003. Neoproterozoic deformation in central Madagascar: a structural section through part of the East African Orogen. *Geological Society, London, Special Publications*, 206(1), 363-379.

Collins, A.S, Razakamanana T and Windley B. F. 2000. Neoproterozoic extensional detachment in central Madagascar; implications for the collapse of the East African Orogen. *Geological Magazine*, 137, 39-51.

Collins, A.S. and Windley, B.F., 2002. The tectonic evolution of the central and northern Madagascar and its place in the final assembly of Gondwana. *Journal of Geology*, 110 (3), 325–339.

Collins, A.S., Kinny, P.D. and Razakamanana, T., 2012. Depositional age, provenance and metamorphic age of metasedimentary rocks from southern Madagascar. *Gondwana Research*, 21, 353-3.

Cornell, C.A., 1968. Engineering seismic risk analysis. *Bulletin of the Seismological Society of America*, 58, 1583-1606.

Cornell, C. A., 1971. Probabilistic analysis of damage to structures under seismic loads. In *Dynamic Waves in Civil Engineering* (edited by D.A. Howells et al.), 473 – 493.

Cox, R., Armstrong, R.A. and Ashwal, L.D., 1998.Sedimentology, geochronology and provenance of the Proterozoic Itremo Group, central Madagascar, and implications for pre-Gondwana palaeogeography. *Journal of the Geological Society (London)*, 155, 1009-1024.

Cox, R., Zentner, D.B., Rakotondrazafy, A.F.M. and Rasoazanamparany, C.F., 2010. Shakedown in Madagascar: occurrence of lavakas (erosional gullies) associated with seismic activity. *Geology*, 38(2), 179-182.

Craig, T., Jackson, J., Priestley, K. and McKenzie, D., 2011. Earthquake distribution patterns in Africa: their relationship to variations in lithospheric and geological structure, and their rheological implications. *Geophysical Journal International*, 185, 403-434.

Cucciniello, C., Le Roex, A.P., Jourdan, F., Morra, V., Grifa, C., Franciosi, L. and Melluso, L., 2018. The mafic alkaline volcanism of SW Madagascar (Ankililoaka, Tulear region): 40Ar/39Ar ages, geochemistry and tectonic setting. *Journal of the Geological Society*, 175(4), 627-641.

Darracott, B.W., 1974. On the crustal structure and evolution of southeastern Africa and the adjacent Indian Ocean. *Earth and Planetary Science Letters*, 24(2), 282-290.

Das, R., Wason, H.R. and Sharma, M.L., 2012. Magnitude conversion to unified moment magnitude using orthogonal regression relation. *Journal of Asian Earth Sciences*, 50, 44-51.

Delvaux, D. and Sperner, B., 2003. New aspects of tectonic stress inversion with reference to the TENSOR program. *Special Publications Geological Society, London*, 212(1), 75-100.

De Wit, M., 2003. Madagascar: heads it's a continent, tails it's an island. *Annual Review of Earth and Planetary Sciences*, 31, 213-248.

Du Toit, A.L., 1937. *Our Wandering Continents.* Oliver and Boyd, London, 366 pp.

Embleton, B.J.J. and McElhinny, M.W., 1975. The palaeoposition of Madagascar: palaeomagnetic evidence from the Isalo Group. *Earth and Planetary Science Letters*, 27, 329-341.

Esteva, L., 1970. *Regionalization Sismica de Mexico para fines de Ingenieria.* Instituto de Ingenieria. UNAM, No. 246, Mexico.

Fasshauer, G.E., 1995. Adaptive least squares fitting with radial basis functions on the sphere. *Mathematical Methods for Curves and Surfaces*, pp. 141-150.

Field, E.H., Jordan, T.H. and Cornell, C.A., 2003. OpenSHA: A developing community-modeling environment for seismic hazard analysis. *Seismological Research Letters*, 74(4), 406-419.

Fitzsimons, I.C.W. and Hulscher, B., 2005. Out of Africa: detrital zircon provenance of central Madagascar and Neoproterozoic terrane transfer across the Mozambique Ocean. *Terra Nova*, 17(3), 224-235.

Förster, R., 1975. The geological history of the sedimentary basin of southern Mozambique, and some aspects of the origin of the Mozambique Channel. *Palaeogeog Palaeoclimat Palaeoecol*., 17, 267-287.

Foster, A.N. and Jackson, J.A., 1998. Source parameters of large African earthquakes: implications for crustal rheology and regional kinematics. *Geophysical Journal International*, 134, 422-448.

Fourno, J.P. and Roussel, J., 1994. Imaging of the Moho depth in Madagascar through the inversion of gravity data: geodynamic implications. *Terra Nova*, 6, 512 - 519.

Frohlich, C., 1992. Triangle diagrams: ternary graphs to display similarity and diversity of earthquake focal mechanisms. *Physics of the Earth and Planetary Interiors*, 75(1-3), 193-198.

Frohlich, C. and Apperson, K.D., 1992. Earthquake focal mechanisms, moment tensor, and the consistency of seismic activity near plate boundaries. *Tectonics*, 11, 279-295.

Gardner, J.K. and Knopoff, L., 1974. Is the sequence of earthquakes in Southern California, with aftershocks removed, Poissonian? *Bulletin of the Seismological Society of America*, 64(5), 1363-1367.

Gasse, F. and Van Campo, E., 2001. Late Quaternary environmental changes from a pollen and diatom record in the southern tropics (Lake Tritrivakely, Madagascar). *Palaeogeography, Palaeoclimatology, Palaeoecology*, 167(3), 287-308.

Geiger, L., 1910. Herdbestimmung bei Erdbeben aus den Ankunfzeiten. *Nachrichten der K. Gesellschaft der Wissenschaften zu Gottingen. Math.-Phys. Klasse*. 331-49.

Geiger, L., 1912. Probability method for the determination of earthquake epicentrals from the arrival time only (translation). *Bulletin of Saint Louis University,* 8, 60-71.

Gephart, J.W. and Forsyth. D.W., 1984. An improved method for determining the regional stress tensor using earthquake focal mechanism data: application to the San Fernando earthquake sequence. *Journal of Geophysical Research*, 89, 9305-9320.

Gephart, J.W., 1990. FMSI: A FORTRAN program for inverting fault/slickenside and earthquake focal mechanism data to obtain the regional stress tensor. *Computers and Geosciences*, 16(7), 953-989.

Giardini, D., Grünthal, G., Shedlock, K.M. and Zhang, P., 1999. The GSHAP global seismic hazard map. *Annals of Geophysics*, 42(6), 1225-1230.

Goldstein, P. and Snoke, A., 2005. SAC availability for the IRIS community. *Incorporated Research Institutions for Seismology Newsletter, 7,* UCRL-JRNL211140.

Grimison, N.L. and Chen, W.P., 1988. Earthquakes in the Davie Ridge-Madagascar region and the southern Nubian-Somalian plate boundary. *Journal of Geophysical Research: Solid Earth*, 93(B9), 10439-10450.

Grünthal, G., Wahlström, R., and Stromeyer, D., 2009. The unified catalogue of earthquakes in central, northern, and northwestern Europe (CENEC)—updated and expanded to the last millennium. *Journal of Seismology*, 13, 517-541.

Gutenberg, B. and Richter, C.F., 1942. Earthquake magnitude, intensity, energy, and acceleration. *Bulletin of the Seismological Society of America*, 32(3), 163-191.

Gutenberg, B., 1945b. Amplitudes of P, PP, and S and magnitude of shallow earthquakes. *Bulletin of the Seismological Society of America*, 35(2), 57-69.

Gutenberg, B., 1945c. Magnitude determination for deep-focus earthquakes. *Bulletin of the Seismological Society of America*, 35(3), 117-130.

Gutenberg, B. and Richter, C.F., 1956. Earthquake magnitude, intensity, energy, and acceleration: (Second paper). *Bulletin of the seismological society of America*, 46(2), 105-145.

Hagos, L.Z. 2006. Earthquake Sources, the Stress Field and Seismic Hazard: A Study in Eritrea and its Surrounding. *PhD thesis, Uppsala University*.

Hanks, T.C., 1979. b values and ω−γ seismic source models: Implications for tectonic stress variations along active crustal fault zones and the estimation of high-frequency strong ground motion. *Journal of Geophysical Research: Solid Earth,* 84(B5), 2235-2242.

Hanks, T.C. and Boore, D.M., 1984. Moment-magnitude relations in theory and practice. *Journal of Geophysical Research: Solid Earth*, 89, 6229-6235.

Hanks, T.C. and Kanamori, H., 1979. A moment magnitude scale. *Journal of Geophysical Research: Solid Earth*, 84(B5), 2348-2350.

Hardebeck, J. L., and Hauksson, E., 2001. Stress orientations obtained from earthquake focal mechanisms: what are appropriate uncertainty estimates? B*ulletin of the Seismological Society of America,* 91, 250-262.

Havskov, J. and Otemöller, L., 2010. *Routine Data Processing in Earthquake Seismology*. Springer.

Hardebeck, J.L. and Hauksson, E. 2001. Crustal stress field in southern California and its implications for fault mechanics. *Journal of Geophysical Research: Solid Earth*, 106(B10), 21859-21882.

Hardebeck, J.L. and Michael, A.J., 2006. Damped regional-scale stress inversions: methodology and examples for southern California and the Coalinga aftershock sequence. *Journal of Geophysical Research: Solid Earth*, 111(B11), B11310, doi:10.1029/2005JB004144

Heath, M.T., Plemmons, R.J. and Ward, R.C., 1984. Sparse orthogonal schemes for structural optimization using the force method. *SIAM Journal on Scientific and Statistical Computing*, 5(3), 514-532.

Hirtz, P., Boulanger, J. and Pavlovsky, R., 1954. Madagascar 1:100,000, (carte géologique). F 59–G 59, Sakamena – Sakoa/Service géologique de Madagascar, Antananarivo. The Ianapera-Ampanihy Suture, SW Madagascar: A major tectonic boundary on the eastern margin of the Mozambique belt *(PDF Download Available)*.

Holtz, R.D., Kovacs, W.D. and Sheahan, T.C., 1981. *An Introduction to Geotechnical Engineering*, Englewood Cliffs, NJ: Prentice-Hall.

Hottin, G., 1972. Représentation schématique du volcanisme, de la tectonique cassante, et des formations précambriennes de Madagascar, scale 1/2.000.000. *Carte publiée par le Bureau de Recherches Géologiques et Minières: carte en couleur.*

Hussein, K. M., Abou, E. I. A., Korrat, I. M., Nader, E., Panza, G. F., and Gabry, M.N., 2008. Integration and magnitude homogenization of the Egyptian earthquake catalogue. *Natural Hazard*, 3, 525-546.

Hutton, K.L. and Boore, D.M., 1987. The M_L scale in southern California. *Bulletin of the Seismological Society of America,* 77, 2074–2094.

Jöns, N., 2006. *Metamorphic events during the formation of the East African Orogeny: case studies from Madagascar and Tanzania*. PhD thesis, Kiel University, Germany.

Jöns, N. and Schenk, V., 2008. Relics of the Mozambique Ocean in the central East African Orogen: evidence from the vohibory block of southern Madagascar. *Journal of Metamorphic Geology*, 26, 17-28.

Jourde, G., 1971. Essai de synthèse structurale et stratigraphique de Précambrien malgache. *Compte Rendu Sociète Géologique Madagascar,* 59-69.

Joyner, W.B., 1984. A scaling law for the spectra of large earthquakes. *Bulletin of the Seismological Society of America*, 74(4), 1167-1188.

Kanamori, H., 1977. The energy release in great earthquakes. *Journal of Geophysical Research*, 82, 2981-2987.

Kanamori, H. and Jennings, P.C., 1978. Determination of local magnitude, ML, from strong-motion accelerograms. *Bulletin of the Seismological Society of America*, 68, 471-485.

Kanamori, H., 1983. Magnitude scale and quantification of earthquakes. *Tectonophysics*, *93*(3-4), 185-199.

Katsushi, S., 2016. A computerized method to estimate friction coefficient from orientation distribution of meso-scale faults. *Journal of Structural Geology*, 89, 44-53.

Khattri, K., 1973. Earthquake focal mechanism studies: a review. *Earth Science*, 9, 19-63.

Kijko, A. and Graham, G., 1998. Parametric-historic procedure for probabilistic seismic hazard analysis part I: estimation of maximum regional magnitude m_{max}. *Pure and Applied Geophysics*, 152(3), 413-442.

Kijko, A. and Graham, G., 1999. "Parametric-Historic" procedure for Probabilistic Seismic Hazard Analysis, Part II: assessment of seismic hazard at specified site. *Pure and Applied Geophysics*, 154, 1-22.

Kijko, A. and Sellevoll, M.A., 1989. Estimation of earthquake hazard parameters from incomplete data files. Part I. Utilization of extreme and complete catalogs with different threshold magnitudes. *Bulletin of the Seismological Society of America*, 79(3), 645-654.

Kijko, A. and Sellevoll, M.A., 1992. Estimation of earthquake hazard parameters from incomplete data files. Part II. Incorporation of magnitude heterogeneity. *Bulletin of the Seismological Society of America*, 82(1), 120-134.

Kijko, A. and Smit, A, 2012. Extension of the Aki-Utsu b-value estimator for incomplete catalogues. *Bulletin of the Seismological Society of America*, 102(3), 1283–1287.

Kijko, A. and Smit, 2014. *Possible effect of hydraulic fracturing on seismic hazard in South Africa*. Report No. K5/2149, Water Research Commission, Pretoria, South Africa.

Kisslinger, C., 1980. Evaluation of S to P amplitude ratios for determining focal mechanisms from regional network observations. *Bulletin of the Seismological Society of America*, 70, 999-1014.

Kramer, S., 1996. *Geotechnical Earthquake Engineering*. Prentice-Hall, Inc.

Kröner, A., Windley, B.F., Jaecke, P., Collins, A.S., Brewer, T.S., Nemchin, A. and Razakamanana, T., 1999. New zircon ages for Precambrian granites, gneisses and granulites from central and southern Madagascar: significance for correlations in East Gondwana. *Gondwana Research*, 2(3), 351-352.

Kusky, T.M., Abdelsalam, M., Stern, R.J. and Tucker, R.D., 2003. Evolution of the East African and related orogens, and the assembly of Gondwana. *Precambrian Research*, 123, 81-85.

Kusky, T.M., Toraman, E. and Raharimahefa, T., 2007. The Great Rift Valley of Madagascar: an extension of the Africa–Somali diffusive plate boundary? *Gondwana Research*, 11(4), 577-579.

Kutina, J., 1975. Tectonic development and metallogeny of Madagascar with reference to the fracture pattern of the Indian Ocean. *Geological Society of America Bulletin*, 86(4), 582-592.

Lahr J.C., 1989. Hypoellipse/Version 2.0: A computer program for determining local earthquake hypocentral parameters, magnitude, and first motion pattern. *U.S. Geological Survey.Open-File Report*, 89/116.

Lahr, J.C., 1999, revised 2012. HYPOELLIPSE: a computer program for determining local earthquake hypocentral parameters, magnitude, and first-motion pattern: U.S. *Geological Survey Open-File Report 99-23*, 1.1, 119.

Laville, E., Pidue, A., Plaziat, J.C., Gioan, P., Rakotomalala, R., Ravololonirina, Y. and Tidahy, E., 1998. Le fosse meridien d'Ankay-Alaotra, temoin d'une extension crustale recente et actuelle a Madagascar. 1998. *Bulletin de la Société Géologique de France*, 169(6), 775-788.

Lee, W., H.K., Nelson, G., Ward, P. L., and Zhao, Z.H., 1981. User's manual for HYPO81A: A program to determine hypocenter and magnitude of local earthquakes using minicomputers.

LeRiche, A., Kalenchuk, K.S. and Diederichs, M.S., 2017. Estimation of in situ stress from borehole breakout for improved understanding of excavation overbreak in brittle-anisotropic rock. In *Proceedings of the Eighth International Conference on Deep and High Stress Mining,* Australian Centre for Geomechanics. 209-222.

Lockridge, J.S., Fouch, M.J. and Arrowsmith, J.R., 2012. Seismicity within Arizona during the Deployment of the Earthscope USArray Transportable Array, *Bulletin of the Seismological Society of America,* 102, 1850-1863.

Lomnitz, C., 1973. Poisson processes in earthquake studies. *Bulletin of the Seismological Society of America*, 63(2), 735-735.

Lund, B. and Townend, J., 2007. Calculating horizontal stress orientations with full or partial knowledge of the tectonic stress tensor. *Geophysical Journal International*, 170, 1328-1335.

Mahoney, J., Nicollet, C. and Dupuy, C., 1991. Madagascar basalts: tracking oceanic and continental sources. *Earth and Planetary Science Letters*, 104(2-4), 350-363.

McKenzie, D.P., 1969. The relation between fault plane solutions for earthquakes and the directions of the principal stresses. *Bulletin of the Seismological Society of America*, *59*(2), 591-601.

Martelat, J.E., Lardeaux, J.M., Nicollet, C. and Rakotondrazafy, R., 2000. Strain pattern and late Precambrian deformation history in southern Madagascar. *Precambrian Research*, 102(1-2), 1-20.

Martelat, J.E., Randrianasolo, B., Schulmann, K., Lardeaux, J.M. and Devidal. J.L., 2014. Airborne magnetic data compared to petrology of crustal scale shear zones from southern Madagascar: a tool for deciphering magma and fluid transfer in orogenic crust. *Journal of African Earth Sciences*, 94, 74-85.

Mascle, J. and Blarez, E., 1987. Evidence for transform margin evolution from the Ivory Coast–Ghana continental margin. *Nature*, 326(6111), 378-381.

Mascle, J., Mougenot, D., Blarez, E., Marinho, M. and Virlogeux, P., 1987. African transform continental margins: examples from Guinea, the Ivory Coast and Mozambique. *Geological Journal*, 22(S2), 537-561.

McGuire, R. K., 1976. FORTRAN program for seismic Risk Analysis, U.S. *Geological Survey Open-file Report*, 76-77.

McGuire, R.K., 1977. Effects of uncertainty in seismicity on estimates of seismic hazard for the east coast of the United States. *Bulletin of the Seismological Society of America*, 67(3), 827-848.

McGuire, R.K., Cornell, C.A. and Toro, G.R., 2005.The case for using mean seismic hazard. *Earthquake Spectra*, 21(3), 879-886.

Meert, J.G., Nédélec, A., Hall, C., Wingate, M.T.D. and Rakotondrazafy, M. 2001. Paleomagnetism, geochronology and tectonic implications of the Cambrian-age Carion granite, central Madagascar. *Tectonophysics*, 340, 1-21.

Menke, W., 1989, *Geophysical Data Analysis; Discrete Inverse Theory*, Revised Edition: Academic Press, San Diego.

Michael, A.J., 1984. Determination of stress from slip data: faults and folds. J*ournal of Geophysical Research: Solid Earth*, 89(B13), 11,517-11,526.

Michael, A., 1987. Use of focal mechanisms to determine stress: a control study. *Journal of Geophysics Research*, 92, 357-368.

Mignan, A., and Woessner, J., 2002. Estimating the magnitude of completeness for earthquake catalogs. Community Online Ressource for Statistical Seismicity Analysis. https://doi.org/10.5078/corssa-00180805.

Mougenot, D., Recq, M., Virlogeux, P. and Lepvrier, C., 1986. Seaward extension of the East African rift. *Nature*, 321(6070), 599 - 603.

Mulabisana, T.F., 2016. *Compiling a homogeneous earthquake catalogue for Southern Africa*. MSc dissertation, University of the Witwatersrand Johannesburg, http://hdl.handle.net/10539/21006.

Nédélec, A., Bouchez, J.L. and Gregoire, V., 2003. Quartz fabric evidence for early Pan-African penetrative east-directed shearing in the Itremo Supracrustal Group of central Madagascar. *Terra Nova*, 15(1), 20-28.

Nicollet, C., 1990. Crustal evolution of the granulites of Madagascar. In *Granulites and Crustal Evolution*. Springer Netherlands, 291-310.

Norton, I.O. and Sclater, J.G., 1979. A model for the evolution of the Indian Ocean and the breakup of Gondwanaland. *Journal of Geophysical Research*, 84, 6803-6830.

Ordaz, M., Martinelli, F., D'Amico, V. and Meletti, C., 2013. CRISIS2008: A flexible tool to perform probabilistic seismic hazard assessment. *Seismological Research Letters*, 84(3), 495-504.

Pagani, M., Garcia-Pelaez, J., Gee, R., Johnson, K., Poggi, V., Styron, R., Weatherill, G., Simionato, M., Viganò, D., Danciu, L. and Monelli, D., 2018. *Global*

Earthquake Model (GEM) Seismic Hazard Map (version 2018.1 - December 2018), DOI: 10.13117/GEM-GLOBAL-SEISMIC-HAZARD-MAP-2018.1.

Panza, G.F., Romanelli, F. and Vaccari, F., 2001. Seismic wave propagation in laterally heterogeneous anelastic media: theory and applications to seismic zonation. *Advances in Geophysics*, 43, 1-95.

Panza, G.F., La Mura, C., Peresan, A., Romanelli, F. and Vaccari, F., 2012. Seismic hazard scenarios as preventive tools for a disaster resilient society. *Advances in Geophysics*, 53, 93-165.

Paquette, J.L. and Nédélec, A., 1998. A new insight into pan-African tectonics in the east-west Gondwana collision zone by U-Pb zircon dating granites from central Madagascar. *Earth and Planetary Science Letters*, 155, 45-56.

Pavlis, G.L., Vernon. V., D.Harvey and Quinlan, D., 2004. The generalized earthquake location (GENLOC) package: an earthquake location library. *Computers and Geosciences*, 30, 1079-1091.

Piqué A., Laville, E., Bignot, G., Rabarimanana, M. and Thouin C., 1999. The initiation and development of the Morondava Basin (Madagascar) from the Late Carboniferous to the Middle Jurassic: sedimentary, palaeontological and structural data. *Journal of African Earth Sciences*, 28, 931-948.

Poggi, V., Durrheim, R., Tuluka, G. M., Weatherill, G., Gee, R., Pagani, M., and Delvaux, D., 2017. Assessing seismic hazard of the East African Rift: a pilot study from GEM and AfricaArray. *Bulletin of Earthquake Engineering*, 15(11), 4499-4529.

Poisson, R.P., 1924. Tremblements de Terre de Tananarive; 1889-1924. *Bulletin Economique de Madagascar, Tananarivo.*

Poisson, R.P., 1930. Tremblement de Terre Malgaches de 1897 à 1905. *Bulletin Economique de Madagascar. Tananarive.*

Pratt, M.J., Wysession, M.E., Wiens, D.A., Nyblade, A., Aleqabi, G.I., Shore, P.J., Rambolamanana, G., Andriampenomanana, F. and Rakotondraibe, T., 2017. Shear-velocity structure of the crust and upper mantle of Madagascar derived from surface wave tomography. *Journal of Geophysical Research*, 456, 405-417.

Rabinowitz, P.D., Coffin, M.F, and David, F., 1983. The separation of Madagascar and Africa. *Science*, 220(4592), 67-69.

Rakotovao, A.P., 2009. Contexte géologique et métallogénique des minéralisations en émeraude du gisement d'Ianapera, bloc de Vohibory, Sud-Ouest de Madagascar. *Ph.D. Thesis, University of Toulouse: Paul-Sabatier*, 226.

Rakotondraibe, T., Nyblade, A.A., Wysession, M.E., Durrheim, R.J., Rambolamanana, G., Aleqabi, G.I., Shore, P.J., Pratt, M.J., Andriampenomanana, F., Rümpker, G. and Rindraharisaona, E., 2020. Seismicity and seismotectonics of Madagascar revealed by the 2011–2013 deployment of the island-wide MACOMO broadband seismic array. *Tectonophysics*, 790, p.228547.

Rakotondrainibe, 1977. Contribution à l'étude de la séismicité de Madagascar. *Thèse Sciences Université d'Antananarivo.*

Rakotondraompiana, S.A., Albouy, Y. and Pique, A., 1999. Lithospheric model of the Madagascar Island [western Indian Ocean]: a new interpretation of the gravity data. *Journal of African Earth Sciences,* 28(4), 961-973.

Rambolamanana, G., 1989. *Détermination par la méthode des ondelettes du facteur de qualité de la région centrale de Madagascar*. Theses Sciences Université d'Antananarivo.

Rambolamanana, G. and Ratsimbazafy, J. B., 1991. Le séisme du 21 avril 1991 localisé dans la région de Famoizankova. *Rapport à l'Académie Malgache*.

Rambolamanana, G., Suhadolc, P. and Panza, G.F., 1997. Simultaneous inversion of hypocentral parameters and structure velocity of the central region of Madagascar as a premise for the mitigation of seismic hazard in Antananarivo. *Pure Applied Geophysics*, 149, 707-730.

Ranganathan, S.R., 1940. Poisson, Simeon Denis (1781–1840). *Current Science*, 207-207.

Rasamimanana G., Bardintzeff, J.M., Rasendrasoa, J., Bellon, H., Thouin, C., Gioan, P., and Piqué, A., 1998. Rifting-related magmatic episodes of south-western Malagasy (Morondava basin). *Compte Rendu de l'Académie des Sciences, Série. II*, 326, 685‑691.

Razafindrakoto, H.N., Rambolamanana, G. and Panza, G.F., 2009. Seismic hazard evaluation for major cities in Madagascar (No.IC--2009/075). *Abdus Salam International Centre for Theoretical Physics*.

Reasenberg, P. 1985. Second-order moment of central California seismicity, 1969–1982. *Journal of Geophysical Research: Solid Earth*, 90(B7), 5479-5495.

Rebetsky, Y.L. and Tatevossian, R.E., 2013. Rupture propagation in strong earthquake sources and tectonic stress field. *Bulletin de la Societe Geologique de France*, 184, 335-346.

Rebetsky, Y.L., Kuchai, O.A., Sycheva, N.A. and Tatevossian, R.E., 2012. Development of inversion methods on fault slip data: Stress state in orogenes of the Central Asia. *Tectonophysics*, 581, 114-131.

Rechenmann, J., 1981. Gravimetrie métallogenique de Madagascar, interpretations et relations avec géologie. *Thèse, Université de Paris Sud*, 175.

Reiter L., 1991. *Earthquake Hazard Analysis.Issues and Insights*, Columbia University Press, New York.

Richter, C.F., 1935. An instrumental earthquake magnitude scale. *Bulletin of the Seismological Society of America*, 25 (1-2), 1-32.

Rindraharisaona, E. J., Rambolamanana, G., 2007, Evaluation de parametres sismiques dans la partie Centrale de Madagascar. *Madarevues* : http://madarevues.recherches.gov.mg/IMG/pdf/MADA-GEO1203.pdf

Rindraharisaona, E.J., Mariangela, G., Abdoulkarim, A. and Rambolamanana, G., 2013. Earth structure and instrumental seismicity of Madagascar: implications on the seismotectonics. *Tectonophysics*, 594, 165-181.

Rivera, L. and Cisternas, A., 1990. Stress tensor and fault plane solutions for a population of earthquakes. *Bulletin of the Seismological Society of America*, 80, 600-614.

Ristau, J., 2009. Comparison of magnitude estimates for New Zealand earthquakes: moment magnitude, local magnitude, and teleseismic body-wave magnitude. *Bulletin of the Seismological Society of America, 99(3),* 1841-1852.

Sabetta, F., and Pugliese, A. 1996. Estimation of response spectra and simulation of nonstationary earthquake ground motions. *Bulletin of the Seismological Society of America,* 86(2), 337-352.

Saria, E., Calais, E., Stamps, D.S., Delvaux, D. and Hartnady, C.J.H., 2014. Present-day kinematics of the East African Rift. *Journal of Geophysical Research, Solid Earth,* 119**,** 3584-3600.

Scordilis, E.M., 2006. Empirical global relations converting MS and mb to moment magnitude. *Journal of Seismology,* 10(2), 225-236.

Segoufin, J. and Patriat, P., 1981. Reconstructions de l9Ocean Indien Occidental pour les epoques des anomalies M21, M2 et 34; Paleoposition de Madagascar. *Bulletin de la Société Géologique de France*, 7(6), 603-607.

Shackleton, R.M., 1996. The final collision between east and west Gondwana: Where is it? *Journal of African Earth Sciences,* 23(3), 271-287.

Shakal, A.F. and Bernreuter, D.L., 1980. *Empirical analyses of near-source ground motion.* Report No. NUREG/CR-2095; UCRL-53028. Lawrence Livermore National Lab., CA (USA).

Shudofsky, G.N., 1985. Source mechanisms and focal depths of the East African earthquakes using Rayleigh-wave inversion and body-wave modeling. *Geophysical Journal International,* 83(3), 563-614.

Sigloch, K., and Barruol, G. 2013. RHUM-RUM investigates La Réunion mantle plume from crust to core. In *EGU General Assembly Conference Abstracts*.

Snoke, J.A., Munsey, J.W., Teague, A.G. and Bollinger, G.A., 1984. A program for focal mechanism determination by combined use of polarity and SV-P amplitude ratio data. *Earthquake Notes,* 55 (3), 15.

Sole'vev, 1965. Seismicity of Sakalin. *Bulletin of Research Institute of Tokyo University*, 43, 95-102.

Stamps, D. S., Calais, E., Saria, E., Hartnady, C., Nocquet, J.M., Ebinger, C.J., and Fernandes, R.M. 2008. A kinematic model for the East African Rift. *Geophysical Research Letters*, 35(5), L05304, doi:10.1029/2007GL032781.

Stein, S. and Wysession, M., 2003. *Introduction to Seismology, Earthquakes, and Earth Structure*. Blackwell, Oxford.

Stepp, J.C., 1972. Analysis of completeness of the earthquake sample in the Puget Sound area and its effect on statistical estimates of earthquake hazard. In *Proceedings of the First International Conference on Microzonation*, Seattle, 2, 897-910.

Stern, R.J., 1994. Arc assembly and continental collision in the Neoproterozoic East Africa Orogen: implications for the consolidation of Gondwanaland. *Annual Review of Earth and Planetary Sciences*, 22, 319-351.

Stigler, S.M., 1981. Gauss and the invention of least squares. *The Annals of Statistics*, 465-474.

Storey, M., Mahoney, J.J. and Saunders, A.D., 1995. Timing of hot spot-related volcanism and the breakup of Madagascar and India. *Science*, 267(5199), 852-855.

Strang, G., 1976. *Linear algebra and its Applications.* Academic Press, New York.

Tarling, D.H., 1971. Gondwanaland, paleomagnetism and continental drift. *Nature*, 229 (5279), 17-21.

Thomas, R.J., De Waele, B., Schofield, D.I., Goodenough, K.M., Key, R.M., Annells, R., Tucker, R.D., Bauer, W., Burton, W.B., Walsh, G.J., Howard, K., Lidke, D., Rabarimanana, M., Rafahatelo, J.M., Ralison, A.V. and Randriamananjara, T., 2008. Crustal architecture of northern Madagascar: results from recent geological mapping. *Gondwana XIII, Dali, China*.

Tilmann, F., Yuan, K., Rümpker, G., Rambolamanana, G. and Rindraharisaona, E., 2013. Investigating the lithospheric structure of southern Madagascar. *AGU Fall Meeting*.

Torsvik, T. H., Tucker, R. D. and Ashwal, L. D. 1998. Late Cretaceous magmatism in Madagascar: palaeomagnetic evidence for a stationary Marion hotspot. *Earth and Planetary Science Letters*, 164(1-2), 221-232.

Tucker, R.D., Ashwal, L.D., Hamilton, M.A., Torsvik, T.H. and Carter, L.M., 1999. Neoproterozoic silicic magmatism of northern Madagascar, Seychelles, and NW India: clues to Rodinia's assembly and dispersal. *Geological Society of America*, 31(7), 317.

Tucker, R.D., Roig, J.Y., Delor, C., Amelin, Y., Goncalves, P., Rabarimanana, M.H., Ralison, A.V. and Belcher, R.W., 2011a. Neoproterozoic extension in the Greater Dharwar Craton: a reevaluation of the ‘‘Betsimisaraka suture’’ in Madagascar. *Journal of Earth Science*, 48, 389-417.

Tucker, R.D., Roig, J.Y., Macey, P.H., Delor, C., Amelin, Y., Armstrong, R.A., Rabarimanana, M.H. and Ralison, A.V., 2011b. A new geological framework for south-central Madagascar and its relevance to the ‘‘out-of-Africa’’ hypothesis. *Precambrian Research*, 185, 109–130.

Tucker, R.D., and Moine, B., 2012. Discussion of: Petrogenesis and Nd-, Pb-, Sr-isotope geochemistry of the Cenozoic olivine melilites and olivine nephelinites (“Ankaratrites”) in Madagascar. *Lithos* 140(141), 255–256.

Vanek, J., Zatopek, A., Karnik, V., Kondorskaya, N.V., Riznichenko, Y.V., Savarensky, E.F., Soloviev, S.L. and Shebalin, N.V., 1962. Standardization of magnitude scale, *Izvestiya Akademii Nauk USSR. Series of Geophysics*, 2, 153-158.

Vavryčuk, V., 2014. Iterative joint inversion for stress and fault orientations from focal mechanisms. *Geophysical Journal International*, 199(1), 69-77.

Waldhauser, F. and Ellsworth, W.L., 2000. A double–difference earthquake location algorithm: method and application to the northern Hayward fault, California. *Bulletin of the Seismological Society of America*, 90(6), 1353 -1 368.

Waldhauser, F., 2001. hypoDD--A Program to Compute Double-Difference Hypocenter Locations (hypoDD version 1.0-03/2001). *US Geological Survey*. Open-File Rept. 01, 113.

Wallace, R.E., 1951. Geometry of shearing stress and relation to faulting. *Journal of Geology*, 59(2), 118-130.

Wegener, A., 1924. *The Origin of Continents and Oceans*. Dutton and Co., New York.

Wessel, P. and Smith, W.H., 1998. New, improved version of Generic Mapping Tools released. *Eos, Transactions American Geophysical Union*, 79, 579.

Wiemer, S., 2001. A software package to analyze seismicity: ZMAP. *Seismological Research Letters*, 72(3), 373-382.

Wiemer, S., and Wyss, M., 2000. Minimum magnitude of completeness in earthquake catalogs: examples from Alaska, the western United States, and Japan. *Bulletin of the Seismological Society of America*, 90(4), 859-869.

Wysession, M., Wiens, D., Nyblade, A., and Rambolamanana, G., 2012. Investigating mantle structure with broadband seismic arrays in Madagascar and Mozambique. *AGU Fall Meeting Abstarct*, B2591.

Zang, A. and Stephansson, O., 2010. Rock fracture criteria. In *Stress Field of the Earth's Crust,* Springer, Dordrecht, 37-62.

Zoback, M.D., Townend, J., and Grollimund, B., 2002. Steady-state failure equilibrium and deformation of intraplates lithosphere. I*nternational Geological Revue*, 44, 383-401.

Appendices

Appendix A: Seismotectonic studies of Madagascar (Published Paper)

Seismicity and seismotectonics of Madagascar revealed by the 2011-2013 deployment of the island-wide MACOMO broadband seismic array

Tectonophysics, 2020, vol. 790, p. 228547.

Tsiriandrimanana Rakotondraibe[1,4], Andrew A. Nyblade[1,2], Michael E. Wysession[3], Raymond J. Durrheim[1], Gérard Rambolamanana[4], Ghassan I. Aleqabi[3], Patrick J. Shore[3], Martin J. Pratt[3], Fenitra Andriampenomanana[1,4], Georg Rümpker[5], and Elisa Rindraharisaona[6]

1. *School of Geosciences, University of the Witwatersrand, Private Bag 3, Wits 2050, Johannesburg, South Africa*

2. *Department of Geosciences, Penn State University, University Park, PA 16802, USA*

3. *Department of Earth and Planetary Sciences, Washington University in St. Louis, Campus Box 1169, 1 Brookings Drive., Saint Louis, MO 63130-4899, USA*

4. *Institut et Observatoire de Géophysique d'Antananarivo, Université d'Antananarivo, Ambohidempona - B.P 3843, Antananarivo 101, Madagascar*

5. Institute of Geosciences, Goethe-University Frankfurt, Altenhöferallee 1, 60438 Frankfurt, Germany

6. *GeoForschungs Zentrum (GFZ), Telegrafenberg, 14473 Potsdam, Germany*

ABSTRACT

The seismicity and seismotectonics of Madagascar have been studied using an island-wide distribution of broadband seismic stations. The 28-station MAdagascar-COmoros-

MOzambique (MACOMO) array was deployed for a 23-month period between 2011 and 2013. MACOMO data were supplemented by seven temporary stations from the Seismological Signatures in the Lithosphere/Asthenosphere system of Southern Madagascar (SELASOMA) project, ten temporary stations from the Réunion Hotspot and Upper Mantle - Réunions Unterer Mantel project (RHUM-RUM), and 11 permanent stations. A total of 695 earthquakes with magnitudes between M_L1 and M_L5.3 located within Madagascar were recorded, a new local magnitude scale was developed, and focal mechanisms were determined for 23 well-recorded events. Most of the seismicity is clustered within central Madagascar, forming NW-SE trends in the Ankaratra region and NE-SW trends in the Alaotra and Ankay regions that roughly align with extensional tectonic features. The northern and southern parts of Madagascar also show seismicity clusters that align parallel to existing tectonic features, primarily Precambrian shear zones. Focal mechanisms exhibit a wide orientation of nodal planes, show predominantly normal faulting throughout Madagascar, and provide no evidence for a sharp east-west striking plate boundary between the Lwandle and Somalian plates in the middle of the island. However, a diffuse plate boundary cannot be excluded. We suggest that topographically-generated extensional stresses is the cause of most seismicity, given that significantly fewer earthquakes are located in the lower elevation areas of the island compared to regions of higher elevations. The frequency-magnitude distribution has a *b*-value of ~1.2 and indicates that events with magnitude M_L5 or greater should occur with an average repeat time of ~1.4 years. However, no earthquake exceeding M_L6 has been recorded in the last century, suggesting that the frequency-magnitude distribution could be truncated.

1. INTRODUCTION

Madagascar, the world's fourth-largest island, is located approximately 1200 km east of the East African Rift (EAR) system, 300 km from mainland Africa and 900 km north of the Southwest Indian Ridge. Most of what is known about seismic activity in Madagascar comes from studies that used data from seismic stations concentrated in the center of the island (*e.g.*, Bertil and Regnoult, 1998). In common with other continental intraplate settings, the earthquakes in Madagascar tend to be small in both number and

magnitude and associated with ancient zones of tectonic activity, such as terrane sutures, failed rifts, and shear zones. The clusters of low-magnitude events are generally aligned with known faults and grabens (Fourno and Roussel, 1993; Bertil and Regnoult, 1998; Rindraharisaona et al., 2013). The level of seismic activity is generally described as 'moderate'. However, the rate of seismicity is somewhat larger than expected for a typical continental intraplate region, with about 90 earthquakes greater than M3 occurring annually and about five in the range of M5 to M6 every decade. However, no earthquakes larger than M6 have been reported since record-keeping began in 1835.

Recent studies based on geodetic, seismic, topographic and bathymetric observations have postulated the existence of several microplates in the region between the East African Rift system and the Southwest Indian Ridge (Chu and Gordon, 1999; Calais et al., 2006), and, more specifically, that the boundary between the Lwandle and Somalian plates passes through the central part of Madagascar (Horner-Johnson et al., 2007; Stamps et al., 2008; Saria et al., 2013, 2014).

We present a study of Madagascan seismicity based on a distribution of broadband stations that provides significantly better coverage than previous studies, particularly in the northern and southern parts of the island. The 28-station 2011-2013 MAdagascar-COmoros-MOzambique (MACOMO) array (Wysession et al., 2012) is supplemented by 7 stations from the 2012-2014 Seismological Signatures in the Lithosphere/Asthenosphere system of Southern Madagascar (SELASOMA) network (Tilmann et al., 2012), 10 stations from the Réunion Hotspot and Upper Mantle – Réunions Unterer Mantel (RHUM – RUM) project (Barruol and Sigloch, 2013) and 11 stations from various permanent networks (GSN, GEOSCOPE, GEOFON, Madagascar National Seismic Network) (Table 3. 1; Figure 3. 10).

The MACOMO and SELASOMA data sets have already been used to investigate the seismic velocity structure of crust and upper mantle of Madagascar (Andriampenomanana et al., 2017; Rindraharisaona et al., 2017; Pratt et al., 2018) and seismic anisotropy (Ramirez et al., 2018). Here we exploit the fairly uniform distribution of seismic stations to investigate the seismicity and seismotectonics of the entire island, and to evaluate the hypothesis that a plate boundary passes through it.

2. GEOLOGIC SETTING

During the Jurassic period, present-day Madagascar (Figure 1. 2) was situated near the heart of the Gondwana supercontinent, close to the suture between Eastern and Western Gondwana (Segoufin and Patriat, 1980; Coffin and Rabinowitz, 1987; Geiger et al., 2004). The island separated from mainland Africa at *ca.* 165 Ma along the Davie Fracture Zone, and India at *ca.* 95 Ma. The transform fault that governed the northeastward movement of the Indian subcontinent bounds the eastern side of the island (Gnos et al., 1997; Phethean et al., 2016). The Archean Antongil and Masora cratons of eastern Madagascar were once part of the larger Western Dharwar Craton of India (Tucker et al., 1999; Paquette et al., 2003). The bulk of the Malagasy highland plateau consists of the Paleoproterozoic Antananarivo Group (Paquette and Nédélec, 1998; Tucker et al., 2007). The Paleo- to Neoproterozoic Bemarivo Group, deformed during the *ca.* 540 Ma East African Orogeny, crops out in northern Madagascar (Thomas et al., 2009). Little is known about the basement rocks of western Madagascar because sediments that accumulated during the ca. 165 Ma rifting from mainland Africa (Rabinowitz et al., 1983; Coffin and Rabinowitz, 1988; Rindraharisaona et al., 2017; Andriampenomanana et al., 2017) cover them.

Major Precambrian shear zones include the Antsaba and Sandrakota in the north (Thomas et al., 2009), the Bongolava in the central region, and the Ranotsara in the south of the island (Figure 1. 3). The Antsaba shear zone is ~15 km wide in the west and narrows to less than 1 km in the east. The Sandrakota shear zone, which separates the Antananarivo and Bemarivo Groups, ranges in width from 4-50 km (Thomas et al., 2009). The Bongolava shear zone is a N-S striking structure that is ~200 km in length (de Wit et al., 2001). The Ranotsara shear zone is a 350-km-long NW-SE-trending structure that correlates with shear zones in southern India and eastern Africa (Reeves, 2014). In addition to these main shear zones, there are several other thrust and shear zones in the northern (Andaparaty) and southern parts of the island (Ampanihy, Vohibory, Betroka, Bekily, and Tranomaro; see (Figure 1. 3).

Volcanic outcrops provide evidence of multiple episodes of magmatism unrelated to island arc subduction (Collins et al., 2003). Tholeiitic basalts erupted in the western part

of the island *ca*. 165 Ma when Madagascar rifted from Africa, and more widespread flood eruptions occured *ca*. 95-85 Ma when Madagascar moved over the Marion hot spot and India rifted away to the northeast (Storey et al., 1995; Torsvik et al., 1998). During the Cenozoic, alkali basalt volcanism occurred in the southwestern, central and northern regions of Madagasar (*e.g.*, Collins, 2000; Buchwaldt, 2006; Tucker and Conrad, 2008; Bardintzeff et al., 2010) (Figure 1. 3).

Previous studies found that seismicity within Madagascar was concentrated in the central part of the island, although this finding could have been an artifact of the limited distribution of seismic stations used in those studies (Bertil and Regnoult, 1998; Rindraharisaona et al., 2013). Published focal mechanisms show predominantly E-W extension (Grimison and Chen, 1988; Rindraharisaona et al., 2013).

3. DATA

Most of the data used to investigate the seismicity of Madagascar comes from the 26 temporary broadband seismic stations deployed at 28 sites during 2011-2013 as part of the MACOMO project (Wysession et al., 2012) (Figure 3. 10, Table S1). These stations, provided by the PASSCAL program of the Incorporated Research Institutions for Seismology (IRIS), were deployed in two phases: Phase A (10 stations) was installed in October 2011 and recorded for two years, except for two stations (VATO, MARO) that were moved to new sites after three month's operation (MAGY, KIRI); while Phase B (an additional 16 stations) was installed in September 2012 and recorded for one year. Phase A primarily targeted near-coastal locations to attain the broadest station distribution possible, while Phase B filled in many of the gaps (Figure 4. 1). The seismograph stations were equipped with broadband sensors (Streckeisen STS-2, Guralp CMG-3, and Nanometrics Trillium 120PA) and Quanterra Q330 data loggers.

The 28 MACOMO stations were supplemented by data from another 28 seismic stations (Figure 4. 1,): four permanent open broadband stations (GSN station ABPO, GEOSCOPE station FOMA and GEOFON stations VOI and SBV); seven permanent short-period stations that belong to the Madagascar National Seismic Network and are maintained by the Institut et Observatoire de Géophysique d'Antananarivo (IOGA) and the Département Analyse, Surveillance, Environnement, France (DASE); seven stations

from the SELASOMA project, which deployed 25 broadband and 23 short-period stations along a SW-NE profile that stretched from coast to coast across the Ranotsara shear zone (Tilmann et al., 2012); and 10 stations from the RHUM – RUM project (Barruol and Sigloch, 2013).

4. METHODS AND RESULTS

4.1 Seismicity

The continuous seismic records were loaded into an Antelope database, which is a commercial software package for seismic data processing developed by Boulder Real Time Technology (BRTT, 2004). Events were identified using the Antelope *dbdetect* routine, which uses a short-term-average/long-term-average (STA/LTA) detector, and initial event association was performed using the routine *dbgrassoc*. P- and S-wave arrivals were then manually picked on the vertical and horizontal components, respectively, using Antelope's *dbpick* routine with an accuracy of 0.1 seconds on 1-10 Hz band-pass filtered seismograms.

Earthquake hypocenters were located using the HYPOELLIPSE program (Lahr, 1999) that uses Geiger's iterative least-squares method (Geiger, 1912) to search for the hypocenter that minimizes the root-mean-square (RMS) residual between the observed and predicted phase arrival times. Only seismic events that were recorded on at least five seismic stations and produced at least eight P- and S-arrival picks were located using an 'average' S-wave velocity model (Figure 1. 6) that we developed. Andriampenomanana et al. (2017) jointly inverted Rayleigh-wave phase velocities and receiver functions at 37 seismic stations that spanned Madagascar. We obtained an 'average' 1D S-wave model for the whole island by weighting these Vs-depth functions (Figure 1. 6) according to the station locations and the mapped geology (Figure 1. 3, Figure 3. 1; see further explanation in supplemental materials). We then determined the corresponding P-wave model (Figure 1. 6 using V_P/V_S ratios of 1.75 and 1.81 for the crust and mantle, respectively (Kvarven et al., 2016, Hyndman, 1979). The validity of using a ratio of 1.75 for the crust was confirmed by a Wadati plot (Figure 1. 6), while the validity of using

1.81 for the mantle is supported by a Pn tomographic study (Andriampenomanana, 2017; Andriampenomanana et al, submitted).

A total of 695 local earthquakes were located with HYPOELLIPSE (Figure 4. 1 Appendix C). This was done in two stages. During the first pass, travel-time residuals were calculated for each phase arrival, and the average of these residuals was calculated and reported as a RMS error for the event. The maximum RMS error for the entire catalog was then determined. The locations were then recalculated, this time applying a reduced weight to each pick that had a residual greater than the maximum RMS error. This revised catalog is listed in Appendix C. The largest RMS error in the entire 695 event catalog is 1.9 s. The event magnitudes range from M_L1 to M_L5.3, with most between M_L2.5 and M_L3.2. Only two of the seismic events (with magnitudes M_L3.5 and 5.3 in our catalogue) are reported in the ISC catalog (with magnitudes M_L2.9 and 5.2; see Table 6. 1). The seismic events are clustered in several regions. There are two broad clusters in central Madagascar, one with a NW-SE trend in the Ankaratra region (ANK), and another that trends NE-SW in the Alaotra region (AL) (Figure 4. 4). A limited amount of seismicity was observed in the southern Bekily region (BEK), around the Vohibory, Ampanihy, and Betroka shear zones (Figure 4. 7). The HYPODD program (Waldhauser, 2001) was used to obtain better relative locations of events in regions where the seismicity is clustered. HYPODD computes new hypocenters that minimize the difference in travel-time residuals for event pairs. HYPODD is better at relocating events if the distance between two hypocenters is small compared to the distance between the events and recording stations. The double-difference inversion can be performed in one of two ways, depending upon the size of the dataset: if it is relatively small (less than 1000 events), a singular value decomposition method (SVD) that is able to quantify errors in the solution is used; alternatively, a least-squares conjugate-gradient method (LSQR) is used. We used the SVD method.

The critical prerequisite for using HYPODD is the identification of groups of clustered earthquakes. The earthquake data are prepared using the *ph2dt* routine (Waldhauser, 2001), which first searches the catalog for event pairs with P- and S-wave arrival-time picks at the same stations, and then links each event pair to neighboring

pairs, thus forming a chain (or cluster) of event pairs. For this study, the manually picked P- and S-arrivals were used as input for the *ph2dt* program to create clusters of event pairs, after which HYPODD was run. During the processing, the data catalog option (*dt.ct*) in the *ph2dt* program was used because this function represents the differential time of the data set from earthquake catalogs for pairs of seismic events. We did not apply the waveform cross-correlation option in the HYPODD program because it proved difficult to identify similar waveforms that could be used as references. This is due to the characteristics of the data from the NDC stations, which are mostly short-period and located in the central part of Madagascar (Fig. 2).

The parameter MINLNK, that defines the minimum number of linked neighboring events, was set to six during the processing. MAXDIST, which defines the maximum distance between the event pair and a particular station, was set at 1000 km, large enough to include all stations in Madagascar. We tested the effect that the maximum distance separating two event pairs (MAXSEP) had on the results, using values of 5 km, 10 km, 15 km and 25 km. In regions where the events were tightly clustered, such as the central-east (Alaotra) and central (Ankaratra) regions, the results were similar. However, in the southern and northern regions of Madagascar (Bekily, Bemarivo), where events are more scattered, the 25-km distance yielded significantly more linked events. The average 1D P-wave velocity model described above was used (Figure 1. 6). A complete list of the parameters used to run HYPODD is provided in Table S4. After identifying possible neighboring events, the double-difference relocation was performed; 422 earthquakes were relocated with residual values less than 0.6 s. The relocated earthquakes lie in four regions, *viz.* northern Bemarivo, east-central Alaotra and Ankay, central Ankaratra and Famoizankova, and southernmost Bekily (Figure 4. 1). The HYPODD locations are only slightly more tightly clustered than the HYPOELLIPSE locations.

4.2 Local Magnitude Determination

A local magnitude scale for Madagascar was determined based on the original Richter (1935) method. The maximum amplitude (zero-to-peak) on the vertical-component seismogram produced by each located earthquake was measured at every

station after correction for the instrumental response and the application of the frequency response of a standard Wood–Anderson torsion seismograph (Kanamori and Jennings, 1978). In the original definition of the magnitude scale (Richter, 1935), the "local magnitude" (M_L) of an earthquake is determined from the difference between the *log* of the measured amplitude of a given seismic signal on a particular seismograph (*log A*) and the *log* of a reference amplitude (*log* A_o)

$$M_L = \log A - \log Ao + \beta \qquad \text{(Equation 1)}$$

where β represents the station correction and *Ao* is a value obtained from an empirically-determined amplitude-distance curve, which is based on the definition that an event with M_L = 3.0 produces a motion with a peak amplitude of 1 mm on a Wood-Anderson seismogram recorded at a station located 100 km away. Hence, the reference amplitude can be expressed by:

$$-\log Ao = n\log\left(\frac{r}{100}\right) + k(r - 100) + 3.0 \qquad \text{(Equation 2)}$$

where *n* is the geometric spreading coefficient, *k* is the anelastic attenuation coefficient, and *r* is the hypocentral distance in kilometers. After combining equations (1) and (2), the observed amplitude at some station *j* is defined by:

$$\log A_j = -n\log\left(\frac{r_j}{100}\right) - k\left(r_j - 100\right) - 3.0 + M_L - \beta_j \qquad \text{(Equation 3)}$$

The values of the coefficients *n*, *k*, and β in equation (3) were obtained by least squares inversion of 5304 amplitude measurements on the 695 located events, yielding the distance-correction function:

$$-\log A_0 = 0.7314\log\left(\frac{r}{100}\right) + 0.0005(r - 100) + 3.0 \qquad \text{(Equation 4)}$$

and a new M_L scale:

$$M_L = \log A + 0.7314\log\left(\frac{r}{100}\right) + 0.0005(r - 100) + 3.0 + \beta_j \qquad \text{(Equation 5)}$$

The station corrections β_j are listed in Table 3. 1.

We compared our attenuation curve for Madagascar with Richter's curve for southern California (Richter, 1935; Hutton and Boore, 1987) and a recently derived attenuation model for eastern Africa (Equation 7; Ebinger et al. 2019).

$$M_L = \text{logA} + 2.56 \log(r) - 1.67 \quad \text{(Equation 6)}$$

$$M_L = \text{logA} + 0.956 \log\left(\frac{r}{17}\right) - 0.000622(r - 17) + 2 \quad \text{(Equation 7)}$$

where r is the hypocentral distance in km. Fig. 5 shows that attenuation is considerably less in Madagascar than southern California, as would be expected as these regions are representative of 'stable' and 'active' continental crust, respectively. The attenuation at epicentral distances greater than 100 km is significantly higher in Madagascar than in regions in eastern Africa. The relatively low attenuation in east Africa is attributed to travel paths through the lower crust and upper mantle, which has properties that resemble the Tanzanian craton (Ebinger et al. 2019).

4.3 Determination of the magnitude of completeness and *b*-value

The empirical Gutenberg-Richter formula is widely used to describe the relationship between the size of earthquakes and their frequency of occurrence (Richter, 1935; Gutenberg-Richter, 1944):

$$\text{logN} = \text{a} - \text{bM} \quad \text{(Equation 8)}$$

with $N = 10^{a-bM}$, where *a* describes the activity rate and *b* is the 'tectonic parameter' that describes the relative abundance of large to small shocks.

We used our 2011 – 2013 catalogs of earthquakes and the Kijko and Sellevoll (1992) method, which is based on the maximum likelihood technique, to calculate the *a*- and *b*-values for Madagascar. While these values will vary depending on the tectonic regime (*e.g*. the regions identified in Figure 4. 1), here we used all data as the time period is quite short (23 months) and the number of events is consequently quite small (695). The data were grouped in 0.2 magnitude bins (Figure 4. 11). We used a moving-time-window approach (Wiemer and Wyss, 2000) to determine a magnitude of completeness

(Mc) of M_L2.8 for our catalog. From the maximum likelihood technique, a frequency magnitude relation is determined

$$\log_{10}(N)=\mathrm{a}-\mathrm{bM}_L = 5.68 - 1.12M_L \qquad \text{(Equation 9)}$$

The observed *b*-value of 1.12 ±0.18 is close to 1, the *b*-value that is generally observed for global distributions of seismicity (Frohlich and Davis, 1999; Stein and Wysession, 2003). We repeated the calculation using a value of M_L3.0 for Mc, based on the observation that conventional methods tend to underestimate Mc by about 0.2 (Woessner and Wiemer, 2005), and obtained a very similar *b*-*v*alue of 1.14 ±0.21.

4.4 Hypocentral depth

We investigated the depth distribution of the 695 local earthquakes and found that nearly 85% were located at depths between 10 and 25 km, *i.e*., in the middle crust (Fig. S4). The average error was estimated to be less than 5 km according to the HYPOELLIPSE program. HYPODD double-difference relocation (Figure 4. 1) reduced the average error to less than 1 km.

4.5 Focal mechanisms

Focal mechanisms were computed using the FOCMEC program (Snoke, 2003) for a selected set of earthquakes that had sufficiently clear first-motion P- and S-wave (SH or SV) polarities on eight or more stations to produce a well-constrained solution. FOCMEC performs a grid search of nodal planes for all combinations of strike, dip, and slip that match a given set of first-motion polarities. A 1º increment was used in the grid search, the maximal azimuthal gap was 180º and maximum take-off angle was 80º.

To improve the reliability of the solutions, data from the MACOMO stations were supplemented by data from stations belonging to the Madagascar National Seismic Network, and the RHUM-RUM and SELASOMA projects. This improved the coverage of the focal sphere by adding stations with other azimuths and take-off angles. Before picking the S-wave polarities, seismograms were rotated along the great-circle path to obtain the radial (SV) and transverse (SH) components. Unfiltered waveforms were used to avoid distortions that might affect the determination of the polarities (Havskov

and Ottemöller, 2010). The source depth, azimuth and take-off angle for each event-station pair were calculated using the HYPOELLIPSE program (Lahr, 1999). Uncertainty in the source depth calculations was assessed by relocating the hypocenters with the source at fixed depths that ranged from the surface to 50 km in 5 km increments and graphing the RMS travel-time residuals (Figure 4. 1). In most cases, the depth determined by HYPOELLIPSE was at a clear minimum in the travel-time residual curve and the uncertainty *ca.* ±5 km, although in a few cases the deeper bound to the RMS curve was not well defined and the uncertainty larger (*e.g.*, events 13 and 21).

FOCMEC was used to determine focal mechanisms for 23 events with magnitudes between M_L2.9 and M_L4.6 (Figure 4. 9, Table 4. 1). The results are classified according to the quality of the phase and polarity picks: A (most picks are clear, with at least 75% absolutely clear), B (many picks are clear, with at least 50% absolutely clear) and C (some picks are clear, with 25% absolutely clear) (See Table 1) Seven of the new focal mechanisms in central Madagascar show normal faulting mechanisms (event IDs 4, 9, 10, 19, 20, 21, 22); while six mechanisms show mainly normal faulting with some strike-slip motion (event IDs 3, 5, 6, 7, 8, 11, 23). The focal mechanisms for two earthquakes in the northern part of the island are normal (event ID 1) and oblique-slip (event ID 2). A variety of focal mechanisms were determined for seven earthquakes in the southern part of the island (event IDs 12, 13, 14, 15, 16, 17, 18), and include extensional, reverse and strike-slip mechanisms with a wide range of nodal plane orientations.

5. **DISCUSSION**

The increased number and wider distribution of seismic stations used in this study has enabled us to develop a new local magnitude scale and gain a better understanding of the seismicity and the seismotectonics of Madagascar. Previous magnitude scales were based on signal duration rather than amplitude, while the seismicity patterns reported in earlier studies may have been influenced by the concentration of seismic stations near the center of the island (Rakotondrainibe, 1977; Bertil and Regnoult, 1998;

Rindraharisaona et al., 2013). The improvement can be assessed by comparing our results (Figure 4. 9) with results from previous studies (Figure 1. 5).

5.1 Seismicity and focal mechanisms

Much of the seismicity in Madagascar occurs within the central part of the island, especially in the Ankaratra and Alaotra regions (Fig. 4). Two of the largest historical earthquakes, both with maximum Mercalli intensities of VII, occurred in this region: one on 14 September 1932 in Mantasoa and the other on 10 November 1955 near the Alaotra rift (Bertil and Regnoult, 1998). Many of the faults in this region are thought to have formed during the separation of Madagascar and India (Torsvik et al., 1998; Bertil and Regnoult, 1998) and been reactivated by Cenozoic tectonic activity associated with Oligocene-to-Holocene volcanism (Collins, 2000; Bardintzeff et al., 2010) (Figure 1. 3 Figure 1. 3), which was possibly caused by lithospheric delamination and asthenospheric upwelling (Pratt et al., 2017).

The focal mechanisms of earthquakes in the Ankaratra and Alaotra regions are mainly normal faulting (Fig. 4), similar to previous studies (Fig. 7; Shudofsky, 1985, Grimison and Chen, 1988; Foster and Jackson, 1998). However, the focal mechanisms shown in Figure 4. 9, as well as others reported by Rindraharisaona et al. (2013), have a wider variation in nodal plane orientations than our focal mechanisms (Figure 1. 5). Thus, while a regional extensional stress regime is supported by the ensemble of focal mechanisms from central Madagascar, the orientation of the stress field may vary locally, possibly reflecting the orientation of pre-existing faults or local perturbations of the stress field by magmatic intrusions (Albaric et al., 2014).

Northern Madagascar has been the site of some of the largest instrumentally-recorded earthquakes (m_b 5.4 on 30 June 1974 and m_b 5.0 on 29 January 1992; Bertil and Regnoult, 1998). We recorded seismic activity near the Sandrakota and Antsaba shear zones and the Andaparaty thrust zone Figure 4. 9). No previous focal mechanisms have been reported for this part of Madagascar; the two focal mechanisms that we determined show a combination of normal and strike-slip motion.

The seismicity distribution in southern Madagascar (Figure 4. 1) resembles earlier work Figure 1. 4). Seismicity occurs mainly within proximity of the Vohibory, Ampanihy, Bekily, Betroka, and Tranomaro shear zones. Focal mechanisms in Figure 4. 9 show a complicated pattern of faulting across southern Madagascar, as do focal mechanisms in Figure 1. 5. Most of the focal mechanism show normal faulting, with a range of nodal plane orientations. However, some strike-slip and reverse faulting mechanism are present in both data sets. Consequently, while it appears that the southern part of the island experiences a regional extensional stress field, there are perturbations that result, at least locally, in compressional stresses. The geodetic strain rate model recently published by Stamps et al. (2018) recognizes a minor amount of compression in the northern and south-central regions of Madagascar; as well as the accumulations of some transtensional and transpressional strain.

5.2 Seismotectonic synthesis

In our effort to understand the main drivers of seismicity in Madagascar, we consider three main observations. This study, in accord with previous work, has found that normal and oblique slip fault mechanisms predominate throughout the island, although the azimuths of the nodal planes vary considerably. Secondly, seismic activity is low in the western sedimentary basins and is greatest in regions where the elevation exceeds 1 km (see inset in Figure 4. 1). Lastly, volcanic activity has occurred during the Cenozoic. While sub-volcanic intrusions most likely contribute to the seismicity in Madagascar, particularly in the Alaotra region (Rechenmann, 1981), we argue that the extensional stresses from the high topography within the uplifted regions of the island are responsible for much of the seismic activity. Other possible sources for the seismicity include volcanic loading and density variations within the crust (van Wyk de Vries and Merle, 1998; Oliva et al., 2019).

The idea that topography and the density variations within the lithosphere affect the stress regime and induce seismicity is not new (*e.g*. Artyushkov, 1973; Mareschal and Kuang, 1986; Fleitout and Froidevax, 1992). Stamps et al. (2010, 2014) calculated the deviatoric stress field for Africa and found that the deviatoric stresses are tensional in

regions with higher elevation and Craig et al. (2011) suggest that elevated topography may play a significant role in deformation and seismicity associated with the East African Rift System. We suggest that buoyancy forces produced by lithospheric delamination and subsequent asthenospheric upwelling beneath Madagascar (Rindraharisaona et al., 2013; Pratt et al., 2017) play a significant role by causing uplift, producing tensional stresses and reactivating old faults.

The plate kinematic model for eastern Africa showing the northern boundary of the Lwandle plate extending W-E across the center of Madagascar predicts W-E strike-slip motion within central Madagascar (Saria et al., 2013, 2014). However, the seismicity pattern and the ensemble of focal mechanisms (Figure 1. 5 and Figure 4. 9) are not consistent with that model. There is no clear W-E pattern of seismicity on the island anywhere; and while a few of the earthquakes show strike-slip motion, most of the events show normal faulting. In addition, for most of those events, the nodal plans are oriented approximately N-S, orthogonal to the orientation of the proposed plate boundary. Instead, our results are more in keeping with the more recent re-evaluation the GPS data by Stamps et al. (2014), who describe the geometry of the Lwandle plate boundary as 'poorly understood'.

5.3 Recurrence of felt earthquakes

If the 23-month period of the MACOMO deployment is representative of typical seismicity levels, the frequency-magnitude distribution suggests that the island of Madagascar should expect, on average, about 180 earthquakes per year with $M_L \geq 3$, about 12 earthquakes per year with $M_L \geq 4$, and one $M_L \geq 5$ earthquakes every one or two years. Extrapolating this distribution would predict one $M_L \geq 6$ earthquake about every 18 years. However, no event of this magnitude is reported in any instrumental or historical catalog, suggesting that the Gutenberg-Richter relationship is truncated, although the present dataset does not allow us to estimate reliably the size of the maximum credible earthquake.

For Madagascar earthquakes during 1979 - 1994, Bertil and Regnoult (1998) found a frequency-magnitude distribution of

$$\log 10(N) = 9.23 - (1.65 \pm 0.10) M_d \quad \text{(Equation 9)}$$

where

$$M_d = 2.04 \log \tau + 0.0004 \Delta - 0.74 + (1.75 * 10^{-7}) \tau^2 \quad \text{(Equation 10)}$$

and M_d is the duration magnitude, Δ is the distance in kilometers, and τ is the duration of the signal in seconds. We believe that the Bertil and Regnoult (1998) value of 1.65 in Equation 8, based upon earthquakes of $M_d \geq 4$, is inappropriately high and biased by the squared term for the duration in Equation 9, which serves to drive down the magnitudes of large events. For example, Equation 7 would predict 427 earthquakes of $M_d \geq 4$ (28 per year), even though their own study detected only 336 earthquakes of $M_L \geq 2.9$ during in their 16-year-long catalog (1979-1994). The fact that the Bertil and Regnoult (1998) *b*-value of 1.65 is too high is more obvious when looking at Madagascar earthquakes of $M_d \geq 3$, where Equation 8 would predict more than 19,000 earthquakes (1190 per year), when, in fact, Bertil and Regnoult (1998) only found 1667 events with $M_d \geq 3$ (104 per year). Their observation of 104 earthquakes per year of $M_d \geq 3$ is similar to this study (117 earthquakes per year of $M_L \geq 3$), although their associated *b*-value is not. However, given that their detection of earthquakes to the north and south of the central regions of Madagascar (where the short-period network is located) is diminished due to a lack of station coverage, their M_d scale is likely offset compared to the M_L scale presented here, with their $M_d = 3$ value corresponding to $M_L > 3$.

Rindraharisaona et al. (2013) located 1221 earthquakes of magnitude ≥ 3 during a 22-year period (1990-2011), which amounts to an average of 56 $M_L \geq 3$ earthquakes per year. Given that their study likely missed at least some M3 earthquakes in the northern or southern regions of the island due to lack of station coverage, their M3 magnitude is probably very similar to a $M_L = 3$ magnitude in the central region of Madagascar in this study.

6. CONCLUSIONS

An analysis of the seismicity and seismotectonics of Madagascar has been carried out using seismic data recorded in a 23-month period during 2011-2013 by both temporary and permanent broadband seismic stations spread fairly evenly across the

island. Hypocenters were determined for 695 earthquakes using P- and S-waves arrival times, and double-difference relocations were obtained for 422 of these events. A new earthquake magnitude scale was determined, the recurrence period of felt earthquakes was estimated, and focal mechanisms were determined for 23 events. A catalog of the events is provided in the supplemental material. The Gutenberg-Richter frequency magnitude distribution has a *b*-value of ~1.2, and suggests that events exceeding M_L5 occur, on average, every 1.4 years. However, there are no instrumental or historical reports of earthquakes exceeding M_L6, suggesting that the maximum credible earthquake may be of this order.

Seismicity occurred mainly in clusters parallel to the extensional tectonic features within the central regions of the island, near the centers of Cenozoic volcanism. However, appreciable amounts of seismicity also occurred in the northern and southern parts of Madagascar, showing geographic clustering that aligns with existing tectonic features. Focal mechanisms indicate predominantly normal faulting throughout Madagascar, and provide little evidence for the postulated W-E boundary between the Somalian plate and Lwandle microplate boundary in the middle of the island.

Some seismicity is likely being related to sub-volcanic intrusion, especially in the center of the island. However, the concentration of seismicity in high-elevation regions compared to the low western basin region supports the hypothesis that topographically-generated extensional stresses are an important cause of seismic activity in Madagascar, as they are thought to be in the East African Rift System (Craig et al., 2011). The topographic uplift may be related to lithospheric delamination and asthenospheric upwelling (Rindraharisaona et al., 2013; Pratt et al., 2017).

ACKNOWLEDGEMENTS

We gratefully acknowledge the field support from IRIS-PASSCAL, which provided the seismic equipment for the MACOMO project (FDSN code: XV, doi:10.7914/SN/XV_2011)*; SELASOMA project (*FDSN code: ZE, *doi:10.14470/MR7567431421), IRIS (*FDSN code: II, *doi:10.7914/SN/II), ,CEA/DASE (FDSN code: RD, doi.org/10.15778/RESIF.RD) GEOFON (*FDSN code: GE, *doi:10.14470/TR560404), and GEOSCOPE (*FDSN code: G,

doi:10.18715/GEOSCOPE.G) for additional seismic data. Figures in this paper have been produced with GMT (Wessel and Smith, 1998). This study was funded by NSF awards EAR-0838426 and 0838387, and supported by the AfricaArray program. R. Durrheim acknowledges the support of the National Research Foundation through the South African Research Chairs Initiative. We also acknowledge two anonymous reviewers and Cynthia Ebinger and Derek Keir for providing insightful reviews that helped to improve the paper.

REFERENCES

Albaric, J., Perrot, J., Deverchere, J., Jakovlev, A. & Deschamps, A., 2014. Deep crustal earthquakes in North Tanzania, East Africa: Interplay between tectonic and magmatic processes in an incipient rift. *Geochem., Geophys., Geosys*., **15**, 374-394.

Andriampenomanana, F., 2017. *The structure of the crust, the uppermost mantle, and the mantle transition zone beneath Madagascar*. PhD thesis, University of the Witwatersrand Johannesburg.

Andriampenomanana, F., Nyblade, A.A., Wysession, M.E., Durrheim, R.J., Tilmann, F., Julià, J, Pratt, M.J, Rambolamanana, G., Aleqabi, G.I., Shore, P.J. & Rakotondraibe, T., 2017. The structure of the crust and uppermost mantle beneath Madagascar, *Geophys. J. Int*., **210(3)**, 1525-1544.

Andriampenomanana, F., Nyblade, A.A., Wysession, M.E., Durrheim, R.J., Tilmann, F., Julià, J, Pratt, M.J, Rambolamanana, G., Aleqabi, G.I., Shore, P.J. & Rakotondraibe, T., submitted, Seismic velocity and anisotropy of the uppermost mantle of Madagascar from Pn Tomography. *Geophys. J. Int.*

Artyushkov, E.V., 1973. Stresses in the lithosphere caused by crustal thickness inhomogeneities. *J. Geophys. Res.*, **78(32)**, 7675-7708.

Bardintzeff, J.M., Liégeois, J.P., Bonin, B., Bellon, H. & Rasamimanana, G., 2010. Madagascar volcanic provinces linked to the Gondwana break-up: Geochemical and isotopic evidences for contrasting mantle sources. *Gondwana Res.*, **18**, 295-314.

Bertil, D. & Regnoult, J.M., 1998. Seismotectonics of Madagascar. *Tectonophysics*, **294,** 57-74.

BRTT (Boulder Real Time Technology), 2004. Evolution of the Commercial ANTELOPE Software, Open file Report, available at: http://www.brtt.com/docs/evolution.pdf (last access: 22 April 2013).

Buchwaldt, R., 2006. *The geology of the Neoproterozoic and Cenozoic rocks of North Madagascar,* Ph.D. Dissertation, Washington University, St. Louis, MO, USA.

Calais, E., Ebinger, C., Hartnady C. & Nocquet, J.M., 2006. Kinematics of the East African Rift from GPS and earthquake slip vector data. *Spec. Pap. Geol. Soc. London,* **259**, 9-22.

Chu, D. & Gordon, R.G., 1999. Evidence for motion between Nubia and Somalia along the Southwest Indian ridge. *Nature*, **398**, 64-67.

Coffin, M.F. & Rabinowitz, P.D., 1987. Reconstruction of Madagascar and Africa: evidence from the Davie fracture zone and western Somali basin. *J. Geophys. Res. Solid Earth*, **92(B9)**, 9385-9406.

Coffin, M.F. & Rabinowitz, P.D., 1988. Evolution of the conjugate East African-Madagascan margins and the western Somali Basin. *Geol. Soc. Am., Spec. Pap*., **226**, 1-79.

Collins, A.S., 2000. The tectonic evolution of Madagascar: its place in the East African Orogen. *Gondwana Res*., **3,** 549 – 552.

Collins, A.S., 2006. Madagascar and the amalgamation of Central Gondwana, *Gondwana Res*., **9,** 3-16.

Collins, A.S., Fitzsimons, I.C.W., Hulscher, B. & Razakamanana, T., 2003. Structure of the eastern margin of the East African Orogen in Central Madagascar. *Precambrian Res.*, **123**, 111-133.

De Wit, M.J., Bowring, S.A., Ashwal, L.D., Randrianasolo, L.G., Morel, V.P. & Rambeloson, R.A., 2001. Age and tectonic evolution of Neoproterozoic ductile shear zones in southwestern Madagascar, with implications for Gondwana studies. *Tectonics*, **20**, 1-45.

Ebinger, C.J., Sarah, J.O., Thi-Quan, P., Katherine, P., Patrick, C., Finnigan, I., Donna, J.S., Natalie, J. A., Ryan, G., Andrew, N. & Gabriel, M., 2019. Kinematics of active deformation in the Malawi and Rungwe Volcanic Province, Africa. *Geochem. Geophys. Geosys*. **20(8)**, 3928-3951.

Fleitout, L. & Froidevaux, C., 1982. Tectonics and topography for a lithosphere containing density heterogeneities. *Tectonics*, **1(1)**, 21-56.

Foster, A.N. & Jackson, J.A., 1998. Source parameters of large African earthquakes: implications for crustal rheology and regional kinematics. *Geophys. J. Int*., **134**, 422-448.

Fourno, J.P. & Roussel, J., 1993. Topographie du Moho sous les hautes terres de Madagascar déduite de l'inversion de données gravimétriques. *C. R. Acad. Sci.*, **316,** 69-75.

Frohlich, C. & Davis, S.D., 1999. How well constrained are well constrained T, B, and P axes in moment tensor catalogs? *J. Geophys. Res.*, **104(B3)**, 4901-4910.

Geiger, L., 1912. Probability method for the determination of earthquake epicenters from the arrival time only (translation). *Bull. St. Louis. Univ.*, **8,** 56-71.

Geiger, M., Clark, D.N. & Mette, W., 2004. Reappraisal of the timing of the breakup of Gondwana based on sedimentological and seismic evidence from the Morondava Basin, Madagascar. *J. Afr. Earth Sci.*, **38(4)**, 363-381.

Gnos, E., Immenhauser, A. & Peters, T.J., 1997. Late Cretaceous/early Tertiary convergence between the Indian and Arabian plates recorded in ophiolites and related sediments. *Tectonophysics*, **271**, 1-19.

Grimison, N.L. & Chen, W.P., 1988. Earthquakes in the Davie Ridge-Madagascar region and the southern Nubian-Somalian plate boundary. *J. Geophys. Res.*, **93,** 10439-10450.

Gutenberg, B. & Richter, C.F., 1949. Seismicity of the Earth and associated phenomena, *Princeton Univ. Press*.

Handke, M.J., Tucker, R.D. & Ashwal, L.D., 1999. Neoproterozoic continental arc magmatism in west-central Madagascar. *Geology*, **27**, 351-354.

Havskov, J. & Ottemöller, L., 2010. Magnitude. In *Routine Data Processing in Earthquake Seismology*, *Springer*., 151-191.

Horner-Johnson, B.C., Gordon, R.G. & Argus, D.F., 2007. Plate kinematic evidence for the existence of a distinct plate between the Nubian and Somalian plates along the Southwest Indian Ridge. *J. Geophys. Res.*, **112,** B05418**,** DOI: 10.1029/2006JB004519.

Hutton, L.K. & Boore, D.M., 1987. The ML scale in southern California. *Bull. Seismol. Soc. Am.*, **77**, 2074-2094.

Hyndman, R.D., 1979. Poisson's ratio in the oceanic crust - a review. In *Developments in Geotectonics*, *Elsevier*, 15, 321-333.

International Seismological Centre, On-line Bulletin, http://www.isc.ac.uk, *Internatl. Seismol. Cent*., Thatcham, United Kingdom, 20XX, http://doi.org/10.31905/D808B830

Kanamori, H. & Jennings, P.C., 1978. Determination of local magnitude, M_L, from strong-motion accelerograms. *Bull. Seism. Soc. Am*., **68**, 471-485.

Kijko, A. & Sellevoll, M.A., 1992. Estimation of earthquake hazard parameters from incomplete data files. Part II. Incorporation of magnitude heterogeneity. *Bull. Seismol. Soc. Am.*, **82(1)**, 120-134.

Kröner, A., Windley, B.F., Jaeckelt, P., Brewer, T.S. & Razakamanana, T., 1999. New zircon ages and regional significance for the evolution of the Pan-African Orogen in Madagascar. *J. Geol. Soc.*, **156**, 1125-1135.

Kvarven, T., Mjelde, R., Hjelsten, B.O., Faleide, J.I., Thybo, H., Flueh, E.R. & Murai, Y., 2016. Crustal composition of Møre Margin and compilation of conjuguate Atlantic margin transect. *Tectonophysics*, 666, 144-157.

Lahr, J.C., 1999 (revised 2012). HYPOELLIPSE: A computer program for determining local earthquake hypocentral parameters, magnitude, and first-motion pattern, U.S. Geological Survey Open-File Report 99-23, version 1.1, 119m and software, available at http://pubs.usgs.gov/of/1999/ofr-99-0023/.

Mareschal, J.C. & Kuang, J., 1986. Intraplate stresses and seismicity: the role of topography and density heterogeneities. *Tectonophysics*, **132(1-3)**, 153-162.

Oliva, S.J., Ebinger, C.J., Wauthier, C., Muirhead, J.D., Roecker, S.W., Rivalta, E. & Heimann, S., 2019. Insights into fault-magma interactions in an early-stage continental rift from source mechanisms and correlated volcano-tectonic earthquakes. *Geophys. Res. Lett.*, **46(4)**, 2065-2074.

Paquette, J.L. & Nédélec, A., 1998. A new insight into Pan-African tectonics in the East-West Gondwana collision zone by U-Pb zircon dating of granites from central Madagascar. *Earth Planet. Sci. Lett.*, **155,** 45-56.

Paquette, J.L., Moine, B. & Rakotondrazafy, M.A., 2003. ID-TIMS using the stepwise dissolution technique versus ion microprobe U – Pb dating of metamict Archean zircons from NE Madagascar. *Precambrian Res.,* **121,** 73-84.

Phethean, J.J., Kalnins, L.M., van Hunen, J., Biffi, P.G., Davies, R.J. & McCaffrey, K.J., 2016. Madagascar's escape from Africa: a high-resolution plate reconstruction for the Western Somali Basin and implications for supercontinent dispersal. *Geochemistry, Geophysics, Geosystems*, **17(12)**, 5036-5055.

Pratt, M.J., Wysession, M.E., Aleqabi, G., Wiens, D.A., Nyblade, A.A., Shore, P., Rambolamanana, G., Andriampenomanana, F., Rakotondraibe, T., Tucker, R.D. & Barruol, G., 2017. Shear velocity structure of the crust and upper mantle of Madagascar derived from surface wave tomography. *Earth Planet. Sci*., **458**, 405-417.

Rabinowitz, P. D., Coffin, M.F. & Falvey, D., 1983. The separation of Madagascar and Africa. *Science,* **220,** 67-69.

Rakotondrainibe, 1977. *Contribution à l' étude de la séismicité de Madagascar*, PhD Thesis, Univ. Antananarivo, Madagascar.

Ramirez, C., Nyblade, A., Wysession, M.E., Pratt, M., Andriampenomanana, F. & Rakotondraibe, T., 2018. Complex seismic anisotropy in Madagascar revealed by shear wave splitting measurements. *Geophys. J. Int.*, **215(3)**, 1718-1727.

Rechenmann, J., 1981. *Gravimètrie de Madagascar: interpretations et relations avec la géologie*. Thèse, Université Paris Sud, 175.

Reeves, C., 2014. The position of Madagascar within Gondwana and its movements during Gondwana dispersal. *J. Afr. Earth Sci*., **94**, 45-57.

Reiss, M.C., Rümpker, G., Tilmann, F., Yuan, X., Giese, J. & Rindraharisaona, E.J., 2016. Seismic anisotropy of the lithosphere and asthenosphere beneath southern Madagascar from teleseismic shear wave splitting analysis and waveform modeling. *J. Geophys. Res. Solid Earth*, **121(9)**, 6627-6643.

Richter, C.F., 1935. An instrumental earthquake magnitude scale. *Bull. Seism. Soc. Am*., **25,** 1-32.

Richter, C.F., 1958. *Elementary Seismology*. Freeman, San Francisco, Calif., 578 pp.

Rindraharisaona, E.J., Guidarelli, M., Aoudia, A. & Rambolamanana, G., 2013. Earth structure and instrumental seismicity of Madagascar: Implications on the seismotectonics. *Tectonophysics*, **594**, 165-181.

Rindraharisaona, E.J., Tilmann, f., Yuan, X., Rümpker, G., Giese,J., Rambolamanana, G. & Barruol, G., 2017. Crustal structure of southern Madagascar from receiver functions and ambient noise correlation: Implications for crustal evolution. *J. Geophys. Res. Solid Earth*, **122(2)**, 1179-1197.

Saria, E., Calais, E., Altamimi, Z., Willis, P. & Farah, H., 2013. A new velocity field for Africa from combined GPS and DORIS space geodetic solutions: Contribution to the definition of the African reference frame (AFREF). *J. Geophys. Res. Solid Earth*, **118**, 1677-1697.

Saria, E., Calais, E., Stamps, D.S., Delvaux, D. & Hartnady, C.J.H., 2014. Present-day kinematics of the East African Rift. *J. Geophys. Res. Solid Earth*, **119,** 3584-3600.

Shudofsky, G.N., 1985. Source mechanisms and focal depths of East African earthquakes using Rayleigh-wave inversion and body-wave modeling. *Geophys. J. Int.*, **83(3)**, 563-614.

Sigloch, K. & Barruol, G., 2013. Investigating La Réunion hot spot from crust to core. *Eos., Trans. AGU*, **94**, 205-207.

Segoufin, J. & Patriat, P., 1980. Existence d'anomalies mésozoïques dans le bassin de Somalie. Implications pour les relations Afrique-Antarctique-Madagascar. *CR Acad. Sci. Paris*, **291(B)**, 85-88.

Snoke, A., 2003. Focal mechanism determination software (FOCMEC package). http://ds.iris.edu/pub/programs/focmec/

Stamps, D.S., Calais, E., Saria, E., Hartnady, C., Nocquet, J.M., Ebinger, C. J. & Fernandes, R.M., 2008. A kinematic model for the East African Rift. *Geophy. Res. Lett.*, **35(5)**, DOI: 10.1029/2007GL032781.

Stamps, D.S, Flesch, L.M., Calais, E, 2010. Lithospheric buoyancy forces in Africa from a thin sheet approach. *Int. J. Earth. Sci*., **99**, 1525-1533.

Stamps, D.S, Flesch, L.M., Calais, E. & Ghosh, A., 2014. Current kinematics and dynamics of Africa and the East African Rift System. *J. Geophys. Res. Solid Earth*, **119**, 5161-5186.

Stamps, D.S., Saria, E. & Kreemer, 2018. A Geodetic Strain Rate model for East African Rift System. *Scientific Reports*, **8(1)**, 732.

Stein, S. & Wysession, M., 2003. *An Introduction to Seismology, Earthquakes, and Earth Structure*. Blackwell, 497 pp.

Storey, M., Mahoney, J.J., Saunders, A.D., Duncan, R.A., Kelley, S.P. & Coffin, M.F., 1995. Timing of hot spot-related volcanism and the breakup of Madagascar and India. *Science*, **267**, 852-855.

Thomas, R.J., De Waele, B., Schofield, D.I., Goodenough, K.M., Horstwood, M., Tucker, R., Bauer, W., Annells, R., Howard, K., Walsh, G. & Rabarimanana, M., 2009. Geological evolution of the Neoproterozoic Bemarivo Belt, northern Madagascar. *Precambr. Res.*, **172,** 279–300.

Tilmann, F., Yuan, X., Rümpker, G. & Rindraharisaona, E., 2012. *SELASOMA Project, Madagascar 2012-2014*, DeutschesGeoForschungsZentrum GFZ, Seismic Network, 829 doi:10.14470/MR7567431421

Torsvik, T. H., Tucker, R.D., Ashwal, L.D., Eide, E.A., Rakotosolofo, N.A. & De Wit, M.J., 1998. Late Cretaceous magmatism in Madagascar: paleomagnetic evidence for a stationary Marion hotspot. *Earth Planet. Sci. Lett.*, **164,** 221-232.

Tucker, R.D., Ashwal, L.D., Hamilton, M.A., Torsvik, T.H. & Carter, L.M., 1999. Neoproterozoic silicic magmatism of northern Madagascar, Seychelles, and NW India: clues to Rodinia's assembly and dispersal. *Geol. Soc. Am. (Abstr)*, **31,** 317.

Tucker, R.D., Kusky, T., Buchwaldt, R. & Handke, M.J., 2007. Neoproterozoic nappes and superposed folding of the Itremo Group, west-central Madagascar. *Gondwana Res.*, **12(4),** 356-379.

Tucker, R.D. & Conrad, J., 2008. 40Ar/39Ar geochronology of Mesozoic and younger igneous rocks of central and northern Madagascar, in Final Report of the BGS-USGS Consortium to the Government of Madagascar, World Bank Project UK-04-0100, Chapter 7.

Tucker, R.D., Peters, S.G., Roig, J.Y., Theveniaut, H. & Delor, C., 2012. *Notice explicative des cartes géologiques et metallogeniques de la République de Madagascar a 1/1.000.000*. Ministère des Mines, PGRM, Antananarivo, République de Madagascar.

Van Wyk de Vries, B. & Merle, O., 1998. Extension induced by volcanic loading in regional strike-slip zones. *Geology*, **26**(11), 983-986.

Waldhauser, F. 2001. hypoDD--A program to compute double-difference hypocenter locations (hypoDD version 1.0). *US Geol. Surv. Open File Rep.,* **01**, 113.

Woessner, J. & Wiemer, S., 2005. Assessing the quality of earthquake catalogues: estimating the magnitude of completeness and its uncertainty. *Bull. Seismol. Soc. Am.*, **95**, 684–698

Wessel, P. & Smith, W.H., 1998. New, improved version of Generic Mapping Tools released. *Eos., Trans. AGU,* **79**, 579-579.

Wiemer, S. & Wyss, M., 2000. Minimum magnitude of completeness in earthquake catalogs: Examples from Alaska, the western United States, and Japan. *Bull. Seismol. Soc. Am.*, **90(4)**, 859-869.

Wysession, M., Wiens, D. & Nyblade, A., 2012. Investigation of sources of intraplate volcanism using PASSCAL broadband instruments in Madagascar, the Comores, and Mozambique. *In AGU Fall Meeting Abstracts.* Doi:10.7914/SN/XV 2011.

Appendix B: Example of input files for HYPOELLIPSE and HYPODD

1. An example of arrival time from Antelope, input files for HYPOELLIPSE. The first column are station name and the phase name (Impulsive –wave phase), the second column is the P-wave arrival time (Year, month, day, hour, minutes, second, milliseconds.), and the last column is the S-wave arrival picks in sec) following the name of the phase. Some of the station don't have S-arrivals if it is difficult to identify them.

```
AMPYIP.0 130125233726.40  45.14ES
ANLAIP.0 130125233856.11
ANTSIP.0 130125233916.32  118.48ES
BAELIP.0 130125233924.99  73.18ES
BANDIP.0 130125233756.62  95.68ES
BANJIP.0 130125234131.84  89.76ES
BARYIP.0 130125233843.57  116.20ES
BATGIP.0 130125233818.354. 7
BERGIP.0 130125233906.32
BITYIP.0 130125233811.73
BKTAIP.0 130125233732.87
CPSMIP.0 130125233738.58  66.85ES
DGOSIP.0 130125234319.80
KIRIIP.0 130125233757.22  95.03ES
LAHAIP.0 130125233932.61
LONAIP.0 130125233719.47
MS04IP.0 130125233716.11
MS07IP.0 130125233724.30  51.10ES
MS10IP.0 130125233733.83
MS12IP.0 130125233738.73  66.95ES
MS16IP.0 130125233749.14
MS19IP.0 130125233759.65
MS23IP.0 130125233807.04  56.93ES
SBVAIP.0 130125233952.63  83.82ES
VINAIP.0 130125233822.80  81.79ES
VOIAIP.0 130125233752.14  88.80ES
ZAKAIP.0 130125233845.86  62.18ES
ZOBEIP.0 130125233834.35
```

2. Example of Input files for HYPODD

```
# 2013 01 19 14 40 39.031 -17.9238 48.4323 10.0000 1.81
0.12465 0.0000 3.4443 7933
ZAKA          2.300   1.000   P
ABPO          28.58   1.000   P
BATG          35.77   1.161   P
ZOBE          21.03   1.000   P
BAND          56.873  1.000   P
```

Appendix C: Earthquake location and relocation lists

1. The 695 earthquake distribution from MACOMO station between 2011 and 2013 where “a” to “d” represent lowest to largest uncertainties

ID_NEW	y/m/d	h/mn/sec	latitude(deg)	longitude(deg)	depth(km)	rms error	mag	Quality
1	2011-10-13	03:26:36.62	-15.4637	48.0983	15.00	0.2340	1.2	b
2	2011-10-16	01:23:53.61	-22.0397	46.1308	14.93	0.4189	2.4	b
3	2011-10-21	08:20:04.32	-23.1010	47.9372	5.00	0.8245	1.1	b
4	2011-10-24	22:25:43.91	-14.4633	49.7155	17.03	1.6521	1.1	d
5	2011-10-27	00:33:50.17	-18.0050	49.3392	26.98	4.1438	2.4	d
6	2011-10-28	11:16:09.13	-23.3550	46.0797	41.52	0.7487	1.0	d
7	2011-11-01	22:43:18.73	-18.3468	48.2082	30.18	0.3269	1.2	d
8	2011-11-07	08:20:36.57	-16.3652	48.2180	15.00	1.4477	2.6	d
9	2011-11-07	05:33:38.65	-19.1823	49.6712	15.00	0.9359	2.7	c
10	2011-11-13	11:26:31.89	-17.4582	48.5358	9.07	0.0012	2.0	c
11	2011-11-13	10:54:57.21	-16.3743	46.8263	32.09	1.8647	2.5	c
12	2011-11-14	15:14:14.15	-19.7048	46.5660	4.00	0.7703	1.3	c
13	2011-11-15	02:38:59.13	-19.6187	47.1232	29.47	0.3650	1.1	c
14	2011-11-18	12:57:48.25	-24.3400	47.1840	6.16	0.7771	3.2	d
15	2011-11-21	06:43:16.96	-18.1130	47.7225	37.13	0.4566	1.3	d
16	2011-11-21	23:24:57.00	-18.0082	49.0370	10.45	0.0439	3.0	d
17	2011-11-22	07:44:00.35	-18.5245	48.7480	34.64	0.6772	3.1	c
18	2011-11-24	00:04:28.71	-19.2943	46.2470	15.82	0.9160	2.0	d
19	2011-11-24	13:33:45.37	-16.8635	49.0270	18.40	0.2063	3.0	c
20	2011-11-25	06:35:03.76	-17.9538	48.4528	6.83	0.2786	1.1	d
21	2011-11-26	12:50:50.72	-18.0425	48.7917	28.43	0.9984	3.1	d
22	2011-11-27	03:00:39.61	-19.4803	46.5800	36.36	0.7140	2.6	b
23	2011-12-08	23:16:44.06	-16.8565	47.8270	15.00	0.7647	3.2	b
24	2011-12-11	10:32:58.85	-18.2210	47.7505	61.67	1.2305	2.7	c
25	2011-12-26	07:16:25.41	-17.4448	48.4038	6.00	0.4151	2.9	d
26	2011-12-30	06:31:08.23	-17.5608	48.6432	32.57	0.6327	2.7	c
27	2011-12-31	20:57:56.29	-17.9555	48.6205	11.71	0.6196	2.3	c
28	2011-12-31	05:06:26.63	-14.9077	49.5323	24.95	0.4921	3.1	b
29	2012-01-02	04:27:36.61	-16.6012	50.0945	6.14	0.5710	2.5	b
30	2012-01-27	01:24:15.69	-14.9293	49.6753	30.92	0.0544	1.5	b
31	2012-01-24	20:59:25.78	-15.6437	49.9962	3.00	1.1973	1.2	b
32	2012-01-28	14:16:00.24	-17.2950	48.4535	0.06	0.3837	3.2	b
33	2012-02-01	22:16:56.83	-16.7442	48.5203	26.78	0.4232	1.2	b
34	2012-02-06	14:57:04.93	-14.6420	49.3707	31.75	0.4720	2.5	d
35	2012-02-06	04:00:28.54	-18.6077	46.2383	2.00	0.8211	3.5	d
36	2012-02-07	00:49:19.26	-24.3750	47.0135	1.00	0.3806	2.1	d
37	2012-02-12	19:34:40.51	-17.6742	48.6747	8.00	0.2740	1.0	d
38	2012-02-12	15:49:54.65	-17.2880	48.5120	22.72	0.4481	2.2	d
39	2012-02-24	22:09:53.44	-18.6425	49.6408	15.00	1.1207	2.3	c
40	2012-02-26	08:23:50.38	-19.0137	47.1823	51.27	0.0004	3.3	c
41	2012-03-05	00:39:20.60	-18.2505	46.5288	24.14	0.4934	1.2	c
42	2012-03-15	00:54:09.36	-14.3115	49.1133	13.71	0.6973	1.2	c
43	2012-03-16	11:56:55.51	-17.5278	48.2978	10.12	1.0150	3.5	c
44	2012-03-20	23:37:18.68	-19.2348	47.5302	25.47	0.4995	2.1	d
45	2012-03-22	00:09:55.00	-18.3035	48.5247	29.92	0.5307	3.6	d
46	2012-03-27	09:33:30.22	-16.1063	48.2082	39.86	0.9940	2.5	d

47	2012-04-05	01:52:35.77	-19.9078	47.0278	32.21	0.3874	2.6	c
48	2012-03-30	08:26:26.80	-18.4325	47.9020	6.00	1.3419	1.2	d
49	2012-04-10	15:43:00.20	-17.4683	47.9895	2.00	1.4461	3.6	c
50	2012-04-23	21:13:15.11	-16.9242	45.5990	15.00	1.2841	2.6	d
51	2012-04-21	19:24:42.95	-15.8975	48.4245	5.08	0.3098	1.5	d
52	2012-05-02	07:46:24.76	-21.0325	45.8970	26.10	0.9857	1.4	b
53	2012-04-29	20:31:12.85	-18.7682	47.6103	25.50	0.1390	1.0	b
54	2012-05-12	02:12:52.71	-16.9065	45.6670	15.00	1.0374	4.1	c
55	2012-05-21	08:20:40.13	-16.7033	50.1650	34.91	0.9210	2.9	d
56	2012-05-14	11:57:50.82	-14.9797	49.3535	31.69	0.3571	1.5	c
57	2012-05-31	16:41:58.58	-19.8913	47.3218	16.35	0.9700	4.2	c
58	2012-05-29	13:50:36.97	-13.9112	49.4832	34.59	0.9760	4.0	b
59	2012-06-17	16:48:13.55	-17.5630	52.6382	6.00	1.4002	1.5	b
60	2012-06-06	22:12:02.38	-23.7402	44.9058	20.22	0.8196	2.8	b
61	2012-06-19	11:25:01.07	-21.4828	45.3802	15.00	0.0003	3.0	c
62	2012-06-17	10:11:35.55	-16.5220	49.2278	16.94	0.6755	3.7	c
63	2012-06-23	11:18:26.28	-20.0395	46.5100	16.21	0.7246	4.2	c
64	2012-06-25	10:56:08.83	-17.4405	48.6610	27.44	0.5795	2.0	c
65	2012-06-26	01:34:43.31	-17.7823	49.2712	43.34	1.3605	1.1	c
66	2012-06-26	00:10:49.86	-21.3883	45.8377	9.72	0.4631	3.2	d
67	2012-07-01	04:43:57.41	-20.2268	46.9322	20.51	1.8805	2.7	d
68	2012-07-04	15:28:04.73	-16.0122	46.0875	59.17	1.5077	3.5	d
69	2012-07-10	13:34:27.76	-17.3165	49.0087	39.46	0.0554	1.5	d
70	2012-07-15	18:17:30.89	-16.1680	48.8905	15.00	1.5798	1.6	d
71	2012-07-15	22:50:57.53	-20.3112	45.5515	1.00	0.5644	3.1	c
72	2012-07-26	04:41:43.38	-17.6900	48.7493	67.86	0.0017	1.5	b
73	2012-07-29	20:36:14.07	-14.5175	49.8643	28.00	1.3729	1.9	b
74	2012-07-30	16:45:51.44	-23.6200	45.0037	15.17	0.4572	3.9	b
75	2012-08-03	18:24:13.05	-15.3605	50.9128	13.50	0.0010	1.7	d
76	2012-08-03	10:34:20.99	-19.0358	48.9510	40.94	1.2529	3.2	d
77	2012-08-05	18:07:10.09	-16.4047	47.5502	0.06	0.1526	3.4	d
78	2012-08-06	02:25:12.11	-18.0513	48.4148	27.80	0.4507	3.0	d
79	2012-08-06	23:54:30.46	-19.1225	47.0698	50.32	0.3985	1.7	d
80	2012-08-08	05:11:14.08	-20.2325	47.2057	20.23	0.2644	1.5	c
81	2012-08-08	08:07:33.28	-17.6565	48.7267	18.84	0.8131	1.5	c
82	2012-08-11	13:57:07.26	-20.1150	46.8208	21.81	0.6055	1.6	c
83	2012-08-11	23:32:12.53	-15.5058	48.0825	29.28	1.2080	3.5	c
84	2012-08-12	17:55:16.52	-17.5490	48.6972	58.02	0.3321	1.4	c
85	2012-08-12	01:09:43.24	-15.3073	47.7853	15.00	0.2035	1.8	b
86	2012-08-16	23:51:06.49	-23.1973	44.9535	0.06	0.5829	2.9	b
87	2012-08-17	10:11:02.18	-17.6542	47.5880	26.88	0.0637	1.6	b
88	2012-08-18	20:07:18.23	-15.3887	48.1832	3.03	1.6955	2.6	d
89	2012-08-18	07:05:33.42	-18.6728	45.7963	15.00	1.2773	4.2	d
90	2012-08-19	21:16:01.13	-18.8327	46.6275	6.00	0.9973	1.6	d
91	2012-08-19	23:50:09.07	-18.0632	47.4720	4.00	1.4088	1.8	d
92	2012-08-21	08:34:46	-19.2203	46.5988	26.26	0.5122	1.3	d
93	2012-08-21	10:07:26.53	-13.7323	48.3992	9.00	0.5566	1.4	c
94	2012-08-21	09:06:22.98	-19.2270	46.6988	3.05	1.5332	1.5	c
95	2012-08-22	23:25:56.75	-24.2510	45.7025	14.43	1.0906	3.2	c
96	2012-08-22	00:35:11.87	-14.2947	48.6165	11.46	1.1010	3.6	c
97	2012-08-23	21:47:11.52	-19.0252	46.7372	1.79	0.7139	1.4	c
98	2012-08-24	01:31:31.46	-17.5585	48.3408	13.09	0.7178	1.7	b
99	2012-08-24	02:35:35.80	-19.0448	46.7627	5.80	0.5739	2.0	b
100	2012-08-24	04:10:38.43	-18.9165	46.8550	52.40	0.8847	2.0	b
101	2012-08-24	04:37:10.77	-19.4863	46.7205	8.37	0.1956	2.2	d
102	2012-08-25	12:24:05.00	-19.3043	46.8440	32.49	1.2376	1.5	d
103	2012-08-25	07:05:25.38	-16.4733	49.8947	11.43	0.5331	1.6	d
104	2012-08-26	02:03:42.01	-19.2472	46.6567	18.80	1.6186	1.4	d
105	2012-08-27	21:46:44.98	-19.0588	46.7577	21.08	0.8409	1.3	d
106	2012-08-28	08:39:35.20	-17.2750	48.0433	5.47	1.2060	3.2	c
107	2012-08-29	18:31:38.09	-19.0000	46.6835	6.00	0.9730	2.7	c
108	2012-08-30	04:34:52.04	-17.4190	48.6088	2.00	1.3733	1.5	c
109	2012-08-30	09:32:12.93	-18.9673	46.7110	8.50	1.6848	3.8	c
110	2012-08-30	07:02:51.96	-17.7543	48.2025	7.80	1.8358	3.8	c

111	2012-08-31	12:50:59.31	-19.4163	46.8748	24.23	1.7650	2.1	b
112	2012-09-01	19:06:41.51	-18.1270	46.5940	17.74	0.6530	2.9	b
113	2012-09-01	18:34:15.64	-19.1023	46.6988	19.26	1.4717	3.0	b
114	2012-09-01	00:07:52.21	-17.8577	48.1337	17.90	1.1015	3.5	d
115	2012-09-01	23:31:12.58	-19.2175	46.7475	26.45	1.4562	3.9	d
116	2012-09-01	10:10:11.04	-23.1927	43.5765	69.18	0.8822	4.0	d
117	2012-09-02	19:41:46.78	-19.3080	46.7703	26.03	1.0951	1.3	d
118	2012-09-02	07:22:42.72	-19.1082	46.7010	18.40	1.0927	1.4	d
119	2012-09-02	20:19:08.92	-19.2650	46.8722	48.59	1.3427	1.5	c
120	2012-09-02	12:20:07.99	-18.9887	46.7143	6.07	0.4226	1.6	c
121	2012-09-03	15:25:29.34	-17.3678	48.0202	16.69	1.2248	1.2	c
122	2012-09-03	01:53:00.59	-20.1503	47.2067	2.18	0.5229	1.3	c
123	2012-09-03	23:27:40.02	-19.8657	46.3642	22.85	0.5865	2.6	c
124	2012-09-03	12:40:30.96	-16.0392	47.8897	17.95	0.9453	3.5	b
125	2012-09-04	18:38:56.73	-20.6447	42.1582	15.00	0.9320	3.7	b
126	2012-09-04	21:31:50.44	-18.9937	46.7018	10.20	1.6438	1.1	
127	2012-09-04	20:34:24.25	-19.3052	46.6928	39.92	1.1523	3.2	b
128	2012-09-05	10:44:52.82	-23.7647	46.1658	12.00	0.5802	1.6	b
129	2012-09-05	04:10:42.82	-18.8747	46.7448	29.95	0.0277	2.4	b
130	2012-09-06	11:52:28.82	-19.1950	46.6868	3.00	0.7887	2.5	d
131	2012-09-04	20:44:25.53	-19.2350	46.7082	11.61	1.0009	1.9	d
132	2012-09-08	20:04:00.35	-18.6850	46.9695	43.41	1.5250	1.7	d
133	2012-09-09	08:07:38.71	-18.7572	45.9618	51.88	0.6031	1.3	d
134	2012-09-09	14:46:28.62	-18.9622	46.6773	10.45	1.3126	2.0	d
135	2012-09-09	12:07:17.96	-18.5537	46.8158	5.12	0.7697	2.1	c
136	2012-09-09	11:12:21.73	-17.8245	48.0197	3.00	0.9639	2.2	c
137	2012-09-10	12:52:57.96	-18.9757	46.7000	8.21	0.5922	1.1	c
138	2012-09-11	01:04:16.22	-13.5690	48.9548	23.12	1.1572	3.0	c
139	2012-09-12	23:56:17.21	-19.1967	47.1602	13.74	0.6767	2.6	c
140	2012-09-13	23:42:35.51	-14.3852	49.4393	21.14	1.3092	2.7	d
141	2012-09-14	13:10:58.74	-23.7670	47.3887	15.00	1.4429	1.1	d
142	2012-09-14	20:12:42.26	-20.7115	47.8217	29.32	1.1876	2.3	d
143	2012-09-15	20:02:00.51	-18.2708	47.6863	5.88	0.8581	1.2	c
144	2012-09-16	20:44:35.64	-14.2875	48.6820	9.00	1.2825	2.2	d
145	2012-09-17	19:25:56.49	-18.2440	47.1132	2.00	0.1676	1.2	c
146	2012-09-17	00:46:49.51	-18.7070	46.9392	3.00	1.1769	3.0	d
147	2012-09-18	22:37:29.02	-24.7385	44.4748	4.38	0.2617	2.0	d
148	2012-09-18	03:32:07.94	-18.6082	47.6038	0.05	1.5568	2.2	b
149	2012-09-18	16:33:39.46	-19.2417	48.4168	12.37	0.9307	2.4	b
150	2012-09-18	14:57:57.37	-20.5693	44.8843	28.12	0.9846	3.1	c
151	2012-09-19	05:17:48.22	-24.4977	45.0817	0.98	0.4079	1.1	d
152	2012-09-20	10:26:06.84	-18.8863	46.7228	57.57	0.3903	1.2	c
153	2012-09-20	15:43:52.09	-14.8055	49.5348	64.12	1.5662	2.2	c
154	2012-09-20	11:13:22.06	-18.9095	46.7172	46.96	1.2515	2.5	b
155	2012-09-21	21:52:17.44	-18.2252	46.3977	58.19	0.8115	1.3	b
156	2012-09-22	06:21:37.14	-20.0595	46.8805	15.99	1.3634	3.9	b
157	2012-09-23	23:37:07.18	-18.4580	47.9577	15.68	0.2216	1.8	b
158	2012-09-23	18:55:12.62	-16.8415	49.2403	26.15	1.3618	2.0	b
159	2012-09-23	20:39:37.17	-18.7867	46.7397	5.68	1.2877	3.7	b
160	2012-09-24	09:12:54.57	-18.9465	46.7433	0.13	0.1383	1.0	d
161	2012-09-25	22:47:05.99	-18.2205	46.3515	20.27	0.2921	1.6	d
162	2012-09-26	14:17:43.58	-19.8423	46.8128	1.96	0.3631	1.4	d
163	2012-09-27	16:41:06.11	-16.2912	45.4200	15.00	0.6533	1.4	d
164	2012-09-27	23:17:37.17	-18.9652	46.7393	27.17	0.8531	3.4	d
165	2012-09-28	12:59:55.65	-18.9738	46.7180	8.05	0.8500	1.3	c
166	2012-09-29	09:55:01.15	-19.2758	47.7063	19.59	0.4669	1.2	c
167	2012-09-29	22:07:53.47	-17.5347	48.2675	11.87	0.7414	2.8	c
168	2012-09-29	16:13:55.53	-19.3782	46.9052	16.06	0.8300	3.5	c
169	2012-09-30	15:38:53.37	-18.9923	46.0483	4.05	0.8417	1.3	c
170	2012-09-30	19:43:27.87	-14.8768	49.5067	12.87	1.6114	2.7	d
171	2012-09-30	08:18:23.72	-16.6878	46.1898	40.62	1.8588	3.1	d
172	2012-09-30	06:08:14.71	-14.9765	49.5405	15.76	1.3055	3.8	d
173	2012-10-01	13:41:56.96	-16.8492	49.1965	3.00	1.9584	1.0	c
174	2012-10-01	19:06:13.63	-17.9698	47.8378	40.37	0.7696	1.3	d

175	2012-10-01	23:47:44.19	-20.9137	46.5893	30.73	0.8983	3.2	c
176	2012-10-02	06:35:30.02	-18.6778	45.5717	15.00	0.8358	1.0	d
177	2012-10-03	22:04:44.31	-20.1572	46.9978	3.00	1.9340	3.3	d
178	2012-10-04	11:15:42.66	-17.6135	48.4692	17.94	1.3361	2.9	b
179	2012-10-05	19:43:00.67	-16.9765	50.4625	15.00	1.3423	2.5	b
180	2012-10-06	22:46:30.75	-15.5488	48.9587	5.85	0.8893	3.6	c
181	2012-10-08	23:21:21.22	-19.4907	46.6693	36.39	1.3185	2.0	d
182	2012-10-08	05:33:48.12	-17.4508	48.5258	24.45	0.7756	3.0	c
183	2012-10-10	05:53:47.83	-18.9603	46.7132	32.00	0.7236	1.0	c
184	2012-10-10	09:21:22.58	-18.7872	46.7582	17.60	0.4126	1.2	b
185	2012-10-10	18:42:50.89	-19.3663	46.7232	22.93	1.6840	2.5	b
186	2012-10-10	04:11:29.01	-18.6092	47.4588	19.95	2.2553	3.4	b
187	2012-10-10	16:27:59.85	-24.4965	45.2723	38.38	0.4029	3.6	b
188	2012-10-11	20:48:59.97	-14.9255	49.7058	7.73	0.5439	1.1	b
189	2012-10-13	09:32:16.15	-14.9040	49.7637	21.50	0.6784	1.1	b
190	2012-10-14	00:52:05.62	-18.4425	46.8060	15.53	0.5518	2.6	d
191	2012-10-15	11:01:10.01	-18.9457	46.7247	0.75	0.1994	1.3	d
192	2012-10-15	18:35:09.05	-18.8912	46.6580	26.84	0.7916	2.3	d
193	2012-10-16	21:02:59.09	-17.0238	47.8402	15.00	0.8569	1.0	d
194	2012-10-16	16:51:47.15	-19.0577	46.7115	0.78	0.6308	1.5	d
195	2012-10-16	22:54:00.48	-18.9408	46.7595	8.31	0.4488	1.6	c
196	2012-10-17	16:24:14.21	-18.2232	46.4210	18.96	1.4828	1.3	c
197	2012-10-17	20:27:35.15	-19.0702	46.6990	24.73	0.0013	1.3	c
198	2012-10-17	00:22:43.76	-18.9037	46.7193	21.00	0.9124	1.8	c
199	2012-10-17	13:47:11.16	-20.1768	46.0138	5.00	1.0091	1.8	c
200	2012-10-17	09:53:59.30	-14.2237	49.3983	34.25	1.8787	2.1	d
201	2012-10-17	08:37:17.89	-14.1490	49.3640	16.34	1.8377	3.1	d
202	2012-10-17	01:51:26.81	-19.3167	46.6837	22.00	0.7196	3.2	d
203	2012-10-18	18:42:23.02	-19.0470	46.7023	16.47	1.8807	1.3	c
204	2012-10-18	10:42:25.86	-19.0657	46.7015	5.47	0.9712	3.0	d
205	2012-10-18	23:39:40.25	-14.2982	49.4267	46.39	1.5296	3.5	c
206	2012-10-18	11:58:05.97	-15.0100	49.3447	37.09	1.3012	3.8	d
207	2012-10-18	12:44:24.70	-20.2703	47.0437	27.53	0.7252	3.9	d
208	2012-10-18	16:12:48.69	-16.8040	49.7427	29.59	1.0176	4.0	b
209	2012-10-18	17:36:06.02	-19.8398	46.9042	16.82	0.7577	4.1	b
210	2012-10-19	01:39:22.43	-14.3553	49.4277	0.14	0.1188	2.8	c
211	2012-10-20	08:52:02.63	-22.9185	45.3032	16.81	0.6493	1.0	d
212	2012-10-20	10:34:11.45	-17.9097	47.0453	25.77	0.3152	1.1	c
213	2012-10-20	18:19:40.84	-18.5152	46.5747	39.30	0.2729	1.6	c
214	2012-10-20	17:53:59.77	-16.0960	49.4192	15.00	0.7403	2.4	b
215	2012-10-21	20:50:39.70	-14.3127	49.4507	0.05	0.4570	3.1	b
216	2012-10-23	11:29:44.18	-19.1580	46.7173	16.31	1.3217	1.4	b
217	2012-10-23	05:06:15.99	-20.5547	45.4208	10.49	0.7973	2.7	b
218	2012-10-25	10:25:45.60	-23.4385	45.0090	10.10	0.9692	1.3	b
219	2012-10-25	05:53:25.82	-18.2170	47.5420	16.85	0.3236	1.6	b
220	2012-10-25	12:42:29.58	-14.3687	49.4570	21.32	0.7340	1.7	d
221	2012-10-26	20:15:04.09	-18.9090	46.7412	20.04	0.4758	1.1	d
222	2012-10-26	17:18:13.71	-18.5903	45.8288	4.03	0.6850	3.4	d
223	2012-10-27	05:40:25.55	-18.3753	46.8827	40.21	0.2197	1.2	d
224	2012-10-28	19:13:02.67	-21.2353	46.5013	15.00	1.8647	1.2	d
225	2012-10-28	12:58:12.15	-17.3040	45.6422	13.42	0.6705	3.1	c
226	2012-10-29	01:24:12.75	-18.1735	48.2137	10.00	1.1396	3.6	c
227	2012-10-31	10:11:29.08	-18.5107	47.4960	35.85	1.0850	2.1	c
228	2012-10-31	00:32:00.00	-18.0445	47.7510	25.00	0.7742	2.4	c
229	2012-11-01	23:40:49.93	-19.0102	46.6182	14.28	0.1335	2.1	c
230	2012-11-01	00:19:28.21	-17.2653	49.0033	11.41	0.8687	4.6	d
231	2012-11-02	20:13:40.52	-17.5217	48.5470	45.11	0.2085	1.2	d
232	2012-11-02	21:57:55.57	-17.7148	46.2067	5.68	0.7108	1.7	d
233	2012-11-03	03:03:57.87	-18.6615	46.1537	11.03	0.6247	2.2	c
234	2012-11-04	01:30:40.85	-18.9903	46.7793	39.28	1.7640	1.1	d
235	2012-11-04	10:05:12.24	-18.1820	47.7722	27.91	1.0191	2.3	c
236	2012-11-04	01:22:33.63	-18.9988	46.7327	55.00	0.5769	2.4	d
237	2012-11-04	01:58:41.55	-19.1342	46.7128	0.06	0.4984	2.5	d
238	2012-11-04	12:49:25.68	-24.4418	44.9618	19.96	0.8060	3.8	b

239	2012-11-05	16:09:10.64	-19.2377	46.8115	17.91	0.3614	1.0	b
240	2012-11-06	08:31:45.83	-16.0808	47.8350	15.00	0.0014	2.1	c
241	2012-11-07	00:51:49.64	-18.3602	47.7603	15.00	0.4580	1.0	d
242	2012-11-07	01:50:41.15	-16.1645	47.8747	15.00	1.3407	1.2	c
243	2012-11-08	17:25:58.23	-17.3175	48.4623	33.37	1.0778	2.3	c
244	2012-11-08	05:29:13.42	-25.5183	44.9445	13.89	1.5069	3.8	b
245	2012-11-11	12:00:32.06	-13.8858	48.5028	16.30	0.4917	1.0	b
246	2012-11-11	07:30:05.91	-18.1472	46.3558	7.00	1.5514	1.4	b
247	2012-11-13	16:13:57.17	-18.3912	47.6967	12.00	1.0624	2.5	b
248	2012-11-13	00:01:50.78	-19.0270	46.8255	11.00	0.4368	4.3	b
249	2012-11-14	20:15:15.65	-18.2127	47.7433	34.20	0.7558	1.2	b
250	2012-11-16	16:40:28.54	-18.1578	45.5272	53.72	0.4269	3.3	d
251	2021-11-20	08:02:57.74	-18.2376	45.5923	12.67	0.0154	2.4	d
252	2012-11-20	00:00:51.88	-20.4418	45.5143	24.35	1.0559	4.3	d
253	2012-11-21	23:17:06.83	-17.3147	47.9875	22.00	1.8858	3.5	d
254	2012-11-22	01:50:41.90	-19.6103	47.0553	11.00	1.8553	1.2	d
255	2012-11-22	09:46:33.15	-19.5867	46.9168	4.56	0.8919	3.4	c
256	2012-11-23	10:27:11.45	-18.7613	46.5750	15.00	0.0019	1.6	c
257	2012-11-23	00:22:52.19	-15.0090	49.2812	22.13	0.4513	3.2	c
258	2012-11-26	06:18:33.74	-19.8922	47.2450	20.89	1.2688	3.6	c
259	2012-11-27	20:22:33.94	-18.2373	46.4773	22.00	0.4403	1.5	c
260	2012-11-27	00:40:11.28	-20.5043	46.6607	16.55	0.8826	1.6	d
261	2012-11-27	09:34:19.48	-17.9030	48.2820	5.17	0.1186	2.8	d
262	2012-11-27	22:23:50.50	-18.0577	44.8993	15.00	0.9588	2.9	d
263	2012-11-29	09:32:11.00	-17.7495	42.7873	18.00	0.0025	3.1	c
264	2012-11-30	20:07:23.05	-17.4675	48.6153	8.00	0.0025	1.1	d
265	2012-12-02	15:55:36.20	-19.2625	46.6830	34.94	0.3187	1.3	c
266	2012-12-02	06:15:40.00	-15.4927	56.6265	15.00	0.3335	3.1	d
267	2012-12-03	18:06:22.42	-18.9802	46.8205	7.67	0.6429	1.9	d
268	2012-12-05	04:47:38.86	-18.5703	46.7160	25.70	0.5611	1.7	b
269	2012-12-06	13:47:50.77	-21.9978	47.5365	3.71	1.2126	1.0	b
270	2012-12-06	07:14:41.03	-17.5188	49.4790	22.37	0.6622	2.0	c
271	2012-12-08	11:26:05.15	-19.0452	46.7012	35.00	0.8424	1.2	d
272	2012-12-10	03:52:20.99	-20.2800	45.5063	12.57	1.1570	2.8	c
273	2012-12-10	23:52:41.50	-15.4738	49.8012	17.20	1.1994	3.7	c
274	2012-12-10	21:30:10.99	-19.9422	43.5662	18.26	0.8565	3.9	b
275	2012-12-11	21:40:55.26	-20.1908	46.8818	28.24	0.7492	2.1	b
276	2012-12-11	01:08:47.76	-19.0297	46.7430	24.03	1.2481	2.7	b
277	2012-12-11	15:06:41.85	-25.6722	45.0078	14.73	0.5057	3.0	b
278	2012-12-12	07:03:42.04	-17.9133	46.0702	22.80	0.8201	2.3	b
279	2012-12-12	16:22:40.56	-18.4775	44.3803	10.78	1.2245	2.7	b
280	2012-12-13	05:54:49.89	-23.2460	46.6870	10.00	1.9476	1.3	d
281	2012-12-13	20:19:55.80	-15.9612	50.4745	15.00	0.0023	2.7	d
282	2012-12-14	15:18:47.31	-15.9935	41.6160	15.00	1.2516	4.1	d
283	2012-12-16	17:33:10.90	-18.9025	46.7348	21.97	0.6505	1.7	d
284	2012-12-16	20:08:52.58	-19.7482	46.5090	21.33	0.7925	2.8	d
285	2012-12-16	23:33:48.50	-19.1748	46.7197	18.61	0.6950	2.8	c
286	2012-12-17	03:39:29.15	-19.0562	46.7325	8.46	0.5428	2.7	c
287	2012-12-20	07:04:53.76	-19.0880	46.6867	23.84	1.2180	1.3	c
288	2012-12-20	14:26:53.06	-19.2002	46.6928	54.00	0.9161	1.4	c
289	2012-12-20	08:07:37.81	-19.7783	46.5825	10.00	1.8600	1.7	c
290	2012-12-21	00:44:46.31	-18.9817	46.7447	4.68	0.7803	2.7	d
291	2012-12-21	23:47:33.42	-19.0032	46.6923	28.21	0.7772	3.5	d
292	2012-12-22	04:58:58.52	-19.2972	46.7207	16.66	0.3159	1.2	d
293	2012-12-22	04:27:07.01	-19.1832	46.7132	33.11	0.9472	1.4	c
294	2012-12-22	08:19:47.31	-19.1382	46.6923	15.00	0.1139	1.4	d
295	2012-12-22	00:17:16.84	-18.9293	46.8088	28.72	0.2507	2.9	c
296	2012-12-22	21:55:26.64	-19.0047	46.5902	24.87	1.8783	3.0	d
297	2012-12-22	03:47:40.23	-19.0633	46.7385	9.00	0.5290	3.1	d
298	2012-12-22	21:29:48.78	-17.2050	50.0707	24.98	1.9152	3.1	b
299	2012-12-23	12:30:37.94	-19.3598	46.7022	10.29	0.5038	1.1	b
300	2012-12-23	04:48:13.38	-18.9245	46.6743	5.01	0.5084	1.7	c
301	2012-12-24	12:17:16.08	-19.0365	46.7303	4.72	0.4630	3.5	d
302	2012-12-25	14:22:07.02	-18.4178	48.1163	16.01	0.6656	2.3	c

303	2012-12-26	16:41:54.56	-20.3267	47.1190	25.09	0.6289	2.2	c
304	2012-12-26	07:28:16.70	-18.7510	47.6723	46.34	1.4851	2.4	b
305	2012-12-26	17:48:55.55	-26.0537	44.8863	5.26	1.9550	3.3	b
306	2012-12-27	09:48:22.12	-16.6318	47.1673	15.00	0.0487	1.0	b
307	2012-12-27	09:57:16.46	-16.3098	48.7400	36.63	1.0390	2.3	b
308	2012-12-27	02:58:09.60	-14.2090	48.5988	8.39	0.8470	2.4	b
309	2012-12-27	01:31:02.16	-17.6977	48.5963	25.52	1.3662	3.5	b
310	2012-12-28	09:08:13.00	-25.6845	44.8430	8.00	0.2880	3.3	d
311	2012-12-28	16:48:59.77	-20.0910	46.3808	10.65	0.9889	3.3	d
312	2012-12-29	09:07:22.44	-25.5370	44.9325	4.64	0.7613	2.8	d
313	2012-12-29	22:56:04.07	-16.4063	48.7460	15.00	1.0973	3.1	d
314	2012-12-29	00:56:43.13	-17.6883	48.6085	15.20	0.9213	3.2	d
315	2012-12-30	18:40:53.39	-23.7780	46.4267	0.05	0.8857	1.7	c
316	2012-12-30	20:57:25.62	-26.1217	44.6378	44.00	0.5260	2.7	c
317	2012-12-30	22:58:20.53	-18.9880	46.7240	4.48	1.0442	3.0	c
318	2012-12-30	01:26:38.04	-18.0410	46.2338	19.56	1.7718	3.2	c
319	2013-01-01	21:53:37.07	-18.9000	46.3725	15.00	0.0362	1.7	c
320	2013-01-01	10:35:32.14	-18.4940	46.7483	39.89	1.3856	1.8	d
321	2013-01-01	17:54:44.64	-19.2255	46.7877	56.05	1.2659	2.0	d
322	2013-01-01	18:24:42.72	-23.6267	43.6812	15.00	0.0017	2.3	d
323	2013-01-01	04:43:16.62	-18.9102	46.6945	1.82	0.8018	2.7	c
324	2013-01-01	05:27:13.88	-18.9388	46.7150	18.31	0.3970	2.7	d
325	2013-01-01	08:39:55.61	-18.9298	46.7068	19.15	1.4130	2.8	a
326	2013-01-01	23:16:08.38	-18.7368	46.6557	1.00	0.5071	2.9	a
327	2013-01-02	14:56:13.35	-19.2433	46.6820	11.12	0.3407	1.0	a
328	2013-01-02	06:46:32.96	-18.9795	46.7040	25.66	0.6836	2.8	a
329	2013-01-02	10:15:14.88	-24.1885	44.8140	19.43	0.9053	2.8	b
330	2013-01-03	23:13:02.26	-14.3682	48.7118	7.86	0.6414	2.7	b
331	2013-01-04	06:35:13.13	-24.4708	44.1763	3.62	0.6274	2.8	b
332	2013-01-04	21:39:50.33	-18.8527	46.7715	17.63	0.6054	2.8	b
333	2013-01-07	11:48:19.37	-18.9990	46.7378	9.75	0.5751	3.1	b
334	2013-01-08	12:02:13.01	-18.9565	46.7632	14.93	0.3955	1.5	b
335	2013-01-08	16:01:19.50	-18.9653	46.8087	15.84	0.8653	2.5	c
336	2013-01-08	21:59:30.07	-18.9875	46.7073	6.00	0.8371	3.9	c
337	2013-01-09	23:54:38.87	-16.9513	45.7072	3.65	0.3134	4.0	c
338	2013-01-10	17:32:09.27	-19.3120	46.6915	15.00	0.0008	1.2	c
339	2013-01-10	00:50:08.88	-14.8762	49.4995	9.88	0.4914	1.5	c
340	2013-01-10	01:08:57.28	-20.9118	45.5928	12.00	1.4487	1.5	c
341	2013-01-13	13:24:54.51	-18.6833	45.9278	13.04	1.1719	4.2	a
342	2013-01-14	23:45:53.22	-18.9888	46.7460	17.97	0.2553	3.7	a
343	2013-01-15	21:55:02.12	-17.3470	47.6790	10.17	1.8051	2.8	a
344	2013-01-15	19:10:20.62	-18.0627	46.5362	36.19	0.1046	3.3	b
345	2013-01-15	15:44:11.45	-19.0252	46.7110	6.39	1.2739	3.4	b
346	2013-01-18	09:25:52.97	-18.9200	46.6350	22.23	0.7877	2.9	b
347	2013-01-18	10:14:58.79	-18.9647	46.6355	22.36	0.6242	3.0	d
348	2013-01-19	23:21:43.61	-18.8858	46.7587	24.68	0.2986	1.3	d
349	2013-01-19	14:40:29.40	-17.2990	48.5760	11.72	1.2955	1.6	d
350	2013-01-19	04:19:03.52	-22.1437	47.0463	55.37	1.1491	3.5	d
351	2013-01-20	12:09:02.87	-18.6773	46.1142	13.62	1.5799	3.0	d
352	2013-01-21	16:04:27.60	-17.3883	47.7395	13.88	1.0916	2.8	c
353	2013-01-21	17:22:04.23	-18.7420	46.5932	16.37	0.3088	2.8	c
354	2013-01-21	07:05:36.24	-25.7002	44.8137	15.00	0.2419	3.0	c
355	2013-01-22	09:26:43.50	-17.0868	49.7805	11.00	0.2642	1.0	c
356	2013-01-23	02:16:03.43	-18.5013	45.7632	7.71	0.8045	3.0	c
357	2013-01-24	13:36:45.28	-25.0235	44.8182	11.00	1.3767	2.4	d
358	2013-01-24	00:44:46.92	-14.2565	48.7082	32.21	0.6062	2.8	d
359	2013-01-24	15:31:00.88	-20.9473	39.8168	40.97	1.9018	2.9	d
360	2013-01-25	01:00:55.01	-24.4718	45.0657	1.54	0.3671	1.2	c
361	2013-01-25	23:37:00.40	-23.5760	43.5002	22.73	1.0845	5.3	d
362	2013-01-26	19:57:14.19	-19.6063	46.9423	25.87	0.8182	3.2	c
363	2013-01-28	23:54:34.98	-23.7787	45.5752	19.97	1.5729	3.3	d
364	2013-01-29	01:43:30.55	-23.8182	44.5857	21.11	1.0844	1.8	d
365	2013-01-29	17:11:33.84	-14.5483	49.5042	9.09	1.6875	2.4	b
366	2013-02-01	12:37:11.69	-22.6210	47.8467	5.50	1.0929	2.9	b

367	2013-02-02	06:24:45.87	-19.0203	46.7637	21.12	0.2883	2.1	c
368	2013-02-03	04:29:50.68	-22.6037	44.3653	54.30	1.7627	1.5	d
369	2013-02-03	07:01:39.73	-14.1495	48.1948	5.98	0.4061	1.5	c
370	2013-02-03	18:34:20.84	-15.6265	49.6200	41.07	1.2099	2.0	c
371	2013-02-03	20:57:57.24	-15.8120	47.8095	0.35	0.0971	1.1	b
372	2013-02-04	20:19:49.49	-20.1353	46.4743	2.80	0.3697	2.8	b
373	2013-02-04	09:21:52.45	-18.1310	46.6865	20.03	0.1702	3.0	b
374	2013-02-05	23:16:47.06	-18.2557	46.4535	15.00	0.6512	2.5	b
375	2013-02-05	06:25:17.82	-18.5657	46.6808	10.54	0.1084	2.8	b
376	2013-02-08	22:15:04.01	-18.5375	47.7235	24.15	0.9266	3.0	b
377	2013-02-08	16:51:58.65	-18.0985	46.4337	3.00	1.6929	3.2	d
378	2013-02-08	02:11:44.51	-18.6517	47.6868	28.55	0.4773	3.3	d
379	2013-02-08	17:48:37.43	-17.4047	48.5923	26.77	1.4427	4.1	d
380	2013-02-10	08:38:06.10	-20.1358	46.7495	18.41	0.8562	2.9	d
381	2013-02-10	01:05:03.00	-17.2628	41.5312	22.40	0.0615	3.2	d
382	2013-02-10	01:36:26.36	-18.1953	46.2160	5.00	1.6710	3.2	c
383	2013-02-11	23:02:48.80	-19.1563	46.6582	20.55	0.5726	2.0	c
384	2013-02-11	11:03:35.14	-18.6283	46.3570	21.09	0.3144	2.3	c
385	2013-02-11	21:47:50.75	-17.6018	48.6647	13.88	0.6429	2.8	c
386	2013-02-13	14:00:48.96	-18.2578	48.1547	18.41	0.1910	2.5	c
387	2013-02-14	13:03:41.22	-13.9068	49.4797	5.00	1.5500	1.2	d
388	2013-02-14	00:35:03.02	-14.5310	49.0488	9.50	0.5151	2.4	d
389	2013-02-15	17:39:55.48	-18.5368	46.5870	38.36	1.7660	1.1	d
390	2013-02-15	13:52:03.38	-18.1152	46.5133	29.19	0.4334	2.0	c
391	2013-02-18	15:19:46.87	-17.2648	48.4420	17.61	1.3283	3.1	d
392	2013-02-18	04:06:33.48	-22.7138	47.5163	26.63	0.9373	3.8	c
393	2013-02-19	23:04:58.67	-19.3602	46.6058	22.07	1.9579	2.1	d
394	2013-02-20	11:58:28.46	-17.9475	47.3657	58.80	0.0011	1.2	d
395	2013-02-20	16:43:41.75	-19.2445	46.6780	31.37	1.2164	1.8	b
396	2013-02-20	14:12:14.07	-18.6880	44.7968	21.00	1.2022	2.5	b
397	2013-02-21	23:36:07.68	-18.9895	46.6992	24.83	1.1797	3.0	c
398	2013-02-21	07:27:14.18	-18.3807	46.5670	0.07	0.4436	3.2	d
399	2013-02-22	01:21:06.47	-18.9645	46.7775	6.89	0.9912	3.0	c
400	2013-02-23	17:55:54.01	-16.8307	45.6535	36.49	1.4066	3.6	c
401	2013-02-24	08:43:13.00	-19.1612	46.1985	15.00	0.0028	1.4	b
402	2013-02-24	14:48:35.32	-18.8300	48.6945	3.09	0.2938	2.5	b
403	2013-02-24	01:31:50.29	-17.7445	48.3030	18.90	0.7623	2.7	b
404	2013-02-25	02:15:20.30	-20.9002	48.6202	15.00	1.2983	1.0	b
405	2013-02-25	23:23:32.70	-14.6270	49.0758	18.92	0.4244	2.6	b
406	2013-02-26	00:53:23.37	-18.8870	46.7623	18.78	0.8806	2.5	b
407	2013-02-27	22:02:25.18	-22.3783	47.3968	0.04	1.3081	1.2	d
408	2013-02-27	02:23:14.11	-18.1962	45.8333	17.81	0.9872	2.4	d
409	2013-02-28	11:56:25.73	-24.5517	46.5285	8.00	0.8527	2.5	d
410	2013-03-01	01:18:57.83	-23.9563	46.0450	18.50	1.9927	1.3	d
411	2013-03-01	00:26:14.89	-17.2182	48.9653	66.16	0.9124	2.5	d
412	2013-03-01	11:03:06.54	-17.7892	47.0570	14.33	0.5697	2.6	c
413	2013-03-02	18:38:35.18	-19.2640	46.6308	38.38	1.5813	2.7	c
414	2013-03-02	16:47:05.67	-25.0110	46.5777	3.16	0.6762	2.8	c
415	2013-03-03	11:12:09.34	-17.7482	46.1730	5.00	0.8995	3.0	c
416	2013-03-03	18:04:31.46	-19.3062	47.0000	0.04	0.7841	3.1	c
417	2013-03-04	12:28:14.94	-19.6192	46.5363	36.44	0.9169	2.8	d
418	2013-03-04	07:57:45.06	-20.2578	46.7642	13.14	0.8269	3.1	d
419	2013-03-04	21:51:17.70	-17.3543	48.9018	28.23	0.6474	3.3	d
420	2013-03-05	05:27:47.30	-18.6895	46.7102	51.69	0.2372	1.9	c
421	2013-03-05	04:03:21.11	-19.0078	46.7272	22.53	0.5796	2.0	d
422	2013-03-05	02:03:03.03	-11.9883	47.4532	15.00	1.2693	3.0	c
423	2013-03-05	15:14:58.16	-11.6973	46.7675	15.00	1.7192	3.0	d
424	2013-03-06	17:46:55.28	-19.4585	46.5587	19.56	1.3958	3.5	d
425	2013-03-07	15:24:28.37	-13.4045	48.3423	3.00	0.4363	3.0	b
426	2013-03-08	14:25:36.61	-13.9650	48.6250	3.00	0.7355	1.5	b
427	2013-03-08	21:00:30.70	-19.0655	46.7247	22.96	0.3766	2.9	c
428	2013-03-08	19:14:56.17	-18.0338	47.8770	0.04	1.6871	3.0	d
429	2013-03-08	20:48:03.08	-19.3082	46.6965	3.93	0.6460	3.0	c
430	2013-03-08	03:23:55.00	-22.5271	46.2034	13.30	0.3258	3.1	c

431	2013-03-09	00:52:31.77	-14.6862	48.8923	39.58	0.9166	1.8	b
432	2013-03-09	23:32:38.80	-18.4168	47.8030	28.66	0.4565	3.0	b
433	2013-03-10	00:38:30.75	-14.9835	49.3082	15.52	0.7427	3.0	b
434	2013-03-11	14:28:57.77	-14.6862	48.8923	39.58	0.9166	1.2	b
435	2013-03-11	17:42:17.56	-18.1795	46.1570	11.72	0.0622	2.8	b
436	2013-03-11	07:12:29.19	-17.5797	48.3587	0.20	0.5168	3.2	b
437	2013-03-11	12:26:09.00	-11.2843	43.2373	13.90	0.3846	4.1	d
438	2013-03-14	20:10:28.77	-15.9185	49.8092	30.35	0.7014	2.9	d
439	2013-03-17	04:57:06.65	-20.8203	47.8482	25.79	1.4741	3.5	d
440	2013-03-18	21:50:52.25	-16.4393	48.0308	5.00	1.0168	3.6	d
441	2013-03-19	00:58:19.36	-18.2222	48.2187	27.38	0.3341	2.6	d
442	2013-03-19	01:20:11.26	-20.3232	47.2172	11.00	1.1453	2.8	c
443	2013-03-20	04:15:19.70	-17.7328	48.4267	7.84	0.5575	1.1	c
444	2013-03-20	05:21:56.00	-11.9918	42.2345	15.87	0.3654	1.4	c
445	2013-03-20	18:26:27.30	-19.4000	46.7198	17.07	1.2874	2.5	c
446	2013-03-21	08:26:00.93	-17.3642	48.7060	59.84	1.1219	3.2	c
447	2013-03-21	02:08:04.52	-17.3438	48.5595	7.94	0.5376	3.3	d
448	2013-03-23	01:58:40.47	-24.8412	45.6550	7.00	1.6925	3.3	d
449	2013-03-24	03:31:37.70	-17.8812	48.0887	14.00	0.5963	1.4	d
450	2013-03-24	09:44:08.00	-19.9152	47.0593	21.96	1.1473	3.2	c
451	2013-03-24	17:44:52.85	-14.7300	49.6082	6.81	1.1589	3.3	d
452	2013-03-26	10:08:39.11	-24.2783	44.5325	30.43	0.9923	1.4	c
453	2013-03-26	21:12:53.56	-24.2863	44.4965	1.34	0.8790	2.7	d
454	2013-03-26	10:08:38.00	-24.2978	44.4268	17.63	1.1555	3.1	d
455	2013-03-26	11:58:15.76	-24.2922	44.5618	33.00	0.8506	3.2	b
456	2013-03-26	23:29:52.89	-24.5070	44.4240	40.39	1.1431	3.2	b
457	2013-03-26	23:02:11.87	-24.3158	44.6107	7.58	0.5945	3.3	c
458	2013-03-26	09:48:39.60	-24.3653	44.4453	9.22	0.9092	3.9	d
459	2013-03-27	05:00:19.44	-23.3447	45.2007	5.00	0.9596	1.8	c
460	2013-03-27	20:26:41.93	-24.2647	44.5610	7.18	0.7155	2.8	c
461	2013-03-28	16:51:03.04	-20.7082	48.2137	33.66	1.7123	1.5	b
462	2013-03-28	04:48:18.33	-17.4243	47.6638	9.78	0.1824	2.8	b
463	2013-03-29	08:57:15.89	-18.3037	48.7753	3.00	1.7326	1.0	b
464	2013-03-29	16:22:19.75	-19.2263	46.7363	6.93	0.4499	1.2	b
465	2013-03-30	12:52:06.13	-19.2048	46.6132	9.86	1.1807	2.8	b
466	2013-03-30	18:21:19.28	-24.8142	45.6785	12.12	1.3506	3.0	b
467	2013-03-31	06:21:38.60	-13.0060	48.8545	10.00	1.7898	1.0	d
468	2013-04-02	01:49:27.46	-16.6590	45.4292	8.00	1.0954	1.4	d
469	2013-04-02	01:26:45.03	-17.8387	47.2380	2.49	0.5368	1.7	a
470	2013-04-02	03:26:02.79	-18.3620	46.7923	18.14	0.5547	2.3	a
471	2013-04-02	09:45:45.91	-24.2403	45.5447	9.58	0.4333	2.8	a
472	2013-04-03	03:01:36.52	-16.2867	46.2447	15.00	0.7461	1.0	a
473	2013-04-03	03:39:00.75	-18.8727	47.4997	33.83	0.0008	1.2	a
474	2013-04-03	00:28:20.42	-13.9435	49.6692	9.52	1.6063	2.3	a
475	2013-04-03	21:46:42.82	-19.3713	46.9845	19.93	1.3569	2.3	a
476	2013-04-04	16:40:42.23	-18.8398	46.7810	0.27	0.4020	2.4	a
477	2013-04-05	13:00:29.07	-18.8517	46.6705	30.70	0.8295	1.0	c
478	2013-04-05	02:33:54.28	-18.0985	46.4307	19.24	0.5373	2.5	a
479	2013-04-05	21:14:38.49	-24.2448	44.5588	0.04	1.1226	3.0	c
480	2013-04-06	09:07:55.77	-19.1902	46.8533	19.11	0.7333	1.0	b
481	2013-04-06	22:05:07.96	-17.6957	48.4980	31.88	0.5616	1.3	a
482	2013-04-06	00:24:48.05	-17.7008	48.2892	26.11	0.0751	1.7	c
483	2013-04-06	00:54:27.71	-20.4325	47.1545	5.00	0.2461	2.6	a
484	2013-04-06	19:37:59.02	-18.6925	47.5718	15.88	0.0007	2.7	d
485	2013-04-06	10:21:10.30	-16.4143	47.6767	1.61	1.9419	2.8	
486	2013-04-06	10:01:13.06	-16.3822	47.5492	16.47	1.9627	2.9	b
487	2013-04-06	01:23:02.63	-21.3982	47.4295	34.21	0.2158	3.3	b
488	2013-04-06	10:05:52.47	-16.4250	47.7263	0.04	1.9266	3.4	b
489	2013-04-06	12:33:16.19	-16.9797	48.3877	40.98	1.4697	3.4	b
490	2013-04-06	11:40:35.77	-19.0582	46.7248	3.12	1.3697	3.7	a
491	2013-04-07	18:29:29.76	-18.6035	44.7177	0.04	0.8723	1.2	a
492	2013-04-07	21:09:32.32	-17.5323	48.2288	21.00	0.6816	2.7	c
493	2013-04-08	01:41:22.66	-17.6983	49.0565	15.00	0.2545	1.5	c
494	2013-04-08	06:24:09.44	-18.4103	46.8657	0.04	0.7543	3.2	c

495	2013-04-10	22:11:12.08	-18.9297	46.8492	15.00	0.0008	1.0	c
496	2013-04-10	22:21:35.67	-19.3653	47.0587	33.17	0.2387	1.0	b
497	2013-04-10	01:21:10.83	-18.4665	44.6182	13.30	0.4005	2.6	
498	2013-04-10	03:58:21.66	-17.8898	47.9157	15.21	0.4538	2.9	d
499	2013-04-10	14:02:34.96	-18.4565	46.6768	5.92	0.3681	2.9	d
500	2013-04-11	11:07:04.05	-19.7290	46.8568	21.64	1.2294	1.2	d
501	2013-04-11	22:38:16.23	-14.6243	49.5043	15.00	0.0017	2.6	d
502	2013-04-11	14:37:18.26	-18.5553	44.7285	0.04	1.2469	2.9	d
503	2013-04-12	05:22:44.35	-24.9368	44.9690	10.89	0.4690	2.0	d
504	2013-04-13	09:23:01.19	-22.8425	48.4260	15.00	1.6322	2.5	a
505	2013-04-13	03:47:09.56	-18.5023	46.2433	5.55	0.5954	3.1	a
506	2013-04-13	02:26:07.48	-17.1067	47.9743	2.79	1.0270	3.2	
507	2013-04-14	08:09:21.98	-24.2660	44.4367	13.44	0.7477	2.8	c
508	2013-04-14	23:18:48.42	-20.8850	46.4215	15.00	1.7944	3.1	d
509	2013-04-15	10:15:13.32	-18.3580	46.8637	41.19	1.9582	1.5	b
510	2013-04-15	11:52:03.82	-19.7855	46.5767	22.65	0.5704	2.7	b
511	2013-04-16	20:04:23.03	-18.8177	46.9505	0.05	0.0797	1.3	b
512	2013-04-18	08:54:39.97	-19.6558	46.5842	15.00	1.2602	3.0	a
513	2013-04-18	00:09:36.24	-19.0360	46.5987	12.67	0.8708	3.5	a
514	2013-04-19	00:02:24.83	-17.6473	45.3505	66.78	0.7823	1.0	a
515	2013-04-19	10:49:56.26	-18.6370	46.1707	6.55	0.8064	3.6	c
516	2013-04-20	10:50:24.49	-19.0107	46.7122	24.52	0.5265	2.8	d
517	2013-04-21	01:09:07.68	-19.0448	46.7112	25.00	1.3553	3.0	d
518	2013-04-22	21:27:17.80	-15.1263	49.9955	37.97	0.7418	2.0	d
519	2013-04-23	13:21:24.49	-19.2032	46.8222	3.04	0.6396	2.7	c
520	2013-04-23	15:29:54.73	-19.0242	46.6733	7.00	1.4992	3.0	a
521	2013-04-24	23:38:15.12	-21.4642	47.2972	21.07	0.8133	2.1	d
522	2013-04-24	18:49:50.75	-19.5428	46.8285	23.63	1.3754	2.7	b
523	2013-04-24	07:10:25.20	-18.3783	46.5062	29.44	0.3658	2.8	b
524	2013-04-25	14:39:34.40	-18.1965	47.1140	7.00	0.2108	3.0	b
525	2013-04-27	06:20:39.17	-20.1732	46.1490	12.00	0.7258	1.6	b
526	2013-04-29	20:06:06.25	-16.0165	49.1647	15.00	0.6260	1.5	c
527	2013-04-29	17:36:14.99	-18.4392	47.6407	26.79	0.5165	2.2	c
528	2013-05-01	22:55:14.52	-19.7788	47.1112	34.37	0.6287	1.9	c
529	2013-05-04	11:55:35.37	-25.3015	44.9103	17.13	0.6792	3.1	c
530	2013-05-05	22:29:10.63	-22.4560	47.7143	15.00	0.5469	2.6	c
531	2013-05-05	06:06:28.33	-22.7887	40.6058	12.77	1.3201	2.9	d
532	2013-05-05	18:23:32.70	-19.0208	46.9758	41.36	0.6982	3.5	d
533	2013-05-06	07:22:21.55	-19.2108	46.7068	9.99	0.7337	1.2	c
534	2013-05-06	01:36:20.18	-15.5458	49.7053	34.44	0.3727	2.2	c
535	2013-05-06	22:39:55.79	-17.6188	48.3322	27.11	0.3198	2.6	d
536	2013-05-06	00:33:00.21	-18.7965	46.6308	9.15	1.3918	3.6	d
537	2013-05-07	15:23:46.99	-18.4063	47.1447	7.00	0.2409	1.2	c
538	2013-05-07	13:46:23.84	-18.9745	46.7687	16.43	0.7143	2.9	d
539	2013-05-10	01:18:04.73	-19.0853	44.6192	11.74	0.3726	1.1	d
540	2013-05-10	11:33:56.84	-21.5650	47.9437	44.00	1.3999	2.3	d
541	2013-05-10	23:22:31.20	-18.3277	46.3152	20.06	0.3440	2.7	a
542	2013-05-11	23:11:04.58	-18.2597	46.9220	6.00	1.8075	2.1	a
543	2013-05-12	00:13:49.12	-18.2497	48.3890	7.76	0.7526	2.3	a
544	2013-05-13	14:40:15.02	-19.0482	46.7363	6.37	0.7373	2.7	a
545	2013-05-14	19:32:54.48	-15.1783	50.2862	37.84	0.9762	1.0	a
546	2013-05-14	04:16:06.64	-17.9905	48.2253	0.04	0.9971	1.2	a
547	2013-05-14	09:50:39.62	-15.4670	49.8062	3.50	1.3966	1.3	c
548	2013-05-14	15:43:11.73	-21.5973	47.3100	34.32	0.8182	2.9	c
549	2013-05-14	21:04:44.90	-19.3218	46.8385	6.03	1.3051	2.9	d
550	2013-05-15	08:22:09.25	-18.4963	46.3900	15.00	0.0052	1.8	d
551	2013-05-15	22:52:57.71	-14.4603	48.7422	20.45	1.0556	2.3	d
552	2013-05-16	06:13:51.05	-20.5525	45.8843	15.00	0.1768	1.0	c
553	2013-05-16	00:44:12.00	-14.2760	49.3642	20.24	1.3034	1.8	c
554	2013-05-16	03:51:48.28	-14.8910	49.5842	4.00	0.7590	2.8	c
555	2013-05-17	09:53:45.50	-17.8497	47.7020	2.51	0.8335	1.0	b
556	2013-05-17	22:22:47.29	-18.3490	46.4478	19.84	0.2824	3.0	b
557	2013-05-17	06:39:54.29	-18.7270	46.1083	17.38	1.5404	4.0	b
558	2013-05-18	22:13:43.11	-17.2400	45.9177	8.26	1.3194	1.2	b

559	2013-05-18	09:26:19.44	-18.7188	46.2788	14.09	0.2705	1.7	d
560	2013-05-18	23:46:52.44	-16.2787	44.2623	15.00	1.9024	2.8	d
561	2013-05-18	00:40:59.77	-25.4813	45.2070	5.00	1.9626	3.0	d
562	2013-05-19	22:53:51.17	-17.5557	47.4890	47.66	1.6375	1.8	d
563	2013-05-19	20:42:07.76	-21.7810	43.3795	20.44	1.9397	2.2	d
564	2013-05-20	06:47:32.99	-18.2705	46.4072	14.89	0.2048	2.4	c
565	2013-05-22	02:35:03.93	-20.8743	47.7300	26.73	0.4707	1.3	c
566	2013-05-23	04:53:56.81	-19.6063	46.9383	44.00	1.1328	2.3	c
567	2013-05-23	02:22:10.97	-17.6633	46.2075	1.00	1.2883	3.0	c
568	2013-05-23	00:17:03.24	-19.1483	46.6560	17.79	0.7142	4.0	c
569	2013-05-24	14:25:28.85	-22.6290	46.0728	19.78	1.4015	2.0	d
570	2013-05-24	02:34:26.10	-18.6633	48.2308	37.14	1.2266	3.6	d
571	2013-05-25	13:43:27.48	-19.9072	45.0733	15.00	0.2715	2.0	d
572	2013-05-25	17:29:07.94	-18.2028	46.0865	12.72	1.0018	2.1	c
573	2013-05-26	07:50:27.09	-17.4780	48.0098	2.00	1.7804	3.3	d
574	2013-05-27	16:33:18.92	-22.8373	45.2112	2.00	0.9833	1.1	c
575	2013-05-27	13:02:39.30	-17.7058	47.4972	0.04	1.2740	2.2	d
576	2013-05-27	03:17:21.30	-19.0727	46.7323	1.93	0.4886	2.3	d
577	2013-05-27	06:31:39.81	-18.9562	46.7435	13.09	0.2844	2.5	b
578	2013-05-27	02:49:14.10	-19.8833	46.6407	1.00	0.6187	2.6	b
579	2013-05-29	20:15:54.24	-19.4107	46.7358	16.86	1.6106	2.5	c
580	2013-05-29	01:54:01.90	-17.6812	45.4928	60.21	0.3295	3.0	d
581	2013-05-30	21:31:07.77	-18.6740	45.9087	15.00	0.6910	1.0	c
582	2013-05-30	02:51:07.43	-23.5398	45.3422	21.93	1.7592	1.8	c
583	2013-05-31	06:12:36.64	-18.2745	46.7007	25.48	0.6629	2.4	b
584	2013-06-02	20:08:39.75	-16.9470	49.7695	16.65	1.2572	2.7	b
585	2013-06-04	02:01:34.08	-18.8363	46.1733	28.65	0.2650	2.7	b
586	2013-06-04	18:03:14.76	-17.6822	46.4715	7.00	1.7472	2.8	b
587	2013-06-04	16:00:43.89	-18.3062	47.4598	22.00	0.3546	2.9	b
588	2013-06-05	14:07:11.15	-20.5952	46.1555	10.90	0.5431	2.7	b
589	2013-06-06	20:49:30.92	-17.2562	47.9795	0.04	0.5897	3.2	b
590	2013-06-07	21:53:55.00	-24.6485	45.0322	25.66	1.0304	2.0	b
591	2013-06-08	02:59:26.01	-17.8748	45.8770	22.44	0.3160	2.0	b
592	2013-06-09	23:34:18.16	-19.4572	46.1085	10.04	0.8406	2.3	d
593	2013-06-09	19:05:55.71	-17.9032	45.9027	7.72	1.2579	3.2	d
594	2013-06-09	02:24:03.19	-17.8450	45.7720	69.18	0.3423	3.3	d
595	2013-06-10	06:25:48.73	-17.9100	47.9275	4.64	0.5838	2.9	d
596	2013-06-11	23:16:10.67	-19.3623	46.9958	7.78	0.8684	3.2	d
597	2013-06-12	04:10:34.66	-12.7943	49.9950	22.63	1.2881	3.2	c
598	2013-06-13	13:37:44.25	-18.3100	47.4781	15.00	0.0014	1.1	c
599	2013-06-13	20:29:39.56	-18.5063	44.7348	10.49	0.7432	1.7	c
600	2013-06-14	11:21:42.99	-23.5103	46.4598	5.08	0.7162	2.2	c
601	2013-06-15	15:03:23.40	-19.2403	47.7100	24.79	1.8392	1.3	c
602	2013-06-15	13:00:07.62	-18.9332	46.7527	0.57	0.0108	1.4	d
603	2013-06-16	10:12:15.23	-18.2037	47.3923	31.54	1.1751	2.8	d
604	2013-06-16	19:12:24.41	-26.0612	45.5420	15.31	1.3089	3.2	d
605	2013-06-17	03:54:19.81	-20.6025	45.7312	24.07	0.4147	2.4	c
606	2013-06-20	05:13:03.63	-18.6932	45.3868	12.23	0.2106	2.4	d
607	2013-06-20	21:27:12.84	-26.2225	45.4088	27.04	0.1964	2.9	c
608	2013-06-20	05:47:35.20	-21.6580	39.1703	15.00	1.0392	3.3	d
609	2013-06-22	21:50:24.78	-20.6780	46.2883	2.00	1.7019	2.6	d
610	2013-06-22	21:32:55.20	-17.8827	45.9072	3.92	0.0016	3.1	b
611	2013-06-22	04:15:15.71	-20.3362	46.5443	19.09	0.5966	3.3	b
612	2013-06-28	02:39:45.19	-18.2637	46.5025	19.37	0.5991	3.0	c
613	2013-07-01	16:54:57.91	-19.2652	46.6337	17.60	1.2610	1.0	d
614	2013-07-02	06:40:06.87	-18.3915	46.5608	5.40	0.6872	3.2	c
615	2013-07-04	13:40:59.08	-24.4833	45.1075	27.72	0.8259	3.2	c
616	2013-07-06	02:06:22.82	-16.2388	50.2352	32.55	1.6496	1.1	b
617	2013-07-06	11:25:48.36	-17.9040	45.8340	34.21	0.2055	2.9	b
618	2013-07-09	00:05:59.57	-17.6552	48.6927	36.83	0.2144	2.4	b
619	2013-07-10	05:23:39.23	-16.2670	47.9547	8.82	0.7926	1.4	b
620	2013-07-10	19:12:59.56	-19.6027	46.7238	54.00	1.1057	2.6	b
621	2013-07-10	19:43:10.82	-18.3877	47.6657	20.84	1.7302	3.5	b
622	2013-07-11	03:39:44.89	-18.7003	49.0533	25.22	0.7630	2.3	d

623	2013-07-12	11:49:20.35	-17.2733	47.6580	14.08	0.6512	1.1	d
624	2013-07-16	07:10:18.34	-17.0095	47.9237	56.00	0.5462	3.3	d
625	2013-07-17	20:11:46.17	-15.0090	49.5870	2.00	0.3617	1.0	d
626	2013-07-17	23:45:34.86	-18.3667	46.4397	33.17	0.0494	2.0	d
627	2013-07-19	03:05:29.63	-19.0573	46.7240	11.11	0.5069	2.7	c
628	2013-07-20	10:50:24.75	-20.1063	47.2438	21.55	0.6574	2.9	c
629	2013-07-23	18:57:11.23	-18.3860	47.6602	17.99	0.5082	2.6	c
630	2013-07-25	15:27:13.81	-24.1428	44.5823	0.07	1.0496	2.9	c
631	2013-07-27	05:43:39.66	-20.6743	45.3410	12.72	1.5539	3.3	c
632	2013-07-28	05:02:34.69	-19.0445	46.6793	8.33	1.6097	2.5	d
633	2013-07-28	19:24:06.78	-17.3745	48.6293	19.02	0.9227	3.4	d
634	2013-08-02	15:46:57.36	-19.7165	46.0448	6.67	0.8043	1.3	d
635	2013-08-02	23:42:41.62	-18.7167	46.9673	40.03	0.8540	3.3	c
636	2013-08-03	06:35:03.78	-18.9985	46.7073	0.04	0.6973	1.3	d
637	2013-08-03	21:15:07.89	-18.4873	45.5707	0.07	0.7320	3.0	c
638	2013-08-04	20:10:28.30	-18.5628	45.9252	12.87	0.6549	2.0	d
639	2013-08-04	22:32:18.05	-14.8578	49.0550	6.42	0.5911	2.8	d
640	2013-08-05	15:39:05.95	-17.8260	48.2447	17.30	1.1756	3.2	b
641	2013-08-10	22:59:56.51	-14.6630	49.8945	21.07	0.3644	1.8	b
642	2013-08-11	04:01:31.83	-18.8538	46.6775	18.81	0.4128	1.8	c
643	2013-08-11	03:24:15.38	-19.4427	46.5843	23.42	1.7572	2.2	d
644	2013-08-11	03:06:24.64	-23.2455	45.8857	5.44	0.9509	3.0	c
645	2013-08-12	00:40:58.33	-20.0147	47.2593	15.42	0.9264	2.1	c
646	2013-08-17	05:41:50.58	-18.2468	46.2265	15.00	0.3596	2.0	b
647	2013-08-18	09:05:56.33	-17.5763	48.8118	15.00	0.8017	3.2	b
648	2013-08-22	21:27:14.45	-17.5090	48.3207	25.40	1.2804	2.8	b
649	2013-08-23	02:02:55.55	-17.4023	48.4828	15.00	1.1751	2.9	b
650	2013-08-23	20:01:06.21	-17.2387	48.3157	40.83	1.2599	3.0	b
651	2013-08-24	06:39:03.85	-18.0453	47.9160	2.62	0.1844	2.6	b
652	2013-08-24	12:47:07.87	-16.3088	49.0810	0.04	1.4279	2.9	d
653	2013-08-26	22:11:43.60	-25.7177	44.8657	9.81	0.7304	3.3	d
654	2013-08-27	10:26:28.44	-17.7742	47.3328	16.88	0.0642	1.6	d
655	2013-08-27	16:15:15.16	-19.9433	47.3578	4.51	0.6843	2.4	d
656	2013-08-27	05:58:33.71	-23.4633	44.7282	48.15	1.7123	2.9	d
657	2013-08-30	17:52:25.48	-25.7868	44.7875	8.00	0.2847	2.9	c
658	2013-08-30	22:25:11.22	-19.3820	46.9217	13.05	0.6477	3.2	c
659	2013-08-31	03:47:55.11	-19.3670	47.0412	26.58	0.9582	3.1	c
660	2013-03-26	20:27:54.05	-18.0962	48.5470	23.45	0.9964	3.2	c
661	2013-03-26	10:05:37.87	-24.1802	44.3892	16.44	1.6299	1.2	c
662	2013-04-06	09:55:23.84	-18.3358	46.4970	15.48	0.4205	2.6	d
663	2013-04-06	10:27:04.85	-16.3350	47.6173	55.00	1.4899	1.6	d
664	2013-04-06	11:42:26.66	-19.0790	46.7830	30.39	1.8786	2.4	d
665	2013-05-15	08:27:25.87	-19.8640	46.6338	18.00	0.0031	2.9	c
666	2013-05-27	03:38:16.90	-21.6482	45.7525	41.06	1.7463	3.2	d
667	2013-08-23	01:55:15.72	-17.4558	48.5517	15.00	1.4253	3.1	c
668	2013-03-26	10:23:02.35	-24.6830	44.2133	61.92	1.1257	3.2	d
669	2013-03-26	23:29:52.99	-24.3800	44.6320	29.86	0.0310	1.2	d
670	2013-03-26	10:06:45.74	-24.2933	44.4347	8.00	1.6370	1.3	b
671	2011-12-23	17:35:34.12	-17.2507	47.6333	15.00	0.0004	2.1	b
672	2012-01-06	19:20:02.86	-17.2465	48.3768	15.00	0.0017	3.1	c
673	2012-06-17	01:11:30.24	-16.2573	49.3003	15.00	0.6996	3.2	d
674	2012-07-03	06:58:50.50	-21.9473	47.6362	0.04	1.9843	3.0	c
675	2012-07-04	18:29:38.08	-16.2750	49.3787	15.00	1.4487	1.2	c
676	2012-08-17	01:32:22.84	-21.9392	40.5932	1.00	1.2049	1.0	b
677	2012-08-25	14:54:56.85	-17.5703	48.7025	4.92	1.7152	2.1	b
678	2012-09-16	08:40:20.68	-22.5850	40.6445	8.10	1.1255	2.9	b
679	2012-10-17	08:40:52.66	-14.4710	49.4510	3.05	1.3735	1.5	b
680	2012-12-09	09:38:00.11	-24.2132	47.3842	17.14	0.3492	1.4	b
681	2012-12-13	05:54:15.36	-22.7303	43.5413	15.00	0.9849	1.7	b
682	2013-01-05	18:39:28.14	-19.8118	46.6575	15.00	0.0004	2.5	d
683	2013-01-06	04:56:30.31	-19.6180	46.6720	15.00	0.0909	3.0	d
684	2013-01-06	05:36:40.27	-19.6270	46.6962	15.00	0.4808	3.1	d
685	2013-01-07	03:27:54.95	-15.1395	46.5100	15.00	4.3263	1.4	d
686	2013-01-11	16:06:58.61	-26.2582	57.0713	15.00	1.7453	2.9	d

687	2013-01-16	10:04:54.43	-18.5300	46.2507	15.00	0.6817	1.5	c
688	2013-01-28	15:12:56.63	-18.4177	45.4832	2.78	0.1744	1.1	c
689	2013-04-04	16:44:02.19	-17.7543	46.1330	8.00	0.1754	2.1	c
690	2013-04-19	22:05:38.40	-17.2577	49.5077	38.09	1.4909	2.8	c
691	2013-04-20	06:23:38.19	-21.1345	48.2303	15.00	0.6510	1.1	c
692	2013-04-20	22:53:29.63	-19.7548	47.6153	14.13	1.8811	1.0	d
693	2013-04-21	04:35:42.42	-18.4967	46.8373	15.00	0.0028	2.9	d
694	2013-04-22	13:43:42.88	-18.5963	46.3850	22.63	1.3801	2.9	d
695	2013-08-26	17:37:08.85	-23.3480	44.6107	5.00	1.2016	1.1	c

2. List of the 422 earthquakes obtained from HYPODD relocations.

ID	LAT(deg)	LON(deg)	DEPTH(km)	DATE(y/m/d)	TIME(h/mn/s)	ERROR(s)	MAG
BEMARIVO							
1	-14.8703	49.5272	9.5	2012-09-30	19:43:28.20	1.220	2.7
2	-14.2335	49.4151	36.8	2012-10-17	09:53:59.68	0.838	2.1
3	-14.1629	49.3885	22.5	2012-10-17	08:37:17.89	1.000	3.1
4	-14.2806	49.4435	43.7	2012-10-18	23:39:40.20	1.013	3.5
5	-15.5074	49.8132	14.4	2012-12-10	23:52:41.80	1.192	3.7
6	-14.2062	48.6149	4.4	2012-12-27	02:58:10.07	1.397	2.4
7	-15.5876	49.6438	36.5	2013-02-03	18:34:21.04	1.691	2.0
8	-14.6764	48.8991	38.9	2013-03-09	00:52:31.71	0.801	1.8
9	-14.6764	48.8991	38.9	2013-03-11	14:28:57.71	0.801	1.2
10	-14.4372	49.4500	2.7	2012-10-17	08:40:52.69	0.973	1.5
11	-14.6318	49.0755	19.1	2013-02-25	23:23:32.72	0.769	2.6
12	-15.1025	49.9562	37.7	2013-04-22	21:27:17.44	0.847	2.0
13	-14.9316	49.5434	12.3	2012-09-30	06:08:14.96	0.932	3.8
14	-14.9320	49.7043	8.8	2012-10-11	20:48:59.86	0.987	1.1
15	-14.9050	49.7520	23.3	2012-10-13	09:32:16.00	1.260	1.1
16	-14.9828	49.3345	32.2	2012-10-18	11:58:06.02	0.766	3.8
17	-14.3536	49.4191	3.8	2012-10-19	01:39:22.36	0.721	2.8
18	-14.3180	49.4406	2.5	2012-10-21	20:50:39.56	1.001	3.1
19	-14.3786	49.4438	27.7	2012-10-25	12:42:29.56	0.933	1.7
20	-13.8869	48.5090	16.0	2012-11-11	12:00:31.96	0.873	1.0
21	-15.0216	49.2833	22.4	2012-11-23	00:22:52.20	0.668	3.2
22	-14.3614	48.7041	8.1	2013-01-03	23:13:02.28	0.855	2.7
23	-14.8836	49.5031	10.4	2013-01-10	00:50:08.83	0.781	1.5
24	-14.2610	48.6991	32.7	2013-01-24	00:44:46.72	1.373	2.8
25	-14.5563	49.4996	9.1	2013-01-29	17:11:33.88	1.463	2.4
26	-14.1426	48.2176	7.3	2013-02-03	07:01:39.51	0.647	1.5
27	-14.5351	49.0506	9.7	2013-02-14	00:35:02.97	0.851	2.4

28	-13.9725	48.6133	1.6	2013-03-08	14:25:36.53	0.920	1.5
29	-15.5261	49.6870	36.0	2013-05-06	01:36:19.86	1.075	2.2
30	-15.4816	49.8020	4.2	2013-05-14	09:50:39.44	1.476	3.2
31	-14.4546	48.7436	20.8	2013-05-15	22:52:57.76	1.130	2.3
32	-14.2951	49.3533	22.5	2013-05-16	00:44:11.89	1.625	1.8
33	-14.8989	49.5823	0.9	2013-05-16	03:51:48.23	1.095	2.8
34	-15.0010	49.5855	0.8	2013-07-17	20:11:46.00	0.578	1.0
35	-14.8544	49.0570	6.6	2013-08-04	22:32:18.02	0.755	2.8
36	-14.6840	49.8796	27.1	2013-08-10	22:59:56.24	0.807	1.8
ALAOTRA							
37	-16.3356	48.2053	18.7	2011-11-07	08:20:36.40	1.313	2.6
38	-15.4727	48.1817	24.2	2012-08-18	20:07:17.78	0.679	2.6
39	-17.4711	48.5318	9.1	2011-11-13	11:26:31.87	0.553	2.0
40	-17.7617	48.1482	41.2	2012-08-30	07:02:52.54	0.794	3.8
41	-16.0763	47.9198	4.5	2012-09-03	12:40:31.08	1.148	3.5
42	-18.1986	47.8129	37.2	2011-11-21	06:43:16.72	2.131	1.3
43	-18.4232	47.9398	10.8	2012-09-23	23:37:07.30	0.696	1.8
44	-18.5198	48.7479	37.0	2011-11-22	07:44:00.90	0.207	3.1
45	-17.5198	48.2995	11.5	2012-09-29	22:07:53.88	0.769	2.8
46	-17.0707	47.8906	14.6	2012-10-16	21:02:59.20	1.637	1.0
47	-17.5084	48.5709	49.9	2012-11-02	20:13:40.12	0.779	1.2
48	-16.0983	47.7948	10.8	2012-11-06	08:31:46.13	0.625	2.1
49	-16.1515	47.9051	18.9	2012-11-07	01:50:41.26	1.981	1.0
50	-17.3016	48.4668	31.4	2012-11-08	17:25:58.40	1.037	2.3
51	-17.9847	48.6081	103.6	2011-12-31	20:57:56.20	0.728	2.3
52	-16.7097	47.3942	16.9	2012-12-27	09:48:21.96	1.263	1.0
53	-16.3796	48.7576	40.0	2012-12-27	09:57:16.45	0.441	2.3
54	-17.6815	48.6331	15.1	2012-12-29	00:56:43.21	0.934	3.2
55	-17.2964	47.7136	9.0	2013-01-15	21:55:02.48	1.565	2.8
56	-17.2489	48.6249	21.5	2013-01-19	14:40:29.51	1.578	1.6
57	-18.4852	47.7174	30.8	2013-02-08	22:15:04.28	1.148	3.0

58	-17.3975	48.5646	40.3	2013-02-08	17:48:37.80	1.320	4.1
59	-17.2440	48.4381	14.3	2013-02-18	15:19:47.15	1.164	3.1
60	-17.9297	47.3915	67.7	2013-02-20	11:58:28.42	0.765	1.2
61	-18.1977	48.2173	37.9	2013-03-19	00:58:19.63	0.527	2.6
62	-17.3924	48.6777	58.7	2013-03-21	08:26:01.44	1.107	3.2
63	-18.3273	48.7673	8.5	2013-03-29	08:57:15.68	0.508	1.0
64	-17.7687	47.2622	13.4	2013-04-02	01:26:46.21	0.720	1.7
65	-17.6219	48.5026	31.8	2013-04-06	22:05:08.02	0.708	1.3
66	-16.3628	47.5045	9.9	2013-04-06	10:01:13.24	1.212	2.9
67	-17.0438	48.3840	22.6	2013-04-06	12:33:15.97	1.078	3.4
68	-16.0851	48.1553	45.6	2012-03-27	09:33:30.00	1.718	2.5
69	-17.5059	48.3663	20.6	2013-05-06	22:39:56.08	0.624	2.6
70	-18.2583	48.4154	6.4	2013-05-12	00:13:49.04	0.774	2.3
71	-17.4976	47.5220	59.0	2013-05-19	22:53:51.18	1.245	1.9
72	-17.5348	47.9540	0.3	2012-04-10	15:43:00.21	0.559	3.6
73	-17.6387	48.6847	41.2	2013-07-09	00:05:59.87	0.773	2.4
74	-17.4077	48.4926	8.8	2013-08-23	02:02:56.00	0.790	2.9
75	-17.2865	48.3179	42.4	2013-08-23	20:01:05.96	1.363	3.0
76	-18.0544	47.9445	3.1	2013-08-24	06:39:04.27	0.501	2.6
77	-18.1551	48.5847	79.7	2013-03-26	20:27:54.60	0.353	3.2
78	-17.5313	48.5280	14.1	2013-08-23	01:55:15.58	1.345	3.1
79	-17.4386	47.6629	7.9	2013-03-28	04:48:18.34	0.915	2.8
80	-17.8779	47.9214	18.6	2013-04-10	03:58:21.95	0.487	2.9
81	-17.4020	48.6180	22.5	2013-07-28	19:24:06.76	1.139	3.4
82	-17.7780	47.3420	14.6	2013-08-27	10:26:28.48	0.605	1.6
83	-18.3427	48.2272	33.4	2011-11-01	22:43:18.84	0.853	1.2
84	-18.1276	47.7927	39.3	2011-11-21	06:43:17.09	1.124	1.3
85	-18.0072	49.0289	104.7	2011-11-21	23:24:56.48	0.911	3.0
86	-17.9127	48.4642	9.0	2011-11-25	06:35:03.75	0.707	1.1
87	-17.9849	48.7890	124.7	2011-11-26	12:50:51.08	1.037	3.1
88	-16.8850	47.8294	15.0	2011-12-08	23:16:43.96	0.835	3.2

89	-18.2357	47.7778	45.0	2011-12-11	10:32:59.51	2.124	2.7
90	-17.4720	48.4076	2.1	2011-12-26	07:16:25.14	0.787	2.9
91	-17.5841	48.6225	34.4	2011-12-30	06:31:07.92	0.804	2.7
92	-17.3113	48.4607	0.5	2012-01-28	14:16:00.15	0.604	3.2
93	-16.6963	48.5155	34.3	2012-02-01	22:16:56.60	0.930	1.2
94	-17.3148	48.4811	22.6	2012-02-12	15:49:54.29	0.748	2.2
95	-17.4968	48.3505	10.1	2012-03-16	11:56:55.76	0.811	3.5
96	-18.3274	48.5302	21.9	2012-03-22	00:09:54.38	0.657	3.6
97	-15.9220	48.3693	8.8	2012-04-21	19:24:42.88	1.034	1.5
98	-16.5345	49.2571	105.7	2012-06-17	10:11:35.58	0.414	3.7
99	-17.4891	48.7078	75.3	2012-06-25	10:56:09.33	0.754	2.0
100	-17.3622	49.0506	142.7	2012-07-10	13:34:28.02	0.178	1.5
101	-16.1414	48.8867	18.2	2012-07-15	18:17:30.60	0.683	1.6
102	-16.3799	47.5493	4.2	2012-08-05	18:07:09.68	0.574	3.4
103	-18.0251	48.3892	32.0	2012-08-06	02:25:11.97	0.786	3.0
104	-17.6244	48.7141	22.0	2012-08-08	08:07:33.26	0.943	1.5
105	-15.4961	48.1174	21.2	2012-08-11	23:32:12.56	0.695	3.5
106	-17.5614	48.6837	46.1	2012-08-12	17:55:16.32	0.840	1.4
107	-17.6715	47.5774	38.3	2012-08-17	10:11:02.05	0.578	1.6
108	-17.5519	48.3485	13.9	2012-08-24	01:31:31.45	0.942	1.7
109	-17.2541	48.0465	4.5	2012-08-28	08:39:35.17	1.259	3.2
110	-17.3975	48.0394	14.9	2012-09-03	15:25:29.13	1.501	1.2
111	-17.8411	48.0523	0.8	2012-09-09	11:12:21.47	0.840	2.2
112	-18.2666	47.6963	4.7	2012-09-15	20:02:00.50	1.155	1.2
113	-17.9872	47.8548	41.1	2012-10-01	19:06:13.32	1.016	1.3
114	-17.5771	48.4969	22.0	2012-10-04	11:15:42.49	1.158	2.9
115	-17.4636	48.5034	28.8	2012-10-08	05:33:48.25	0.860	3.0
116	-17.9083	47.0692	29.1	2012-10-20	10:34:11.49	0.788	1.1
117	-18.2165	47.5499	13.8	2012-10-25	05:53:25.86	0.758	1.6
118	-17.3201	49.0454	73.9	2012-11-01	00:19:28.69	0.840	4.6
119	-18.2583	47.7501	39.4	2012-11-14	20:15:15.00	1.253	1.2

120	-17.8968	48.2767	8.0	2012-11-27	09:34:19.53	0.699	2.8
121	-18.4087	48.1052	16.7	2012-12-25	14:22:07.09	1.078	2.3
122	-17.6518	48.5758	24.8	2012-12-27	01:31:02.15	0.959	3.5
123	-16.4199	48.7306	17.7	2012-12-29	22:56:04.04	0.557	3.1
124	-17.3839	47.7413	17.9	2013-01-21	16:04:27.73	1.166	2.8
125	-15.8587	47.7818	3.8	2013-02-03	20:57:57.10	0.647	1.1
126	-18.6092	47.7002	33.0	2013-02-08	02:11:44.38	0.908	3.3
127	-17.5956	48.6477	17.0	2013-02-11	21:47:50.52	0.765	2.8
128	-18.2363	48.1283	18.7	2013-02-13	14:00:49.16	0.568	2.5
129	-17.7275	48.2945	20.3	2013-02-24	01:31:50.26	0.802	2.7
130	-17.2221	48.9785	56.3	2013-03-01	00:26:15.11	0.822	
131	-17.7847	47.0764	7.8	2013-03-01	11:03:06.31	0.607	2.6
132	-17.3522	48.8598	30.6	2013-03-04	21:51:17.44	0.764	3.3
133	-18.4119	47.8011	30.0	2013-03-09	23:32:38.64	0.924	3.0
134	-17.5790	48.3578	2.2	2013-03-11	07:12:29.24	0.785	3.2
135	-16.4282	48.0251	2.0	2013-03-18	21:50:52.00	1.090	3.6
136	-17.7213	48.4294	9.4	2013-03-20	04:15:19.58	0.882	1.1
137	-17.3502	48.5618	10.3	2013-03-21	02:08:04.39	0.880	3.3
138	-17.6904	48.2854	31.8	2013-04-06	00:24:47.77	0.580	1.7
139	-17.5411	48.2336	0.2	2013-04-07	21:09:32.16	0.793	2.7
140	-17.1504	47.9507	5.7	2013-04-13	02:26:07.65	1.118	3.2
141	-18.4120	47.6524	35.3	2013-04-29	17:36:15.10	0.765	2.2
142	-18.6299	48.2226	37.4	2013-05-24	02:34:26.04	0.687	3.6
143	-17.8929	47.9150	3.7	2013-06-10	06:25:48.84	0.922	2.9
144	-18.1952	47.4332	32.0	2013-06-16	10:12:15.14	1.298	2.8
145	-16.2474	47.9325	7.6	2013-07-10	05:23:39.49	1.139	1.4
146	-18.3878	47.6628	31.9	2013-07-10	19:43:10.80	1.239	3.5
147	-17.2832	47.6830	11.8	2013-07-12	11:49:20.45	1.039	1.1
148	-17.0596	47.9382	2.5	2013-07-16	07:10:18.28	1.220	3.3
149	-18.3840	47.6917	16.9	2013-07-23	18:57:11.20	0.890	2.6
150	-17.8278	48.2545	19.6	2013-08-05	15:39:05.88	0.842	3.2

151	-17.5843	48.7663	15.8	2013-08-18	09:05:55.95	1.236	3.2
152	-17.5036	48.3705	22.5	2013-08-22	21:27:14.02	1.141	2.8
153	-16.8907	49.1917	81.7	2012-09-23	18:55:12.82	0.752	2.0
154	-17.2576	49.5077	38.1	2013-04-19	22:05:38.40	1.121	2.5
155	-17.7830	49.2704	43.4	2012-06-26	01:34:43.31	1.838	2.8
156	-17.5184	49.4796	22.3	2012-12-06	07:14:41.03	1.468	2.0
157	-17.0881	49.7796	0.1	2013-01-22	09:26:43.49	1.224	1.0
158	-16.8489	49.1966	0.0	2012-10-01	13:41:56.96	1.560	1.0
159	-16.8638	49.0269	18.4	2011-11-24	13:33:45.37	1.560	3.0
ANKARATRA							
160	-19.1517	46.6228	22.4	2012-08-21	20:34:46.34	0.866	1.3
161	-18.9156	46.8479	53.3	2012-08-24	04:10:38.42	0.961	2.0
162	-19.4448	46.7571	10.5	2012-08-24	04:37:10.97	1.175	2.2
163	-19.2951	46.8483	38.9	2012-08-25	00:24:04.82	0.876	1.5
164	-19.2679	46.6441	23.6	2012-08-26	02:03:41.98	1.308	1.4
165	-18.9316	46.7089	3.2	2012-08-30	09:32:12.70	0.755	3.8
166	-19.4336	46.8855	40.4	2012-08-31	12:50:59.10	1.212	2.1
167	-18.1185	46.5410	16.0	2012-09-01	19:06:41.84	0.834	2.9
168	-19.6490	46.5758	0.0	2011-11-14	15:14:13.58	0.132	1.3
169	-19.1299	46.7021	21.6	2012-09-01	18:34:15.72	0.801	2.9
170	-19.2462	46.7258	13.8	2012-09-01	23:31:12.32	1.060	3.9
171	-19.3252	46.7512	30.6	2012-09-02	19:41:46.92	1.190	1.3
172	-19.1162	46.7113	13.6	2012-09-02	07:22:42.82	0.718	1.4
173	-19.1750	46.8501	51.5	2012-09-02	20:19:09.26	1.736	1.5
174	-20.1508	47.2066	3.9	2012-09-03	01:53:00.80	0.970	1.3
175	-19.0004	46.7066	5.5	2012-09-04	21:31:50.06	0.634	1.1
176	-18.7153	46.9139	35.5	2012-09-08	20:04:00.40	1.607	1.4
177	-18.9638	46.7166	16.0	2012-09-09	14:46:28.11	0.313	2.0
178	-18.8873	46.0799	4.6	2012-09-30	15:38:53.68	1.186	1.3
179	-19.4638	46.7326	44.8	2012-10-08	23:21:21.20	1.063	2.0
180	-18.4513	46.8052	4.3	2012-10-14	00:52:05.27	0.915	2.6

181	-18.2128	46.4331	18.3	2012-10-17	16:24:14.77	1.572	1.3
182	-19.0737	46.6922	32.1	2012-10-17	20:27:35.28	0.484	1.3
183	-19.0350	46.6923	19.4	2012-10-18	18:42:23.06	0.951	1.3
184	-18.4910	46.5745	36.2	2012-10-20	18:19:40.68	0.866	1.6
185	-18.8614	46.7544	12.7	2012-10-26	20:15:04.36	0.580	1.1
186	-18.9511	46.6835	4.6	2012-11-01	23:40:49.44	0.938	2.1
187	-18.9523	46.7223	17.0	2012-11-04	01:30:40.23	0.889	1.1
188	-19.6055	47.2365	5.8	2012-11-22	01:50:41.85	2.280	1.2
189	-18.7025	46.6431	1.6	2012-11-23	10:27:10.51	0.308	1.6
190	-20.2000	46.8332	40.0	2012-12-11	21:40:55.44	1.080	2.1
191	-18.9714	46.7306	22.1	2012-12-11	01:08:47.96	0.660	2.7
192	-19.1442	46.6993	19.5	2012-12-16	23:33:48.88	1.032	2.8
193	-19.0860	46.7078	14.3	2012-12-20	07:04:53.59	0.803	1.3
194	-19.1311	46.7397	55.0	2012-12-22	04:27:06.89	0.888	1.4
195	-19.1503	46.6932	12.0	2012-12-22	08:19:47.35	0.434	1.4
196	-18.9594	46.6575	26.4	2012-12-22	21:55:26.12	1.232	3.0
197	-20.0526	46.4129	11.1	2012-12-28	16:48:59.96	0.886	3.3
198	-18.0464	46.2730	14.2	2012-12-30	01:26:38.51	0.841	3.2
199	-19.2027	46.7978	51.4	2013-01-01	17:54:44.72	0.991	2.0
200	-18.0771	46.5074	45.1	2013-01-15	19:10:20.44	0.544	3.3
201	-20.1108	46.4876	0.3	2013-02-04	20:19:49.58	0.656	2.8
202	-18.2635	46.4521	13.3	2013-02-05	23:16:47.26	0.713	2.5
203	-18.1049	46.4065	6.4	2013-02-08	16:51:59.04	1.739	3.2
204	-20.1678	46.8134	42.5	2013-02-10	08:38:06.22	0.827	2.9
205	-18.4689	46.6238	59.5	2013-02-15	17:39:55.46	0.912	1.1
206	-19.3617	46.4956	31.6	2013-02-19	23:04:58.48	0.849	2.1
207	-19.2660	46.7056	45.2	2013-02-20	16:43:41.78	0.943	1.8
208	-18.9703	46.7272	26.1	2013-02-21	23:36:07.88	1.202	3.0
209	-19.2199	46.6192	71.8	2013-03-02	18:38:34.42	1.165	2.5
210	-19.5611	46.7004	71.7	2013-03-04	12:28:14.61	0.826	2.8
211	-18.6589	46.7202	47.6	2013-03-05	05:27:47.14	0.953	1.9

212	-19.4532	46.5044	32.2	2013-03-06	17:46:54.48	0.871	3.5
213	-19.0875	46.7244	29.6	2013-03-08	21:00:30.68	0.494	2.9
214	-18.1895	46.1587	10.4	2013-03-11	17:42:17.70	0.853	2.8
215	-19.1829	46.7400	8.7	2013-03-29	16:22:20.09	0.693	1.2
216	-18.7473	46.6568	41.2	2013-04-05	13:00:29.42	0.394	1.0
217	-19.1024	46.8601	16.8	2013-04-06	09:07:56.31	1.082	1.0
218	-18.9127	46.8586	20.3	2013-04-10	22:11:12.28	0.216	1.0
219	-19.3804	47.0756	42.6	2013-04-10	22:21:35.48	1.115	1.0
220	-19.7186	46.8590	29.9	2013-04-11	11:07:04.34	1.281	1.2
221	-18.4793	46.2429	3.9	2013-04-13	03:47:09.71	0.548	3.1
222	-18.2452	46.7923	57.1	2013-04-15	10:15:13.02	1.981	1.5
223	-18.5947	46.1590	2.0	2013-04-19	10:49:56.43	0.627	3.6
224	-19.5334	46.8134	32.2	2013-04-24	18:49:51.04	1.262	2.7
225	-18.2090	47.1037	0.7	2013-04-25	14:39:34.50	0.322	3.0
226	-20.1593	46.1325	0.6	2013-04-27	06:20:39.16	0.686	1.6
227	-19.7510	47.1043	43.0	2013-05-01	22:55:14.52	1.701	1.9
228	-19.1785	46.7251	3.3	2013-05-06	07:22:21.69	0.780	1.2
229	-18.8056	46.6629	1.8	2013-05-06	00:32:59.70	0.491	3.6
230	-19.2941	46.8216	1.7	2013-05-14	21:04:44.72	0.659	2.9
231	-18.6885	46.1887	18.1	2013-05-17	06:39:55.29	0.805	4.0
232	-18.1954	46.0857	9.4	2013-05-25	17:29:07.92	1.299	2.1
233	-19.8632	46.7167	2.3	2013-05-27	02:49:13.99	0.671	2.6
234	-19.4328	46.7346	18.5	2013-05-29	20:15:53.88	0.966	2.5
235	-18.4032	46.6676	85.1	2013-05-31	06:12:37.30	1.129	2.4
236	-17.8987	45.8996	5.7	2013-06-09	19:05:55.94	0.805	3.2
237	-17.9011	45.9099	4.2	2013-06-22	21:32:55.28	0.430	3.1
238	-19.2880	46.6465	22.0	2013-07-01	16:54:58.07	0.514	1.0
239	-18.2514	46.2285	5.6	2013-08-17	05:41:50.30	0.622	2.0
240	-19.0786	46.7554	17.4	2013-04-06	11:42:26.64	1.187	2.4
241	-17.7713	46.1306	1.4	2013-04-04	16:44:02.19	0.310	2.1
242	-18.5326	46.4355	16.6	2013-04-22	13:43:42.92	1.258	2.9

243	-18.9709	46.7122	5.0	2012-09-02	12:20:08.09	0.538	1.6
244	-18.9682	46.6488	20.1	2013-01-18	10:14:58.86	0.666	3.0
245	-18.8755	46.7654	4.1	2013-04-04	16:40:42.25	0.559	2.4
246	-18.1013	46.4238	19.3	2013-04-05	02:33:54.27	0.848	2.5
247	-17.6417	45.3431	61.5	2013-04-19	00:02:24.45	0.426	1.0
248	-19.2196	46.8220	2.5	2013-04-23	13:21:24.45	1.021	2.7
249	-18.4146	46.4875	76.2	2013-04-24	07:10:25.21	0.426	2.8
250	-18.2715	46.4069	14.6	2013-05-20	06:47:32.98	0.631	2.4
251	-17.7152	45.5449	57.5	2013-05-29	01:54:01.64	0.336	3.0
252	-17.9054	45.8799	40.5	2013-06-08	02:59:25.90	0.557	2.0
253	-18.9452	46.7461	1.2	2013-06-15	13:00:07.61	0.298	1.4
254	-18.2624	46.4936	22.1	2012-03-05	00:39:20.59	0.493	1.9
255	-19.8580	47.0183	18.0	2012-04-05	01:52:36.67	0.154	2.6
256	-20.0712	46.5593	12.6	2012-06-23	11:18:26.46	0.781	4.2
257	-19.1350	47.0205	46.5	2012-08-06	23:54:30.56	1.018	1.7
258	-20.2259	47.2286	13.4	2012-08-08	05:11:14.00	0.462	1.5
259	-20.1255	46.8262	20.2	2012-08-11	13:57:07.25	0.570	1.6
260	-18.6614	45.8384	11.8	2012-08-18	07:05:33.66	0.629	4.2
261	-19.0391	46.7338	4.1	2012-08-23	21:47:11.44	0.538	1.4
262	-19.0389	46.7699	3.8	2012-08-24	02:35:35.67	0.435	2.0
263	-19.0608	46.7423	26.1	2012-08-27	21:46:45.16	0.738	1.3
264	-19.0110	46.7026	2.5	2012-08-29	18:31:38.08	0.525	2.7
265	-19.2476	46.7264	9.9	2012-09-04	20:34:25.48	0.826	1.9
266	-18.8447	46.7283	33.5	2012-09-05	04:10:42.71	0.734	2.4
267	-19.2358	46.7112	1.2	2012-09-06	11:52:28.72	0.732	2.5
268	-18.7297	45.9558	50.7	2012-09-09	08:07:38.20	0.624	1.3
269	-18.9890	46.7093	6.7	2012-09-10	12:52:58.03	0.508	1.1
270	-19.2318	47.1320	16.5	2012-09-12	23:56:17.04	0.806	2.6
271	-18.8842	46.7221	51.2	2012-09-20	10:26:07.09	0.785	1.2
272	-18.9082	46.7341	52.8	2012-09-20	11:13:21.90	1.567	2.5
273	-18.2115	46.4173	43.9	2012-09-21	21:52:17.36	0.690	1.3

274	-20.0567	46.8836	26.3	2012-09-22	06:21:37.47	1.221	3.9
275	-18.9669	46.7357	2.3	2012-09-24	09:12:54.65	0.570	1.0
276	-19.8321	46.7904	1.5	2012-09-26	14:17:43.38	0.421	1.4
277	-18.9613	46.7412	2.1	2012-09-27	23:17:37.38	0.568	3.4
278	-19.0027	46.7215	9.4	2012-09-28	12:59:55.51	0.484	1.3
279	-18.8005	46.7545	14.4	2012-10-10	09:21:22.74	0.614	1.2
280	-18.9555	46.7139	3.9	2012-10-15	11:01:10.04	0.455	1.3
281	-18.8949	46.6649	35.8	2012-10-15	18:35:09.08	0.844	2.3
282	-19.0511	46.7056	2.2	2012-10-16	16:51:47.27	0.482	1.5
283	-18.9662	46.7443	8.9	2012-10-16	22:54:00.60	0.649	1.6
284	-19.0379	46.7150	3.4	2012-10-18	10:42:25.92	0.562	3.0
285	-20.2459	47.0156	30.1	2012-10-18	12:44:24.59	0.760	3.9
286	-19.8322	46.8975	16.4	2012-10-18	17:36:06.00	0.836	4.1
287	-18.5689	45.8117	5.4	2012-10-26	17:18:13.52	0.482	3.4
288	-17.7437	46.2199	5.9	2012-11-02	21:57:55.52	0.926	1.7
289	-18.6911	46.1178	15.5	2012-11-03	03:03:57.97	0.712	2.2
290	-19.0127	46.7246	1.5	2012-11-04	01:22:33.49	0.626	2.4
291	-18.1702	45.5861	51.8	2012-11-16	16:40:28.28	0.287	3.3
292	-19.5877	46.9067	4.9	2012-11-22	09:46:33.12	1.326	3.4
293	-19.8932	47.2026	18.9	2012-11-26	06:18:33.83	1.134	3.6
294	-20.4672	46.6548	19.1	2012-11-27	00:40:11.44	0.767	1.6
295	-18.9655	46.7977	11.5	2012-12-03	18:06:22.84	0.745	1.9
296	-18.5806	46.7098	31.1	2012-12-05	04:47:38.96	0.790	1.7
297	-17.9236	46.0170	82.2	2012-12-12	07:03:40.45	0.949	2.3
298	-18.9043	46.7430	21.0	2012-12-16	17:33:10.96	0.528	1.7
299	-19.7460	46.5211	24.8	2012-12-16	20:08:52.64	0.810	2.8
300	-19.0369	46.7233	5.0	2012-12-17	03:39:29.26	0.376	2.7
301	-18.9831	46.7336	3.5	2012-12-21	00:44:46.24	0.607	2.7
302	-18.9400	46.7860	36.9	2012-12-22	00:17:16.71	0.879	2.9
303	-19.0562	46.7235	3.0	2012-12-22	03:47:40.36	0.462	3.1
304	-18.9457	46.6910	5.9	2012-12-23	04:48:13.42	0.497	1.7

305	-19.0363	46.7268	4.1	2012-12-24	12:17:16.10	0.419	3.5
306	-20.3037	47.0926	29.1	2012-12-26	16:41:54.49	0.640	2.2
307	-19.0002	46.7324	3.4	2012-12-30	22:58:20.52	0.728	3.0
308	-18.9425	46.7123	4.6	2013-01-01	04:43:16.57	0.575	3.0
309	-18.9470	46.7012	20.4	2013-01-01	05:27:13.94	0.553	2.7
310	-18.9583	46.7137	21.0	2013-01-01	08:39:55.66	0.629	2.7
311	-18.9606	46.7034	21.8	2013-01-02	06:46:33.06	1.061	2.8
312	-18.8618	46.7709	17.6	2013-01-04	21:39:50.50	0.449	2.8
313	-18.9934	46.7356	8.2	2013-01-07	11:48:19.54	0.632	3.1
314	-18.9687	46.7524	14.1	2013-01-08	12:02:12.96	0.503	1.5
315	-18.9721	46.8120	13.0	2013-01-08	16:01:19.52	0.676	2.5
316	-18.6693	45.9425	9.9	2013-01-13	13:24:54.57	0.541	4.2
317	-19.0026	46.7331	19.4	2013-01-14	23:45:53.16	0.486	3.7
318	-19.0301	46.7251	7.6	2013-01-15	15:44:11.62	0.520	3.4
319	-18.9345	46.6452	25.9	2013-01-18	09:25:53.11	0.597	2.9
320	-18.6945	46.0739	13.1	2013-01-20	12:09:02.65	0.688	3.0
321	-18.7563	46.5999	15.1	2013-01-21	17:22:04.36	0.582	2.8
322	-18.4920	45.7712	5.9	2013-01-23	02:16:03.31	0.519	1.0
323	-19.6023	46.9174	22.6	2013-01-26	19:57:13.98	1.253	3.2
324	-19.0321	46.7510	29.6	2013-02-02	06:24:45.82	0.569	2.1
325	-18.1368	46.6757	20.3	2013-02-04	09:21:52.47	0.848	3.0
326	-18.5723	46.6737	7.1	2013-02-05	06:25:17.80	0.302	2.8
327	-18.6256	46.3633	78.8	2013-02-11	11:03:35.19	0.297	2.3
328	-18.1248	46.5113	40.9	2013-02-15	13:52:03.29	0.766	2.0
329	-18.3605	46.5538	0.4	2013-02-21	07:27:14.18	0.659	3.2
330	-18.9766	46.7646	6.9	2013-02-22	01:21:06.53	0.804	3.0
331	-18.9067	46.7527	18.1	2013-02-26	00:53:23.35	0.744	2.5
332	-18.2374	45.8239	20.9	2013-02-27	02:23:14.12	0.732	2.4
333	-17.7488	46.1903	3.4	2013-03-03	11:12:09.29	0.793	3.0
334	-20.2214	46.7462	11.1	2013-03-04	07:57:45.12	0.914	3.1
335	-19.0161	46.7311	19.2	2013-03-05	04:03:21.04	0.678	2.0

336	-19.3001	46.6855	3.0	2013-03-08	20:48:03.04	0.663	3.0
337	-19.2414	46.6467	8.9	2013-03-30	12:52:05.86	0.772	2.8
338	-18.3714	46.7740	13.3	2013-04-02	03:26:03.02	0.640	2.3
339	-19.3832	46.9626	27.3	2013-04-03	21:46:42.76	1.173	2.3
340	-19.0551	46.7236	2.8	2013-04-06	11:40:35.80	0.425	3.7
341	-18.4140	46.8265	1.4	2013-04-08	06:24:09.44	0.894	3.2
342	-18.4715	46.6736	6.6	2013-04-10	14:02:35.03	0.378	2.9
343	-19.8091	46.5738	19.7	2013-04-15	11:52:03.10	0.850	2.7
344	-19.0597	46.6074	15.4	2013-04-18	00:09:36.17	0.846	3.5
345	-19.0211	46.7228	0.9	2013-04-21	01:09:07.48	0.457	3.0
346	-19.0116	46.9430	45.4	2013-05-05	18:23:32.42	1.194	3.5
347	-18.9736	46.7472	14.0	2013-05-07	13:46:23.83	0.590	2.9
348	-18.3514	46.3078	17.5	2013-05-10	23:22:31.24	0.600	2.7
349	-19.0555	46.7236	4.7	2013-05-13	14:40:15.04	0.427	2.7
350	-18.3518	46.4425	17.1	2013-05-17	22:22:47.24	0.606	3.0
351	-19.1703	46.6603	15.3	2013-05-23	00:17:03.14	0.638	4.0
352	-19.0543	46.7233	4.8	2013-05-27	03:17:21.43	0.515	2.3
353	-18.9735	46.7375	14.2	2013-05-27	06:31:39.78	0.495	2.7
354	-18.8210	46.1377	31.8	2013-06-04	02:01:33.70	0.669	2.1
355	-17.8815	45.7957	63.0	2013-06-09	02:24:03.15	0.333	3.3
356	-19.3568	46.9785	10.2	2013-06-11	23:16:10.56	0.931	3.2
357	-18.6435	45.4413	12.1	2013-06-20	05:13:03.70	0.381	2.4
358	-18.2624	46.4973	16.4	2013-06-28	02:39:45.20	0.627	3.0
359	-18.4060	46.5680	5.6	2013-07-02	06:40:06.94	0.681	3.2
360	-17.9102	45.8758	38.5	2013-07-06	11:25:47.92	0.768	2.9
361	-18.3561	46.4271	35.2	2013-07-17	23:45:34.52	0.606	2.0
362	-19.0561	46.7281	10.7	2013-07-19	03:05:29.71	0.414	2.7
363	-20.1092	47.2120	24.0	2013-07-20	10:50:24.56	0.774	2.9
364	-19.0845	46.6850	12.6	2013-07-28	05:02:34.46	0.611	2.5
365	-18.7384	46.9500	5.6	2013-08-02	23:42:41.72	0.732	3.3
366	-18.4917	45.5701	1.7	2013-08-03	21:15:07.72	0.504	3.0

367	-18.5851	45.9014	16.9	2013-08-04	20:10:28.26	0.839	2.0
368	-20.0016	47.2161	18.4	2013-08-12	00:40:58.33	0.843	2.1
369	-19.9492	47.3633	5.7	2013-08-27	16:15:15.00	1.288	2.4
370	-19.4041	46.9285	12.4	2013-08-30	22:25:11.16	1.128	3.2
371	-19.4095	47.0188	16.4	2013-08-31	03:47:55.26	1.079	3.1
372	-18.8354	46.7492	6.5	2012-09-23	20:39:37.44	0.469	3.7
373	-18.2193	46.3558	20.6	2012-09-25	22:47:06.02	0.750	1.6
374	-16.6555	45.4243	0.5	2013-04-02	01:49:27.51	1.468	1.4
375	-17.2392	45.9166	8.1	2013-05-18	22:13:43.12	1.738	1.2
376	-16.9239	45.5991	15.0	2012-04-23	21:13:15.12	0.953	2.6
377	-16.9080	45.6619	14.4	2012-05-12	02:12:52.76	1.435	4.1
378	-17.3019	45.6426	13.5	2012-10-28	12:58:12.15	1.253	3.1
379	-16.9517	45.7089	3.8	2013-01-09	23:54:38.86	1.332	4.0
380	-16.8334	45.6551	36.9	2013-02-23	17:55:53.96	1.467	3.6
381	-18.4688	44.6179	13.3	2013-04-10	01:21:10.83	1.180	2.6
382	-18.6854	44.7975	0.0	2013-02-20	14:12:14.06	1.407	2.5
383	-18.5548	44.7289	0.0	2013-04-11	14:37:18.26	1.243	2.9
384	-18.5074	44.7336	10.5	2013-06-13	20:29:39.56	1.075	1.7
385	-19.4574	46.1085	10.0	2013-06-09	23:34:18.16	1.153	2.3
386	-19.7163	46.0448	6.7	2013-08-02	15:46:57.36	1.153	1.3
BEKILY							
387	-24.7374	44.4723	3.2	2012-09-18	22:37:29.06	0.606	2.0
388	-24.4777	45.2486	41.4	2012-10-10	16:27:59.63	1.534	3.6
389	-23.4418	44.9963	7.4	2012-10-25	10:25:45.82	1.643	1.3
390	-25.0237	44.8397	5.4	2013-01-24	13:36:45.24	0.847	2.4
391	-24.2756	44.5292	29.8	2013-03-26	10:08:39.09	0.843	1.4
392	-24.2881	44.4996	0.8	2013-03-26	21:12:53.62	1.125	2.7
393	-24.2950	44.4213	16.5	2013-03-26	10:08:38.07	0.898	3.1
394	-23.4650	44.7536	48.4	2013-08-27	05:58:33.52	2.154	2.9
395	-24.1671	44.3830	17.1	2013-03-26	10:05:37.90	1.485	1.2
396	-24.3761	44.6299	29.3	2013-03-26	23:29:52.96	0.723	3.2

397	-24.2897	44.4385	0.9	2013-03-26	10:06:45.70	0.892	1.3
398	-23.6172	45.0040	52.7	2012-07-30	16:45:51.38	1.421	3.9
399	-23.7414	44.8965	89.5	2012-06-06	22:12:02.40	0.867	2.8
400	-23.2015	44.9539	1.7	2012-08-16	23:51:06.40	0.850	2.9
401	-24.4959	45.0884	1.0	2012-09-19	05:17:48.22	0.919	1.1
402	-24.4439	44.9622	19.8	2012-11-04	12:49:25.69	0.839	3.8
403	-24.2005	44.8125	17.8	2013-01-02	10:15:14.93	1.057	2.8
404	-24.4739	44.1831	4.1	2013-01-04	06:35:13.05	0.852	2.8
405	-24.4718	45.0664	1.1	2013-01-25	01:00:55.04	0.874	1.2
406	-23.8206	44.5830	20.9	2013-01-29	01:43:30.55	1.441	1.8
407	-26.0533	44.8818	5.3	2012-12-26	17:48:55.56	0.882	3.3
408	-25.5187	44.9511	14.1	2012-11-08	05:29:13.40	0.942	3.8
409	-25.6724	45.0018	14.5	2012-12-11	15:06:41.87	0.894	3.0
410	-25.6850	44.8419	0.9	2012-12-28	09:08:13.01	0.744	3.3
411	-25.5365	44.9310	4.7	2012-12-29	09:07:22.44	0.857	2.8
412	-26.1181	44.6469	0.7	2012-12-30	20:57:25.56	0.989	2.7
413	-25.7180	44.8685	9.8	2013-08-26	22:11:43.60	0.754	3.3
414	-22.1439	47.0456	14.4	2013-01-19	04:19:03.52	0.844	3.5
415	-22.6200	47.8471	5.5	2013-02-01	12:37:11.69	1.245	2.9
416	-22.7147	47.5163	19.1	2013-02-18	04:06:33.49	1.186	3.8
417	-24.2507	45.7033	14.4	2012-08-22	23:25:56.76	1.033	3.2
418	-23.7649	46.1661	11.9	2012-09-05	10:44:52.82	0.852	1.6
419	-23.9563	46.0454	18.6	2013-03-01	01:18:57.83	1.032	1.3
420	-23.7783	46.4255	0.1	2012-12-30	18:40:53.40	1.070	1.7
421	-23.1927	43.5766	69.2	2012-09-01	10:10:11.04	0.476	4.0
422	-23.5760	43.5000	92.7	2013-01-25	23:37:00.40	0.476	5.3

Appendix D: Example of FOCMEC input files

1. Example of input files for FOCMEC

The first shows the information about the seismic event (Year-month-day-hour-minute-second-latitude-longitude-depth -event identity). The following lines are the phase polarities information. First column indicates the station code, second column is the azimuth, the third column is the takeoff angle following the phase identity (U: Compression, up, D: Dilatational D, B upswings for $S_{H,}$ F downswings for $S_{H,}$ L downswings for $S_{V,}$ and R upswing for S_V)

20120811233211921 5S2614 48E 699 1293 17 89 55 1
ANLA 150.00   48.00D
ANLA 150.00   48.00D
BAEL   35.00   68.00U
BAEL   35.00   68.00B
BANJ   10.00   48.00U
BARY 215.00   48.00U
BERG 252.00   75.00U
BERG 252.00   75.00B
ZOBE 197.00   48.00U
MAJA 260.00   48.00U
MAJA 260.00   48.00L
MAJA 260.00   48.00F
ANTS 348.00   75.00D
ANTS 348.00   75.00B

2. Example of input files parameters for FOCMEC

FM_1_SV_SH.out Output file name [focmec.out]

Sakhalin: 8 BB stations no ratios, 0 polarity errors: ak135 with no crust

/* Previous line comment (up to 80 char) Next line input file [focmec.iknp]

FM_1_SV_SH.inp

correct file [y]

relative weighting..[y]

y Total polarity option

0 allowed polarity erors..[0]

100 exit after this many acceptable solutions...[100]

minimum B trend [0]

1 B increment [5]

359 maximum B trend [355]

min B plunge..[0]

1 increment [5]

89 maximum..[90]

minimum Angle..[0]

1 increment [5]

179 maximum [175]

EOT

Different angles are shown in this table such as

- The minimum and maximum B trend angles indicate the limits for the B axis trend. I choose the value of 1 for the increment to get best fit of the solutions instead of 5, I set 1 at the increment for each calculation, then I must set the angle into **359**, because this B-axis trend is turning from **0 to 360** degrees.
- The minimum and maximum angle for the B-axis plunge, maximum value is set to 89 after setting the increment value into 1 because this axis is turning from 0 to 90 degrees.
- About the A angle, which is the angle that N makes with the plane defined by the vertical (down) and the B-axis trend, the choice of the increment value is the same as for B axis with the same reason and if I set it into 1, I have to change the maximum

angle into 179 in order to get 180 degrees. All values presented inside square brackets in Table 2 and Table 3 are the default values of the FOCMEC.

3. Flow chart showing the different steps to determine focal mechanism solutions

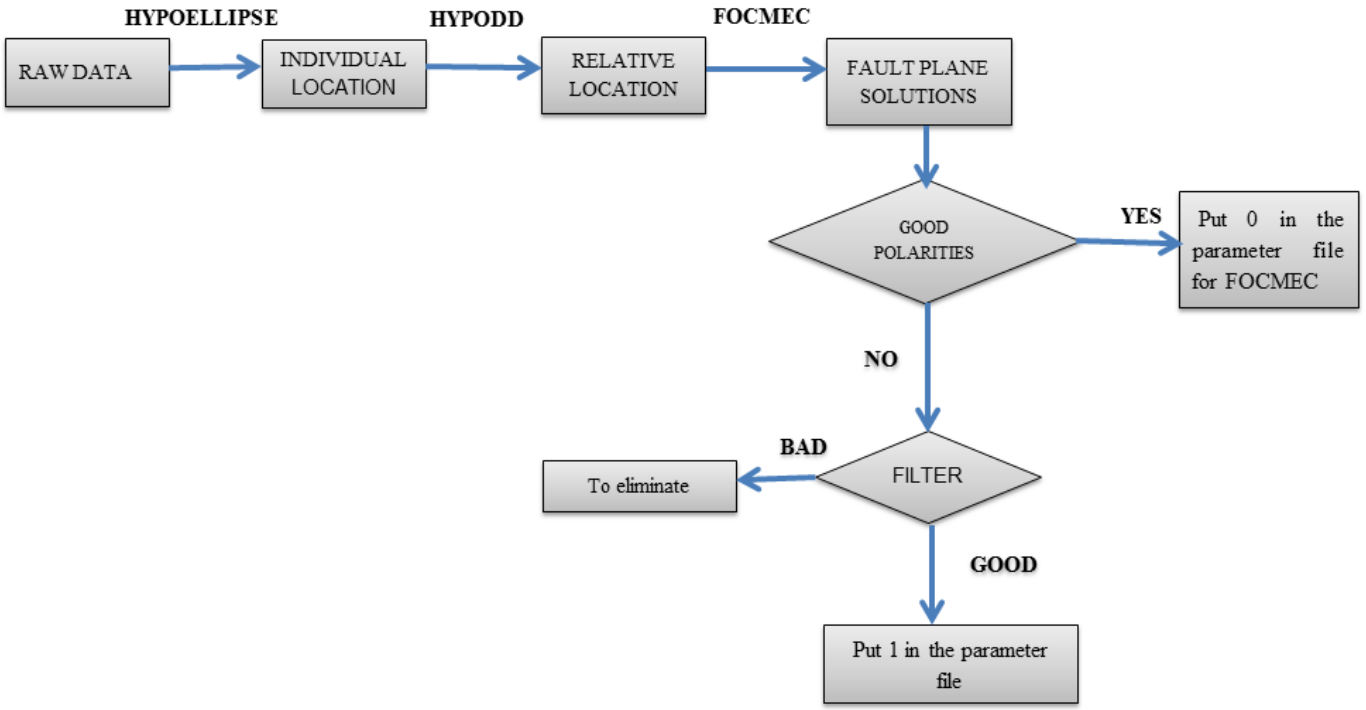

Appendix E: Paper about Stress field in Madagascar paper (In Prep.)

Determining the stress field in Madagascar using focal mechanism data

Tsiriandrimanana Rakotondraibe[1], Andrew A. Nyblade[1,2], Michael E. Wysession[3], Raymond Durrheim[1], Gérard Rambolamanana[4], Ghassan Aleqabi[3], Patrick Shore[3], Martin J. Pratt[3], Fenitra Andriampenomanana[1], Georg Rümpker[5], Elisa Rindraharisaona[6].

1. *School of Geosciences, University of the Witwatersrand, Private Bag 3 - 2050 Wits, Johannesburg, South Africa*. E-mail: tsitsikel@gmail.com.

2. *Department of Geosciences, Penn State University, University Park, PA 16802, USA.*

3. *Department of Earth and Planetary Sciences, Washington University in St. Louis, Campus Box 1169, 1 Brookings Dr., Saint Louis, MO 63130-4899, USA.*

4. *Institut et Observatoire de Géophysique d'Antananarivo, Université d'Antananarivo, Ambohidempona - B.P 3843, Antananarivo 101, Madagascar.*

5. Institute of Geosciences, Geothe-University Frankfurt, Altenhöferallee 1, 60438 Frankfurt, Germany.

6. *DeutschesGeoForschungsZentrum (GFZ), Telegrafenberg, 14473 Potsdam, Germany.*

ABSTRACT

Stress field inversion in the whole part of Madagascar has been investigated using focal mechanisms data computed from seismograms recorded by the local permanent stations and the MAdagascar-COmoros-MOzambique (MACOMO) temporary seismic network. In order to characterize the direction of the main axis for stress, a subset of 182 focal mechanisms solutions from earthquake data between 2000 and 2016 with magnitude $M_L \geq 2.5$ was inverted after dividing the area into six regions. The inversion follows Michael's method based on a linear procedure. Focal depths of the selected earthquake are ranging between 1 km and 45 km. With 182 focal mechanisms, shape ratio and friction values from each region are obtained also the direction of the minimum and maximum principal stress. The results show domination of normal faulting in the central region and a tendency for strike-slip and thrust faulting in the northern and southern regions of Madagascar according to the direction of the principal stress. The observations may infer a potential effect caused by the separation of Madagascar from Africa, India, and Somalia.

Keywords: Stress direction, focal mechanisms, shape ratio, frictions, Madagascar.

1. INTRODUCTION

In this study, we deal with the question of how a tectonic stress in the crust in Madagascar is estimated using focal mechanisms data. We target on some regions in Madagascar such as in Bemarivo, Alaotra, Famoizankova, Ankaratra, Itremo, and Bekily regions, where some clusters of earthquakes data were presented.

As proposed previously, the tectonic framework of Madagascar is characterized by its detachment from the Gondwana supercontinent and later to the Indo-Australian Plate (Coffin & Rabinowitz 1987; 1988; de Wit 2003). The separation of Madagascar from Somalia and the east Africa led to an extensional regime accompanying the volcanism in the late Cretaceous and Cenozoic (Eocene and Miocene) (Storey *et al.* 1995), whereas in the south, an extensive volcanism is associated to the second rifting caused by the extension of the east African rift (Collins *et al*. 2000). The drifting of Madagascar gave way to the extreme extension in central Madagascar and formed the Neoproterozoic to Cambrian association of Gondwana that dominated the geology in northern and central part of Madagascar. While geological structure of Madagascar holds some deformation, some previous studies did not explain how intraplates faults literally achieves this. It can be explained by seismotectonic study in the whole part of the island which is less known except in the central area of Madagascar because of the scarcity of the earthquakes data (*e.g*., Rindraharisaona *et al*. 2013). High extensional E-W direction in the central region of Madagascar was seen using seismic data from the local permanent seismic station in Madagascar. The identified high seismic active zones are Famoizankova, Alaotra, and Ankaratra regions (*e.g*., Bertil & Regnoult 1998). Since, not only large historic earthquakes such as on November 3rd, 1897 in Itasy and on September 14th, 1932 in Mantasoa (with intensity VIII and VII on Mercalli scale, respectively) occurred in Madagascar but also some recent seismic events in Famoizankova on April 21st, 1991. They took place along the seismic zone and gave tendency to reveal the relation between seismic activity and fault activity. On this background, seismotectonic observation was performed in the whole part of Madagascar using

data from the permanent seismic stations and the temporary seismic stations of MACOMO (Pratt *et al.* 2017), SELASOMA (Rindraharisaona *et al.* 2013) and RHUM-RUM (Stähler *et al.* 2016) projects (Table 3. 1).

Our main object for studying stress in Madagascar is to afford an interpretation of crustal seismicity in regard of longer deformation; stress reduced brittle failure mechanism for regional distributed crustal strain.

2. SEISMOTECTONIC SETTING

2.1 Geology and tectonics

Madagascar is divided into two major domains: metamorphosed and migmatized Precambrian rocks comprise the eastern two-thirds of the island; while a younger sedimentary basin, which includes some volcanic rocks, covers the western third (Bésairie 1971, 1973; Hottin 1972). The main geological units, boundaries of major tectonic domains and traces of major shear zones are shown in Figure 1. 3.

The northern part of Madagascar is characterized by metamorphosed and migmatized Archean rocks (around 2600-3000 *Ma*) (Caen-Vachette 1979). Various tectonic units are observed in this zone. The Bemarivo belt defined as the northernmost Precambrian terrane. The Antongil belt consists of east-west-striking metasediments, granites and gneiss (Tucker *et al*. 1999). This region intersected and is subdivided into the Antananarivo cratons and the Neoproterozoic Anaboriana belt (Bauer *et al*. 2011), it is characterized by the Sandrakota and Andaparaty shear zones which are prominent tectonic features (Figure 1. 3) including the Archean Antogil belt that consists of the Antananarivo craton and the Neoproterozoic Anaboriana belt (Bauer *et al*. 2011). The separation of Madagascar from Somalia might cause the Neoproterozoic structure in this area which gave away to the southward motion of Sandrakota, Andaparaty, and Takarindoha shear zones along two strike-slip zones (Collins *et al.* 2000, Bauer *et al*. 2011). The volcano-sedimentary sequence occurs predominantly talong the coast in the western part of Bemarivo belt. Although it is still debate about the fault structure

in the northern part of the island, the increasing numbers of earthquakes around the different shear zones are important for this study. This block was separated from East Africa (Fitzsimons & Hulscher 2005) and deformed during an early Neoproterozoic orogenesis (Collins *et al*. 2003, Collins 2006).

The central of Madagascar is dominated by the Antananarivo block, in which forms the largest pre-Paleozoic tectonic unit of Madagascar (Figure 1. 3). During the Neogene (*ca.* 10 - 15 *Ma*), an extensive uplift zone is observed in the central and northern part of Madagascar (De Wit 2003). This is caused by the African rifting system (Collins 2000). In addition to this, the lavakas or channels that correlate to the seismic activity (Cox et al. 1998) characterize central area of Madagascar. Several major shear zones cut through the Antananarivo block, notably the NNE-striking Pan-African of Angavo shear zone cuts through the Antananarivo block (Grégoire *et al.* 2009). It is sub parallel to the Alaotra-Ankay rift (Figure 1. 3), which lies along the southeastern margin of the Antananarivo block. The Alaotra - Ankay rift has similar morphology to the East African Rift system (Bertile & Regnoult 1998) and the Alaotra and- Ankay basins are separated by the NE-SW trending high zone of Andaingo. This region is also defined as an uplift zone defined by the existing volcanism in this area. Some Quaternary volcanic rocks are found in Antananarivo block, such as in the Ankaratra and Itasy regions. The volcanic area of Ankaratra is formed from the processes triggered by intra-continental rifting and the overlaying Precambrian basement or Neogene volcanic rocks (Berger *et al*. 2014). It is localized in the southwest of Antananarivo (Figure 1. 3).

.

The southern part of the island is represented by the main shear zone of Ranotsara that showing the boundary between the Ikalamavony and the Anosyen domains. In addition, the Beraketa shear zone that trends N-S with strike-slip shear zone is also seen in the southern part of Madagascar and following by the Anosyen and Androyen domains (*e.g*. Martelat *et al*. 2000, 2014). The Ampanihy shear zone is also seen that trends N-S and parallel to the Beraketa shear zone (Figure 1. 3). The south-central part of Madagascar is defined by the Itremo group which is banded by the Betsileo

shear zone and interpreted to be a dipping thrust fault that formed an extensional detachment (Collins *et al*. 2000). The Betsileo shear zone is caused by the post collisional extension deformation in central Madagascar (Collins *et al*. 2000). From Martelat *et al*. 2000, the west-central region of Madagascar is composed by the Ifanadiana shear zone which correlates with the Angavo shear zones in the central of Madagascar.

The 200 km NW-trending Ranotsara Shear Zone (RSZ) cuts across the crystalline shield of southeastern Madagascar. The region south by the RSZ is characterized by several N-S trending tectonic belts such as the Vohibory, Ampanihy, Bekily, Betroka (Windley *et al*. 1994), Beraketa, and Tranomaro (De Wit *et al*. 2003; Martelat *et al*. 2000; 2014).

Seismicity in Madagascar is attributed to the reactivation of zones of weakness in the crust that were formed during the Pan African orogenesis and the separation of Madagascar from Africa and India (Bertil & Regnoult 1998, Fourno & Roussel 1994) and a thermally-driven bulge of the lithosphere (Bertil & Regnoult 1998; Rambolamanana 1989).

The source mechanism of earthquakes occurring in Madagascar has previously been studied by Bertil & Regnoult (1998), Rindraharisaona *et al*. (2013), and Rakotondraibe *et al*. (submitted). Grimison & Chen (1988) obtained a normal fault striking north-south near the Davie ridge after selecting the seismic events on May 18th, 1965. They used waveform and absolute amplitude of P-and SH-waves. An NNE trending along the eastern coast of Madagascar was detected after Segoufin & Patriat (1981), but a N8°W direction feature in the Ankaratra volcanic area was established by Kutina *et al.* (1975). Shudofsky (1985) used Rayleigh wave inversion and body-wave modeling to obtain a thrust fault mechanism for the 4 April 1975 with M_w= 5.4 earthquake characterized by strike=245°, dip=85° and rake=140°. Poisson (1924, 1930) realized that Madagascar is under regulating seismic activity. Most of the earthquake events occurred in the central part of the island as defined in Figure 5.

1, and they are still occurring in this area (Rakotondraibe *et al.* submitted). In addition to this study, data from the local permanent seismic station including data from the temporary stations are introduced into the research. According to the obtained focal mechanisms, domination of normal faulting is seen with depth varying 1 km to 45 km (Rakotondraibe *et al*. submitted).

Rakotondraibe *et al*. (submitted) located the hypocenters of 695 Malagasy earthquakes and found that they are distributed throughout the crust. From previous studies, an extension direction of N10°E trending was observed in the central area of Madagascar with hypocenters located at depth of 15 km – 21 km in the Alaotra and Ankay regions and 12 km -25 km in the Famoizankova area (Rindraharisaona *et al*. 2013).

2.3 Clustered volcanic events

A major magmatic event occurred during the late Cenozoic, mainly in the central regions (Ankaratra, Itasy) and in the north (Takarindoha) (Tucker *et al*., 2011). From Gasse & Campo 2001, De Wit 2003; the volcanic of Ankaratra occurred during the Late Pleistocene and the late Cenozoic magmatism and is associated with intracontinental rifting, thus the central area of Madagascar is represented by an extension of the Somalian-African diffusive plate boundary.

A Quaternary volcanic field is found in the Itasy-Ankaratra region in central Madagascar (southwest of Antananarivo). It has been proposed that the Itasy area is experienced by uplift during the past 10-15 *Ma*, which is caused by a thermal bulge (De Wit 2003; Bertil & Regnoult 1998).

3. METHODOLOGY

3.1 Data

In this study, focal mechanisms results from seismic events recorded by the Madagascar National Data Center (NDC) stations including the MACOMO stations (Pratt *et al*. 2017, Rakotondraibe *et al.* submitted) during 2000-2016 are analyzed. A

total number of 182 focal mechanisms from initial hypocenter locations are taken for the analysis. All data are selected according to their distribution and the characteristics of the tectonic unit. Locations of the seismic stations are displayed in Figure 3. 1 and distribution of focal mechanisms from the selected local earthquakes is presented in Figure 5. 2.

With respect to the structure depending to the seismic activity that occurred in Madagascar, we divided the area into six regions and selected the clustered events from each region (Figure 5. 2). Characteristics of seismic stations and the data are defined and supplemented in Figure 5. 2 and in the Appendix F, respectively.

3.2 Methods

Earthquake relocation

In order to make the processing reliable, high-quality seismic events from the combined bulletin NDC and MACOMO between 2000-2016 are relocated using the double difference method of HYPODD (Waldhauser 2000, 2001) program providing a calculated 1-D velocity model using results Fenitra Andriampenomanana et al. submitted). (Figure 1. 6). The improved focal mechanisms distribution with magnitude and depth classification is illustrated as example in Figure 4. 8. Parameter files introduced for the double-difference method are listed in Table 2. 2

Focal mechanisms

Focal mechanism determination is the most important field to understand the tectonic process from the earthquake data. To retrieve the focal mechanisms solutions, we applied the grid-search method of FOCMEC program (Snoke 2004) using first P-wave polarities and some clear S-wave polarities. This technique is based on the seismic station distributions in order to cover the earthquake seismic sources. In addition to the results obtained from Rakotondraibe *et al.* submitted, we determined more focal mechanisms using data from the local permanent stations and applying the same method and the same program with FOCMEC software. We first

estimated the azimuth and take-off angles of the rays arriving at each station using results from HYPOELLIPSE program (Lahr 1999) after introducing the calculated average local crustal model using results from Andriampenomanana *et al*. (2017), and then we inserted all values of take-off angle and azimuth into FOCMEC program. Parameter files used for focal mechanism determination are listed in Appendix D. Focal mechanisms solutions from the 182 earthquakes are shown in Figure 5. 2

Inversion for stress from earthquake mechanisms

Stress inversion

In order to manage comprehensive focal mechanism inversion to determine relative magnitude and stress orientations in the whole part of Madagascar, several methods have been proposed (Angelier 1984, Gephart & Forsyth 1984, and from Michael 1984, 1987). All of the methods assume (1) the uniformity of the stress in an area; (2) the occurrence of the earthquake in a various orientation in a region; (3) the point of the slip vector in the direction of shear stress on the fault (Wallace-Bott hypothesis, Wallace 1951, Bott 1959); and (4) the non-interaction of the earthquakes with each other and the non-distortion in the background tectonic stress. Generally, the stress tensor is with the normalized maximum compressive stress (Michael 1987) and is determined according to the type of focal mechanism (normal, strike-slip, and thrust faulting).

In this study, we applied a linear stress-inversion technique by Michael (1984, 1987) in the STRESSINVERSE package (Vavryčuk 2014) that depends on an iterative calculation for the determination of the principal stress σ_1, σ_2, σ_3, the shape ratio, and the friction values (Equation 1). The shape ratio value represents the relative magnitude of the principal stress calculated according to the geology and the tectonic structure of the area study, while the friction values characterize the fractures in the rocks

The shape ratio value is defined by the following formula (after Angelier 1984):

$$R = \frac{\sigma_2 - \sigma_3}{\sigma_1 - \sigma_3}$$ (equation 1)

where σ_1, σ_2 and σ_3 are the stress axes and R is the shape ratio value.

Application was done after introducing 182 varieties of focal mechanisms within Madagascar between 2000 and 2016 in which the condition of uniform tectonic stress may be reasonable to assume (Figure 5. 2). With respect to the structure depending to the seismic activity that occurred in Madagascar, we divided the area into six regions and selected the clustered events from each region (Figure 5. 2). According to the distribution of the earthquake data, we subdivided the region of Alaotra and Ankaratra into three (A, B, C) and two (D, E), respectively (Figure 5. 2). Large amounts of normal mechanisms have been determined in the central region of Ankaratra, Famoizankova and Alaotra (ANK, AL, FAM) (Figure 4. 2) and some strike-slip and reverse faulting are seen in the northern and southern regions of Madagascar (BE, BEK) (Figure 5. 2).

Summary description of the focal mechanism in each region is given in Table 5. 1: according to the various sub-regions (A, B, C, D, and E).

4. RESULTS

The inserted focal mechanisms for each region are classified on the ternary diagrams (Figure 5. 3) where the three principal modes of faulting are connected to different corners (Frohlich & Apperson 1992). All mechanisms were selected with 65% confidence for the stress field inversion in order to get the best orientation of the principal stress.

For each of the six regions containing focal mechanisms, the individual observations are presented in four different manners as seen in Figure 5. 4 as example. The individual T- and P- axes are plotted as a stereograph with different symbols, included the shape ratio value distribution (R), the Mohr Coulomb plot, and the confidence of the principal stress axes from each region.

The direction of the maximum and the minimum compressive stresses (σ_1) in red color and (σ_3) in blue color, respectively, from each focal solution are also presented. We proceed to show results of each of the six regions in more detail.

4.1 Bemarivo

After the inversion of 20 focal mechanisms data, azimuths and plunges of the three principal stresses axes σ_1, σ_2, σ_3 are presented, for the maximum stress azimuth and plunge values are equal to 21° and 86°, respectively (Figure 5. 5). Average stress direction for σ_1, σ_2, and σ_3 are trending 247°, 151°, and 345°, respectively. Values of the shape-ratio vary from 0.30 to 0.70, and the friction value is equal to 0.71.

4.2 Bekily

In the southern region of Madagascar the σ_1-axis change their direction in average from 308° and plunging 5.8° from the horizontal after introducing 23 focal mechanisms. The spatial variation of the intermediate stress and minimum stress σ_2 and σ_3 trend 218° and 99.7°, and plunge 3.1° and 83.34°, respectively (Figure 5. 7). Value of the shape ratio varies from 0.2 to 0.5 and the friction value is equal to 0.75.

4.3 Famoizankova

Domination of normal faulting was seen in the Famoizankova region. A total number of 15 focal mechanisms were introduced into the inversion for stress determination. We found that the direction of the P- and T- axes is mostly uniform (Figure 5. 9) with average azimuthal value of 195° and 37° for σ_1 and σ_3 direction, respectively; and plunging 79.1° and 10° down from the horizontal. The intermediate stress direction trends 306° and plunges 4°. This direction is consistent to the average dip of P-axis. For the σ_3 principal stress axis, the direction trends from N343°W which tend to be horizontal. Obtained results are consistent to the average dip of T-axis.

4.4 Alaotra

Majority of the main orientation of the strike are noted in the range between 170° - 260° for all sub-regions and both nodal planes show dips that can be either relatively gentle from about 40° - 53°, and the rake present peak in the range of -90° to -84°. The cluster denotes a major tendency for normal faulting.

Characteristic of stress in the Alaotra region was obtained from the 86 inverted focal mechanisms after subdividing the region into three sub-areas. The earthquake magnitude M_L values ranged from 2.5 to 5 (Figure 5. 10). In general, the stress inversion results in the Alaotra region is obtained from 78 normal focal mechanisms that are grouped into three sub-zones (A, B, and C). Quality of the results according to the sub-zone is different after the inversion. In the sub-zone A; the blue direction that represents the minimum stress is trending in an average 66°and plunges 6.4° (See Figure 5. 13) while the red directions for the maximum stress axes are mostly trending 221° and plunges 83° (See Figure 5. 13), shape ratio values vary from 0.8 to 1. In the sub-zone B; the direction of the minimum stress axis (blue) direction is not uniform, some of them trend NW-SE and some trends NE-SW and the maximum stress as well, but for the observed clustered events, the maximum stress trends in the direction NW-SE. The values of shape-ratio vary from 0.9 to 1. And in the sub-zone C, the average direction of maximum stress is trending NE-SW and the minimum stress is trending NW-SE, shape ratio value is between 0.7 and 1. Characteristics of the obtained values of stresses are listed in Table 5. 1 and observed in Figure 5. 13

4.5 Ankaratra

Focal mechanisms from this region were calculated from only 30 events that having good coverage of seismic stations and good polarities. Results of the inversion from all focal mechanisms in this area are seen in Figure 5. 14 and Figure 5. 15, also the direction of the stress. From this study, predominant faulting and its scatter are also projected into a scatter of the P/T axes, which form clusters of a specific shape and presented in Figure 5. 14 and Figure 5. 15

After the inversion, we obtained the principal stress directions with 65% confidence. It yields orientations of the principal stress axes and the shape ratio values varying from 0.8 to 0.9 which measure the relative magnitude of the intermediate principal stress. The Mohr Coulomb failure criteria that shows the relation between the plane orientation and the normal shear is presented in Figure 5. 14. The average calculated direction of the maximum compressive stress, intermediate stress and minimum stress directions trend 242°, 193° and 101°, respectively; and plunge 79°,6.5°, and 8.5°, respectively. All results are presented in Figure 5. 14 and presented in Table 5. 1

4.6 Itremo

Results of stress inversion in Itremo region are obtained from 16 focal mechanisms (Figure 5. 17. Domination of normal faulting was seen in the Itremo region. The orientation of the principal stress (σ_1) trends from the 226° that plunging 78° from the horizontal and consistent to the average dip of P-axis. The intermediate stress trends 107°and plunges 6° while the minimum stress direction σ_3 trends from the azimuth 16° and plunge 10°. Values of the shape ratio and friction are 0.91 and 0.55, respectively.

5. DISCUSSION

Stress inversion in the whole part of Madagascar has not been estimated previously. Only characteristic of the fault direction was well determined using focal mechanisms solutions *e.g.*, Bertil & Regnoult (1998). Several geological and geophysical studies have been conducted to identify the characteristics of faulting in Madagascar (*e.g.*, Collins 2000; Bertil & Regnoult 1998). However, in this study the results of the stress inversion from focal mechanisms data set show the characteristic of the principal stress axis that is responsible of the fault direction in the study area.

Stress orientations can be well-resolved if diverse focal mechanisms are available. Based on the spatial variations of σ_1 and σ_3, the regional stress configuration of Madagascar was determined. Various stress directions are distinguished in some

local tectonic area of Madagascar after dividing the area study into six regions. Our results from this study suggest that the stress field, the faulting characteristics and focal mechanisms are predominantly a manifestation of extensional structure in the central part of the island of Madagascar. Interpretations of the results are presented according to each region.

5.1 Central region

From this study, results obtained in the central region such as in Alaotra, Ankaratra and Famoizankova areas show in a majority a domination of normal faulting which is consistent to the previous study (*e.g*., Bertil & Regnoult 1998).

The central area of Madagascar is one of the most seismically active where massive number of seismic events is seen in this area between 2000 and 2016 (Figure 5. 1). The main reason of the seismic activity in the central Madagascar is defined by different rifting, such as the Somalian plate and the Africa plate (Grimison & Chen 1988) following a high concentration of lavakas or erosional gullies in which correlate with the seismicity (Cox *et al*. 2010). It has been attributed by many authors using seismological data such as Bertil & Regnoult 1998; Rindraharisaona *et al*. (2013). Such different regions in central Madagascar are defined as active (Rindraharisaona *et al.* 2013) *e.g*., Ankaratra, Famoizankova, and Alaotra regions which are characterized by a number of small earthquakes and active hot spring (Bertil & Regnoult 1998). According to this study, from the selected events, quite large scatter in the distribution of the T- and P- axes are seen (Figure 5. 13). The average direction of the maximum horizontal principal stress that is derived from the individual earthquake focal solutions is about rotating clock ways 210°N and plunge 80° from the horizontal. While indicating consistence to the P- axis direction and to the existing structure presented in the region that shows domination normal environment in central Madagascar with sub-horizontal maximum and minimum extensional axes. The obtained uniform stress field in the central region of Madagascar can be interpreted that the area is manifested by thermal modulates strain rates as defined Zoback *et al.*

(2002). And direction of the main stress is corresponding to the tectonic feature in this area.

The central part of the island *e.g.,* in Ankaratra region is also volcanic and its latest eruption was during the quaternary (de Wit 2003*)*. The maximum compressional axis σ_1 is vertical and the minimum compressional axis is perpendicular to that in the surrounding area. Collected seismic data are consistent with the active regional stress field which is characterized by an almost and NE trending σ_1 and σ_3 lying horizontally. According to the value of friction, which is in an average number of 0.6, that indicates that faults located in Earth's crust are similar (Vavryčuk 2011)

Thus, we can interpret that both σ_2 and σ_3 are equal to the lithostatic stress in the central region of Madagascar around the existing faulting of Angavo and the seismically active area of Famoizankova, Ankaratra, and Alaotra.

5.2 Northern region

From this study, spatial variation of compressional stresses axis σ_1 and σ_3 in the northern part of Madagascar is not well determined because of the number of the data but results from the presented data give an interesting feature about the stress direction. According to the characteristic of fault plane solutions obtained in this area, domination of strike-slip faulting is presented (Figure 5. 5). After the inversion, direction of the maximum stress that rotated clock ways 247°N indicates that stress orientations vary between 30° and 10° from the existing thrust direction. It is related to the extensive medasedimentary rocks around the Andaparaty thrust also in the northern part of the Bemarivo Belt that occurred by the younger volcano-sedimentary structure (Tucker *et al.* 1999).

The compressive σ_1 is not seen as vertical as the results in the central region of Madagascar. Some strike slip faulting is seen around Sandrakota shear zone and Andaparaty thrust (See Figure 5. 5). After the inversion, orientation of the maximum

stress direction is parallel to the Sandrakota shear zone in the north that trends NW-SE direction, it can be explained that strong deformation of rock might occurred in this area and might create fracture in the surface that will be parallel to the existing shear zone.

About the relative magnitude of the three principal stresses, the stress ratio R-value from the inversion in the northern part of Madagascar is about 0.7 which is close to the unity and indicates $\sigma_2 \approx \sigma_3$.

5.3 Southern region

The southern part of Madagascar is seen as striking and thrusting. After inverting focal mechanism solutions from some events, direction of the maximum main stress is trending NW-SE and the minimum stress direction follow ENE-SWS next to the Ampanihy and Beraketa shear zones (Figure 5. 7). Next the Ampanihy shear zone, σ_1 and σ_3 are almost horizontal that trending NW-SE and ENE-SWS directions. The results are suited for the strike slip faulting on the N-S or E-W oriented vertical planes of the existing shear zone. No investigations have attempted about stress using focal mechanism data in this region.

On the other hand, value of R is closely equal to 0.5 around the southern active area of Madagascar. It can be interpreted as the non-uniformity of the horizontal compressive stress directions which is approximately less than 30° from the existing shear zone of Ampanihy presented in Figure 4. 7 to NW-SE.

6. CONCLUSION

We have subsequently used the obtained mechanisms of 182 in the whole area of Madagascar in order to get the direction of the stress using Michael's method (1984, 1987). The results gave the characteristics of the different stress axes, the magnitude of stress that defined the shape ratio value and the friction value that characterize the fracture on the rocks. A general view of normal faulting persists in

the central area with some reverse mechanisms and strike-slip faulting in northern and southern regions.

Regularity of the stress is seen in the central area that can be explained by the uplift structure in the central part of Madagascar and the separation of Madagascar from Africa, India, and Somalia. The most dominant direction-trend observed in the central Madagascar is NW-SE. This trend is compatible with the previous results of fault mechanisms in the defined active area of Madagascar. Stress results showing extension indicated by the faults existing in the study area support the suggestion that the stress should be characterized as correlate with the existing structure and formation beneath the area study. Our results in the central Madagascar show that this region is generally occurred by an extensional structure, the general direction of the principal stress E-W suggests that the extension could be the main cause of this stress regime. The stress distributions in the northern and southern of Madagascar regions are identical to the existing tectonic structure in these two regions.

From this work, we underline the importance of knowing the level of the background seismic activity and the reason why clustered events are observed in these two areas. Results from this present work must be improved after introducing more data from other method *e.g.*, GPS data. Based on this study, the main stress regime in Madagascar has been determined and could be helpful of the seismic hazard studies and the geodynamics analysis in the future.

ACKNOWLEDGEMENTS

This study is supported by the AfricaArray program under grant by the NSF awards EAR-0838426 and 083838. We acknowledge the support of the National Research Foundation trough the South African Research Chairs Initiative. All figures in this paper have been created with GMT (Wessel & Smith 1998) and MATLAB.

Appendix F. Focal mechanism list for stress determination

List of 182 focal mechanisms and defined by each regions using FOCMEC program. They are characterized by their locations, mechanisms, magnitude, their identities and their qualities.

ID	Date	Long	Lat	Depth	Mag	S1	D1	R1	S2	D2	R2
	d/m/year	(Deg)	(Deg)	(Km)							
BEMARIVO											
1	26-11-2002	49.3735	-14.9730	37.6	3	121	66	38	302	46	12
2	21-08-2003	48.6335	-14.3130	22.8	3.2	91	87	48	301	67	28
3	21-11-2004	49.5388	-14.6865	44.6	3.5	94	55	39	114	65	59
4	05-01-2005	49.6281	-14.6246	2	3.2	98	61	44	108	54	60
5	05-01-2005	50.1059	-14.6941	2	3.5	115	59	38	299	48	15
6	02-11-2005	50.0019	-14.8647	20	2.5	106	68	48	112	54	46
7	05-03-2007	49.5200	-14.8327	22.9	3.47	102	84	36	99	57	54
8	14-05-2010	49.5993	-14.9508	59.6	3.2	171	68	35	324	45	15
9	30-09-2011	49.5225	-14.9102	7.1	2.7	161	78	54	312	68	57
10	29-05-2012	49.4832	-13.9112	20.02	4	206	85	67	212	74	68
11	11-08-2012	48.0825	-15.5058	11.16	3.5	352	72	47	13	68	34
12	03-09-2012	47.8897	-16.0392	7.88	3.5	246	43	-41	8.95	62	-125
13	30-03-2014	49.4065	-14.6278	31.4	3.2	112	66	33	333	64	57
14	04-08-2014	48.7145	-14.3915	18	2.8	142	64	40	328	65	45
15	22-09-2013	49.4560	-14.3380	9.1	3.6	165	57	35	338	54	37
16	22-09-2014	49.3065	-14.9895	29.2	3.6	118	68	45	258	64	39
17	08-10-2014	49.0757	-14.6270	13.5	1.8	155	60	35	300	68	59
18	4-10-2015	49.4353	-14.3587	19.5	3.6	112	78	28	357	76	28
19	15-11-2015	49.6203	-14.7395	23.2	3.4	156	69	36	320	68	56
20	23-05-2016	49.4022	-14.3562	40.8	5	98	82	31	225	68	47
FAMOIZANKOVA											
1	5/12/2012	45,2349	-18,0897	15	4.1	119	55	-96	302	30	-92
2	8/18/2012	45,5372	-18,5244	23.2	4.2	148	26	-88	310	28	-91
3	1/9/2013	45,6362	-16,8375	41.9	4	123	35	-56	113	45	-70

4	1/13/2013	45,68357	-17,6629	23.5	4.2	301	22	-92	120	44	-91
5	4/16/2015	45,6962	-16,9472	25	5.3	114	56	-96	322	54	-85
6	5/24/2015	45,7553	-17,3136	25	4	311	56	-87	176	48	-90
7	5/30/2015	45,7554	-18,0194	25	4.4	160	55	-75	323	45	-86
8	6/18/2015	45,7688	-18,3690	25	5.1	321	56	-87	184	54	-94
9	8/5/2015	45,7856	-17,6873	2	3.7	112	32	-91	318	44	-84
10	9/23/2015	45,8137	-18,6778	2	4.2	136	32	87	321	41	82
11	10/24/2015	45,8240	-17,7532	25	4.8	125	69	-68	287	71	-78
12	10/27/2015	45,8626	-17,7397	2	4.6	187	33	-65	208	60	-87
13	10/29/2015	45,9019	-18,3996	25	3.7	135	55	-89	328	54	-91
14	10/30/2015	45,9265	-18,6908	25	3.2	124	26	-92	280	31	-90
15	12/24/2015	46,0399	-18,733675	25	4.1	110	77	-91	308	66	-93
ALAOTRA											
1	05-12/2003	48.3893	-17.7777	26.79	4.3	251	77	-91	87	68	-89
2	24-08-2005	48.6024	-15.8755	14.92	3.5	154	66	135	111	66	86
3	09-10-2005	48.5273	-17.4528	13	2.5	268	18	-97	108	58	-94
4	18-06-2006	48.5547	-17.3372	6.345	2.9	12	55	-105	215	45	-87
5	04-12-2006	48.5664	-18.1306	4.963	2.7	106	83	-112	323	84	-87
6	22-02-2007	48.1372	-15.5505	9.99	3	98	78	-66	225	56	-97
7	30-06-2007	48.2458	-18.6713	7.7	2.5	332	56	-90	115	58	-87
8	19-08-2007	48.6083	-17.2993	8.51	3	256	32	-24	123	34	-36
9	02-09-2007	48.6340	-17.3783	22.85	3.1	341	73	125	144	71	98
10	02-11-2008	48.6916	-17.5796	5.5	3.9	273	86	169	115	84	97
11	06-08-2009	48.3037	-17.7443	16.7	3.4	338	45	-79	144	45	-88
12	06-10-2009	48.6540	-17.5922	7.65	3.4	34	88	-115	210	88	-87
13	01-01-2010	48.4002	-16.9588	24.89	2.5	236	65	-76	155	66	-87
14	04-02-2010	48.6633	-17.5660	16.97	4	356	63	-125	162	56	-97
15	25-05-2010	47.1783	-19.9263	26.6	2.1	321	73	-79	136	65	-94
16	24-10-2010	47.8728	-18.4185	25.87	2.1	278	63	-78	144	67	-93
17	08-12-2011	47.8320	-16.8553	5.01	3.2	351	48	-65	138	44	-97
18	11-12-2011	47.7528	-18.2208	16.2	2.7	127	87	161	322	86	97
19	26-12-2011	48.3937	-17.4450	9.945	2.8	289	71	-87	123	65	-94
20	05-04-2012	47.0212	-19.9055	8.7	2.6	149	88	163	310	84	98
21	21-04-2012	48.4238	-15.8993	19.347	2.9	325	67	-93	154	63	-91
22	26-05-2012	47.9992	-17.4966	10.07	3.3	275	68	-89	158	54	-95
23	30-08-2012	48.2025	-17.7543	39.92	3.8	341	40	-82	151	50	-97

24	01-11-2012	49.0033	-17.2653	25.12	3.5	196	90	50	106	40	-180
25	03-09-2013	47.8460	-16.0180	3.65	3.5	190	88	126	222	87	98
26	12-09-2013	47.1692	-19.1985	2.64	2.6	225	85	-98	135	87	-99
27	10-10-2013	47.5718	-18.6263	2.44	3.4	235	86	136	129	83	99
28	21-11-2013	47.9733	-17.3140	6.79	3.5	321	66	-75	128	67	-89
29	26-11-2013	47.2092	-19.8773	27.8	3.6	48	45	145	43	147	56
30	15-01-2014	47.7622	-17.2870	3.65	2.8	355	76	154	112	58	136
31	03-02-2014	47.8178	-15.8290	8.487	3.1	295	46	-93	133	44	-99
32	08-02-2014	47.6505	-18.3592	2.84	3	144	77	136	244	74	144
33	08-02-2014	47.6798	-18.6502	2.57	3.3	180	72	112	312	56	98
34	12-02-2014	48.3865	-17.5565	7.394	3.3	247	88	-106	153	57	-114
35	13-02-2014	48.1553	-18.2467	12.5	2.5	349	87	-96	156	84	132
36	03-03-2014	47.0157	-19.3057	14.1	3.1	325	45	-96	144	45	-92
37	08-03-2014	47.8795	-18.0355	3.65	3	114	87	155	285	45	126
38	09-03-2014	47.8050	-18.4175	24.32	3	205	33	-95	45	33	-95
39	18-03-2014	48.0303	-16.4428	1.84	3.6	142	84	136	289	84	95
40	24-03-2014	47.0593	-19.9152	13	3.2	245	75	65	65	74	91
41	28-03-2014	47.6560	-17.4357	3.5	2.8	231	43	-66	87	44	-85
42	06-04-2014	47.5972	-16.3892	20	2.9	135	45	-87	325	45	-95
43	07-04-2014	48.2295	-17.5110	9.94	2.7	189	78	53	312	65	54
44	10-04-2014	47.9468	-17.8770	23.74	2.9	352	50	-91	168	64	-87
45	13-04-2014	47.9807	-17.1128	25	3.2	334	82	-57	164	84	-69
46	17-05-2014	48.4150	-19.2405	23.5	4	262	26	-107	68	35	-97
47	31-05-2014	47.0193	-19.9493	14	4.2	325	78	90	145	74	92
48	06-06-2014	47.9807	-17.2665	9.474	3.2	249	54	132	76	54	92
49	10-06-2014	47.9320	-17.9077	11.1	2.9	292	77	114	45	54	98
50	10-07-2014	47.6657	-18.3877	37.42	3.5	263	67	-90	83	23	-90
51	16-07-2014	47.9387	-17.0243	15	3.3	113	74	149	330	56	98
52	23-07-2014	47.6690	-18.3895	17.96	2.6	324	45	90	120	58	92
53	05-08-2014	48.2325	-17.8188	12.8	3.2	47	78	49	244	74	62
54	18-08-2014	48.3662	-17.5788	13.814	3.2	345	57	-87	135	54	-94
55	24-08-2014	47.8500	-18.0543	10.48	2.6	235	75	-95	56	74	-112
56	31-08-2014	47.0757	-19.3790	0.42	3.1	277	47	-97	89	41	-120
57	22-09-2014	48.0505	-18.6392	42.5	2.9	197	63	54	331	56	68
58	22-04-2015	48.7152	-17.3536	20.8	3.3	285	56	-170	128	54	-168
59	04-07-2015	48.6633	-17.7262	11.942	3.7	350	74	138	178	74	98
60	17-03-2015	48.3700	-18.0332	55.36	3.6	280	66	-69	144	54	-87
61	18-03-2015	48.6348	-17.4255	43.121	4.1	324	51	-80	133	44	-90
62	25-03-2015	48.3533	-17.5273	13.4	4.3	356	76	-97	153	57	123

63	22-04-2015	48.5671	-19.6609	17.668	3.1	322	88	-87	136	48	-97
64	07-05-2015	48.5658	-17.6732	21.3	3.6	349	61	-114	179	60	-97
65	24-05-2015	48.5811	-17.7561	11	4	5	88	-158	188	87	-147
66	28-05-2015	47.7698	-19.0881	13.3	4.2	241	45	90	78	44	92
67	07-06-2015	48.6460	-17.3650	32.5	4.2	63	77	-79	244	68	-91
68	19-06-2015	48.3378	-17.5388	16.2	4.25	322	44	118	166	54	157
69	30-08-2015	48.7302	-18.5195	55.2	3.2	61	70	-74	231	70	-91
70	10-11-2015	48.4563	-17.2542	6.431	3.6	62	36	-107	248	34	-91
71	20-12-2015	48.3493	-17.9158	13.1	3.7	315	35	-71	123	44	-98
72	24-12-2015	48.4000	-17.6633	31.704	4.1	324	55	-60	132	54	-94
73	05-01-2016	48.4108	-17.3317	12	4.1	347	75	-79	168	74	-81
74	20-04-2016	48.5952	-18.1410	3.519	3.1	299	76	-98	154	38	-95
75	05-05-2016	48.2446	-18.2933	15.54	2.6	231	43	-66	79	56	-97
76	18-08-2016	48.5443	-17.6688	17.34	3	292	75	-83	121	66	-94
77	02-09-2016	47.8318	-18.3465	9.63	4.1	340	81	177	136	58	147
78	07-09-2016	48.5210	-18.3017	5.145	3.2	190	56	101	28	54	90
ANKARATRA											
1	2/3/2002	46.7377	-18.7868	22.4	3.4	145	28	-99	321	25	-97
2	27-04-2002	46.9367	-19.6083	32.8	3	332	44	-96	133	41	-95
3	19-04-2003	47.0157	-19.3057	9.7	3.3	114	22	-88	301	28	-94
4	02-10-2003	47.4561	-17.9370	25	3.2	205	58	-95	78	51	-95
5	14-10-2003	46.5660	-19.4600	29	3	123	31	-87	310	28	-96
6	13-11-2003	46.6872	-19.3212	4.6	3.2	121	32	-78	308	34	-94
7	30-05-2005	47.4575	-18.1891	2	3	235	65	77	89	62	94
8	16-12-2007	47.5159	-17.4624	25	4.2	310	45	-95	118	44	-93
9	09-11-2008	47.4890	-17.5737	2	3.9	166	62	-85	280	61	-95
10	07-02-2009	47.3198	-18.4428	2	3.4	165	43	-87	285	44	-90
11	26-07-2010	47.0193	-19.9493	45.5	3.7	59	44	-171	218	59	-98
12	03-09-2012	47.8897	-16.0392	7.8	3.5	246	43	-41	8.95	62	-125
13	08-02-2012	46.9673	-18.7167	25	3	147	31	-99	321	30	-98
14	27-09-2012	46.7393	-18.9652	21.1	3.4	272	63	-31	17	63	-149
15	21-12-2012	46.6923	-19.0032	7.8	3.5	272	63	-31	17	63	-149
16	01-09-2012	46.7475	-19.2175	23.1	3.9	296	7	-90	116	82	-90
17	03-01-2013	45.9278	-18.6833	19.3	4.2	210	82	-31	187	62	-31
18	29-09-2012	46.9052	-19.3782	4.4	3.5	334	42	-89	321	25	-66
19	17-05-2013	46.1083	-18.7277	26.4	4	316	42	-67	322	52	-77
20	06-03-2013	46.5587	-19.4585	21.3	3.5	220	58	-26	324	68	-146
21	11-07-2015	46.9383	-19.6766	10	3	310	45	-99	121	42	-120
22	19-07-2015	46.9198	-19.8467	26.5	3.1	325	45	-97	123	41	-110
23	24-08-2015	47.2092	-19.8773	28.3	3.7	88	43	-99	209	44	-100

24	01-09-2015	47.5136	-18.7872	25	3.7	210	65	-84	79	62	-94
25	21-10-2015	47.3542	-18.4367	25	3.7	98	55	-94	255	54	-110
26	18-12-2015	47.3666	-18.0329	60	3.9	191	26	-88	79	25	-94
27	04-01-2016	46.6837	-19.0112	34.2	4.5	239	75	75	68	74	86
28	04-01-2016	46.6920	-19.0032	15.6	3.6	314	42	-88	132	44	-92
29	28-01-2016	46.7465	-19.0617	13.4	3.1	301	45	-91	118	44	-90
30	17-08-2016	46.9133	-19.3755	16.1	3.1	147	65	120	328	60	90
ITREMO											
1	12-04-2004	47.0038	-20.8927	30.9	3.1	321	53	-92	123	54	-90
2	01-10-2010	46.6270	-20.9305	27.4	3.2	144	54	-88	298	54	-90
4	19-01-2013	212.0000	56.0000	-78	3.5	45	90	220	45	90	45
3	28-01-2013	45.5752	-23.7787	9.31	3.3	17	56	-53	143	48	-132
5	14-05-2013	47.3100	-21.5973	2.1	2.9	212	56	-78	11	36	107
6	06-04-2014	47.0263	-20.0353	45	3.3	143	63	-91	284	63	-90
7	22-06-2014	46.5387	-20.3342	13	3.3	137	58	-96	289	35	-92
8	27-07-2014	45.3272	-20.6618	24.6	3.3	145	52	-92	279	51	-79
9	23-11-2014	46.8129	-20.1308	2	3.6	132	52	-87	289	51	-90
10	11-12-2014	45.6284	-20.7324	25	3.3	140	51	-88	287	50	-90
11	29-12-2014	45.5642	-20.6124	25	3.3	136	36	-87	297	39	-90
12	26-06-2014	45.5562	-20.4457	25	3.5	139	65	-89	300	60	-87
13	12-08-2014	45.5557	-20.3484	25	3.2	136	32	-87	299	34	-92
14	31-03-2015	47.6590	-20.6569	2	3.6	151	51	-88	300	56	-92
15	10-08-2015	47.4760	-20.2401	2	3.6	140	42	-90	305	56	-91
16	18-08-2016	45.9962	-17.6604	9.8	3.7	322	44	-71	125	45	-98
BEKILY											
1	23-12-2002	46.5773	-24.5067	2.5	3.5	154	36	49	320	34	56
2	09-01-2003	47.0978	-23.1448	9.1	3.6	145	35	45	312	24	54
3	01-06-2004	45.2078	-23.6855	17.9	3.1	132	47	58	301	51	69
4	02-03-2006	45.1173	-24.4712	19.8	4.4	321	68	40	123	65	54
5	11-08-2006	44.8565	-23.3395	37.8	3	99	45	39	212	41	56
6	18-11-2011	46.3797	-24.4118	31.4	3.2	221	35	79	78	41	85
7	22-09-2012	46.8805	-20.0595	13.8	3.9	146	43	-86	320	47	-94
8	30-07-2012	45.0037	-23.6200	30.7	3.9	77	70	52	322	42	149
9	26-03-2013	44.4453	-24.3653	19.9	3.9	223	61	-90	43	29	-90
10	04-07-2013	45.1075	-24.4833	12.9	3.2	95	44	-60	236	53	-115
11	04-11-2012	44.9495	-24.4465	29.4	3.8	154	33	47	300	52	57
12	28-01-2014	45.6375	-23.7232	21.5	3.3	111	45	35	301	42	38
13	23-03-2014	45.6693	-24.7940	3	3.3	189	55	45	78	56	57
14	26-03-2014	44.5038	-24.3168	54.1	3.8	147	59	48	289	56	59
15	26-03-2013	44.5792	-24.3178	19.1	3.2	166	45	36	300	57	56

16	14-02-2014	46.2202	-23.2320	2	3.3	145	56	54	287	54	68
17	10-03-2014	45.7822	-23.9362	2	4.1	156	80	58	297	81	56
18	03-04-2014	45.5005	-22.8927	2	3.9	132	79	58	336	74	59
19	06-06-2014	45.4469	-23.7742	2	3.2	178	65	49	348	61	59
20	28-06-2014	46.7898	-24.7551	2	3.4	121	86	48	336	84	58
21	07-08-2015	44.6804	-22.8972	20	4.3	93	54	67	240	52	62
22	30-03-2016	45.7333	-24.8325	18.3	3	235	55	84	78	54	72
23	08-06-2016	47.1181	-22.8019	15	4.2	156	56	45	300	52	60

Appendix G: Paper about Seismic hazard (In prep.)

Probabilistic Seismic Hazard study for Madagascar

Tsiriandrimanana Rakotondraibe[1,4], Raymond Durrheim[1], Andrew A. Nyblade[1,2], Michael E. Wysession[3], Gérard Rambolamanana[4], Fenitra Andriampenomanana[1,4]

1. School of Geosciences, University of the Witwatersrand, Private Bag 3 - 2050 Wits, Johannesburg, South Africa. E-mail: tsitsikel@gmail.com

2. Department of Geosciences, Penn State University, University Park, PA 16802, USA.

3. Department of Earth and Planetary Sciences, Washington University in St. Louis, Campus Box 1169, 1 Brookings Dr., Saint Louis, MO 63130-4899, USA.

4. Institut et Observatoire de Géophysique d'Antananarivo, Université d'Antananarivo, Ambohidempona - B.P 3843, Antananarivo 101, Madagascar.

ABSTRACT

Seismic hazard assessment for Madagascar based on Probabilistic analysis method (PSHA) is carried out after determining the three main parameters such as the mean seismic activity rate (λ), the *b*-value called Gutenberg-Richter value, and the maximum magnitude m_{max}. An earthquake catalogue was compiled from data combined between two sets of bulletins by the MACOMO and NDC databases. Duplicate events were removed, and the catalogue was homogenized to moment magnitude (M_W) scale before being declustered. A seismotectonic model for Madagascar developed from latter studies was used for the delineation of seismic source zones. A total of seven areal source zones were introduced in this study. Each zone is characterized in terms of its recurrence parameters and maximum magnitude using the homogenized catalogue. Seismic hazard calculations were performed for a grid spacing of 0.5° x 0.5° throughout the country. The logic tree formalization was implemented to account for uncertainties in the input parameters. The hazard values from 10% and 2% probabilities of exceedance for 50 years are estimated with the spectral accelerations for periods 1.0 s and 3.0 s. Relatively high hazard values were observed within the central regions of Madagascar comparing results from previous studies.

Keywords: Probabilistic seismic hazard analysis, Madagascar, peak ground acceleration (PGA), areal zone.

1. INTRODUCTION

Within the past century, high numbers of seismic activity have been recorded within central Madagascar *e.g.*, the volcanic region of Itasy and Ankaratra (Bertil & Regnoult 1998). The northern and southern parts of the country exhibit relatively low levels of seismic activity although several faults have been identified in these regions (Rakotondraibe et al., submitted). A number of destructive events have affected Madagascar with some having intensities up to VIII (Table 1. 1). An assessment of the hazard posed by these earthquakes within Madagascar is necessary.

Seismic hazard is defined as the probable level of ground shaking associated with recurrence of earthquakes (Giardini *et al.* 1999). In general, two commonly approaches are used for seismic hazard analysis, the deterministic and probabilistic methods. The deterministic approach is aimed on estimating the value of hazard parameter for a particular earthquake magnitude that happened at a fixed source-site distance (Reiter 1991). While the probabilistic approach considers the level of ground motion to which a location may be subjected within a given time period from different possible sources by taking into account the randomness in magnitude, the unpredictable nature of future earthquakes, (Cornell 1968, McGuire 1977). The Probabilistic Seismic Hazard Assessment (PSHA) method aims on quantifying the uncertainties from the earthquake location, the earthquake's size, and the resulting intensity of the future earthquakes.

For Madagascar, Razafindrakoto et al. (2009) conducted the first seismic hazard assessment using the Neo-deterministic method (Panza et al., 2001, 2012) by modeling a few seismic events recorded from the local permanent seismic stations. In their study, peak ground displacements, velocity, and acceleration were calculated using synthetic seismograms. Given the recent station installation and subsequent acquired seismicity information, it is pertinent to update the seismic hazard assessment for Madagascar. In this study, we applied the PSHA methodology to estimate the hazard for Madagascar. Calculation was done for 10% and 2%

probabilities of exceedance in 50 years after following logic-tree scheme based on various uncertainties from the ground motion prediction equation (GMPE) model, magnitude values and the depth. The spectral acceleration was also estimated for the period 1.0 s and 3.0 s, respectively.

2 Data and method

2.1 Catalogue homogenization and declustering process

Earthquake catalogues for Madagascar have been improved through revision of local and regional earthquake catalogues (Rakotondraibe et al., submitted). Earthquake data between 1897 and 2016 obtained from the combined bulletins Madagascar National Data Center (NDC) and Madagascar - COmoros and MOzambique (MACOMO) project (Rakotondraibe et al., submitted) were introduced in the present study. During the preliminary data processing, we applied pass band filters between 1 and 10 Hz in order to identify the local earthquake data and then identifying all earthquake sources using HYPOELLIPSE program (Lahr 1999). The combined catalogue was preprocessed to remove duplicate events then it was homogenized to the moment magnitude (Mw) using relation by Hanks & Kanamori (1979).

A total number of 7,020 events, that includes aftershock and seismic swarms, were identified and removed during the declustering process. The cluster method using ZMAP program (Wiemer 2001) was applied for declustering implemented seismic data. The final homogenious, declustered catalogue containing 11;950 seismic events is shown in Figure 5. 1.

In seismic hazard analysis, the commonly used magnitude scale is the moment magnitude (M_W). This scale is distant invariant and does not saturate at large magnitudes (Hanks & Kanamori 1979). It is therefore necessary to unify magnitudes in the catalogue into M_w. Because of this idea, we selected the moment magnitude relation for South Africa, from the Council of Geoscience (CGS) (Mulabisana 2016) to be applied in this study see equation (1). The reason of choosing their relation based on the numbers of events that they have been used and on the characteristics of the events that occurred in this area including the geological tectonic features existing

in this area. Their calculation relation was based on the maximum likelihood from SEISAN program (Havskov & Ottomoller 1999) using MAG function. In order to improve results of the relation, they insert another step using 358 earthquakes (Figure 5. 3) and derived the following equation

$$Mw = 0.796M_L + 0.539 \qquad \text{(Equation 1)}$$

With RMS 0.515

2.3 Catalogue completeness.

Catalogue completeness must be assessed before the recurrence parameters determination. An earthquake catalogue can be completed above a given magnitude Mc (magnitude of completeness) over a period Tc (period of completeness) if all earthquakes with magnitude values equal to or greater than Mc that have occurred during the period Tc. It is necessary to consider this aspect of the catalogue to avoid biasing the estimation of the recurrence parameters which would affect the final hazard results. Data completeness is largely dependent upon availability and is governed by factors including the time interval in question, geographical region, and recording instrumentation used. It is fair to assume that with time, data availability will improve in most regions given the implementation of superior monitoring methods. In this study, we used the method catalogue-based. Calculation is done after running the program written by Kijko et al. (2016) called HA3 program based on statistical approach e.g (Stepp 1972, Wiemmer and Wyss, 2000; Beauval and Scotti, 2003). The determination of the maximum curvature gives value of magnitude of completeness (M_C) after inserting all data in each source zone (See Figure 6. 6).

2.4 Seismic source model

Development of a seismic source model for seismic hazard calculations requires knowledge of both seismicity and geological setting of the region. In this study we

utilized the seismotectonic model developed by Rakotondraibe et al. (2020) to generate the seismic sources. Seven area sources, that are composed of 18,970 events (without declustered), were identified that lies within longitude 43º to 51º E and latitude 26º to 12º S (Figure 3. 9). According to the results from recent studies (Rakotondraibe et al, submitted), central and central-west of Madagascar are dominated by an extensional faulting *e.g.* in Ankaratra, Alaotra, Famoizankova, and Itremo. While the northern and southern part of the island are presented by strike-slip and thrust faulting *e.g.* in Bemarivo and Bekily regions (Figure 5. 2).Seven different area sources are classified as described after the declustering method as follows:

- Zone 1 (BEM) called Bemarivo zone: 300 events are located in this zone which is characterized by the presence of the Andaparaty thrust. The thrust runs northward at a low angle and about several hundred meters thick (Thomas et al. 2009) (Figure 6. 2).
- Zone 2 (AL) described as Alaotra and Ankay zone: This zone is visibly active as indicated by high seismicity and shown in previous studies (De Wit 2003; Laville *et al.* 1998, Bertil & Regnoult, 1998). A total number of 4954 seismic events are located in this zone (see Figure 6. 2) The two areas Alaotra and Ankay were grouped into one zone because of their similarity in geological features. First, Alaotra basin is characterized by minor volcanic which is a continuation of the Neogene-Quaternary magmatic field of Ankaratra (Brenon and Buissière 1959; Bésairie, 1964; Laville *et al.* 1998). And the Ankay basin is similar to the Alaotra structure, covered by basal conglomerates, lake and swamp deposits (Bésairie 1964). They are networking through the active river within the Alaotra-Ankay rift that is considered as a surface re-adjustment into recent tectonic activity (Bertil & Regnoult, 1998). According to Rakotondraompiana et al. (1999), cluster events occurring around the rift system and a main extension features were detected (Mougenot *et al.* 1986; Bertil & Regnoult, 1998).

- Zone 3 (ANK) the Ankaratra- Itasy zone: This zone is characterized by visible normal faulting observed from geological features. It covers the central parts of the island. A total number of 2546 earthquake events were recorded in the current catalogue. Recorded earthquakes are almost shallow with focal depth ranging from 5 to 39 km. This zone is also characterized by a volcanic field and consider as very active with abundant seismically tectonic active regions.
- Zone 4 and 5 (ITR) The Itremo zone is located in the west part from the central domain (Figure 6. 2). This zone constitutes an abundant volcanic-clastic-metasediment. A total number of 318 seismic events were located in this zone
- Zone 5 (IKL): The Ikalamavony zone is located in the east part from the central domain with a total of 1,224 seismic events recorded within this zone. An important main shear zone is shown under this zone called the Ranotsara shear zone (Figure 5. 2).
- Zone 6 (BEK) Bekily zone: It is located in the extreme southern part of Madagascar and consists of different thrust structure such as Ampanihy and Beraketa domains. A few thrust faults were determined in this zone. 110 earthquakes were reported. Maximum-recorded earthquake was M_L4.8.
- Zone 7 (FAM) the Famoizankova zone: It is characterized by relatively high seismic activity with relatively large events reaching a maximum magnitude value of 5.6. The seismic events are mainly caused by the existing NE-SW trending faults (Rakotondraibe *et al.* submitted). A total number of 2498 seismic events were selected and occurring in depth varying 5 to 39 km.

2.5 Determination of recurrence parameters

In order to assess the seismic hazard at a specific site, the seismic sources need to be characterised in terms of their earthquake recurrence, *i.e.* the relative frequency of occurrence of earthquakes with different sizes, as well as the maximum magnitude for each source. Calculations were carried out using the hazard program (HA3) from Kijko *et al.* (2016). The seismicity of all sources is assumed to follow a truncated

exponential (Gutenberg- Richter, Equation 2) distribution characterised by the following parameters:

- The m_{max} values are defined as the maximum possible earthquake magnitude for each source zone.
- The *b-value* represents the slope of the Gutenberg-Richter relation (Equation 2) and controls the relative frequency of occurrence of earthquakes of different magnitudes.
- The activity rate, *a*, is the intercept of the Gutenberg-Richter relation (Equation. 2) and represents the number of earthquakes occurring each year.

Ideally, all three parameters characterising the recurrence relations are determined jointly. However, in the present case, the time span of our data is too short to allow a good level of constraint on m_{max} values; hence this parameter was assessed separately, based on the maximum observed magnitude values.

$$\text{Log } N = a - b\text{m} \qquad \text{(Equation 2)}$$

where *a* and *b* values are defined above, and *N* represents the number of earthquakes. The *a*- and *b*-values are also summarised in

and the cumulative values for each source zone are presented in Figure 6. 6. These parameters were derived from the declustered catalogue data, using a maximum-likelihood approach to determine the best fit to the data over the magnitude range for which it can be considered complete ($m_{min,CALC}$ to $m_{max, CALC}$).

In general, methods for assessing m_{max} are classified into two types: deterministic and probabilistic. Deterministic approach consists of the empirical relationships between the m_{max} and some parameters related to the fault dimensions while probabilistic approach estimates m_{max} using seismic event catalogue and statistical estimation methods. In this study, we applied a statistical procedure for evaluating value of the m_{max}. Techniques as previously presented by Kijko & Sellevol (1989, 1992) were applied to estimate m_{max} values (Table 6. 6).

Kijko and Sellevoll (1989, 1992) (K-S) developed a probabilistic approach that takes into account the incompleteness of a catalogue as well as some pre-instrumental catalogue (Equation. 3) and this was applied for our study.

$$m_{max} = \frac{m_{max}^{obs} + \partial^{\frac{1}{q+2}} exp\,[\frac{nr^q}{1-r^q}]}{\acute{\beta}} \Gamma\left(-\frac{1}{q, \partial r^q}\right) - \Gamma(-\frac{1}{q, \partial}) \qquad \text{(Equation 3)}$$

Where, $r=p/(p + m_{max} - m_{min})$, $p = \bar{\beta}/(\acute{\sigma}\beta)^2$, and $q = (\frac{C_1}{\sigma\beta})^2$, β= bln(10), $\acute{\bar{\beta}}$ denotes the mean value of β, $\sigma\beta$ is the standard deviation of β and Cβ is a normalizing coefficient which is equal to

$\{1-[p/(p + m_{max} - m_{min})]q\}-1$, and,

$c_1=exp[-n\,(i-C\beta)]$, $\sigma=nC\beta$ *and* $\Gamma(.,.)$ is the incomplete Gamma Function.

Historical and complete instrumental data are important for the K-S approach. In this study, earthquake data are reported within Madagascar for the period from 1897 to 1992. A total of 17 largest earthquake events is recorded during this span of time (Table 6. 4) including the complete instrumental data. The catalog is subdivided into

three sub-catalogues such as: from 01 January 1993 to 31 December 2008, from 01 January 2009 to October 2013, and from 01 November 2013 to December 2016. The choice of these periods based on the fact that if older earthquake is less accurate the obtained information from the catalogue encompasses the time span 1897-1992. Characteristics of the largest earthquakes between November 1897 and December 1992 are presented in Table 6. 4 and structure of the Kijko and Sellevol method (K-S) is illustrated in Figure 2. 30.

2.6 Ground motion prediction equation (GMPE)

Ground Motion Prediction Equations (GMPEs) are used to relate a ground-motion parameter (*e.g.*, peak ground acceleration) to a set of variables describing the earthquake source, wave propagation path and local site conditions (*e.g.*, Douglas 2003). Some recent models go further to account for other factors affecting earthquake ground motions (*e.g.*, hangingwall effects). Given that hundreds of equations have been published in recent times, it is a daunting task to identify suitable models for a given project.

The choice of the GMPE model used is a fundamental component for any seismic hazard analysis. In this study, we selected two models in order to capture the epistemic uncertainties associated with the selection of GMPEs and utilized the logic tree formalism for PSHA (*e.g.*, Bommer and Scherbaum 2008). We selected the model developed by Boore et al (2014) for the NGA and Chiou & Youngs (2014) defined by the following two equations, respectively.

$$F_{source}(M)=C_1+C_2M+C_3M^2+f_{mech} \qquad \text{(Equation 5)}$$

where C_1, C_2, C_3 are the regression coefficients, M is the magnitude values and f_{mech} varies according to the normal, strike-slip or reverse source mechanism.

The model developed by Boore et al (2014) for the NGA shows good agreement for shallow crustal earthquakes in active tectonic region, and useful for regional

variability in earthquake source. While the model developed by Chiou and Youngs (2014), which is an update of 2008 NGA, is adopted for active shallow crustal earthquakes also and related to the effect of the style of faulting and the hangingwall effects. Valid magnitude range is from 3 to 8 which our data is quite similar to their characteristics with a valid distance range between 0 and 300 km. These equations were selected because the prevalent normal faulting and thrust faulting within the Alaotra and Ankaratra regions are similarly experienced. The range of magnitude values of earthquakes used to derive the two equations started with a minimum magnitude greater than 3.0 (Mw). The attenuation relation characterizes earthquake ground motion that decreases as the distance to the earthquake increases. It is related to the ground motion prediction relation for investigating.

2.7 Seismic Hazard Analysis

This Section describes the performance of the probabilistic seismic hazard analysis (PSHA) using the Cornell & McGuire methodology earthquakes (Cornell 1968, McGuire *et al.* 2005). This method aims on quantifying the uncertainties from the earthquake location, size, and the resulting intensity of the future earthquakes. All uncertainties were combined to create an explicit description of the future shaking that may occur at the site of the interest.

Delineating the seismic active zones is the main concept of this method that depends on the seismicity distribution (Cornell 1968, McGuire *et al.* 2005) as shown in the following equation:

$$P[Z \geq z] = \int_{m_{min}}^{m_{max}} \int P[Z \geq z|m,r]\, f_M(m) f_{R|m}(r|m) dr dm \qquad \text{(Equation 6)}$$

where Z and z are earthquake ground motion, $P[Z \geq z]$is the probability values, *m* is a given magnitude at an epicentral distance *r*; f_M and $f_{R|m}(r|m)$ are the Probability Density Function (PDF) of earthquake magnitude and the conditional PDF of the epicentral distance, respectively.

Seismic hazard for Madagascar was calculated for a 0.5^{o} interval for the entire country using the CRISIS2015 software (Ordaz *et al.* 2015) which implements the probabilistic seismic hazard method. PSHA was performed for 10 % and 2 % probabilities in order to evaluate the variation of the PGA values and to estimate the spectral acceleration for 1.0 s and 3.0 s. The PSHA required the characteristic of seismic zone which illustrated in Table 6. 6.

.

The logic-tree approach is used in seismic hazard analyses to incorporate epistemic uncertainty (uncertainty related to the lack of data or knowledge) by considering and ranking alternative options (Bommer *et al.* 2005). Different branches separate all uncertainties and each branch is inserted for each of the parameters. The calculation of the hazard followed all branches throughout the logic -tree and the analysis created a single hazard curve that shows the ground motion *vs*. annual frequency of exceedance. The weighting value is obtained by multiplying the weights along the branches.

In the current study, the logic-tree created contains 28 branches that were set up for each source and each represents an alternative seismic hazard scenario. Uncertainties associated with the Gutenberg–Richter recurrence relationship, the depth characteristics as well as the GMPE were presented. Magnitude of completeness values in the different mentioned areas are quite different, so we made the calculation for Mc2.3 and Mc 5.0. Figure 6. 11represent an example of one source-branche used in this present study.

3. RESULTS AND DISCUSSION

Seismic hazard maps for Madagascar are presented in Figure 5. 14 and Figure 5. 15 Results correspond to spatial distribution of PGA and SA at 1.0 s and 3.0 s that are computed for 10% and 2% probability of exceedance in 50 years, which correspond to return period of 474- and 2,475- years, respectively. Results show higher

exceedance PGA values of 0.090 g for 2% probabilities while 0.04 g for 10% probabilities, in the central part of Madagascar (*i.e.* in Famoizankova, Ankaratra, Alaotra, and Itremo regions) compared to other regions (Bemarivo, Bekily, and Ikalamavony regions). In the northern part of the island, lower PGA values are observed, which range between 0.098 g for 2% probabilities whie 0.023 g for 10 % probabilities. (Figure 6. 12)

Comparing our results, which are from probabilistic method, with previous ones, which used neodeterministic approach, large difference of PGA values were observed. The result from the neodeterministic approach was based on the data that are clustering in the central area of Madagascar, where the stations are concentrated, and events are close to all stations (Razafindrakoto *et al.* 2009). Results obtained from neodeterministic approach by Giardini et al (1999) and Razafindrakoto *et al*. (2009) (Figure 6. 16) gave maximum PGA values of 0.03 g; however, the probabilistic curve represents that the probability occurrence of an event is only 0.02 g. Values are quite in a very low probability event with 474-year return period (10% probabilities). Razafindrakoto *et al*. (2009) showed that the PGA values were mainly influenced by the earthquake event in April 21, 1991, where more damage occurred such as cracks in the house (90% people's house in Ambohimanarina, 84% in Kiranomena, 33% in Beanana, and 30% in Fenoarivo Be) (Rambolamanana & Ratsimbazafy 1991).

On the other hand, in the current probabilistic studies, high value of PGA varied from 0.07 g to 0.09 g. This can be attributed to the influence the time span catalogue (1897 to 2016), in which earthquake number and seismic stations were increased, hence, yield well characterized earthquakes (especially the magnitude). Also, the number of seismic stations and, thus, seismic events were increased; hence, yield well characterized earthquakes (especially the magnitude). It is known that PGA values depend on the distance between the source and the site, the earthquake magnitude, the local site conditions and the earthquake source characteristics.

Most of the earthquakes occurred around the depth of 15 km and 35 km. The selected GMPE models compatible to these depths of occurrence apparently influenced the results of PGA values according to their characteristics. In our study, the choice of GMPE model was based on the fault structure of the study area as proposed Boore *et al.* (2014) and Chiou & Youngs (2014). Although their model is not compatible and difficult to correlate to our seismic source zone, our results appeared to be consistent with our source zone. It is highly recommended to elaborate a new GMPE model for Madagascar in the future.

The capital of Madagascar is in Antananarivo, in the central part of the island, it means a place of industrial structures and large constructions. But according to the results from this study, higher values of PGA are presented in this area (in the center zone of Madagascar); these results can be useful for alarming the population in this area about the quality of the buildings that they want to construct in the future because numbers of population and numbers of building will increase time to time in the future.

4. CONCLUSION

The present study shows an update of PSHA for Madagascar. Seismic hazard assessment for Madagascar was carried out on a 0.5^{o} x 0.5^{o} grid using CRISIS software based on the Cornell (1968) methodology and following a logic tree formalism based on the uncertainties from the depth and the GMPE model. All hazard parameters are determined after using Kijko et al. (2016) based on stochastic methods.

PGA and spectral acceleration (SA) map are shown for different natural periods with 10 % and 2 % probabilities of exceedance in 50 years. The output of the regional hazard analysis was consisted of a set of probabilistic hazard maps for PGA, spectral accelerations of 1.0 s and 3.0 s. According to the calculation, the highest seismic hazard values occur in the central region that experienced the largest recorded

earthquakes. This study shows significant results and notices new PGA values in the northern and southern region of the island comparing to the results from Razafindrakoto *et al.* (2009).

Finally, it is necessary to say that, although the presented results have been calculated using recent data and information from each source zones, it can be interpreted as preliminary results because of the choice of models. Compared to Poggi *et al.* (2017), PGA and SA values are less, with maximums of about 0.25 g and 0.3 g for 10% probability of exceedance in 50 years.

Appendix H: Moment magnitude determination

Moment magnitude determination using MACOMO earthquake data

All calculation was done using SAC program. Measurement was done starting picking waveform at 0.5s before and 0.5s after the picked P-wave for all selected local earthquake. Seismogram analysis was done from the displacement spectra of 11 local earthquakes.

A fast Fourier Transform was applied on the vertical displacement component using a log scale and using SAC program (Goldstein and Snoke, 2005). Calculation based on the following equations that give the relation between moment magnitude and seismic moment. Results from Table D.1 of density, source distance, velocity of the P-wave (m/s), and the radiation effect correction are used to determine the seismic moment and moment magnitude values.

Table D1: Selected 11 local events within their characteristics for determining M_w

ID	Date	Time	Density (ρ[kg/m])	P-wave velocity[m/s]	S-wave velocity[m/s]
1	2011-12-31	05:06:26.63	2740	6400	3600
2	2012-06-17	10:11:35.55	2740	6400	3600
3	2012-08-22	00:35:11.87	2740	6400	3600
4	2012-10-18	17:36:06.02	2740	6400	3600
5	2012-10-18	16:12:48.69	2740	6400	3600
6	2012-11-01	00:19:28.21	2740	6400	3600
7	2012-11-20	00:00:51.88	2740	6400	3600
8	2013-01-13	13:24:54.51	2740	6400	3600
9	2013-03-18	21:50:52.25	2740	6400	3600
10	2013-03-26	09:48:39.60	2740	6400	3600
11	2013-01-25	23:37:26.10	2740	6400	3600